Doctor of Philosophy degree in Biomedical Sciences and Biotechnology

Cycle XXXII

"Mechanistic and functional studies of free and anchored antimicrobial peptides for biomaterial applications"

Ph.D. candidate:
Gerard Boix Lemonche

Advisors:
Prof. Irene Mavelli

Dr. Barbara Skerlavaj

2020

Table of Contents

Acknowledgments

Firstly, I would like to express my sincere and warm gratitude to my advisor Dr. Barbara Skerlavaj for the continuous support to my Ph.D. study and related research, for her patience, guidance, motivation, sustain and transmitted knowledge. Thank you for giving me the chance to mature and develop personally and professionally. I am also very grateful to my advisor Prof. Irene Mavelli and to all members of Dr. Skerlavaj's group, in particular to Dr. Francesca D'Este for her precious support and inspirational discussions.

Besides my advisors, I would also like to thank Dr. José María Manero (Biomaterials, Biomechanics and Tissue Engineering (BiBiTE); Department of Materials Science and Engineering; Polytechnic University of Catalonia; Catalonia; Spain), who gave me the chance to perform a stage in his research group. Special thanks to Dr. Jordi Guillem Martí (Biomaterials, Biomechanics and Tissue Engineering (BiBiTE); Department of Materials Science and Engineering; Polytechnic University of Catalonia; Catalonia; Spain), for his support and helpful discussion.

For this dissertation, I would like to express my gratitude to the reading committee members: Prof. Karl Lohner, Institute of Molecular Sciences, University of Graz, Austria and Prof. Renato Gennaro, Department of Life Sciences, University of Trieste, Italy, for their time, interest, and helpful comments. I would also like to thank very much the thesis committee for their insightful suggestions, questions and encouragement.

Secondly, I want to thank all the co-authors which contributed to the publications and communications related to this thesis. This dissertation would not have been possible without your hard and brilliant work and feedback.

I would like to thank Prof. Alessandro Tossi, Department of Life Sciences, University of Trieste, Italy, for help in peptide synthesis and analytical HPLC facilities, assistance in mass spectrometry and helpful discussion, to Dr. Filomena Guida, Department of Life Sciences, University of Trieste, Italy, for peptide synthesis and analytical HPLC guidance, to Prof. Nicolò Dossi, Department of Agricultural, Food, Environmental and Animal Sciences, University of Udine, Italy, for preparative HPLC facilities and to Dr. Alessandra Arzese, Department of Medicine, University of Udine, Italy, for helpful discussion. Dr. Davide Porrelli and Dr. Gianluca Turco, Department of Medicine, Surgery and Health Sciences, University of Trieste, Italy, are gratefully acknowledged for technical assistance in SEM analysis. I am also very grateful to Prof. Lorenzo Fedrizzi, Polytechnic Department of Engineering and Architecture, University of Udine,

I will always remember my fellow labmates and colleagues in University of Udine for the fun time we spent together. Thanks to Dorota, Kristel, Annalisa, Giorgio and Eros for the nice moments in the department. Thanks to Hari, Yammanappa, Gretta and Ashraf for our unforgettable moments, talks and good food. And specially thanks to Sara with whom I shared flat in Barcelona, Cristian, Rossella, Jacopo, Denise, Francesco, Matteo, Marzia, Bruno, Ehsan and Ruben for our great talks, aperitivos, dinners and many great moments. Special thanks to Rabail and Haseeb for our remarkable deep talks and your incredible Biryani, Rosario for our D&D games and nerd nights, Salvo for your crazy mood, you are a laugh machine ;-), Maria for all your support, wisdom and laughs. I will never forget all the *aperitivi*, the scientific and personal support, the lunches and dinners together, the good and bad moments, the beers, the laughs. Thank you for being there!

For the last but not the least, I could not finish this text without thanking all my family and friends in Spain, Switzerland, New Zeland, Netherlands, Japan and Germany who gave me so much support even from the distance… And a special thank to Marc, who gave me support many times via skype, and also against the Big Waaagh!

And most of all, a special thank you to Gina for encouraging and supporting me. She shared with me all the stress and the great moments, and has been a faithful support during the final stages of this Ph.D. which I appreciate much. Thank you.

Thank you all.

Co-Authorship Statement

This thesis contains information included in papers published prior to concluding the thesis (reported in the Annex). The articles were collaborations of our research group, Biochemistry (Department of Medicine, University of Udine, Italy), with Prof. Alessandro Tossi from Trieste research group (Department of Life Sciences, University of Trieste, Italy) and with Dr. Jordi Guillem Martí and Prof. José María Manero from Biomaterials, Biomechanics & Tissue Engineering (BiBiTE) research group (Polytechnic University of Catalonia, Spain).

Preparation of Titanium samples and their physicochemical characterization were performed at the Polytechnic University of Catalonia.

Peptide purification and characterization *via* HPLC and Mass Spectrometry were performed at the University of Trieste.

The biological characterization of the prepared Titanium samples were performed at the University of Udine.

List of Abbreviations

Ahx   6-aminohexanoic acid

AMPs   Antimicrobial Peptides

APTES   (3-aminopropyl)triethoxysilane

ATCC   American Type Culture Collection

BHI   Brain Hearth Infusion

BMAP   Bovine Myeloid Antimicrobial Peptide

CA   Contact Angle

CCCP   Carbonyl cyanide 3-chlorophenylhydrazone

CFU   Colony Forming Unit

CLSI   Clinical and Laboratory Standards Institute

CLSM   Confocal Laser Scanning Microscopy

DiBAC$_4$(3)   Bis-(1,3-Dibutylbarbituric Acid)Trimethine Oxonol

diSC$_3$(5)   3,3'-Dipropylthiadicarbocyanine Iodide

DMSO   Dimethyl Sulfoxide

FCCP   Carbonyl cyanide 4-(trifluoromethoxy)phenylhydrazone

FE-SEM   Field Emission Scanning Electron Microscope

FRET   Fluorescence Resonance Energy Transfer

HPLC   High-performance liquid chromatography

LUVs   Large Unilamellar Vesicles

MIC   Minimum Inhibitory Concentration

MBC   Minimum Bactericidal Concentration

MH   Mueller-Hinton

MH-PBS   Mueller-Hinton - Phosphate Buffered Saline

MPA   3-mercaptopropionic acid

MW   Molecular Weight

PBS   Phosphate Buffered Saline

PBS-glc   Phosphate Buffered Saline supplemented with glucose

PI   Propidium Iodide

QCM-D   Quartz Crystal Microbalance and monitoring Dissipation

SEM   Scanning Electron Microscope

Ti   Titanium

XPS   X-ray Photoelectron Spectroscopy

Abstract

The covalent immobilization of antimicrobial molecules on biomedical devices could represent an effective strategy to prevent bacterial colonization of implants and reduce the use of antibiotics. The antimicrobial peptides (AMPs) are emerging as promising candidates in this regards due to potent microbicidal properties that can be retained upon immobilization.

In the present thesis the widely used biocompatible material Titanium (Ti) was functionalized *via* thiol-maleimide chemistry with BMAP27(1-18), an α-helical cathelicidin peptide previously shown to retain potent staphylocidal activity when immobilized on agarose beads. Contact angle, Quartz Crystal Microbalance with Dissipation monitoring and X-ray Photoelectron Spectroscopy analyses confirmed successful peptide functionalization. A contact killing effect was observed on a reference biofilm-forming *S. epidermidis* strain, regardless of peptide C- or N- terminal orientation, by using CFU counts and SEM analyses. The immobilized peptide was not toxic to osteoblasts, which adhered and spread better on functionalized Ti also when co-cultured with bacteria, compared to non-coated surfaces.

An optimal design of antimicrobial coating requires a deep understanding of the mode of action of the immobilized molecules on whole bacteria. A part of this thesis was dedicated to the development of a rapid fluorescence microplate assay based on the combination of the potential-sensitive dye 3,3'-Dipropylthiadicarbocyanine Iodide, Propidium Iodide and CFU counts, which allows to distinguish between membrane depolarization due to ion movements across the membrane and membrane permeabilization due to pore formation. Applying this novel method, BMAP27(1-18) free and anchored to a model support *via* C- or N- terminus was evaluated for its membrane perturbing and bactericidal activity. Results showed a clear permeabilizing effect in solution, while alternative/additional mechanisms could be implicated for the immobilized peptide.

This assay could be applied in 'mode of action' studies of other soluble and immobilized membrane active AMPs and could be useful to further improve the design of peptide coated biomaterials. In the case of BMAP27(1-18), results obtained with grafted titanium support its potential for biomedical applications.

Reading notes

Chapter 1 Introduction - Global introduction to biomaterials, antimicrobial peptides and coating strategies.

Chapter 2 Aim of this thesis

Chapter 3 Covalent Anchoring of an alpha-helical Cathelicidin Peptide to reduce Staphylococcal Adhesion to Titanium surfaces - This chapter is based on the covalent attachment of BMAP27(1-18) to Titanium surface and its antimicrobial activity. It contains published data.

Chapter 4 Development of a rapid fluorescence-based microplate assay to obtain mechanistic insights on the interaction of membrane active peptides with whole bacterial cells - This chapter is focused on development of a novel microplate assay to distinguish bacterial membrane depolarization and permeabilization. It contains unpublished data.

Chapter 5 Mode of action of AMPs in the immobilized state - This chapter presents data related to the mode of action of free and anchored BMAP27(1-18). It contains unpublished data.

Chapter 6 Osteoblasts compatibility of peptide-functionalized titanium samples and the "Race for the surface" concept - This chapter provides information about capacity of osteoblasts to adhere and spread on functionalized Titanium samples also in the presence of bacteria. It contains published and unpublished data.

Chapter 7 General conclusions and future outlook

Chapter 1 – Introduction

1.1. Material used for bone replacement
1.1.1. Biomaterials

Biomaterial is an external material to the body designed to substitute a specific function or a part of the patient in a safe and physiologically acceptable way[1–3].

Biomaterials have been used in humans since about 2000 years. Ancient civilizations, such as ancient Romans and Aztecs used gold, silver, wood and animal bones as dental replacement, and tendons and fibers as suture material. These kind of substitutions were not successful due to the use of incorrect materials and their subsequent infections due to non-aseptic procedures. During the 1860s, aseptic surgery technique was developed, and the implantation of devices was improved, promoting an increment of the use of stainless steel and of the material engineering for biomedical applications.
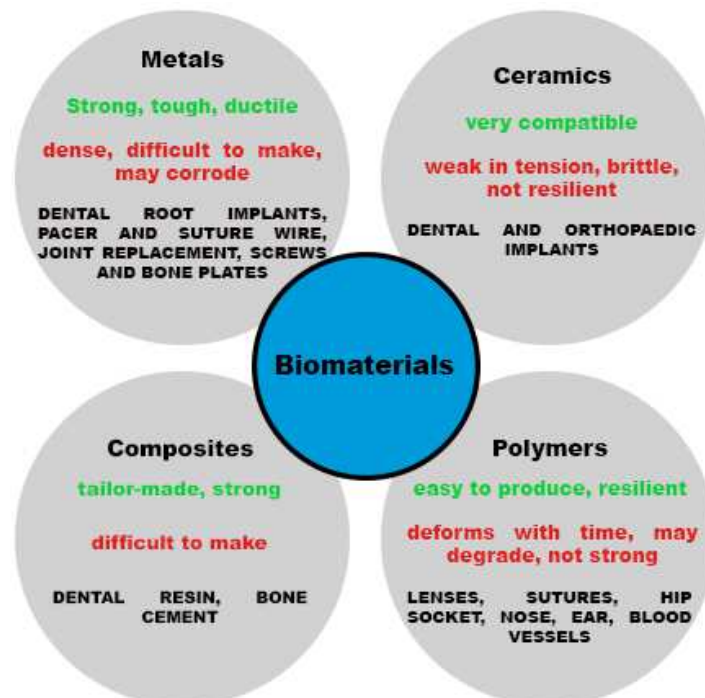
Figure 1.1. *Different biomaterials with advantages (green), drawbacks (red) and their applications in medicine.*

Biomaterials can be classified grouping them into several families: glasses, metals, ceramics, polymers and composites materials (**Figure 1.1.**)[4,5].

Biomaterials find a high number of applications in the medicine field. Some of these are hip prostheses, dental implants, knee prostheses, cardiac valves, intraocular lenses and left ventricular assist devices (**Table 1.1.**).

Table 1.1.: *Some Applications of Synthetic Materials and Modified Natural Materials in Medicine. Obtained from Ratner et al. 2004[6].*

Application	Types of materials
Skeletal system	
Joint replacements (hip, knee)	Titanium, Ti–Al–V alloy, stainless steel, polyethylene
Bone plate for fracture fixation	Stainless steel, cobalt–chromium alloy
Bone cement	Poly(methyl methacrylate)
Bony defect repair	Hydroxyapatite
Artificial tendon and ligament	Teflon, Dacron
Dental implant for tooth fixation	Titanium, Ti–Al–V alloy, stainless steel, polyethylene Titanium, alumina, calcium phosphate
Cardiovascular system	
Blood vessel prosthesis	Dacron, Teflon, polyurethane
Heart valve	Reprocessed tissue, stainless steel, carbon
Catheter	Silicone rubber, Teflon, polyurethane Polyurethane
Organs	
Artificial heart	Polyurethane
Skin repair template	Silicone–collagen composite
Artificial kidney (hemodialyzer)	Cellulose, polyacrylonitrile
Heart–lung machine	Silicone rubber
Senses	
Cochlear replacement	Platinum electrodes
Intraocular lens	Poly(methyl methacrylate), silicone rubber, hydrogel
Contact lens	Silicone-acrylate, hydrogel
Corneal bandage	Collagen, hydrogel

Titanium is the most used biomaterial for dental implants, but it is also extensively employed in orthopaedics, where higher mechanical requirements exists[7,8].

1.1.2. Titanium as biomaterial

Titanium (Ti) is the ninth element most abundant in the world, discovered by William Gregor in 1791. During the 1940s, some researchers performed animal studies in order to analyse the bioactivity of stainless steel, CrCoMb and Ti, and they discovered that Ti

had the lowest elastic modulus, ductility, high strength and good biocompatibility[9]. This promoted the use of Ti as a material for implants[6,10].

Regarding physical properties, Ti is a transition element such as iron, nickel or cobalt. Ti can be considered a lightweight metal, with an excellent relationship between resistance/density. It has a high melting point, which allows its handling at high temperature. Moreover, it is important to highlight its low thermal capacity, comparable to stainless steel, its low conductivity coefficient and low thermal expansion.

Concerning Ti chemical properties, it can be noted that it has 5 stable isotopes, with atomic weights between 46 and 50. The most abundant is Ti^{48}. One of the most important characteristics of Ti is its thermal reactivity at high temperatures. Titanium thermal reactivity is highly increased, which can be observed with the extreme reactivity between titanium and oxygen or other gases at high temperatures that are spread to the crystalline titanium network. This high reactivity with oxygen results in a fast formation of an oxide surface layer (passivation) with heterogeneous grading depending on the diffusion. This layer is impermeable, allows the metal to be completely protected, and for that reason, titanium has the characteristic of high corrosion resistance[6,10].

Usually Ti has a low mechanical resistance. The mechanical properties of Ti depend on the percentage of contaminant interstitial elements (oxygen, nitrogen, carbon and hydrogen). For this reason, different degrees of commercially pure titanium are defined based on the content of these elements (which determine resistance and fragility) and iron (which affects their resistance to corrosion). Extra Low Interstitial (ELI) alloys are also defined with very low contents in interstitial elements, which guarantee good plasticity and low toxicity[6,10].

Table 1.2. reports the classification of commercially pure titanium according to ISO 5832-2, as well as the mechanical properties of the different Ti purity grades[10,11].

Table 1.2. *Mechanical properties of titanium depending on purity degree for biomedical applications. Obtained from Brunette et al. 2001 and Adamovic et al. 2018[10,11].*

Properties	CP Ti grade 1	CP Ti grade 2	CP Ti grade 3	CP Ti grade 4
Yield strength (MPa)	170	275	380	485
Tensile strength (MPa)	240	345	450	550
Elongation (%)	24	20	18	15
Reduction in area (%)	30	30	30	25

Titanium grade 2 has bone-like mechanical properties, chemical stability, a good corrosion resistance and biocompatibility. For these reasons, it is the most widely used material in medicine[6,10–12] in particular for use in bone prostheses, dental implants and in other medical applications[4,10–12].

1.2. Problems derived from the interaction prosthesis-body

During the last century, the increment of degenerative diseases of the bone such as wear or excessive loading, deficiency of biological self-healing processes, degeneration of human joints, generated a rise of the use of biocompatible materials for bone replacement. A 70-80% of biomedical implants are composed of metallic materials[8]. In addition, the number of elder people demanding a substitution for failed-tissue is rapidly growing and the population life expectance is increasing. Furthermore, approximately a 90% of population over 40 is affected by some kind of degenerative disease[13].

Nevertheless, an increment of replacement surgery is directly related to a rise in revision surgery for prosthesis failure. The implant failure can be caused by factors such as host response, allergy, stress shielding effect, poor osseointegration and infection.

1.3. Host response

Once a prosthesis is implanted in the body, this causes a response that is named foreign body reaction where the macrophages, lymphocytes and neutrophils try to start the wound healing process and at the same time neutralize the foreign material. It is important to prevent any exaggerated response caused by the implant during the healing process, because it could alter tissue repair, promoting pathological inflammation, and lead to implant failure.

1.3.1. Wound healing process

Wound healing process is composed by four combined and overlapping phases: hemostasis, inflammation, proliferation and tissue remodelling[14–16] (***Table 1.3.***). The process could be affected resulting in a chronic wound. If any phase is interrupted, aberrancies are promoted or prolonged in time[16].

Table 1.3. *Normal Wound-healing process. Obtained from Guo et al. 2010[16].*

Phase	Cellular and Bio-physiologic Events
Hemostasis	1. Vascular constriction
	2. Platelet aggregation, degranulation, and fibrin formation (thrombus)
Inflammation	1. Neutrophil infiltration
	2. Monocyte infiltration and differentiation to macrophages
Proliferation	1. Re-epithelialization
	2. Angiogenesis
	3. Collagen synthesis
	4. ECM formation
Tissue remodelling	1. Collagen remodelling
	2. Vascular maturation and regression

1.3.2. Foreign body reaction

Subsequently to prosthesis implantation, the body has an inflammatory and wound healing response where the foreign body reaction (FBR) is the final-phase response. FBRs to titanium and other materials have been studied in material sciences and orthopaedics for long time and are considered as multifactorial, immune-modulated, and complex healing processes where a high number of cells and mediators are implicated[17].

The reaction of the host depends on physico-chemical implant characteristics and starts 2-4 weeks after implantation although this response is always present at the tissue-material interface[18]. It involves macrophages and giant body cells that can affect the biocompatibility of the implanted prostheses. After surgical implantation, a protein layer composed by fibrinogen, albumin, fibronectin and other proteins, adheres to prosthesis surface where its interaction with adhesion receptors present on inflammatory cell populations can regulate the subsequent inflammatory and wound healing process[19].

1.4. Infection

During the last decades, biomedical implants have transformed medicine, but unfortunately these devices also promoted an infection risk increment[20]. One of the principal problems of implants is their infection that implies complex interactions between the biomaterial, the pathogen and the host immune response.

In the infection associated to prosthesis, the implant induces an on-site tissue reaction that usually involves acute and chronic inflammation, a foreign body reaction, granulation tissue formation and fibrous encapsulation that make the implant susceptible to bacterial colonization, infection and subsequent biofilm formation[21]. Bacterial pathogenicity is mainly correlated to the capacity to adhere onto materials[22,23] and develop a multi-layered biofilm. The biofilm is composed of an aggregate of microorganisms, where the bacteria, often enclosed within a self-produced matrix of extracellular polymeric substances, adhere to each other and/or to the surface[24]. Biofilm formation allows pathogens to remain as reservoirs and to overcome innate immune defences resulting in long-term persistence of these infections[25]. Biofilm formation is composed of two phases. The first is the attachment of microbial cells to the surface, which depends on the physicochemical forces between the material and bacterial surface proteins, and the specific recognition between bacterial receptors and plasma and connective tissue proteins which cover prosthetic devices once implanted[26]. The second phase is the multiplication and accumulation of microorganisms, leading to the formation of multi-layered bacteria clusters *via* expression of specific polysaccharides and proteins on the surface of colonizing bacteria[27]. The orthopaedic prosthetic infections are usually caused by Gram-positive staphylococci, such as *Staphylococcus aureus* but also by some opportunistic pathogens, otherwise considered commensals, such as *Staphylococcus epidermidis*[20,28].

An international team from USA and EU reported differences in geographical distribution of orthopaedic implant infections caused by staphylococci. Specifically, they observed that *S. aureus* was the most frequent pathogen associated with total arthroplasty in the USA, whereas *S. epidermidis* was slightly more common in Europe (**Table 1.4.**). In the USA, 25.6% of all healthcare-associated infections are caused by infections related to biomedical devices[29]. A vast review of published reports

considering the distribution of causative agents of prosthetic joint infections indicated that coagulase-negative staphylococci, such as *S. epidermidis*, and *S. aureus* were found in equal proportions (about 30%)[30]. In infections caused by *S. aureus*, methicillin-resistant *S. aureus* (MRSA) was predominant in early infections, while methicillin-sensitive *S. aureus* (MSSA) was predominant in delayed and late infections[30]. Antibiotic resistance is a critical question in orthopaedic implant infections[23]. Nearly 32% *S. aureus* and 40% *S. epidermidis* strains recollected from orthopaedic postsurgical and prosthesis-associated infections were observed to be resistant to gentamicin[31,32].

Table 1.4. *Major implant-infecting bacteria causing orthopaedic infections. Obtained from Arciola et al. 2018*[20]

Species	Prevalence in medical device infections (%)	Prevalence in knee arthroplasty infections (%)	Prevalence in hip arthroplasty infections (%)	Prevalence in infections involving external fixation (%)	Prevalence in infections involving internal fixation (%)	Refs
Staphylococcus aureus	31.7	21.1	22.2	54.5	47.8	[33]
	33.8	26.4	24.4	47.8	42.5	[34]
	13.0 (EU)[a] – 31.0 (US)[a]	12.1 (EU)[a] – 29.6 (US)[a]	13.6 (EU)[a] – 32.6 (US)[a]	ND	ND	[35]
Coagulase-negative staphylococci	20.2 (US)[a] – 39.3 (EU)[a]	21.7 (US)[a] – 37.0 (EU)[a]	18.4 (US)[a] – 40.7 (EU)[a]	ND	ND	[35]
Staphylococcus epidermidis	39.0	52.6	48.1	18.2	26.1	[33]
	31.5	41.8	43.6	15.2	21.9	[34]
Coagulase-negative staphylococci other than *Staphylococcus epidermidis*	11.6	ND	ND	ND	ND	[33]
	12.8	ND	ND	ND	ND	[34]
Streptococcus spp. and *Enterococcus* spp.	10.3 (US)[a] – 14.5 (EU)[a]	10.3 (US)[a] – 14.5 (EU)[a]	9.1 (US)[a] – 12.1 (EU)[a]	ND	ND	[35]
Enterococcus faecalis	2.4	2.6	0.0	0.0	6.5	[33]
	4.4	0.5	3.5	8.7	5.3	[34]
Gram-negative bacteria	ND	4.5 (EU)[a] – 6.4 (US)[a]	4.2 (EU)[a] – 6.8 (US)[a]	ND	ND	[35]
Pseudomonas aeruginosa	6.1	10.5	3.7	18.2	4.3	[33]
	6.7	4.4	2.9	14.1	8.9	[34]
Escherichia coli	2.4	5.3	0.0	0.0	0.0	[33]
	1.6	ND	ND	ND	ND	[34]

EU, data from a European reference clinical setting; ND, not determined; US, data from a US reference clinical setting. [a]Infections after total arthroplasty

1.5. Antimicrobial coatings

Some of the first attempts to perform antimicrobial coatings for orthopaedic implants were made with conventional antibiotics, such as vancomycin and gentamicin[36]. However their limited antimicrobial activity and the delivery of these drugs at sub-MIC levels could evoke bacterial resistance[37,38]. Antibiotic-resistant bacteria are considered by the World Health Organization as one of the greatest threats to human health in the future and, specifically, as an important problem in orthopaedic implant infections[39]. It has been reported that some bacteria, such as *S. aureus*, show high rates of antibiotic resistance, and other species, such as *S. epidermidis* are developing an increase of antibiotic resistance[40].

Consequently, it is crucial to adopt strategies to prevent bacterial adhesion to and biofilm formation on the implant surfaces. Several approaches already exist, such as the screening and decolonization of MRSA in carriers, application of prophylactic antibiotics before implant surgery, skin preparation immediately before incision with an antiseptic solution, and others[28]. As they are not enough, it is important to improve the perioperative preventative measures, and to develop osteoblast-compatible biomaterials resistant to bacterial infection.

The many events that happen upon prosthesis implantation can be described by the 'race for the surface' concept. In the case that the tissue cells win this race, the implant surface is coated by tissue and would be more resistant to bacterial colonization. But if bacteria win this competition, they will promote the formation of biofilm on the implant surface reducing the possibility of tissue integration (***Figure 1.2.***)[41–43].
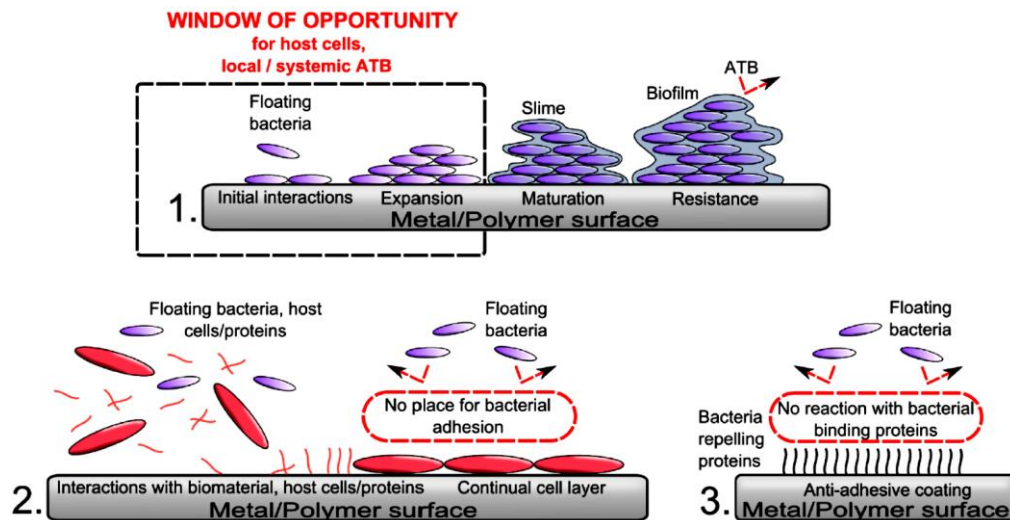
Figure 1.2. *Representative illustration of the process of biomaterial colonization starting from individual bacteria adhesion micro-colonies towards formation and maturation of biofilm (1); Schematic illustration about the "Race for the surface" Concept (2); illustrative image about the repulsion on bacteria in suspension caused by anti-adhesive coating. (3). Obtained from Gallo et al. 2014[44].*

Nowadays, diverse strategies are under study for orthopaedic applications[36,44,45], which try to prevent the bacterial adhesion and adsorption, such as anti-adhesive polymers[46,47], super-hydrophobic surfaces[48,49], nano-patterned surface[50,51], application of hydrogels[52,53]; or which attempt to kill bacteria via inorganic coatings, such as silver nanoparticles[54,55], zinc[56,57], selenium[58,59] and copper ions[60]; or organic coatings, such as chitosan derivatives[61,62], cytokines[63] or enzymes[64], surfaces covalently coated with antibiotics[65,66], and also by using AMPs[67,68]. Among these strategies the formation of biomaterials with antimicrobial peptides attached to the surface could represent an effective approach to prevent bacterial colonization[67,69,70].

1.6. Antimicrobial Peptides

Antimicrobial peptides (AMPs) represent an untapped reservoir of natural molecules with antimicrobial properties[71,72]. They are potential candidates as bactericidal agents, which have demonstrated their efficacy as a part of innate immunity[73]. AMPs or "host defense peptides" are components of the innate immune system, present in all living species, including bacteria, fungi, plants, insects, amphibians as well as other eukaryotes[74]. AMPs are molecules with high variability in size (<100 amino acids) and sequence. They are usually small, cationic and amphipathic. Many of them are membrane-active[75,76], usually with broad spectrum activity including bacteria, fungi and,

in some cases parasites, enveloped viruses, and even cancerous cells[73,77]. There is no definite consensus about the amino acid sequence determining their biological activity. Nevertheless, some conserved traits exist, such as charge, hydrophobicity, and amphipathicity. These features helped to define a well-accepted classification, based on the secondary structure. It divides AMPs into four groups: α-helical peptides, β-sheets, mixed structures and extended peptides (*Figure 1.3.*)[78,79].
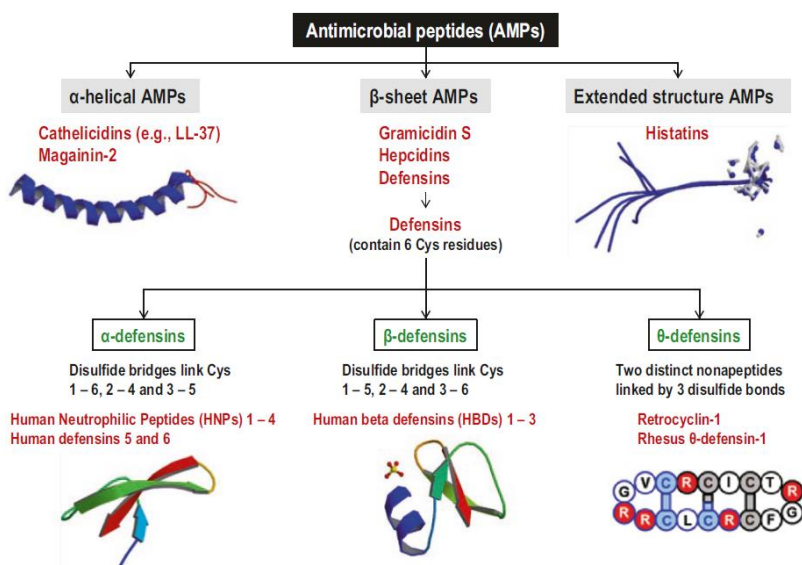
Figure 1.3. Classification of AMPs based on their structure. Obtained from Chakraborti et al.(chapter 5) 2018[80] and corrected with Lehrer et al. 2012[81].

A detailed description of the various classes of AMPs goes beyond the scope of this thesis. The experimental part of this study is focused on the α-helical peptides, which appear the most suitable for prosthetic coatings applications due to their mode of action (see below). They are one of the most abundant AMPs that are present in insects, amphibian, and mammals. The AMPs of the cathelicidin family have been isolated from many different species of mammals. Cathelicidin proforms share a well-conserved N-terminal prodomain (cathelin domain), for its more than 70% homology to cathelin, and inhibitor of cathepsin L.[82]. Nevertheless, these molecules are considerably different in the C-terminal antimicrobial domain, corresponding to the mature AMP, which becomes active upon its release from the holoprotein. Taking into account the structure of this domain, cathelicidins are additionally classified into cyclic and linear molecules. The cyclic peptides could contain one disulphide bond (e.g. cyclic dodecapeptide[83]), two disulphide bonds (e.g. protegrins[84]), could be rich in tryptophan residues (e.g. indolicidin[85]) or with a short tandem-repeat sequences (e.g. bovine bactenecins Bac5

and Bac7 [86]). However, the major part of cathelicidin peptides are linear with 23-40 amino acids, which adopt an α-helical conformation in anisotropic environments like the biological membranes (some examples of α-helical cathelicidins are rabbit CAP-18 [87], mice CRAMP[88], porcine PMAP-36 [89] and -37 [90], ovine SMAP-29 [91] and -34 [92], bovine BMAP-27, -28 [93] and -34 [94] and human hCAP-18 [95] and LL-37 [96,97]).

Most of these molecules have a mode of action based on membrane permeabilization. This accounts for a broad spectrum activity including antibiotic-resistant clinical isolates[98], efficacy against biofilm-embedded microorganisms, and low level of resistance induction[76,99–101]. Taking into consideration the increment of antibiotic-resistance problem[102], thanks to these properties AMPs may represent an advantage respect to other strategies.

As was mentioned previously, AMPs are molecules with high variability in sequences and size, thus they also have many different target sites or in other words many mechanisms of action depending on their targets. Currently, the first contact between AMPs and bacteria occurs at the microbial surfaces. As peptides are mainly cationic molecules, they interact with the anionic phospholipids of bacterial cytoplasmic membranes, such as the phosphate groups on Gram-negative outer membrane lipopolysaccharide (LPS), or the teichoic acids of Gram-positive bacterial peptidoglycan[103,104]. After the first contact with microbial surface, these peptides can interact in some different ways, such as disrupting the membrane integrity leading to cellular inactivation, or crossing the bacterial membrane without membrane permeabilization to reach intracellular targets that are essential for microbial metabolic pathways[105]. Currently, AMPs with membranolytic activity have two principal mechanisms, which depend on the relative position of the peptide respect to the bacterial membrane surface, that are called "carpet-like model" and "toroidal-pore model" (*Figure 1.4.*)[75,106].
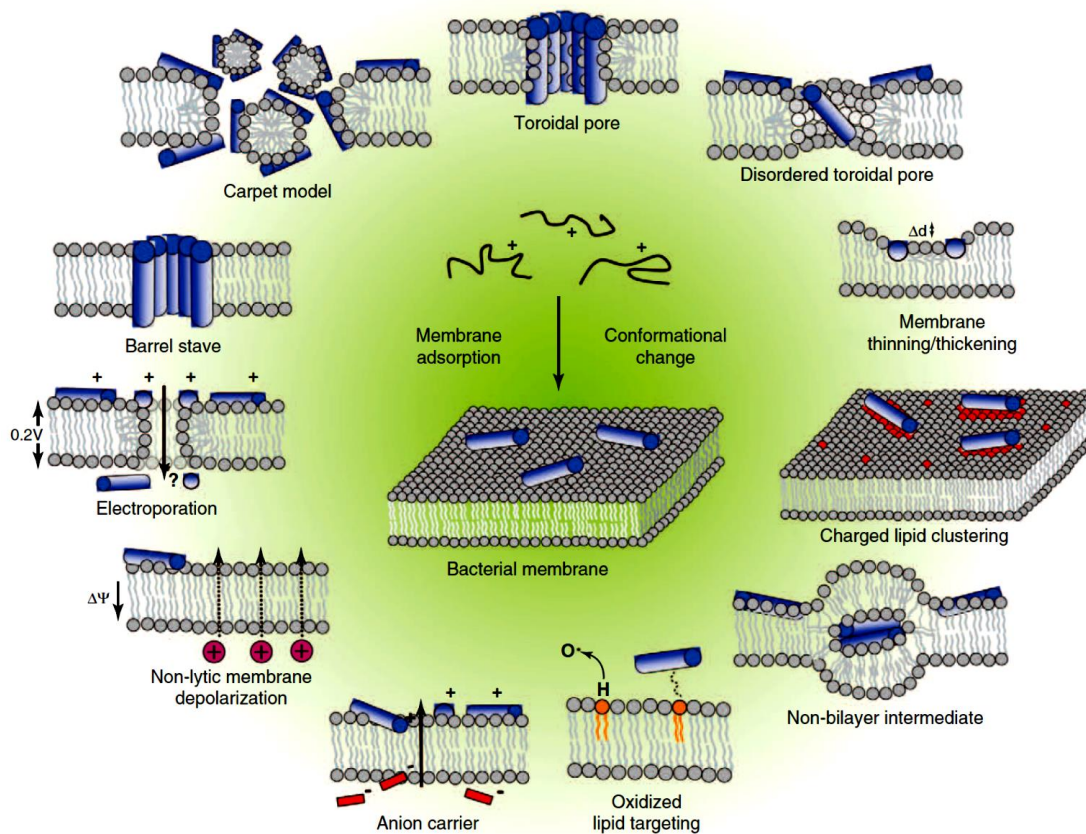
Figure 1.4. Schematic representation of the diverse events happening at the bacterial cytoplasmic membrane since initial AMP adsorption. These phenomena are not exclusive of each other and neither are inclusive. In this figure are described the classical models of membrane disruption (Toroidal pore model, Carpet-like model and Barrel stave model), other less common such as disordered toroidal pore, membrane thinning, charged lipid clustering, non-bilayer intermediate and also more specific situations as electroporation, non-lytic membrane depolarization, anion carrier and oxidized lipid targeting. Obtained from Nguyen et al. 2011[75].

In the toroidal-pore model peptides lying onto the membrane are adsorbed with their axes parallel to bacterial surface, forcing the lipids to fold inwards, building a pore delimited by lipid headgroups and associated peptides[103,106]. Moreover, another version exists, called "disordered toroidal pore model" which involves the stochastic formation of the pore with lower peptides participation[107]. However, the resulting pores induce a strong membrane depolarization and escape of the cytoplasmic components which cause the cell death[103]. In the carpet-like model, the molecules of AMPs always remain positioned in parallel to the bacterial membrane surface and cover it in a disordered manner until they reach a critical concentration where the membrane integrity is affected losing its electrostatic interactions and consequently collapsing to micellar

form[108,109]. In the barrel stave model, peptide aggregate and reorientate, inserting perpendicular into the bacterial membrane with their hydrophobic regions aligned with acyl fatty chains and hydrophilic regions towards the central aqueous lumen, forming a membrane-spanning pore such as a classical protein pore[110]. Anyway, the insertion of any molecule into the bacterial membrane would modify the membrane stability and the membrane-protein functions. The formation of pores and channels, or less defined lesions could provoke a distinct leakage of essential cytoplasmic components, which could induce the membrane depolarization and membrane permeabilization phenomena. Hence, once AMPs reach the bacterial membrane surface or pass through the membrane arriving into the intracellular space, they can interact with crucial targets and promote cell degradation by induction of hydrolases or inhibiting cell-wall synthesis or metabolic enzymatic activity, and finally inducing cell death[103,109,111,112].

Moreover, several AMPs possess modulatory host cell functions[71], also in the bone environment, such as LL-37 that promotes bone regeneration *in vivo* by diverse mechanisms implicating stimulation of other cell types[113–115], or the β-defensins that elicit stimulatory effects on osteoblast proliferation and differentiation[116]. In view of these characteristics, AMPs could be helpful not only to kill bacteria, but also to promote bone regeneration. Hence, prosthetic implants functionalized with AMPs would be an interesting target to study the "Race for the Surface" concept.

Several recent publications show successful binding of short cationic antimicrobial peptides to titanium (Ti) or other metals by using several different coupling methodologies[117–125]. These approaches include substantially the decision of tethering position (N- or C-terminus) and the nature and size of a possible spacer[67,69,126]. However, many researchers discuss about the antimicrobial efficacy of AMPs upon surface anchoring[127–130]. The efficacy depends on several variables associated to structural characteristics of the peptide and to coupling strategies. This means that an immobilized peptide could show distinct antimicrobial properties respect to the free peptide[131–133]. Numerous examples of antimicrobial peptides covalently immobilized to titanium are reported in the upper part of *Table 1.5.* Other useful information concerning coupling strategies and functional characterization are also provided. In addition, the lower part

of this table lists numerous examples of studies where AMPs were non covalently incorporated in various matrices for controlled release upon implantation.

Taking into consideration covalent surface immobilization, membrane-active AMPs arise as the most appropriate candidates as they would not require to penetrate into the bacterial cell to reach intracellular targets. Moreover, the creation of short antimicrobial sequences would have a positive impact on the production costs.

Table 1.5. *Examples of AMPs immobilized on titanium with different strategies. Obtained from Andrea et al. 2018[134].*

Biomaterial	AMP	Sequence	Coating Method	Bacteria	In Vitro Testing	In Vivo Testing	Biocompatibility Tested on	Ref.
Immobilized								
Titanium disks or hollow round casings	Melimine	CTLISWIKNKRKQRPRVSRRRR RRGGRRRR	Three-step: 1. Silanization with APTES[1] through vapour deposition. 2. Cross-linker addition sulfo-SMCC[2] by immersion. 3. Cys-peptide addition by immersion.	*S. aureus* strain 38 *P. aeruginosa* PAO1	Bacterial adhesion via fluorescence microscopy	Mouse and rat subcutaneous infection models. CFU determination	n/a	135
Titanium, commercially pure Grade II disks	GL13K	GKIIKLKASLKLL-NH$_2$	Two-step: 1. Silanization with (3-chloropropyl)triethoxysilane. 2. Peptide addition on the silane by immersion.	*Streptococcus gordonii* strain ML-5	Drip Flow Bioreactor Culture CFU assay, ATP assay, L/D staining BacLight, SEM	n/a	n/a	136
Titanium	GZ3163	4-methylhexanoyl-Cys-D-Dab-Dab-Dab-Leu-D-Phe-Dab-Dab-Leu-NH$_2$	Three-step: 1. Silanization with APTES[1]. 2. PEGylation with NHS-PEG$_{24}$-MAL[3] ester, by immersion. 3. Peptide coating by immersion.	*E. coli* DH5α *P. aeruginosa* ATCC27853 *S. aureus*[10]	CFU assay, L/D staining BacLight, SEM	n/a	Mouse blood cells lysis assay	137
Titanium, platelets	LL-37	CLLGDFFRKSKEKIGKEFKRIVQ RIKDFLRNLVPRTES	Three-step: 1. Silanization with APTES[1]. 2. PEG linker NHS-PEG-Mal[4]. 3. Incubation with peptide.	*E. coli* strain K12	Bacterial killing assay (Propidium iodide staining)	n/a	n/a	138
Titanium, deposited on silicon wafer	Tet213	KRWWKWWRRC	Three-step: 1. Copolymer brushes[5] synthesized on Ti. 2. Modification of the grafted chains using 3-maleimidopropionic acid *N*-hydroxysuccinimide ester. 3. Peptide conjugation via cysteine residue.	*P. aeruginosa* PA01 (*luxCDABE*)	CFU assay, luminescence	n/a	n/a	139
Titanium, deposited on silicon wafer	Tet-20	RWRIRVRVIRKC	Three-step: 1. Silanization with APTES[1] through vapour deposition. 2. N-substituted polyacrylamide brushes. 3. One-end tethering of AMP.	*P. aeruginosa* PA01 (*luxCDABE*)	CFU assay, luminescence, SEM	Rat subcutaneous infection model	MG-63 human osteoblast-like cells, Platelet activation, Complement activation analysis	140
Titanium, commercially pure Grade II	hLF1-11	MPA-Ahx-Ahx-Ahx-GRRRRSVQWCA-NH$_2$[6]	Three-step: 1. Silanization with APTES[1]. 2. Bifunctional cross-linker iodoacetic acid *N*-hydroxysuccini- mide ester 3. Peptide addition, by immersion.	*S. sanguinis*[10] *L. salivarius*[10]	CFU assay, L/D staining BackLight, CLSM, BacTiter-Glo Reagent for biofilm	n/a	Human foreskin fibroblasts	121

Material	Peptide name	Peptide sequence	Immobilization method	Bacteria	In vitro assay	In vivo	Cytocompatibility	Ref
Titanium, commercially pure Grade II	hLF1-11	MPA-Ahx-Ahx-Ahx-GRRRRSVQWCA-NH$_2$ [6]	Three-step: 1. Silanization with either APTES [1] or CPTES [7]. 2. Addition of the bifunctional cross linker 3-(maleimide)propionic acid N-hydroxysuccinimide ester. 3. Peptide addition, by immersion.	*S. sanguinis* [11] *L. salivarius* [11]	CFU assay, SEM, luminescence BacTiter-Glo Reagent for biofilm	n/a	Human foreskin fibroblasts	120
Titanium, commercially pure Grade II	GL13K	GKIIKLKASLKLL-NH$_2$	Two-step: 1. Silanization with CPTES [7]. 2. Peptide addition by immersion.	*Porphyromonas gingivalis* ATCC 33277	ATP assay, CFU assay	n/a	Human gingival fibroblasts (HGF) and MC3T3-E1 murine osteoblasts	141
Titanium foils 99.2% pure	Ti-binding-linker-JPH8194	RKLPDA-PAPAP-KRLFRRWQWRMKKY	Chimeric peptide, with titanium-binding domain.	*S. gordonii* ATCC 51656, *S. sanguis* ATCC 10556	L/D staining BacLight, CLSM	n/a	MC3T3-E1 Osteoblasts Culture	142
Titanium alloy, Ti6AL4V	Bacitracin	Ile-Cys-Leu-d-Glu-Ile-cy(Lys-d-Orn-Ile-d-Phe-His-d-Asp-Asp)	Polydopamine	*S. aureus* ATCC 25923, MRSA	n/a	Rat model, Ti rods were implanted into the femurs. CFU on the implant and at the peri-implant tissues.	Histopathology evaluation of the bone tissue around the Ti rod implant. nephrotoxicity of bacitracin-modified Ti in vivo	143
Titanium	SESB2V	[(RGRKVVRR)$_2$K]$_2$KK	Polydopamine	*S. aureus* ATCC 29213 *P. aeruginosa* ATCC 9027	L/D staining BacLight	rabbit keratitis model, CFU/cornea	n/a	144
Titanium alloy, Ti6Al4V	SESB2V	[(RGRKVVRR)$_2$K]$_2$KK	Polydopamine	*B. cereus* ATCC 14579 *E. coli* ATCC 35218	L/D staining, fluorescent microscopy	n/a	Human corneal stroma cells from donors tissue	142
Titanium, grade V powder	AMP1 / AMP2	LKLLKKLLKLLKKL / KWKRWWWWR	Chimeric peptide, with titanium-binding domain.	*E. coli* ATCC 2592 *S. mutans* ATCC 25175 *S. epidermidis* ATCC 29886	SYTO9 green fluorescent nucleic acid stain fluorescent microscopy	n/a	n/a	145
Release								
Titanium	HHC-36	KRWWKWWRR-NH$_2$	hydrogel, cathehol functionalised, addition of AMP	*P. aeruginosa* *E. coli* *S. aureus* *S. epidermidis*	CFU assay, SEM	n/a	human mesenchymal stem cells	146
Titanium	OP-145	Ac-IGKEFKRIVERIKRFLRELVRPLR-NH$_2$	PLEX [8] coating, mixed with peptide. Immersion for in vitro testing, spraying for in vivo.	*S. aureus* clinical strain JAR060131	CFU assay, Crystal violet	Mouse subcutaneous and Rabbit intramedullary nail infection models. Biopsy fom skin, subcutaneous tissue and implant.	n/a	147

Substrate	AMP	Sequence	Functionalization	Bacterial strain	Antibacterial assay	In vivo	Cytocompatibility	Ref
Titanium	Tet213	KRWWKWWRRC	Calcium phosphate by electrolytic deposition, soaking in the AMP solution.	*P. aeruginosa* H1001: *lux-CDABE* *S. aureus* ATCC 25293	CFU assay, luminescence	n/a	MG-63 human osteoblast-like cells	148
Titanium	HHC-36	KRWWKWWRR-NH$_2$	LBL [9] coating. Three layers of vertically oriented TiO$_2$ nanotubes, a thin layer of calcium phosphate coating and a phospholipid.	*P. aeruginosa* H1001: *lux-CDABE* *S. aureus* ATCC 25293	CFU assay, SEM	n/a	MG-63 human osteoblast-like cells Platelet activation Red blood cell (RBC) haemolysis assay	149
Titanium	GL13K	GKIIKLKASLKLL-NH$_2$	TiO$_2$ nanotubes.	*F. nucleatum* ATCC 25586 *P. gingivalis* ATCC 33277	CFU assay	n/a	MC3T3-E1 cells, a clonal mouse preosteoblastic cell line, J774A.1 mouse macrophage	150
Titanium[1]	HHC36	KRWWKWWRR	TiO$_2$ nanotubes, adsorption via a simple vacuum-assisted physical adsorption method.	*S. aureus* ATCC 25293	CFU assay, SEM	n/a	n/a	151
Titanium alloy, Ti6Al4V	Cateslytin	RSMRLSFRARGYGFR	Hydrogel made of natural polysaccharide, sodium alginate, modified by catechol groups along the polymer chain.	*P. gingivalis* ATCC 33277	Alamar Blue cell viability assay CFU assay	n/a	Gingival fibroblasts HGF-1	152
Titanium, solid medical grade implants	SAAP-145	Ac-LKRLYKRLAKLIKRLYRYLKKPVR-NH$_2$	Biodegradable PLEX was mixed with peptide.	*S. aureus* JAR060131, MDR *S. aureus* LUH15101	Propidium iodine fluorescence	mouse model of subcutaneous biomaterial-associated infection. CFU on the implant and at the peri-implant area. Biopsies.	n/a	153
Titanium plaHNUtes	Tet213	KRWWKWWRRC	layer-by-layer assembly, chitosan, hyaluronic acid. AMP was covalently linked to free amines of collagen IV	*S. aureus* ATCC 25923, *P. gingivalis* ATCC 33277	CFU and fluorescent microscopy	mice, intraperitoneal administration	Cytotoxicity Assay. HaCaT cells Human erythrocytes, haemolysis assay In vivo immunotoxicity assay.	154

[1] APTES: 3-Aminopropyl triethoxysilane; [2] Sulfo-SMCC: 4-(*N*-maleimidomethyl)cyclohexane-1-carboxylic 3-sulfo-*N*-hydroxysuccinimide ester; [3] NHS-PEG$_{24}$-MAL: succinimidyl-[*N*-maleimidopropionamido]-poly(ethylene glycol); [4] NHS-PEG-Mal: α-*N*-hydroxysuccinimidyl-ω-maleimidyl-PEG; [5] Copolymer brushes: *N,N*-dimethylacrylamide-*co*-*N*-(3-aminopropyl)-methacrylamide hydrochloride); [6] Ahx: 6-aminohexanoic acid, as spacer, MPA: 3-mercaptopropionic acid, as anchoring group; [7] CPTES: (3-chloropropyl)triethoxysilane; [8] PLEX: biodegradable Polymer-Lipid Encapsulation MatriX, consisting of poly lactic-*co*-glycolic acid, dipalmitoyl phosphatidyl choline, distearoyl phosphatidyl choline and cholesterol; [9] LBL: Layer-by-Layer; [10] Strains not specified; [11] *Streptococcus sanguinis* (CECT 480, Colección Española de Cultivos Tipo (CECT), Spain) and *Lactobacillus salivarius* (CCUG 17826, Culture Collection University of Göteborg (CCUG), Sweden). n/a: not applicable, CFU: Colony Forming Units, L/D staining: Live/Dead staining, SEM: Scanning Electron Microscopy, CLSM: Confocal laser scanning microscopy.

1.7. References

1. Williams, D. F. *Definitions in biomaterials : proceedings of a consensus conference of the European Society for Biomaterials, Chester, England, March 3-5, 1986. European Society for Biomaterials* **4**, (1986).

2. Grainger, D. W. The Williams dictionary of biomaterials. *Materials Today* **2**, 29 (1999).

3. Williams, D. F. On the nature of biomaterials. *Biomaterials* **30**, 5897–5909 (2009).

4. Ratner, B. D. Biomaterials Tutorial, an Introduction to Biomaterials. *University of Washington Engineered Biomaterials* (2004). Available at: http://www.uweb.engr.washington.edu/research/tutorials/introbiomat.html. (Accessed: 13th May 2015)

5. Park, J. & Lakes, R. S. *Biomaterials: An introduction: Third edition. Biomaterials: An introduction: Third edition* (2007). doi:10.1007-978-0-387-37880-0

6. Ratner, B. D., Hoffman, A. S., Schoen, F. J. & Lemons, J. E. *biomaterials science: An Introduction to Materials in Medicine. Chemical Engineering* (2004).

7. Li, H., Zheng, Y. & Qin, L. Progress of biodegradable metals. *Prog. Nat. Sci. Mater. Int.* **24**, 414–422 (2014).

8. Li, Y. *et al.* New Developments of Ti-Based Alloys for Biomedical Applications. *Materials (Basel).* **7**, 1709–1800 (2014).

9. Bothe, R. T., Beaton, L. E. & Davenport, H. A. Reaction of bone to multiple metallic implants. *Surg. Gynecol. Obs.* **71**, 598–602 (1940).

10. Brunette, D. M., Tengvall, P., Textor, M. & Thomsen, P. *Titanium in Medicine. Springer- Verlag: Heidelberg and Berlin* (Springer Berlin Heidelberg, 2001). doi:10.1007/978-3-642-56486-4

11. Adamovic, D., Ristic, B. & Zivic, F. Review of Existing Biomaterials—Method of Material Selection for Specific Applications in Orthopedics. in *Biomaterials in Clinical Practice* (eds. F., Z. et al.) 47–99 (Springer International Publishing, 2018). doi:10.1007/978-3-319-68025-5_3

12. Chouirfa, H., Bouloussa, H., Migonney, V. & Falentin-Daudré, C. Review of titanium surface modification techniques and coatings for antibacterial applications. *Acta Biomater.* **83**, 37–54 (2019).

13. Geetha, M., Singh, A. K., Asokamani, R. & Gogia, A. K. Ti based biomaterials, the ultimate choice for orthopaedic implants – A review. *Prog. Mater. Sci.* **54**, 397–425 (2009).

14. Rajendran, N. K., Kumar, S. S. D., Houreld, N. N. & Abrahamse, H. A review on nanoparticle based treatment for wound healing. *J. Drug Deliv. Sci. Technol.* **44**, 421–430 (2018).

15. Gonzalez, A. C. de O., Costa, T. F., Andrade, Z. de A. & Medrado, A. R. A. P. Wound healing - A literature review. *An. Bras. Dermatol.* **91**, 614–620 (2016).

16. Guo, S. & Dipietro, L. a. Factors affecting wound healing. *J. Dent. Res.* **89**, 219–29 (2010).

17. Trindade, R., Albrektsson, T., Tengvall, P. & Wennerberg, A. Foreign Body Reaction to Biomaterials: On Mechanisms for Buildup and Breakdown of Osseointegration. *Clin. Implant Dent. Relat. Res.* **18**, 192–203 (2016).

18. Trindade, R. *et al.* Osseointegration and foreign body reaction: Titanium implants activate the immune system and suppress bone resorption during the first 4 weeks after implantation. *Clin. Implant Dent. Relat. Res.* **20**, 82–91 (2018).

19. Anderson, J. M., Rodriguez, A. & Chang, D. T. Foreign body reaction to biomaterials. *Semin. Immunol.* **20**, 86–100 (2008).

20. Arciola, C. R., Campoccia, D. & Montanaro, L. Implant infections: adhesion, biofilm formation and immune evasion. *Nat. Rev. Microbiol.* **16**, 397–409 (2018).

21. Anderson, J. M. Future challenges in the in vitro and in vivo evaluation of biomaterial biocompatibility. *Regen. Biomater.* **3**, 73–77 (2016).

22. Geipel, U. Pathogenic organisms in hip joint infections. *Int. J. Med. Sci.* **6**, 234–240 (2009).

23. Campoccia, D., Montanaro, L. & Arciola, C. R. The significance of infection related

to orthopedic devices and issues of antibiotic resistance. *Biomaterials* **27**, 2331–2339 (2006).

24. Vert, M. *et al.* Terminology for biorelated polymers and applications (IUPAC Recommendations 2012). *Pure Appl. Chem.* **84**, 377–410 (2012).

25. Rafii, F. Antimicrobial resistance in clinically important biofilms. *World J. Pharmacol.* **4**, 31 (2015).

26. Busscher, H. J., Norde, W. & van der Mei, H. C. Specific Molecular Recognition and Nonspecific Contributions to Bacterial Interaction Forces. *Appl. Environ. Microbiol.* **74**, 2559–2564 (2008).

27. Heilmann, C. Adhesion Mechanisms of Staphylococci. in 105–123 (2011). doi:10.1007/978-94-007-0940-9_7

28. Hitchman, L. H., Smith, G. E. & Chetter, I. C. Prosthetic infections and high-risk surgical populations. *Surg.* **37**, 38–44 (2019).

29. Magill, S. S. *et al.* Multistate Point-Prevalence Survey of Health Care–Associated Infections. *N. Engl. J. Med.* **370**, 1198–1208 (2014).

30. Guo, G., Wang, J., You, Y., Tan, J. & Shen, H. Distribution characteristics of *Staphylococcus spp.* in different phases of periprosthetic joint infection: A review. *Exp. Ther. Med.* **13**, 2599–2608 (2017).

31. Campoccia, D. *et al.* Molecular epidemiology of *Staphylococcus aureus* from implant orthopaedic infections: Ribotypes, agr polymorphism, leukocidal toxins and antibiotic resistance. *Biomaterials* **29**, 4108–4116 (2008).

32. Campoccia, D. *et al.* Cluster analysis of ribotyping profiles of *Staphylococcus epidermidis* isolates recovered from foreign body-associated orthopedic infections. *J. Biomed. Mater. Res. Part A* **88A**, 664–672 (2009).

33. Montanaro, L. *et al.* Scenery of *Staphylococcus* implant infections in orthopedics. *Future Microbiol.* **6**, 1329–1349 (2011).

34. Arciola, C. R., An, Y. H., Campoccia, D., Donati, M. E. & Montanaro, L. Etiology of Implant Orthopedic Infections: A Survey on 1027 Clinical Isolates. *Int. J. Artif.*

Organs **28**, 1091–1100 (2005).

35. Aggarwal, V. *et al.* Organism Profile in Periprosthetic Joint Infection: Pathogens Differ at Two Arthroplasty Infection Referral Centers in Europe and in the United States. *J. Knee Surg.* **27**, 399–406 (2014).

36. Eltorai, A. E. *et al.* Antimicrobial technology in orthopedic and spinal implants. *World J. Orthop.* **7**, 361 (2016).

37. Stigter, M., Bezemer, J., de Groot, K. & Layrolle, P. Incorporation of different antibiotics into carbonated hydroxyapatite coatings on titanium implants, release and antibiotic efficacy. *J. Control. Release* **99**, 127–137 (2004).

38. Price, J. S., Tencer, A. F., Arm, D. M. & Bohach, G. A. Controlled release of antibiotics from coated orthopedic implants. *J. Biomed. Mater. Res.* **30**, 281–286 (1996).

39. Campoccia, D., Montanaro, L. & Arciola, C. R. A review of the clinical implications of anti-infective biomaterials and infection-resistant surfaces. *Biomaterials* **34**, 8018–8029 (2013).

40. Li, B. & Webster, T. J. Bacteria antibiotic resistance: New challenges and opportunities for implant-associated orthopedic infections. *J. Orthop. Res.* **36**, 22–32 (2017).

41. Subbiahdoss, G., Kuijer, R., Grijpma, D. W., van der Mei, H. C. & Busscher, H. J. Microbial biofilm growth vs. tissue integration: "The race for the surface" experimentally studied. *Acta Biomater.* **5**, 1399–1404 (2009).

42. Gristina, A. Biomaterial-centered infection: microbial adhesion versus tissue integration. *Science (80-.).* **237**, 1588–1595 (1987).

43. Godoy-Gallardo, M. *et al.* Anhydride-functional silane immobilized onto titanium surfaces induces osteoblast cell differentiation and reduces bacterial adhesion and biofilm formation. *Mater. Sci. Eng. C* **59**, 524–532 (2016).

44. Gallo, J., Holinka, M. & Moucha, C. Antibacterial Surface Treatment for Orthopaedic Implants. *Int. J. Mol. Sci.* **15**, 13849–13880 (2014).

45. Campoccia, D., Montanaro, L. & Arciola, C. R. A review of the biomaterials technologies for infection-resistant surfaces. *Biomaterials* **34**, 8533–8554 (2013).

46. Follmann, H. D. M. *et al.* Antiadhesive and Antibacterial Multilayer Films via Layer-by-Layer Assembly of TMC/Heparin Complexes. *Biomacromolecules* **13**, 3711–3722 (2012).

47. Muszanska, A. K. *et al.* Antiadhesive Polymer Brush Coating Functionalized with Antimicrobial and RGD Peptides to Reduce Biofilm Formation and Enhance Tissue Integration. *Biomacromolecules* **15**, 2019–2026 (2014).

48. Zhu, H., Guo, Z. & Liu, W. Adhesion behaviors on superhydrophobic surfaces. *Chem. Commun.* **50**, 3900 (2014).

49. Poncin-Epaillard, F. *et al.* Elaboration of highly hydrophobic polymeric surface — a potential strategy to reduce the adhesion of pathogenic bacteria? *Mater. Sci. Eng. C* **33**, 1152–1161 (2013).

50. Singh, A. V. *et al.* Quantitative Characterization of the Influence of the Nanoscale Morphology of Nanostructured Surfaces on Bacterial Adhesion and Biofilm Formation. *PLoS One* **6**, e25029 (2011).

51. Truong, V. K. *et al.* The influence of nano-scale surface roughness on bacterial adhesion to ultrafine-grained titanium. *Biomaterials* **31**, 3674–3683 (2010).

52. Zhao, C. *et al.* Dual Functionality of Antimicrobial and Antifouling of Poly(N -hydroxyethylacrylamide)/Salicylate Hydrogels. *Langmuir* **29**, 1517–1524 (2013).

53. Drago, L. *et al.* Does Implant Coating With Antibacterial-Loaded Hydrogel Reduce Bacterial Colonization and Biofilm Formation in Vitro? *Clin. Orthop. Relat. Res.* **472**, 3311–3323 (2014).

54. Godoy-Gallardo, M. *et al.* Silver deposition on titanium surface by electrochemical anodizing process reduces bacterial adhesion of *Streptococcus sanguinis* and *Lactobacillus salivarius*. *Clin. Oral Implants Res.* **26**, 1170–1179 (2015).

55. Knetsch, M. L. W. & Koole, L. H. New Strategies in the Development of Antimicrobial Coatings: The Example of Increasing Usage of Silver and Silver

Nanoparticles. *Polymers (Basel).* **3**, 340–366 (2011).

56. Elizabeth, E., Baranwal, G., Krishnan, A. G., Menon, D. & Nair, M. ZnO nanoparticle incorporated nanostructured metallic titanium for increased mesenchymal stem cell response and antibacterial activity. *Nanotechnology* **25**, 115101 (2014).

57. Hu, H. *et al.* Antibacterial activity and increased bone marrow stem cell functions of Zn-incorporated TiO2 coatings on titanium. *Acta Biomater.* **8**, 904–915 (2012).

58. Webster, T. J. & Tran. Selenium nanoparticles inhibit *Staphylococcus aureus* growth. *Int. J. Nanomedicine* 1553 (2011). doi:10.2147/IJN.S21729

59. Holinka, J., Pilz, M., Kubista, B., Presterl, E. & Windhager, R. Effects of selenium coating of orthopaedic implant surfaces on bacterial adherence and osteoblastic cell growth. *Bone Joint J.* **95**-**B**, 678–682 (2013).

60. Hoene, A. *et al.* In vivo evaluation of copper release and acute local tissue reactions after implantation of copper-coated titanium implants in rats. *Biomed. Mater.* **8**, (2013).

61. Tan, H., Ma, R., Lin, C., Liu, Z. & Tang, T. Quaternized Chitosan as an Antimicrobial Agent: Antimicrobial Activity, Mechanism of Action and Biomedical Applications in Orthopedics. *Int. J. Mol. Sci.* **14**, 1854–1869 (2013).

62. Renoud, P., Toury, B., Benayoun, S., Attik, G. & Grosgogeat, B. Functionalization of Titanium with Chitosan via Silanation: Evaluation of Biological and Mechanical Performances. *PLoS One* **7**, e39367 (2012).

63. Li, B. & McKeague, A. L. Emerging Ideas: Interleukin-12 Nanocoatings Prevent Open Fracture-associated Infections. *Clin. Orthop. Relat. Res.* **469**, 3262–3265 (2011).

64. Thallinger, B., Prasetyo, E. N., Nyanhongo, G. S. & Guebitz, G. M. Antimicrobial enzymes: An emerging strategy to fight microbes and microbial biofilms. *Biotechnol. J.* **8**, 97–109 (2013).

65. Antoci, V. *et al.* Covalently Attached Vancomycin Provides a Nanoscale Antibacterial Surface. *Clin. Orthop. Relat. Res.* **PAP**, 81–87 (2007).

66. Hickok, N. J. & Shapiro, I. M. Immobilized antibiotics to prevent orthopaedic implant infections. *Adv. Drug Deliv. Rev.* **64**, 1165–1176 (2012).

67. Costa, F., Carvalho, I. F., Montelaro, R. C., Gomes, P. & Martins, M. C. L. Covalent immobilization of antimicrobial peptides (AMPs) onto biomaterial surfaces. *Acta Biomater.* **7**, 1431–1440 (2011).

68. Rapsch, K., Bier, F. F., Tadros, M. & von Nickisch-Rosenegk, M. Identification of Antimicrobial Peptides and Immobilization Strategy Suitable for a Covalent Surface Coating with Biocompatible Properties. *Bioconjug. Chem.* **25**, 308–319 (2014).

69. Onaizi, S. A. & Leong, S. S. J. Tethering antimicrobial peptides: Current status and potential challenges. *Biotechnol. Adv.* **29**, 67–74 (2011).

70. Riool, M., de Breij, A., Drijfhout, J. W., Nibbering, P. H. & Zaat, S. A. J. Antimicrobial peptides in biomedical device manufacturing. *Front. Chem.* **5**, 1–13 (2017).

71. Yeung, A. T. Y., Gellatly, S. L. & Hancock, R. E. W. Multifunctional cationic host defence peptides and their clinical applications. *Cell. Mol. Life Sci.* **68**, 2161–2176 (2011).

72. Wang, G. *et al.* Antimicrobial Peptides in 2014. *Pharmaceuticals* **8**, 123–150 (2015).

73. Hancock, R. E. W. & Sahl, H.-G. Antimicrobial and host-defense peptides as new anti-infective therapeutic strategies. *Nat. Biotechnol.* **24**, 1551–7 (2006).

74. Ageitos, J. M., Sánchez-Pérez, A., Calo-Mata, P. & Villa, T. G. Antimicrobial peptides (AMPs): Ancient compounds that represent novel weapons in the fight against bacteria. *Biochem. Pharmacol.* **133**, 117–138 (2017).

75. Nguyen, L. T., Haney, E. F. & Vogel, H. J. The expanding scope of antimicrobial peptide structures and their modes of action. *Trends Biotechnol.* **29**, 464–472 (2011).

76. Tossi, A., Skerlavaj, B., D'Este, F. & Gennaro, R. Structural and functional diversity of Cathelicidins. in *Antimicrobial Peptides: Discovery, Design and Novel*

Therapeutic Strategies (ed. Wang, G.) 20–48 (CABI, 2017).

77.   Gaspar, D., Veiga, A. S. & Castanho, M. A. R. B. From antimicrobial to anticancer peptides. A review. *Front. Microbiol.* **4**, 1–16 (2013).

78.   Hancock, R. E. W. & Lehrer, R. Cationic peptides: a new source of antibiotics. *Trends Biotechnol.* **16**, 82–88 (1998).

79.   Mojsoska, B. & Jenssen, H. Peptides and Peptidomimetics for Antimicrobial Drug Design. *Pharmaceuticals* **8**, 366–415 (2015).

80.   Segal, B. H. *Management of Infections in the Immunocompromised Host*. (Springer International Publishing, 2018). doi:10.1007/978-3-319-77674-3

81.   Lehrer, R. I., Cole, A. M. & Selsted, M. E. θ-Defensins: Cyclic Peptides with Endless Potential: FIGURE 1. *J. Biol. Chem.* **287**, 27014–27019 (2012).

82.   Zanetti, M., Gennaro, R. & Romeo, D. Cathelicidins: a novel protein family with a common proregion and a variable C-terminal antimicrobial domain. *FEBS Lett.* **374**, 1–5 (1995).

83.   Romeo, D., Skerlavaj, B., Bolognesi, M. & Gennaro, R. Structure and bactericidal activity of an antibiotic dodecapeptide purified from bovine neutrophils. *J. Biol. Chem.* **263**, 9573–5 (1988).

84.   Kokryakov, V. N. *et al.* Protegrins: leukocyte antimicrobial peptides that combine features of corticostatic defensins and tachyplesins. *FEBS Lett.* **327**, 231–236 (1993).

85.   Selsted, M. E. *et al.* Indolicidin, a novel bactericidal tridecapeptide amide from neutrophils. *J. Biol. Chem.* **267**, 4292–5 (1992).

86.   Frank, R. W., Gennaro, R., Schneider, K., Przybylski, M. & Romeo, D. Amino acid sequences of two proline-rich bactenecins. Antimicrobial peptides of bovine neutrophils. *J. Biol. Chem.* **265**, 18871–4 (1990).

87.   Larrick, J. W. *et al.* Antimicrobial activity of rabbit CAP18-derived peptides. *Antimicrob. Agents Chemother.* **37**, 2534–2539 (1993).

88. Gallo, R. L. *et al.* Identification of CRAMP, a Cathelin-related Antimicrobial Peptide Expressed in the Embryonic and Adult Mouse. *J. Biol. Chem.* **272**, 13088–13093 (1997).

89. Storici, P., Scocchi, M., Tossi, A., Gennaro, R. & Zanetti, M. Chemical synthesis and biological activity of a novel antibacterial peptide deduced from a pig myeloid cDNA. *FEBS Lett.* **337**, 303–307 (1994).

90. Tossi, A., Scocchi, M., Zanetti, M., Storici, P. & Gennaro, R. PMAP-37, a Novel Antibacterial Peptide from Pig Myeloid Cells. cDNA Cloning, Chemical Synthesis and Activity. *Eur. J. Biochem.* **228**, 941–946 (1995).

91. Skerlavaj, B., Benincasa, M., Risso, A., Zanetti, M. & Gennaro, R. SMAP-29: a potent antibacterial and antifungal peptide from sheep leukocytes. *FEBS Lett.* **463**, 58–62 (1999).

92. Brogden, K. A. *et al.* The Ovine Cathelicidin SMAP29 Kills Ovine Respiratory Pathogens In Vitro and in an Ovine Model of Pulmonary Infection. *Antimicrob. Agents Chemother.* **45**, 331–334 (2001).

93. Skerlavaj, B. *et al.* Biological Characterization of Two Novel Cathelicidin-derived Peptides and Identification of Structural Requirements for Their Antimicrobial and Cell Lytic Activities. *J. Biol. Chem.* **271**, 28375–28381 (1996).

94. Gennaro, R., Scocchi, M., Merluzzi, L. & Zanetti, M. Biological characterization of a novel mammalian antimicrobial peptide. *Biochim. Biophys. Acta - Gen. Subj.* **1425**, 361–368 (1998).

95. Cowland, J. B., Johnsen, A. H. & Borregaard, N. hCAP-18, a cathelin/pro-bactenecin-like protein of human neutrophil specific granules. *FEBS Lett.* **368**, 173–176 (1995).

96. Agerberth, B. *et al.* FALL-39, a putative human peptide antibiotic, is cysteine-free and expressed in bone marrow and testis. *Proc. Natl. Acad. Sci.* **92**, 195–199 (1995).

97. Larrick, J. W. *et al.* Human CAP18: a novel antimicrobial lipopolysaccharide-

binding protein. *Infect. Immun.* **63**, 1291–7 (1995).

98. Zanetti, M., Gennaro, R., Skerlavaj, B., Tomasinsig, L. & Circo, R. Cathelicidin Peptides as Candidates for a Novel Class of Antimicrobials. *Curr. Pharm. Des.* **8**, 779–793 (2002).

99. Strempel, N., Strehmel, J. & Overhage, J. Potential application of antimicrobial peptides in the treatment of bacterial biofilm infections. *Curr. Pharm. Des.* **21**, 67–84 (2015).

100. Batoni, G., Maisetta, G. & Esin, S. Antimicrobial peptides and their interaction with biofilms of medically relevant bacteria. *Biochim. Biophys. Acta - Biomembr.* **1858**, 1044–1060 (2016).

101. Koprivnjak, T. & Peschel, A. Bacterial resistance mechanisms against host defense peptides. *Cell. Mol. Life Sci.* **68**, 2243–2254 (2011).

102. ECDC. *European Centre for Disease Prevention and Control. Surveillance of surgical site infections in Europe 2010–2011*. (2013). doi:10.2900/90271

103. Brogden, K. A. Antimicrobial peptides: pore formers or metabolic inhibitors in bacteria? *Nat. Rev. Microbiol.* **3**, 238–250 (2005).

104. Malanovic, N. & Lohner, K. Antimicrobial Peptides Targeting Gram-Positive Bacteria. *Pharmaceuticals* **9**, 59 (2016).

105. Mookherjee, N. & Hancock, R. E. W. Cationic host defence peptides: Innate immune regulatory peptides as a novel approach for treating infections. *Cell. Mol. Life Sci.* **64**, 922–933 (2007).

106. Yang, L., Harroun, T. A., Weiss, T. M., Ding, L. & Huang, H. W. Barrel-Stave Model or Toroidal Model? A Case Study on Melittin Pores. *Biophys. J.* **81**, 1475–1485 (2001).

107. Sengupta, D., Leontiadou, H., Mark, A. E. & Marrink, S.-J. Toroidal pores formed by antimicrobial peptides show significant disorder. *Biochim. Biophys. Acta - Biomembr.* **1778**, 2308–2317 (2008).

108. Oren, Z. & Shai, Y. Mode of action of linear amphipathic α-helical antimicrobial

peptides. *Biopolymers* **47**, 451–463 (1998).

109. Hale, J. D. F. & Hancock, R. E. W. Alternative mechanisms of action of cationic antimicrobial peptides on bacteria. *Expert Rev. Anti. Infect. Ther.* **5**, 951–959 (2007).

110. Ehrenstein, G. & Lecar, H. Electrically gated ionic channels in lipid bilayers. *Q. Rev. Biophys.* **10**, 1–34 (1977).

111. Zasloff, M. Antimicrobial peptides of multicellular organisms. *Nature* **415**, 389–395 (2002).

112. Choi, K.-Y., Chow, L. N. Y. & Mookherjee, N. Cationic Host Defence Peptides: Multifaceted Role in Immune Modulation and Inflammation. *J. Innate Immun.* **4**, 361–370 (2012).

113. Kittaka, M. *et al.* The antimicrobial peptide LL37 promotes bone regeneration in a rat calvarial bone defect. *Peptides* **46**, 136–142 (2013).

114. Zhang, Z. & Shively, J. E. Generation of Novel Bone Forming Cells (Monoosteophils) from the Cathelicidin-Derived Peptide LL-37 Treated Monocytes. *PLoS One* **5**, e13985 (2010).

115. Zhang, Z. & Shively, J. E. Acceleration of Bone Repair in NOD/SCID Mice by Human Monoosteophils, Novel LL-37-Activated Monocytes. *PLoS One* **8**, e67649 (2013).

116. Kraus, D. *et al.* Human β-defensins differently affect proliferation, differentiation, and mineralization of osteoblast-like MG63 cells. *J. Cell. Physiol.* **227**, 994–1003 (2012).

117. Costa, F. M. T. A., Maia, S. R., Gomes, P. A. C. & Martins, M. C. L. Dhvar5 antimicrobial peptide (AMP) chemoselective covalent immobilization results on higher antiadherence effect than simple physical adsorption. *Biomaterials* **52**, 531–538 (2015).

118. Mishra, B. & Wang, G. Titanium surfaces immobilized with the major antimicrobial fragment FK-16 of human cathelicidin LL-37 are potent against multiple antibiotic-resistant bacteria. *Biofouling* **33**, 544–555 (2017).

119. Nie, B. *et al.* Covalent immobilization of KR-12 peptide onto a titanium surface for decreasing infection and promoting osteogenic differentiation. *RSC Adv.* **6**, 46733–46743 (2016).

120. Godoy-Gallardo, M. *et al.* Covalent immobilization of hLf1-11 peptide on a titanium surface reduces bacterial adhesion and biofilm formation. *Acta Biomater.* **10**, 3522–3534 (2014).

121. Godoy-Gallardo, M. *et al.* Antibacterial properties of hLf1-11 peptide onto titanium surfaces: A comparison study between silanization and surface initiated polymerization. *Biomacromolecules* **16**, 483–496 (2015).

122. Lin, W. *et al.* Multi-biofunctionalization of a titanium surface with a mixture of peptides to achieve excellent antimicrobial activity and biocompatibility. *J. Mater. Chem. B* **3**, 30–33 (2015).

123. Makihira, S. *et al.* Titanium Immobilized with an Antimicrobial Peptide Derived from Histatin Accelerates the Differentiation of Osteoblastic Cell Line, MC3T3-E1. *Int. J. Mol. Sci.* **11**, 1458–1470 (2010).

124. Zhou, L. *et al.* Biofunctionalization of microgroove titanium surfaces with an antimicrobial peptide to enhance their bactericidal activity and cytocompatibility. *Colloids Surfaces B Biointerfaces* **128**, 552–560 (2015).

125. Chen, C.-P., Jing, R.-Y. & Wickstrom, E. Covalent Attachment of Daptomycin to Ti6Al4V Alloy Surfaces by a Thioether Linkage to Inhibit Colonization by *Staphylococcus aureus*. *ACS Omega* **2**, 1645–1652 (2017).

126. Masurier, N. *et al.* Site-specific grafting on titanium surfaces with hybrid temporin antibacterial peptides. *J. Mater. Chem. B* **6**, 1782–1790 (2018).

127. Wadhwani, P., Heidenreich, N., Podeyn, B., Bürck, J. & Ulrich, A. S. Antibiotic gold: tethering of antimicrobial peptides to gold nanoparticles maintains conformational flexibility of peptides and improves trypsin susceptibility. *Biomater. Sci.* **5**, 817–827 (2017).

128. Gao, G. *et al.* Biomembrane Interactions Reveal the Mechanism of Action of

Surface-Immobilized Host Defense IDR-1010 Peptide. *Chem. Biol.* **19**, 199–209 (2012).

129. Soares, J. W., Kirby, R., Doherty, L. A., Meehan, A. & Arcidiacono, S. Immobilization and orientation-dependent activity of a naturally occurring antimicrobial peptide. *J. Pept. Sci.* **21**, 669–679 (2015).

130. Rai, A. *et al.* High-density antimicrobial peptide coating with broad activity and low cytotoxicity against human cells. *Acta Biomater.* **33**, 64–77 (2016).

131. Bagheri, M., Beyermann, M. & Dathe, M. Mode of action of cationic antimicrobial peptides defines the tethering position and the efficacy of biocidal surfaces. *Bioconjug. Chem.* **23**, 66–74 (2012).

132. Hilpert, K. *et al.* Screening and Characterization of Surface-Tethered Cationic Peptides for Antimicrobial Activity. *Chem. Biol.* **16**, 58–69 (2009).

133. Bagheri, M., Beyermann, M. & Dathe, M. Immobilization Reduces the Activity of Surface-Bound Cationic Antimicrobial Peptides with No Influence upon the Activity Spectrum. *Antimicrob. Agents Chemother.* **53**, 1132–1141 (2009).

134. Andrea, A., Molchanova, N. & Jenssen, H. Antibiofilm Peptides and Peptidomimetics with Focus on Surface Immobilization. *Biomolecules* **8**, 27 (2018).

135. Chen, R., Willcox, M. D. P., Ho, K. K. K., Smyth, D. & Kumar, N. Antimicrobial peptide melimine coating for titanium and its in vivo antibacterial activity in rodent subcutaneous infection models. *Biomaterials* **85**, 142–151 (2016).

136. Chen, X., Hirt, H., Li, Y., Gorr, S. & Aparicio, C. Antimicrobial GL13K Peptide Coatings Killed and Ruptured the Wall of *Streptococcus gordonii* and Prevented Formation and Growth of Biofilms. *PLoS One* **9**, e111579 (2014).

137. De Zoysa, G. H. & Sarojini, V. Feasibility Study Exploring the Potential of Novel Battacin Lipopeptides as Antimicrobial Coatings. *ACS Appl. Mater. Interfaces* **9**, 1373–1383 (2017).

138. Gabriel, M., Nazmi, K., Veerman, E. C., Nieuw Amerongen, A. V. & Zentner, A.

Preparation of LL-37-Grafted Titanium Surfaces with Bactericidal Activity. *Bioconjug. Chem.* **17**, 548–550 (2006).

139. Gao, G. *et al.* Antibacterial Surfaces Based on Polymer Brushes: Investigation on the Influence of Brush Properties on Antimicrobial Peptide Immobilization and Antimicrobial Activity. *Biomacromolecules* **12**, 3715–3727 (2011).

140. Gao, G. *et al.* The biocompatibility and biofilm resistance of implant coatings based on hydrophilic polymer brushes conjugated with antimicrobial peptides. *Biomaterials* **32**, 3899–3909 (2011).

141. Holmberg, K. V. *et al.* Bio-inspired stable antimicrobial peptide coatings for dental applications. *Acta Biomater.* **9**, 8224–8231 (2013).

142. Tan, X. W. *et al.* Dual functionalization of titanium with vascular endothelial growth factor and β-defensin analog for potential application in keratoprosthesis. *J. Biomed. Mater. Res. Part B Appl. Biomater.* **100B**, 2090–2100 (2012).

143. Nie, B. *et al.* Immobilizing bacitracin on titanium for prophylaxis of infections and for improving osteoinductivity: An in vivo study. *Colloids Surfaces B Biointerfaces* **150**, 183–191 (2017).

144. Tan, X. W. *et al.* Effectiveness of Antimicrobial Peptide Immobilization for Preventing Perioperative Cornea Implant-Associated Bacterial Infection. *Antimicrob. Agents Chemother.* **58**, 5229–5238 (2014).

145. Yucesoy, D. T. *et al.* Chimeric Peptides as Implant Functionalization Agents for Titanium Alloy Implants with Antimicrobial Properties. *JOM* **67**, 754–766 (2015).

146. Cheng, H. *et al.* Mussel-Inspired Multifunctional Hydrogel Coating for Prevention of Infections and Enhanced Osteogenesis. *ACS Appl. Mater. Interfaces* **9**, 11428–11439 (2017).

147. de Breij, A. *et al.* Prevention of *Staphylococcus aureus* biomaterial-associated infections using a polymer-lipid coating containing the antimicrobial peptide OP-145. *J. Control. Release* **222**, 1–8 (2016).

148. Kazemzadeh-Narbat, M. *et al.* Antimicrobial peptides on calcium phosphate-

coated titanium for the prevention of implant-associated infections. *Biomaterials* **31**, 9519–9526 (2010).

149. Kazemzadeh-Narbat, M. *et al.* Multilayered coating on titanium for controlled release of antimicrobial peptides for the prevention of implant-associated infections. *Biomaterials* **34**, 5969–5977 (2013).

150. Li, T. *et al.* Antibacterial activity and cytocompatibility of an implant coating consisting of TiO_2 nanotubes combined with a GL13K antimicrobial peptide. *Int. J. Nanomedicine* **Volume 12**, 2995–3007 (2017).

151. Ma, M. *et al.* Local delivery of antimicrobial peptides using self-organized TiO_2 nanotube arrays for peri-implant infections. *J. Biomed. Mater. Res. Part A* **100A**, 278–285 (2012).

152. Mateescu, M. *et al.* Antibacterial Peptide-Based Gel for Prevention of Medical Implanted-Device Infection. *PLoS One* **10**, e0145143 (2015).

153. Riool, M. *et al.* Controlled Release of LL-37-Derived Synthetic Antimicrobial and Anti-Biofilm Peptides SAAP-145 and SAAP-276 Prevents Experimental Biomaterial-Associated *Staphylococcus aureus* Infection. *Adv. Funct. Mater.* **27**, 1606623 (2017).

154. Shi, J. *et al.* Biological and immunotoxicity evaluation of antimicrobial peptide-loaded coatings using a layer-by-layer process on titanium. *Sci. Rep.* **5**, 16336 (2015).

Chapter 2 – Aim of the thesis

2.1. Aim

Bacterial infection of orthopaedic implants represents one of the major challenges in orthopaedic surgery being associated with huge morbidity, and healthcare and social costs. The problem is critical also in view of the increment of antibiotic resistance, particularly in hospital settings. The development of infection-resistant biomaterials could represent an effective strategy to prevent bacterial colonization of implants, reducing the need for antibiotics. The antimicrobial peptides are receiving increasing attention in this regard due to their potent antimicrobial and antibiofilm properties also upon immobilization, and low tendency to induce resistance[1].

Bovine cathelicidin BMAP-27 is a well-characterized α-helical peptide expressed by bovine neutrophils[2]. It displays potent antimicrobial activity against bacteria and fungi but also relevant cytotoxicity towards mammalian cells[3]. Previous studies focused on a fragment of this peptide, BMAP27(1-18), which maintained high bactericidal activity while displaying significantly lower cytotoxicity[2,4]. Specifically, this BMAP27 derivative was effective against Gram-positive isolates, its activity was retained also in the presence of biological components such as serum, hyaluronic acid and synovial fluid and proved biocompatible to osteoblasts, highlighting its potential for orthopaedic applications[4]. Notably, BMAP27(1-18) immobilized on solid support showed potent killing capacity against *Staphylococcus aureus* and *Staphylococcus epidermidis*[4].

In view of all these properties, it was decided to covalently immobilize BMAP27(1-18) peptide onto Titanium (Ti), a widely and routinely used metal for orthopaedic implants[5,6], in order to possibly exploit the BMAP27(1-18) properties to inhibit bacterial colonization and enhance osseointegration of implants. The covalent immobilization was performed *via* thiol-maleimide chemistry and the functionalized Ti samples were physicochemically characterized and tested against a reference biofilm forming strain of

S. epidermidis[7]. Furthermore, osteoblast biocompatibility was evaluated in bacteria-osteoblasts co-cultures in the frame of the "Race for the Surface" concept.

In order to analyse the mechanism of action of the immobilised BMAP27(1-18) peptide, a relevant fraction of this thesis was dedicated to the development of a novel assay to get mechanistic and kinetic insights on the interaction of membrane active peptides with cytoplasmic membranes of whole bacteria. This rapid fluorescence based microplate assay was initially set up for soluble peptides using peptides with well-known mechanism of action as standards. In a subsequent step, this test was also applied to surface anchored peptides to gain mechanistic information that could be useful to further improve the design of peptide coated biomaterials.

2.2. References

1. Riool, M., de Breij, A., Drijfhout, J. W., Nibbering, P. H. & Zaat, S. A. J. Antimicrobial peptides in biomedical device manufacturing. *Front. Chem.* **5**, 1–13 (2017).

2. Skerlavaj, B. *et al.* Biological Characterization of Two Novel Cathelicidin-derived Peptides and Identification of Structural Requirements for Their Antimicrobial and Cell Lytic Activities. *J. Biol. Chem.* **271**, 28375–28381 (1996).

3. Risso, A., Zanetti, M. & Gennaro, R. Cytotoxicity and Apoptosis Mediated by Two Peptides of Innate Immunity. *Cell. Immunol.* **189**, 107–115 (1998).

4. D'Este, F., Oro, D., Boix-Lemonche, G., Tossi, A. & Skerlavaj, B. Evaluation of free or anchored antimicrobial peptides as candidates for the prevention of orthopaedic device-related infections. *J. Pept. Sci.* **23**, 777–789 (2017).

5. Bauer, S., Schmuki, P., von der Mark, K. & Park, J. Engineering biocompatible implant surfaces. *Prog. Mater. Sci.* **58**, 261–326 (2013).

6. Khorasani, A. M., Goldberg, M., Doeven, E. H. & Littlefair, G. Titanium in Biomedical Applications—Properties and Fabrication: A Review. *J. Biomater. Tissue Eng.* **5**, 593–619 (2015).

7. Sabaté Brescó, M. *et al.* Pathogenic Mechanisms and Host Interactions in *Staphylococcus epidermidis* Device-Related Infection. *Front. Microbiol.* **8**, (2017).

Chapter 3 – Covalent Anchoring of an alpha-helical Cathelicidin Peptide to reduce Staphylococcal to Titanium surfaces

3.1. Introduction

As was mentioned in the previous chapter, the infection of implanted prostheses is the most serious trouble in arthroplasty procedures and it may lead to prosthetic failure[1]. Medical treatment is arduous mainly due to microbial biofilm formation on device surfaces[1–3]. Bacterial biofilms are less sensitive to antibiotics compared to planktonic organisms, and only few antibiotics with anti-biofilm efficacy are available[3–5]. The principal microorganisms which cause prosthetic joint infections are Gram-positive bacteria[6], mainly *Staphylococcus aureus* (20 – 30 % of cases) and coagulase-negative staphylococci (20 – 30 % of cases)[4]. In healthy subjects, *Staphylococcus epidermidis* is an inoffensive commensal bacteria, but is being considered an opportunistic pathogen in immunocompromised patients, and patients with inserted medical devices[7]. Additionally, its ability to adhere and form biofilm on biomedical surfaces is recognized as a true virulent factor[8]. Taking into consideration all this information, it is crucial to adopt strategies for the prevention of bacterial adhesion to and biofilm formation on the prosthetic surfaces.

At present, many strategies are under study for orthopaedic applications[9–11]. Among these, the development of biomaterials coated with antimicrobial peptides (AMPs) could represent an effective approach to prevent bacterial colonization of implants[12–14]. Some AMPs have been reported to regulate host cell functions[15], also in the bone environment[16–18]. In this respect, several studies report on successful coating of Titanium (Ti) or other metals with short cationic AMPs by applying diverse linking strategies[19–27] which differ principally by the nature and length of a possible spacer and by tethering orientation (N- or C-terminus) of the selected peptide[12,13,28]. It is important to keep in mind that depending on coupling strategies and peptide structural

characteristics, an immobilized peptide could have different antimicrobial properties with respect to its soluble form[29–31].

At the beginning of my doctorate I was involved in the characterization of a cathelicidin derived α-helical peptide, namely BMAP27(1-18), which was selected for immobilization on solid support[32]. In solution this peptide presented potent bactericidal activity against Gram-positive clinical isolates, was active also in the presence of relevant biological components such as serum, hyaluronic acid and synovial fluid, and was biocompatible to osteoblasts[32]. Moreover, an N-biotinylated analogue bound to streptavidin resin beads exhibited potent killing capacity against *S. aureus* and *S. epidermidis*[32].

Based on these characteristics, in this part of my thesis a derivative of BMAP27(1-18) was covalently immobilized on the surface of titanium, which is a widely and routinely used metal for orthopaedic implants[33,34]. Functionalized Ti samples were characterized by contact angle (CA), quartz crystal microbalance with dissipation monitoring (QCM-D) and X-ray photoelectron spectroscopy (XPS). Their antimicrobial efficacy was investigated against a biofilm-forming *S. epidermidis* reference strain by colony forming unit (CFU) counts, evaluation of metabolic activity, and scanning electron microscopy (SEM). The aim was to assess whether Ti-immobilized BMAP27(1-18) was able to inhibit bacterial colonization in order to exploit the potential of this peptide for the production of infection-resistant titanium surfaces.

3.2. Results and Discussion
3.2.1. Coupling strategy

In collaboration with Biomaterials, Biomechanics & Tissue Engineering research group (BiBiTE) of the Polytechnic University of Catalonia (Barcelona, Catalonia, Spain), we decided to covalently bind BMAP27(1-18) to titanium surface *via* maleimide-thiol chemistry. To this purpose, the peptide was modified by attaching at the N-terminus three units of 6-aminohexanoic acid (Ahx) as a spacer and one unit of 3-mercaptopropionic acid (MPA) as anchoring moiety bearing a free thiol. The derivative MPA-(Ahx)$_3$-BMAP27(1-18) is hereafter referred to as B27(1-18)^{SH}. In order to check whether the antimicrobial properties of the peptide derivative B27(1-18)^{SH} have been affected by this modification, the minimum inhibitory concentrations (MIC) of both peptides against representative Gram-positive and Gram-negative bacterial species were determined (***Table 3.1.***). Apparently, B27(1-18)^{SH} lost efficacy against gram-negative bacteria, maintained efficacy against *S. aureus* and improved against *S. epidermidis* (***Table 3.1.***), but given the small differences in MIC values (one well corresponding to one double concentration), these can be regarded as negligible.

Table 3.1. *Antimicrobial activity of soluble peptides against reference strains.*

	BMAP27(1-18) [32]	B27(1-18)^{SH}
	MIC (µM)^{a,b}	
S. epidermidis ATCC 35984	2	1
S. aureus ATCC 25923	4	4
E. coli ATCC 25922	2	4
P. aeruginosa ATCC 27853	2	4

[a] Determined in MH broth.

[b] Data are means of at least 3 independent experiments.

Given the long year experience of the BiBiTE research group in peptide coupling to various metals, we decided to apply the simple strategy that already gave satisfactory results with the cell adhesive RGD peptide, and the antimicrobial peptide hLF1-11 tethered to tantalum and titanium, respectively[22,23,35] and which is schematically illustrated in ***Figure 3.1***. By using this procedure, B27(1-18)^{SH} was covalently anchored

to titanium *via* its N-terminus and the coating was performed using two different peptide concentrations in the coupling solution.
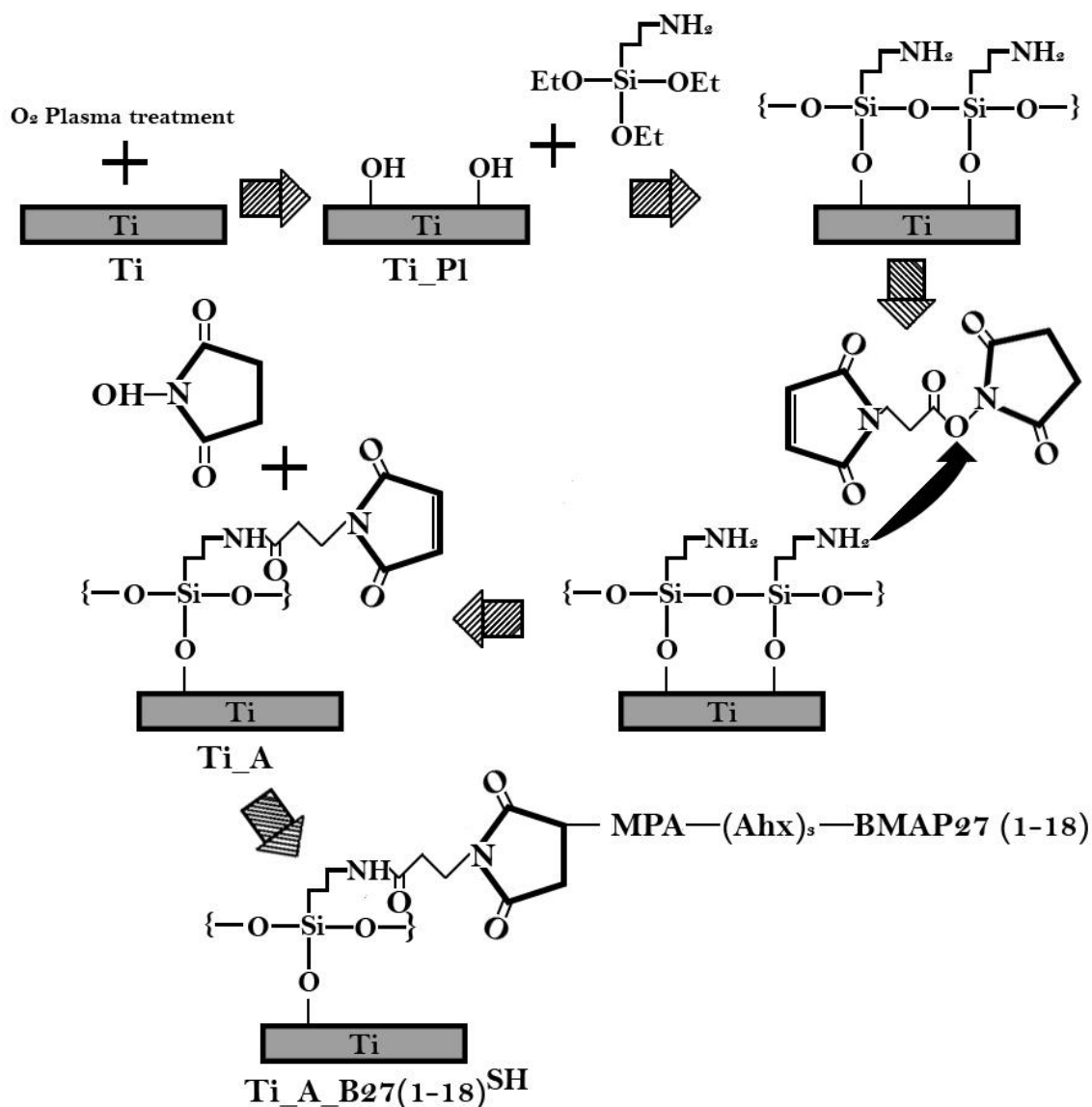
Figure 3.1. *Schematic representation showing the coupling procedure of B27(1-18)^{SH} to titanium by maleimide-thiol chemistry.*

The procedure consists in the modification of Ti disks surface (Ti) with oxygen plasma treatment (Ti_Pl) to produce hydroxyl groups, required for the subsequent silanization of samples with the (3-aminopropyl)triethoxysilane (APTES). Afterwards, the surface is treated with the bifunctional crosslinker N-succinimidyl-3-maleimidopropionate (SMP), which reacts with the amino groups of the organosilane and bears the maleimide function (Ti_A), needed for the reaction with the thiol group on the peptide N-terminus (Ti_A_B27(1-18)^{SH}) (***Figure 3.1.***).

3.2.2. Physicochemical characterization of titanium samples

To verify whether Ti functionalization was successful, Ti samples underwent physicochemical characterization by static contact angle (CA) measurements and XPS. CA technique allows to determine the hydrophilicity/hydrophobicity of the Ti surface (*Figure 3.2.*), which is supposed to change following the various treatments. CA thus gives information about physical modifications of the surfaces during the coupling procedure.
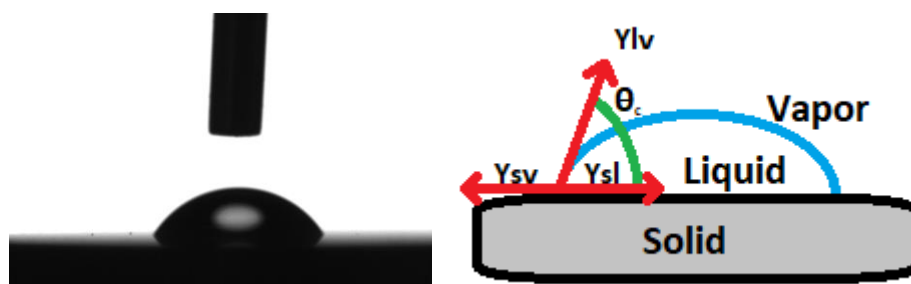
Figure 3.2. Representative image of a water drop on Titanium. Ysv=interfacial energy between solid-vapor; Ylv= interfacial energy between liquid-vapor; Ysl = interfacial energy between solid-liquid.; ϑ: contact angle of the liquid (L) and solid (S).

CA analysis showed considerable and statistically significant modifications in wettability as a result of plasma treatment (Ti_Pl *vs*. Ti samples), as well as upon silanization (Ti_A *vs*. Ti_Pl). The subsequent peptide coupling caused significant modifications respect to controls (Ti_A_B27(1-18)[SH] 100 µM *vs*. Ti_Pl, and Ti_A_B27(1-18)[SH] 100 µM *vs*. Ti_A; Ti_A_B27(1-18)[SH] 200 µM *vs*. Ti_Pl, and Ti_A_B27(1-18)[SH] 200 µM

Table 3.2. Average values of contact angles and calculation of surface free energy and of its polar and dispersive components.

	CA_w (°)	POL (mJ/m²)	DISP (mJ/m²)	SFE (mJ/m²)
Ti	70.4 ± 0.5	8.0 ± 0.3	37.0 ± 0.2	45.1 ± 0.2
Ti_Pl	7.5 ± 0.2 [a]	32.4 ± 0.1 [a]	46.5 ± 0.1 [a]	78.9 ± 0.1 [a]
Ti_A	62.7 ± 0.9 [a, b]	12.0 ± 0.5 [a, b]	36.8 ± 0.5 [b]	48.9 ± 0.6 [a, b]
Ti_A_B27(1-18)[SH] 100 µM	68.3 ± 0.9 [b, c]	8.6 ± 0.4 [b, c]	38.4 ± 0.5 [a, b]	47.0 ± 0.6 [a, b]
Ti_A_B27(1-18)[SH] 200 µM	67.4 ± 0.5 [a, b, c]	9.1 ± 0.4 [a, b, c]	38.3 ± 1.1 [b]	47.4 ± 0.9 [a, b]

CA_w: contact angle water; POL: polar component; DISP: dispersive component and SFE: surface free energy.

[a] Statistically significant differences versus control Ti ($P < 0.05$).

[b] Statistically significant differences vs. Ti_Pl ($P < 0.05$).

[c] Statistically significant differences vs. Ti_A ($P < 0.05$).

vs. Ti_A) (**Table 3.2.**). However, no difference was noted between samples obtained with the two different concentrations (i.e. 100 *vs*. 200 μM) of B27(1-18)[SH]. Based on these results we can conclude that the expected changes have occurred and that data are overall in line with others found in the literature[22,23,35], obtained by using the same coupling strategy.

The high-resolution spectra recorded using X-ray photoelectron spectroscopy (XPS) showed the chemical composition of the modified Ti surfaces (**Figure 3.3.A**). The presence of silicon (Si 2p) and the increment in carbon (C 1s) and nitrogen (N 1s) content in Ti_A vs. Ti disks favours proper silanization of samples. Moreover, the increment of carbon (C 1s) and nitrogen (N 1s), and the decrement of oxygen (O 1s) and titanium (Ti 2p) percentage in Ti_A_B27(1-18)[SH] 100 μM samples, respect to Ti_A and Ti disks,
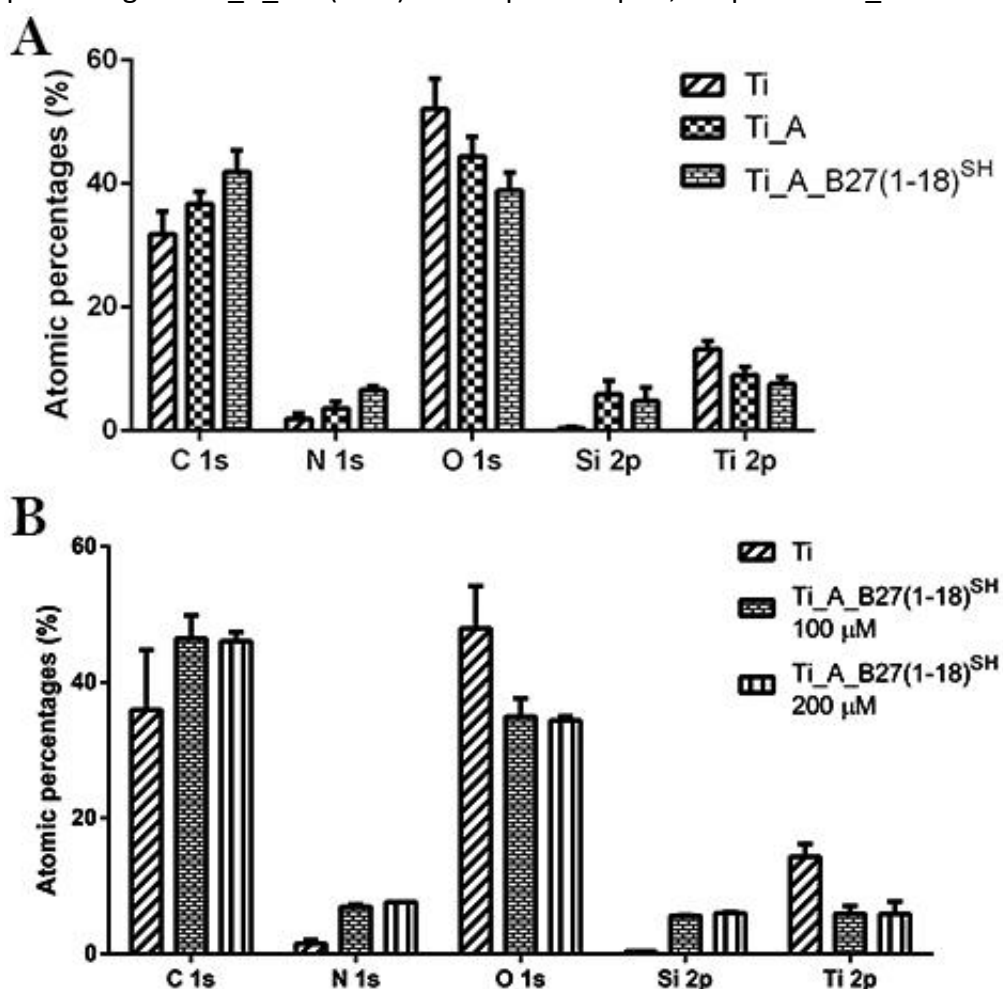
Figure 3.3. *Chemical composition (atomic percentage) obtained by XPS analysis of the indicated titanium surfaces. (A) Comparison of chemical compositions of Ti, Ti_A and Ti_A_B27(1-18)[SH] 100 μM. (B) Comparison of chemical compositions of Ti, Ti_A_B27(1-18)[SH] 100 μM and Ti_A_B27(1-18)[SH] 200 μM. Results are the means ± SD of at least two independent experiments performed in duplicate.*

respectively, indicates that the peptide molecules are stably and strongly bound to the silanized metal surfaces. Moreover, the chemical composition of samples obtained with different peptide coupling concentrations was very similar (***Figure 3.3.A and B***), in keeping with the findings reported for functionalization of titanium with the antimicrobial peptide hLF1-11 [22]. Thus, the XPS data confirm that the employed procedure for peptide tethering to titanium was sound and reliable.

To quantify the peptide layer generated on Ti surface, the Quartz Crystal Microbalance with Dissipation monitoring (QCM-D) was used. This technique allows to quantify masses in the ng/cm^2 range[36]. It is based on monitoring the resonance frequency of a suitable piezoelectric sensor crystal, which decreases proportionally to the adsorbed mass (defined as "adlayer") on the surface of the sensor itself. Additionally, monitoring the dissipation factor enables a more accurate mass estimation because it takes into account the contribution of the adsorbed water to the adlayer mass[37].
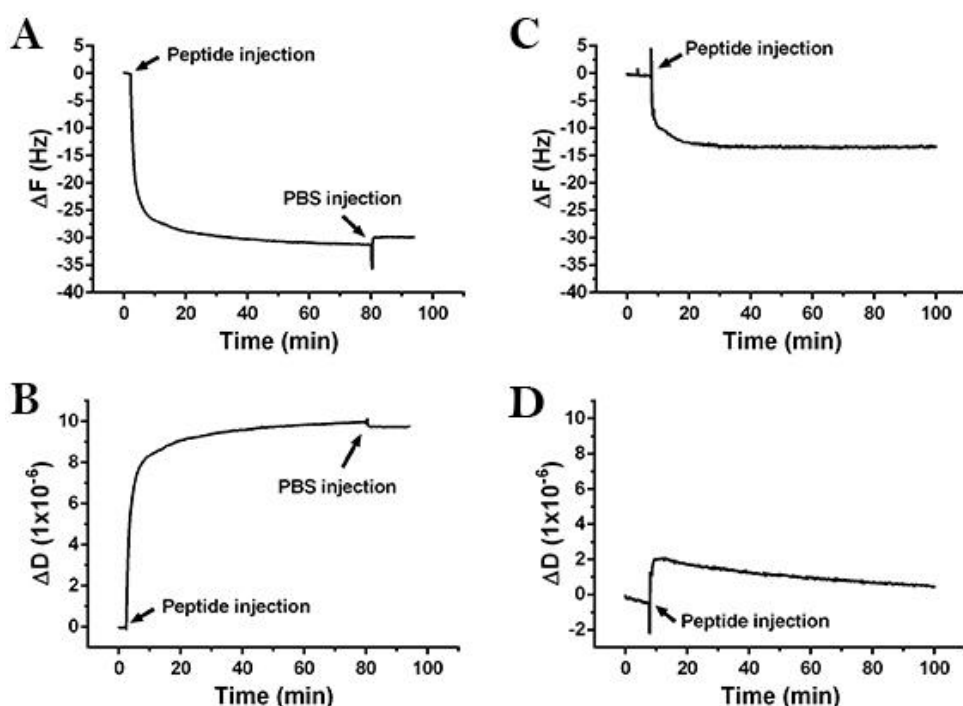
Figure 3.4. *Resonance frequency (A, C) and dissipation (B, D) of a Ti crystal sensor upon addition of 100μM (A, B) and 200μM (C, D) B27(1-18)^{SH} solution in a QCM-D assay. Prior to addition of peptide solution in PBS, the sensor has been treated as described in Materials and Methods. Data were fitted in the Voigt viscoelastic model to obtain surface mass density and thickness values.*

In our case, to quantify the molecular layer formed by the peptide bound covalently to titanium, titanium crystal sensors were first treated with oxygen plasma, APTES and crosslinker, as described above for Ti disks, and extensively washed with PBS. Then, 100 µM or 200 µM peptide solution was added and, as expected, changes in resonant frequency (*ΔF*, ***Figure 3.4.A, 3.4.C***) and dissipation (*ΔD*, ***Figure 3.4.B, 3.4.D***) were observed. The curves shown in ***Figure 3.4.C*** and ***3.4.D*** indicate that at 200 µM peptide concentration the deposition of B27(1-18)[SH] did not occur properly. One possible explanation could be the formation of peptide dimers in the more concentrated peptide solution. In this case, the thiols would be engaged in disulfide bond formation and would not be available for the reaction with the maleimide groups. On the contrary, the changes observed after addition of 100 µM peptide solution (***Figure 3.4.A*** and ***3.4.B)*** indicated a stable layer deposition with a rapid *ΔF* drop, corresponding to a rapid *ΔD* increase, in the first 5 - 6 min, followed by stabilization of both parameters in the next 15 – 20 min. The peptide solution was then replaced by PBS and the resonance frequency and dissipation were monitored for the subsequent 80 min without observing appreciable modifications, suggesting the formation of a stable peptide monolayer over the silanized surface. An average surface mass density of 456.32 ± 7.61 ng/cm^2 and a layer thickness of 3.08 ± 0.06 nm were calculated after fitting data using the Voigt model[38].

The results obtained with QCM-D measurements are in line with the values reported for cell-adhesive peptides adsorbed to CoCr sensors[39] and for antimicrobial peptides attached to Ti sensors[40]. Moreover, the peptide layer thickness is equivalent to that achieved by a basically similar binding strategy for the antimicrobial peptide Dhvar5 grafted on chitosan[19] and for the titanium bound lactoferrin peptide[23], both monitored by ellipsometry. Our surface mass density data are comparable to those obtained by other researchers with colorimetric methods[19,20]. Taking into consideration the physicochemical data, these indicate effective functionalization of Ti disks with the cathelicidin peptide derivative B27(1-18)[SH] at 100 µM. Hence, the analysis of the antimicrobial properties was performed on samples obtained by using this peptide concentration.

3.2.3. Analysis of antimicrobial properties of titanium samples

The antimicrobial efficacy of peptide-functionalized surfaces was analysed in two steps, first testing the bacterial adhesion inhibition, and second, monitoring the bacterial ability to grow after being in contact with the functionalized surface.

The adhesion of microorganisms is the first and crucial step for the bacterial colonization of implants and consequently its prevention would logically avoid the development of infection.

Titanium samples were exposed to a suspension of *Staphylococcus epidermidis* ATCC 35984, a reference strain with a well-documented biofilm-forming ability[7], that is related to the pathogenicity of this commonly harmless microorganism[2,7].

S. epidermidis was allowed to adhere to Ti samples for 2h at 37°C, at that time planktonic cells were washed away and survived bacteria adhered to Ti surface recovered by a two-step vortexing procedure. The colony forming units (CFU) of *S. epidermidis* found on Ti_A_B27(1-18)[SH] disks were significantly less than those recovered from both controls, i.e. Ti and Ti_A samples (**Figure 3.5.**). These data would indicate that bacteria have been killed as a result of their contact with the peptide-functionalized titanium, and/or their adhesion to Ti_A_B27(1-18)[SH] disks has been hindered in some manner.
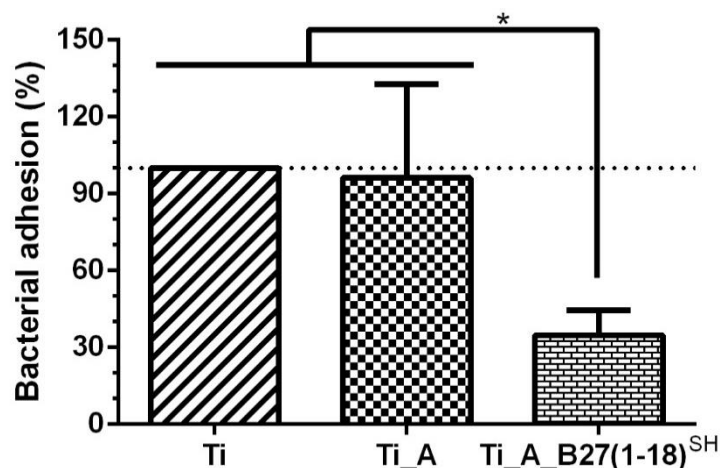
Figure 3.5. *Adhesion of S. epidermidis to the indicated Ti samples. Following 2 h incubation at 37 °C, the CFUs of adherent microorganisms were recovered by a vortexing procedure, serial dilutions and plating on solid medium. Results are expressed as percent CFU respect to CFU recovered from bare titanium (Ti) and are the means ± SD of at least three independent experiments performed in triplicate. * Statistically significant difference vs. Ti and vs. Ti_A (P < 0.05).*

In order to understand the events that take place at the metal surface during staphylococcal adhesion, in parallel to CFU determination, the morphology of the attached bacteria was analysed by SEM. This analysis revealed remarkable differences in the morphology of *S. epidermidis* cells on the different substrata (***Figures 3.6.1.-3.6.3.***).
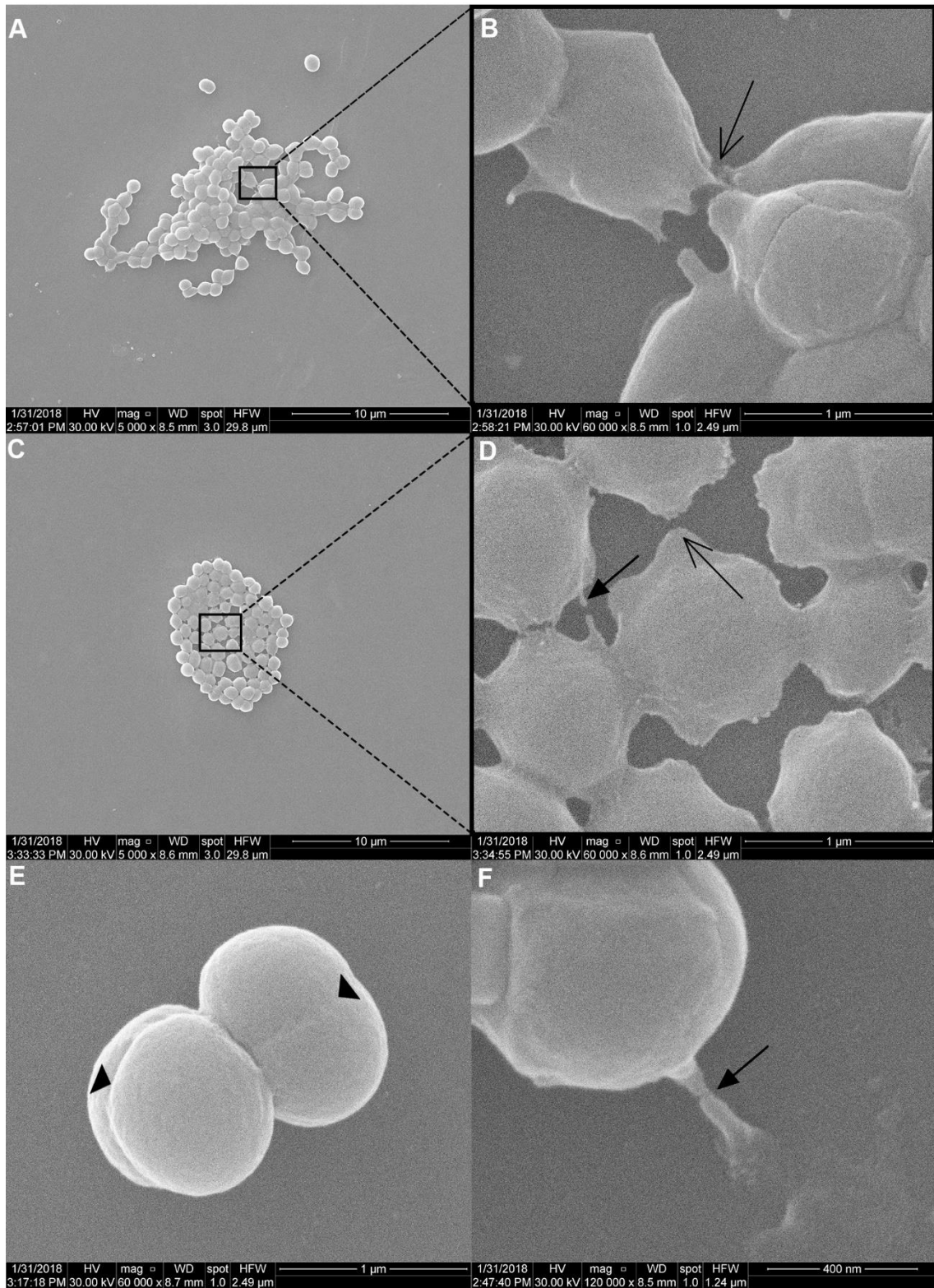
Figure 3.6.1. *Morphology of S. epidermidis on titanium samples analysed by SEM (Panels A – F). Upon 2 h incubation samples were rinsed, fixed and processed for SEM analysis. Panel B and D are a higher magnification of the images presented in Panel A and C, respectively. Arrows indicate, division septa (▲), contact junctions (↑), pseudopod-like structures (↑). Representative images from two experiments performed in duplicate are shown.*

S. epidermidis cells on control Ti samples were opaque, round in shape, with smooth surface and with division septa clearly evident (***Figures 3.6.1.E*** and ***3.6.2.E***).
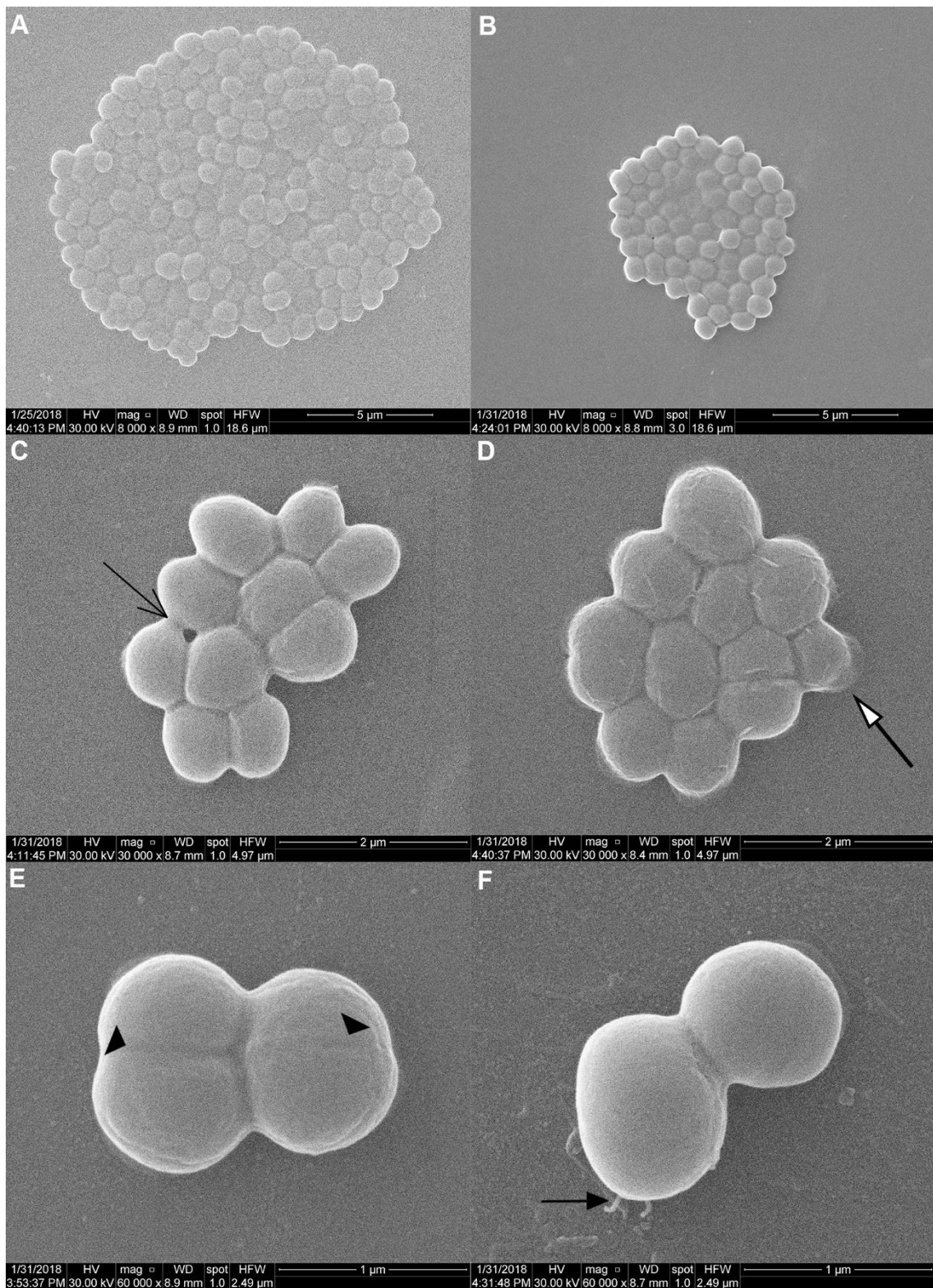
Figure 3.6.2. *Morphology of S. epidermidis on Ti_A samples analysed by SEM (Panels A – F). Arrows indicate, respectively, division septa (▲), contact junctions (↑), halos (⬆), pseudopod-like structures (↑). Representative images from two experiments performed in duplicate are shown.*

Bacteria presented the expected size, with average diameter values between 0.55 μm to 0.85 μm. Dividing microorganisms were frequent. This means that bacteria on bare titanium and Ti_A were viable and growing (***Figures 3.6.1.E and 3.6.2.C-F***). There were also many microbial agglomerates covered by a dense and grey layer, similar to a blanket (***Figures 3.6.1.A, 3.6.1.C-D and 3.6.2.A-D***). Single bacteria were tightly related to each other and connected by junctions (***Figures 3.6.1.B, 3.6.1.D and 3.6.2.C***). Moreover, in several clusters a halo surrounding the bacteria at the contact interface between bacterial and Ti surfaces was observed (***Figure 3.6.2.D***). In some groups of bacteria it was possible to see fimbriae-like surface appendages connecting bacteria to Ti (***Figure 3.6.1.F and 3.6.2.F***). All the observed elements probably represent extracellular matrix components and/or adhesion structures, what indicates early biofilm formation[41–43]. The morphological characteristics of bacteria visualized by SEM are in agreement with the well-known biofilm forming properties of *S. epidermidis* ATCC 35984, which is a recognized heavy matrix producer[7,8]. Remarkably, we did not see significant morphological differences between bacteria adhered to bare Ti (***Figure 3.6.1***) and those attached to silanized Ti disks (***Figure 3.6.2***).

On the contrary, Ti_A_B27(1-18)[SH] samples presented a lower number of *S. epidermidis* remaining attached to their surfaces, and bacterial morphology was dramatically affected (***Figure 3.6.3***). Dead *S. epidermidis* cells showed increased size and elongated shapes, and remarkably, bacteria lost their division septa (***Figure 3.6.3.D***). Furthermore, bacterial surface did not have a smooth appearance, many bacterial cells were collapsed, deflated, and appeared embedded into a layer of amorphous material deposited on Ti surface (***Figures 3.6.3.A-D***). In numerous cases, the dead elongated bacteria, similar to ghosts, were surrounded by an empty circle (***Figure 3.6.3.E***), and in some of them it was possible to observe extrusion of cytoplasmic material out of the cell (***Figure 3.6.3.F***).
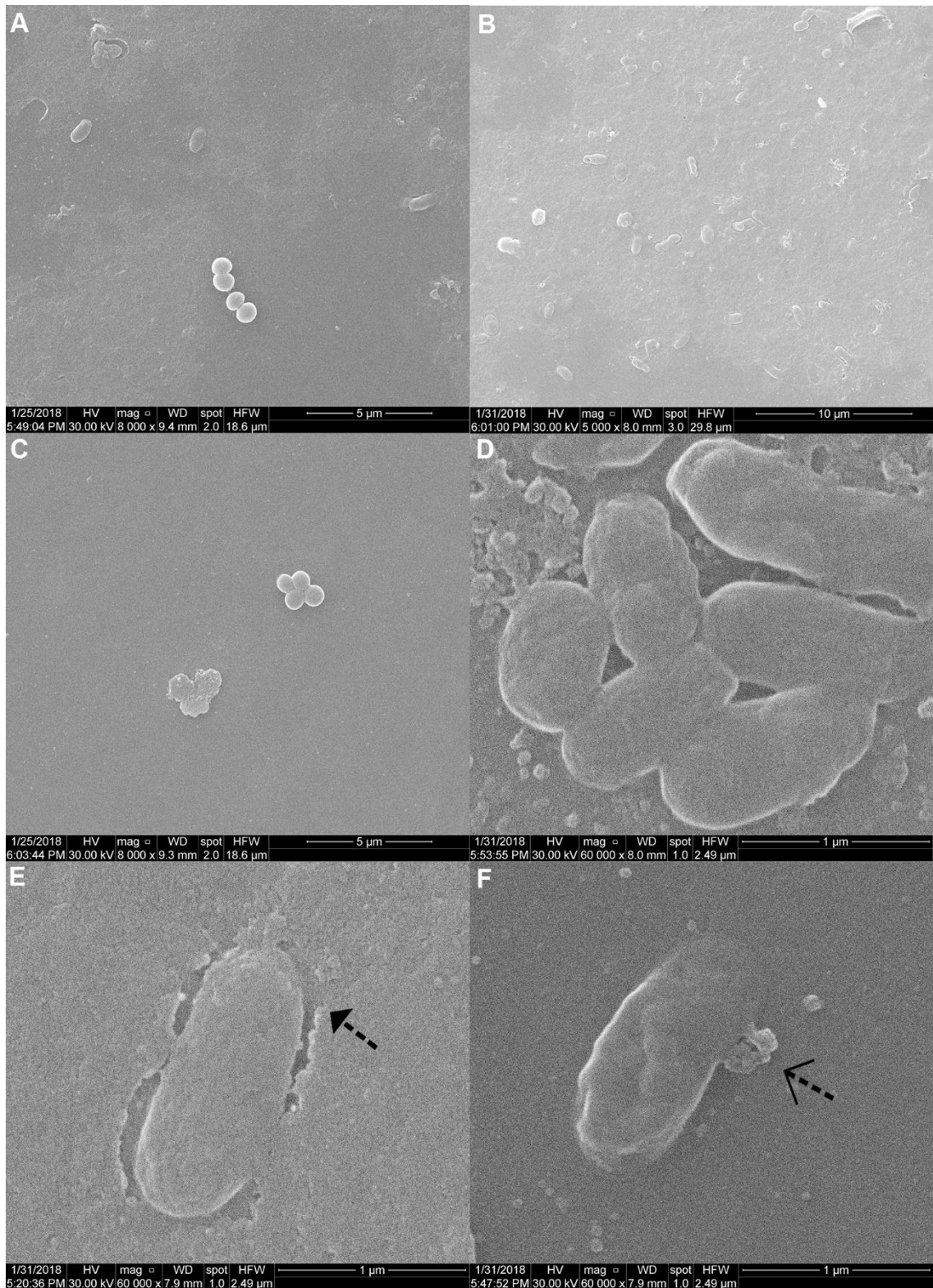
Figure 3.6.3. *Morphology of S. epidermidis on Ti_A_B27(1-18)^{SH} samples analyzed by SEM (Panels A – F). Arrows indicate, respectively, empty circles (↑), extruded cytoplasmic material (↑). Representative images from two experiments performed in duplicate are shown.*

These severe modifications of bacterial morphology pointed out that microbial cell growth has been impaired, as well as the cell division process, which is normally accomplished through formation of the division septum. In addition, the layer of amorphous material present on these samples could plausibly derive from dead *S. epidermidis* such as those appearing collapsed. In any case, the bacteria "deflated bag" morphology, in the absence of evident surface damage such as blebs or holes[44], would indicate that digestion of bacterial content has occurred from inside, possibly upon activation of autolytic enzymes[45]. The changes in morphology observed in Ti_A_B27(1-18)[SH] samples matched with the reduction in CFUs, demonstrating killing ability of Ti-immobilized B27(1-18)[SH]. This finding was not unexpected, taking into consideration that BMAP27(1-18) has proved able to kill staphylococci when N-terminally attached to a model support[32].

However, all the collected data make us wonder what was the mode of action of B27(1-18)[SH] covalently anchored to a surface. The antibacterial activity of this peptide free in solution relies on its ability to perturb microbial membranes, and is closely correlated to its ability to adopt an amphipathic conformation[46,47]. It looks quite evident that, considering their limited mobility, the peptide molecules attached to Ti surface could interact only with superficial components of the bacterial cell. This means that the mode of killing action could be totally different from that displayed by this type of peptides in solution[44,46,47]. It is important to recall that the bovine cathelicidin BMAP-27, i.e. the molecule from which B27(1-18) was derived, shares highly similar structural and membrane perturbing properties with other α-helical AMPs of the same family such as for example the sheep cathelicidin SMAP-29[48]. In this respect, it is intriguing to note that the staphylococci adhered to peptide-functionalized Ti (***Figure 3.6.3***) were remarkably different from those examined in a previous study after treatment with the sheep peptide SMAP-29 free in solution, where bacteria presented extensive surface roughening and blebbing[44]. Such modifications were ascribed to the potent permeabilizing activity of this alpha-helical peptide in solution[44]. Interestingly, both peptides, SMAP-29 and BMAP-27, demonstrated antimicrobial efficacy when anchored to a solid support, but their mode of action in the immobilized state has not been elucidated yet[49,50].

It could be that the negatively charged bacteria were initially attracted by the highly cationic B27(1-18)[SH] (net charge +10 [32]), but the microorganisms were killed upon their contact/adhesion to the metal surface, according to what suggested by other authors[21,30]. The morphological modifications could be the consequence of events triggered by a peptide-induced perturbation at the bacterial surface, as described with free peptides in solution[45,51,52], and also suggested for immobilized AMPs[30,53].

Although Ti_A_B27(1-18)[SH] samples presented dead or heavily damaged bacteria, occasionally microcolonies with normal appearance adjacent to dead bacteria were also found (**Figure 3.6.3.A** and **3.6.3.C**). This result prompted us to investigate whether the surviving bacteria could be able to regrow. Considering this objective, Ti samples have been exposed to a *S. epidermidis* suspension for 2 h as above and, after removal of planktonic bacteria and washings, the incubation has been extended for additional 22 h in fresh MH broth. As the presence of metal disks in the wells would not allow optical density measurements, bacterial growth was kinetically monitored by the PrestoBlue® dye, which emits fluorescence upon conversion by metabolically active microorganisms.
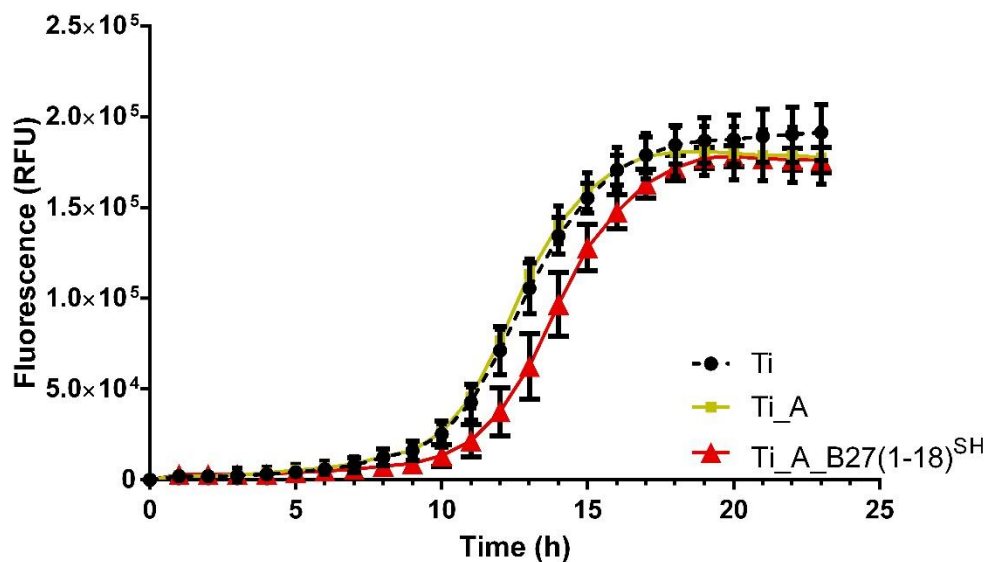
Figure 3.7. Growth kinetics of S. epidermidis on the indicated Ti samples (Ti, circles; Ti_A, squares; Ti_A_B27(1-18)[SH], triangles). After 2 h incubation and washing, fresh MH supplemented with the metabolic dye PrestoBlue® was added and adherent bacteria were allowed to grow overnight at 37 °C. Growth kinetics was monitored by measuring fluorescence emission that is directly proportional to microbial viability. Results are reported as relative fluorescence units (RFU) and are the means ± SD of at least three independent experiments performed in triplicate.

S. epidermidis growth on control Ti disks (Ti and Ti_A) became detectable at 7 - 8h post-adhesion, with an exponential phase between 10 - 15 h, and a final plateau at 18-20 h. On Ti_A_B27(1-18)[SH] samples, the survived bacteria showed an about 1.5-h delay both at the beginning and onset of the exponential growth phase, supposedly associated with their decreased initial number, in accordance with the results of bacterial adhesion assays (***Figure 3.5.***). Therefore, a reduction or total inhibition of early bacterial adhesion remains critical for long-lasting antimicrobial efficacy[10].

It must be emphasized that the experimental settings applied in our *in vitro* assays such as for instance a relatively high initial inoculum, could be different from those occurring in clinical conditions where a possible bacterial contamination would take origin from a very low bacterial number, as also verified by animal model studies[54,55]. According to what suggested by other authors[20], one could reasonably expect a more effective protection under medically relevant conditions with only few bacteria present at the implant surface thanks to strictly antiseptic surgical procedures.

3.3. Conclusions

- Data acquired by contact angle, XPS and QCM-D analyses indicate successful attachment of B27(1-18)^{SH} to titanium surface.

- The attempt to increase peptide concentration in the coupling solution did not increase surface coverage. To improve it, I would probably need to modify the coupling strategy substantially.

- The bacterial inhibition tests showed that the adhesion of *S. epidermidis* to peptide-functionalized titanium disks was remarkably inhibited respect to bare titanium, suggesting effective coupling of B27(1-18)^{SH} to the metal surface in a form that preserves its activity.

- Regarding the titanium anchored peptide, the remarkable changes in bacterial morphology observed by SEM suggest a different mode of action respect to that displayed in solution.

- The results obtained in the present study are promising, highlighting the potential of B27(1-18)^{SH} for the development of biomaterials refractory to microbial contamination.

3.4. Experimental procedure

3.4.1. Peptide synthesis and characterization

3.4.1.1. Reagent for peptide synthesis and characterization

Polyethylene glycol–polystyrene (PEG-PS) resins, coupling reagents for peptide synthesis and 9-fluorenylmethoxy carbonyl (Fmoc)-amino acids have been purchased from Applied Biosystems, Novabiochem and ChemImpex. Peptide synthesis-grade N,N,dimethylformamide (DMF), dichloromethane, piperidine and HPLC-grade acetonitrile have been purchased from Biosolve (Valkenswaard, The Netherlands). Trifluoroacetic acid (TFA), trifluoroethanol and N-methylmorpholine have been purchased from Acros Chimica. (Beerse, Belgium). 6-aminohexanoic acid (Ahx) and 3-mercaptopropionic acid (MPA) were purchased from Fluorochem Ltd (Hadfield, Derbyshire, UK).

3.4.1.2. Peptide synthesis

All peptides have been synthesized on a Biotage Initiator+ microwave-assisted automated peptide synthesizer in standard solid-phase using Fmoc-chemistry, according to published procedures[32].

The amino acid sequence of the α-helical cathelicidin derived peptide BMAP27(1-18) [32] has been modified at the N-terminus by addition of three units of 6-aminohexanoic acid (Ahx) and one unit of 3-mercaptopropionic acid (MPA) as spacer and anchoring group, respectively. The resulting peptide MPA-(Ahx)$_3$-BMAP27(1-18) is hereafter referred to as B27(1-18)^{SH} (***Table 3.3.***).

Table 3.3. *Amino acid sequence of the selected AMP and its modifications at the N-terminus.*

Peptide	Sequence
BMAP27(1-18)	GRFKRFRKKFKKLFKKLS-NH$_2$
B27(1-18)^{SH}	HS-MPA-(Ahx)$_3$-GRFKRFRKKFKKLFKKLS

After cleavage and deprotection, the peptide was purified by reverse phase high performance liquid chromatography (RP-HPLC) on a C18 Delta-Pak column (Waters; USA) and confirmed by mass spectrometry using a Q-STAR hybrid quadrupole time-of-flight mass spectrometer (Applied Biosystems/MDS Sciex, Concord, ON, Canada) equipped with an electrospray ion source.

3.4.2. Determination of peptide concentration

The concentration of the peptides in **Table 3.3.** has been determined in aqueous solution by measuring the UV absorbance at 257 nm taking into account the molar extinction coefficient (195.1 cm^{-1}M^{-1}) for each phenylalanine (Phe) residue[32].

3.4.3. Reverse phase chromatography

Peptide purification was carried out with a semi-preparative reverse-phase high performance liquid chromatography (RP-HPLC) with a linear aqueous acetonitrile gradient containing 0.05% TFA on a C18 Delta-Pak column.

3.4.4. Mass Spectrometry

The Mass spectrometry is a sensitive and powerful analytical technique that provides qualitative and quantitative measures on nanomolar to attomolar amounts of molecules[56]. It is primary composed by an ion source, where the molecules may be ionized, a mass analyser that distributes ions according to their mass-to-charge ratio (m/z), a detector which measures the abundances of the separated ions as an electrical signal, and the recording device which modifies the detector signal into appropriate way for subsequent study and processing[56]. Mass spectra have been acquired and analysed to validate the peptide synthesis (Bruker Daltonics Esquire 4000).

3.4.5. Peptide Immobilization on Solid support
3.4.5.1. Titanium Preparation

Commercially pure Titanium (Ti) grade II disks have been obtained from Technalloy S.A. (Sant Cugat del Vallès, Spain). The disks of 10 mm diameter and 2 mm height, have been polished with wet abrasive paper (800, 1200 and 2400 – European P-grade standard) and smoothed with an alumina suspension (1 µm and 0.05 µm particle size) on cotton clothes. Before the activation and silanization process, the samples were ultrasonically washed with cyclohexane, isopropanol, distilled water, ethanol and acetone and finally stored dried under vacuum.

3.4.5.2. Activation and Silanization of titanium samples

Ti surfaces have been activated by 10 min oxygen plasma treatment at 100W power in a Standard Plasma System (FEMTO, Diener electronic GmbH, Germany). Samples have been silanized with (3-aminopropyl)triethoxysilane (APTES) (2%, v/v) (Sigma-Aldrich, St

Louis, MO, USA) in anhydrous toluene for 1 h at 70 °C under agitation and nitrogen atmosphere. Ti samples have been sonicated for 5 min and rinsed with toluene, isopropanol, distilled water, ethanol and acetone, and dried with nitrogen. Thereafter, aminosilanized samples have been immersed in a 7.5 mM solution of N-succinimidyl-3-maleimidopropionate (SMP) bi-functional cross-linker agent in N,N-dimethylformamide (DMF) for 1 h under agitation at room temperature. At last, aminosilanized samples with SMP group (Ti_A) have been washed with DMF, distilled water, ethanol and acetone, and dried with nitrogen.

3.4.5.3. Immobilization of peptide onto Ti samples

B27(1-18)[SH] peptide has been dissolved in phosphate buffered saline (PBS), pH 6.5 at 100 µM final concentration. Afterwards, it has been deposited onto the Ti_A samples (100 µL/disk) and incubated overnight at room temperature. Successively, B27(1-18)[SH] peptide functionalized titanium samples have been rinsed with PBS and dried with nitrogen. These samples have been designated as Ti_A_B27(1-18)[SH].

3.4.6. Physicochemical Characterization of the Biofunctionalized Titanium Surfaces

3.4.6.1. Static Contact Angle Measurements and Surface Energy Calculations

The sessile drop method has been used to determine the hydrophilicity of the Ti surfaces by a Contact Angle System (OCA15 plus, Dataphysics, Filderstadt, Germany). All measurements have been done at room temperature using Ultrapure distilled water (Millipore Milli-Q, Merck Millipore Corporation, USA) and diiodomethane (Sigma-Aldrich, Spain) as wetting liquids (drop volume of 1 µL and 1 µL/min dosing rate). Static contact angles have been calculated using Laplace-Young fitting with SCA 20 software (Dataphysics). Young described the contact angle as the mechanical equilibrium of a liquid drop on an ideal solid surface under the action of three interfacial tensions[57].

$$\gamma_S = \gamma_{SL} + \gamma_L \cos\theta \qquad (1)$$

$$\gamma_L(1 + \cos\theta) = 2\left(\left(\gamma_L^d \gamma_S^d\right)^{1/2} + \left(\gamma_L^p \gamma_S^p\right)^{1/2}\right) \qquad (2)$$

where γ^d_L, γ^d_S is the dispersive part and γ^P_L, γ^p_S is the polar part, respectively, of the liquid and solid surface tension (γ_L and γ_S). θ is the contact angle of the liquid (L) and solid (S).

The surface free energy and its dispersive and polar components have been determined by Young-Laplace (1) and Owens, Wendt, Rabel and Kaeble (2) equations applied to both water and diiodomethane measurements[22,58].

Data are means of five measurements per disk for three sample replicates.

3.4.6.2. X-ray photoelectron spectroscopy (XPS)

X-ray photoelectron spectroscopy (XPS) is a technique to allow the semiquantitative analysis of surface composition. XPS can determine the elemental composition, empirical formula, chemical state and electronic state of the elements within a material. It is mainly composed by X-ray source, chamber sample, electron energy analyser and detector. It is based on the irradiation of a solid surface with a beam of X-rays while simultaneously measuring the kinetic energy and electrons that are emitted from the first 10nm of the material surface being analysed.

The chemical composition of the surface of the Ti functionalized samples have been analysed using an XPS equipment (D8 advance, SPECS Surface Nano Analysis GmbH, Germany) with an Mg anode XR50 source operating at 150W and a Phoibos 150 MCD-9 detector. High-resolution spectra have been registered with pass energy of 25 eV at 0.1 eV steps at a pressure below 7.5×10^{-9} mbar. Binding energies have been referenced to the C1s signal at 284.8 eV. Two samples were studied for each working condition. Finally, data were analysed using the CasaXPS software (Version 2.3.16, Casa Software Ltd., Teignmouth, UK).

3.4.6.3. Quartz Crystal Microbalance and Dissipation monitoring (QCM-D)

Quartz Crystal Microbalance and Dissipation monitoring (QCM-D) is a reliable and sensitive method to measure very small masses in the order of ng/cm^2. In this technique a piezoelectric quartz sensor undergoes oscillation upon application of an alternating electric field across the crystal. If a material is adsorbed on the crystal, the resonant frequency decreases proportionally to the mass of the component. The contribution of water to the mass of the adsorbed layer can be estimated from the dissipation factor.

QCM-D measurements were performed on titanium crystal sensors (QSX 310, Q-Sense, Sweden) in a D-300 instrument (Q-sense, Sweden), in order to quantify and characterize the peptide layer attached to the surfaces. Ti sensors, have been washed

as previously described[39], have been activated with O_2 plasma and subsequently treated with APTES and SMP as described above for Ti_A samples. Before studying the adsorption of B27(1-18)^{SH}, the baseline was stabilized with PBS for 30 - 60 min. Subsequently, the B27(1-18)^{SH} derivative was added (100 µM in PBS, pH 6.5) and changes in resonant frequency and dissipation was monitored at 25 °C for 100 minutes, in real-time employing a Qsoft software (Q-Sense, Sweden). Frequency and dissipation curves were fitted to a Voigt viscoelastic model[38] to yield the adsorbed mass and thickness of the peptide layer, as well as kinetic information, by using the Q-tool data analysis software (Q-Sense, Sweden).

3.4.7. Bacteria and antimicrobial activity assays

The bacterial assays were performed with the reference strains *Staphylococcus epidermidis* ATCC 35984, *Staphylococcus aureus* ATCC 25923, *Escherichia coli* ATCC 25922 and *Pseudomonas aeruginosa* ATCC 27853. Bacteria were cultured either in liquid Brain Hearth Infusion (BHI) (both *Staphylococcus* species) or in Mueller-Hinton (MH) (both Gram-negatives) overnight at 37 °C. Antimicrobial activity of the titanium bound peptide was tested with *S. epidermidis* ATCC 35984. Stationary phase bacteria were harvested by 10 min centrifugation at 1000 x g and resuspended in sterile PBS (pH 7.4). Bacterial density was assessed by turbidity at 600 nm, with reference to previously determined standards. For the experiments, bacterial suspensions was prepared in MH broth at optimal density.

3.4.7.1. Determination of the Minimum Inhibitory Concentration (MIC)

The MIC of B27(1-18)^{SH} in solution was determined by a broth microdilution assay in 96-well microtiter plates, using MH broth with logarithmic-phase microorganisms at 5×10^5 CFU/mL, as previously reported[32], following Clinical and Laboratory Standards Institute (CLSI) guidelines.

3.4.7.2. Evaluation of bacterial adhesion to titanium surface

The evaluation of bacterial adhesion was studied by adapting a previously described protocol[23]. Before use in antimicrobial assays Ti, Ti_A and Ti_A_B27(1-18)^{SH} samples were sterilized by 30 min treatment with 70 % ethanol, and washed with sterile PBS. Titanium samples were placed in a 24-well plate for better handling of samples and incubated with 1 mL of *S. epidermidis* at 1×10^5 CFU/mL for 2 h at 37 °C. The medium

containing planktonic bacteria was then aspirated and the samples rinsed three times with sterile PBS. Subsequently, disks were transferred to sterile tubes containing 1 mL of 50 % Mueller-Hinton in sterile PBS (MH-PBS), and adherent bacteria were detached by 10 min vortexing. To make sure that dislodging of bacteria from the surfaces was effective, after the first vortexing step the disks were transferred in new sterile tubes containing 1 mL of MH-PBS and vortexed again for 5 min. Bacterial suspensions from each vortexing step were then serially diluted in MH-PBS and seeded on BHI agar plates. The plates were incubated at 37 °C for 24 h and the resulting colonies counted. All experiments were performed in triplicate for each type of surface.

3.4.7.3. Scanning Electron Microscopy (SEM)

Scanning Electron Microscopy (SEM) is a technique to easily visualize specimens displayed as three-dimensional objects. Electron microscopes use electrons for imaging in a similar way that light microscopes use visible light. Specifically, SEM employ the electrons that are reflected or knocked off the near-surface region of a sample to create an image that is displayed on the computer screen.

Nowadays, SEM is one of the best techniques among others to observe bacteria in a 3D-high resolution.

S. epidermidis morphology, when adhered to titanium samples, was studied by means of SEM (Quanta250 SEM, FEI, Oregon, USA) operated in secondary electron detection mode. The working distance was adjusted in order to obtain the suitable magnification; the accelerating voltage was set to 30 kV. SEM was performed in duplicate for each sample. Briefly, upon 2 h incubation as described above, all samples were rinsed three times with filtered sterile PBS, fixed with 2.5 % (v/v) glutaraldehyde for 30 min at 4 °C, washed three times with filtered sterile PBS and MilliQ ultrapure water, and dehydrated in graded series of ethanol solutions (20 min each). Immediately prior to SEM analysis, samples were sputter-coated with gold (Sputter Coater K550X, Emitech, Quorum Technologies Ltd, UK).

3.4.7.4. Bacterial growth kinetics on titanium surfaces

Titanium samples, placed in triplicate into 48-well plates, were immersed in 1 mL of *S. epidermidis* (6×10^4 CFU/mL) suspension in MH for 2 h. The medium containing

planktonic bacteria was removed, titanium disks washed with sterile PBS, and adherent bacteria allowed to grow at 37 °C for 22 h in fresh MH medium supplemented with 10 % (v/v) PrestoBlue® metabolic dye. Bacterial growth kinetics was monitored fluorometrically according to PrestoBlue® manufacturer's instructions by using a Multimode Plate Reader (EnSpire™ 2300, PerkinElmer, Waltham, MA, USA).

3.4.8. Statistical analysis

Data, presented as mean values ± standard deviations, have been analysed by a non-parametric U Mann-Whitney test (IBM SPSS Statistics 20 software, Armonk, NY, USA). Statistical significance was set at *P* value <0.05.

3.5. References

1. Tande, A. J. & Patel, R. Prosthetic Joint Infection. *Clin. Microbiol. Rev.* **27**, 302–345 (2014).

2. Arciola, C. R., Campoccia, D., Speziale, P., Montanaro, L. & Costerton, J. W. Biofilm formation in Staphylococcus implant infections. A review of molecular mechanisms and implications for biofilm-resistant materials. *Biomaterials* **33**, 5967–5982 (2012).

3. Gbejuade, H. O., Lovering, A. M. & Webb, J. C. The role of microbial biofilms in prosthetic joint infections. *Acta Orthop.* **86**, 147–158 (2015).

4. Moriarty, T. F. *et al.* Orthopaedic device-related infection: current and future interventions for improved prevention and treatment. *EFORT Open Rev.* **1**, 89–99 (2016).

5. Taha, M., Abdelbary, H., Ross, F. P. & Carli, A. V. New Innovations in the Treatment of PJI and Biofilms—Clinical and Preclinical Topics. *Curr. Rev. Musculoskelet. Med.* **11**, 380–388 (2018).

6. Matthews, P. C., Berendt, A. R., McNally, M. A. & Byren, I. Diagnosis and management of prosthetic joint infection. *BMJ* **338**, b1773–b1773 (2009).

7. Sabaté Brescó, M. *et al.* Pathogenic Mechanisms and Host Interactions in *Staphylococcus epidermidis* Device-Related Infection. *Front. Microbiol.* **8**, (2017).

8. Fey, P. D. & Olson, M. E. Current concepts in biofilm formation of *Staphylococcus epidermidis*. *Future Microbiol.* **5**, 917–33 (2010).

9. Campoccia, D., Montanaro, L. & Arciola, C. R. A review of the biomaterials technologies for infection-resistant surfaces. *Biomaterials* **34**, 8533–8554 (2013).

10. Gallo, J., Holinka, M. & Moucha, C. Antibacterial Surface Treatment for Orthopaedic Implants. *Int. J. Mol. Sci.* **15**, 13849–13880 (2014).

11. Eltorai, A. E. *et al.* Antimicrobial technology in orthopedic and spinal implants. *World J. Orthop.* **7**, 361 (2016).

12. Costa, F., Carvalho, I. F., Montelaro, R. C., Gomes, P. & Martins, M. C. L. Covalent immobilization of antimicrobial peptides (AMPs) onto biomaterial surfaces. *Acta Biomater.* **7**, 1431–1440 (2011).

13. Onaizi, S. A. & Leong, S. S. J. Tethering antimicrobial peptides: Current status and potential challenges. *Biotechnol. Adv.* **29**, 67–74 (2011).

14. Riool, M., de Breij, A., Drijfhout, J. W., Nibbering, P. H. & Zaat, S. A. J. Antimicrobial peptides in biomedical device manufacturing. *Front. Chem.* **5**, 1–13 (2017).

15. Yeung, A. T. Y., Gellatly, S. L. & Hancock, R. E. W. Multifunctional cationic host defence peptides and their clinical applications. *Cell. Mol. Life Sci.* **68**, 2161–2176 (2011).

16. Kraus, D. *et al.* Human β-defensins differently affect proliferation, differentiation, and mineralization of osteoblast-like MG63 cells. *J. Cell. Physiol.* **227**, 994–1003 (2012).

17. Kittaka, M. *et al.* The antimicrobial peptide LL37 promotes bone regeneration in a rat calvarial bone defect. *Peptides* **46**, 136–142 (2013).

18. Zhang, Z. & Shively, J. E. Acceleration of Bone Repair in NOD/SCID Mice by Human Monoosteophils, Novel LL-37-Activated Monocytes. *PLoS One* **8**, e67649 (2013).

19. Costa, F. M. T. A., Maia, S. R., Gomes, P. A. C. & Martins, M. C. L. Dhvar5 antimicrobial peptide (AMP) chemoselective covalent immobilization results on higher antiadherence effect than simple physical adsorption. *Biomaterials* **52**, 531–538 (2015).

20. Mishra, B. & Wang, G. Titanium surfaces immobilized with the major antimicrobial fragment FK-16 of human cathelicidin LL-37 are potent against multiple antibiotic-resistant bacteria. *Biofouling* **33**, 544–555 (2017).

21. Nie, B. *et al.* Covalent immobilization of KR-12 peptide onto a titanium surface for decreasing infection and promoting osteogenic differentiation. *RSC Adv.* **6**, 46733–46743 (2016).

22. Godoy-Gallardo, M. *et al.* Covalent immobilization of hLf1-11 peptide on a

titanium surface reduces bacterial adhesion and biofilm formation. *Acta Biomater.* **10**, 3522–3534 (2014).

23. Godoy-Gallardo, M. *et al.* Antibacterial properties of hLf1-11 peptide onto titanium surfaces: A comparison study between silanization and surface initiated polymerization. *Biomacromolecules* **16**, 483–496 (2015).

24. Lin, W. *et al.* Multi-biofunctionalization of a titanium surface with a mixture of peptides to achieve excellent antimicrobial activity and biocompatibility. *J. Mater. Chem. B* **3**, 30–33 (2015).

25. Makihira, S. *et al.* Titanium Immobilized with an Antimicrobial Peptide Derived from Histatin Accelerates the Differentiation of Osteoblastic Cell Line, MC3T3-E1. *Int. J. Mol. Sci.* **11**, 1458–1470 (2010).

26. Zhou, L. *et al.* Biofunctionalization of microgroove titanium surfaces with an antimicrobial peptide to enhance their bactericidal activity and cytocompatibility. *Colloids Surfaces B Biointerfaces* **128**, 552–560 (2015).

27. Chen, C.-P., Jing, R.-Y. & Wickstrom, E. Covalent Attachment of Daptomycin to Ti6Al4V Alloy Surfaces by a Thioether Linkage to Inhibit Colonization by Staphylococcus aureus. *ACS Omega* **2**, 1645–1652 (2017).

28. Masurier, N. *et al.* Site-specific grafting on titanium surfaces with hybrid temporin antibacterial peptides. *J. Mater. Chem. B* **6**, 1782–1790 (2018).

29. Bagheri, M., Beyermann, M. & Dathe, M. Mode of action of cationic antimicrobial peptides defines the tethering position and the efficacy of biocidal surfaces. *Bioconjug. Chem.* **23**, 66–74 (2012).

30. Hilpert, K. *et al.* Screening and Characterization of Surface-Tethered Cationic Peptides for Antimicrobial Activity. *Chem. Biol.* **16**, 58–69 (2009).

31. Bagheri, M., Beyermann, M. & Dathe, M. Immobilization Reduces the Activity of Surface-Bound Cationic Antimicrobial Peptides with No Influence upon the Activity Spectrum. *Antimicrob. Agents Chemother.* **53**, 1132–1141 (2009).

32. D'Este, F., Oro, D., Boix-Lemonche, G., Tossi, A. & Skerlavaj, B. Evaluation of free

or anchored antimicrobial peptides as candidates for the prevention of orthopaedic device-related infections. *J. Pept. Sci.* **23**, 777–789 (2017).

33. Bauer, S., Schmuki, P., von der Mark, K. & Park, J. Engineering biocompatible implant surfaces. *Prog. Mater. Sci.* **58**, 261–326 (2013).

34. Khorasani, A. M., Goldberg, M., Doeven, E. H. & Littlefair, G. Titanium in Biomedical Applications—Properties and Fabrication: A Review. *J. Biomater. Tissue Eng.* **5**, 593–619 (2015).

35. Mas-Moruno, C., Garrido, B., Rodriguez, D., Ruperez, E. & Gil, F. J. Biofunctionalization strategies on tantalum-based materials for osseointegrative applications. *J. Mater. Sci. Mater. Med.* **26**, 1–12 (2015).

36. Marx, K. A. Quartz crystal microbalance: A useful tool for studying thin polymer films and complex biomolecular systems at the solution - Surface interface. *Biomacromolecules* **4**, 1099–1120 (2003).

37. Rodahl, M. & Kasemo, B. A simple setup to simultaneously measure the resonant frequency and the absolute dissipation factor of a quartz crystal microbalance. *Rev. Sci. Instrum.* **67**, 3238–3241 (1996).

38. Höök, F. *et al.* Variations in coupled water, viscoelastic properties, and film thickness of a Mefp-1 protein film during adsorption and cross-linking: A quartz crystal microbalance with dissipation monitoring, ellipsometry, and surface plasmon resonance study. *Anal. Chem.* **73**, 5796–5804 (2001).

39. Castellanos, M. I. *et al.* Functionalization of CoCr surfaces with cell adhesive peptides to promote HUVECs adhesion and proliferation. *Appl. Surf. Sci.* **393**, 82–92 (2017).

40. Corrales Ureña, Y. R. *et al.* Influences of the pH on the adsorption properties of an antimicrobial peptide on titanium surfaces. *Appl. Adhes. Sci.* **3**, 7 (2015).

41. Williams, D. L. & Bloebaum, R. D. Observing the Biofilm Matrix of *Staphylococcus epidermidis* ATCC 35984 Grown Using the CDC Biofilm Reactor. *Microsc. Microanal.* **16**, 143–152 (2010).

42. Valdez-Salas, B. *et al.* In Vitro Assessment of Early Bacterial Activity on Micro/Nanostructured Ti6Al4V Surfaces. *Molecules* **22**, 832 (2017).

43. Cao, P. *et al.* Coupling Plant-Derived Cyclotides to Metal Surfaces: An Antibacterial and Antibiofilm Study. *Int. J. Mol. Sci.* **19**, 793 (2018).

44. Skerlavaj, B., Benincasa, M., Risso, A., Zanetti, M. & Gennaro, R. SMAP-29: a potent antibacterial and antifungal peptide from sheep leukocytes. *FEBS Lett.* **463**, 58–62 (1999).

45. Wilmes, M. *et al.* Killing of Staphylococci by θ-Defensins Involves Membrane Impairment and Activation of Autolytic Enzymes. *Antibiotics* **3**, 617–631 (2014).

46. Skerlavaj, B. *et al.* Biological Characterization of Two Novel Cathelicidin-derived Peptides and Identification of Structural Requirements for Their Antimicrobial and Cell Lytic Activities. *J. Biol. Chem.* **271**, 28375–28381 (1996).

47. Lee, E. K., Kim, Y.-C., Nan, Y. H. & Shin, S. Y. Cell selectivity, mechanism of action and LPS-neutralizing activity of bovine myeloid antimicrobial peptide-18 (BMAP-18) and its analogs. *Peptides* **32**, 1123–1130 (2011).

48. Zanetti, M. The role of cathelicidins in the innate host defenses of mammals. *Curr. Issues Mol. Biol.* **7**, 179–96 (2005).

49. Soares, J. W., Kirby, R., Doherty, L. A., Meehan, A. & Arcidiacono, S. Immobilization and orientation-dependent activity of a naturally occurring antimicrobial peptide. *J. Pept. Sci.* **21**, 669–679 (2015).

50. Rapsch, K., Bier, F. F., Tadros, M. & von Nickisch-Rosenegk, M. Identification of Antimicrobial Peptides and Immobilization Strategy Suitable for a Covalent Surface Coating with Biocompatible Properties. *Bioconjug. Chem.* **25**, 308–319 (2014).

51. Müller, A. *et al.* Daptomycin inhibits cell envelope synthesis by interfering with fluid membrane microdomains. *Proc. Natl. Acad. Sci.* **113**, E7077–E7086 (2016).

52. Scheinpflug, K. *et al.* Antimicrobial peptide cWFW kills by combining lipid phase separation with autolysis. *Sci. Rep.* **7**, 44332 (2017).

53. Chen, X., Hirt, H., Li, Y., Gorr, S. & Aparicio, C. Antimicrobial GL13K Peptide Coatings Killed and Ruptured the Wall of *Streptococcus gordonii* and Prevented Formation and Growth of Biofilms. *PLoS One* **9**, e111579 (2014).

54. Southwood, R., Rice, J., McDonald, P., Hakendorf, P. & Rozenbilds, M. Infection in experimental hip arthroplasties. *J. Bone Joint Surg. Br.* **67**-**B**, 229–231 (1985).

55. Vidlak, D. & Kielian, T. Infectious Dose Dictates the Host Response during Staphylococcus aureus Orthopedic-Implant Biofilm Infection. *Infect. Immun.* **84**, 1957–1965 (2016).

56. Mellon, F. A. MASS SPECTROMETRY | Principles and Instrumentation. in *Encyclopedia of Food Sciences and Nutrition* **17**, 3739–3749 (Elsevier, 2003).

57. Young, T. III. An essay on the cohesion of fluids. *Philos. Trans. R. Soc. London* **95**, 65–87 (1805).

58. Godoy-Gallardo, M. *et al.* Antibacterial Coatings on Titanium Surfaces: A Comparison Study Between in Vitro Single-Species and Multispecies Biofilm. *ACS Appl. Mater. Interfaces* **7**, 5992–6001 (2015).

Chapter 4 – Development of a rapid fluorescence-based microplate assay to obtain mechanistic insights on the interaction of membrane active peptides with whole bacterial cells

4.1. Introduction

The World Health Organization identified Antibiotic-resistant bacteria as one of the greatest threats to human health in the future. Antimicrobial Peptides (AMPs) are potential candidates as bactericidal agents, which have demonstrated their efficacy as part of innate immunity[1]. For development of novel antimicrobials, an interesting target is represented by bacterial cytoplasmic membrane where vital processes take place[2]. Membrane interactions of AMPs have been extensively investigated by using model membrane systems[3–5]. However interactions of AMPs with whole bacteria could be different due to complexity of living microbial membranes[6]. The membrane-targeting AMPs can alter the membrane function rising the membrane ion-permeability, promoting the formation of ion-conducting membrane pores or simulating an ion carrier[7–9]. For this reason, one of the key experiments to analyse the mode of action of membrane-targeting AMPs is the evaluation of membrane permeability. Nowadays, membrane impermeable fluorescent dyes such as Propidium Iodide (PI) [10] or SYTOX green[11] are employed to detect alterations in membrane permeability. These nucleic acid staining dyes increment their fluorescence when the membrane integrity is critically damaged or large pores are formed[11–13], but they are not useful to detect modifications in membrane potential[14]. The modifications in ion permeability could be studied using membrane potential-sensitive fluorescent distributional probes, for example oxonols, such as Bis-(1,3-Dibutylbarbituric Acid)Trimethine Oxonol (DiBAC$_4$(3)) [15], or cationic dyes such as 3,3'-Dihexyloxacarbocyanine Iodide (DiOC$_6$(3)) [16] and 3,3'-Dipropylthiadicarbocyanine Iodide (diSC$_3$(5)) [17].

In this chapter we described the development of a rapid fluorescence based microplate assay, by combining a potential sensitive dye with a nucleic acid stain, to get mechanistic and kinetic insights on the interaction of membrane active peptides with cytoplasmic membranes of whole bacteria, by monitoring simultaneously the phenomena of membrane depolarization, due to ion movements across the membrane, and membrane permeabilization, due to pore formation, in *Staphylococcus* species.

4.2. Results and Discussion

### 4.2.1. Compatibility between the fluorescent dyes

The fluorescent dyes used to develop this assay were DiBAC$_4$(3), diSC$_3$(5) and PI. DiBAC$_4$(3) is a membrane-potential sensitive *bis*-oxonol dye that can penetrate bacterial cells and bind to intracellular proteins or to the membrane when these cells are depolarized[15]. This is observed as an increment of DiBAC$_4$(3) fluorescence caused by a higher influx of the anionic dye into the microorganisms where it binds to the hydrophobic residues of the proteins[15]. On the other hand, Propidium Iodide is a classical intercalating dye which displays increase in fluorescence upon binding to nucleic acids[18].

Table 4.1. *Reported fluorescent excitation and emission wavelengths of the tested dyes.*

	Molecular Weight	Solubility	Charge	Excitation (λ)	Emission (λ)	References
DiBAC$_4$(3)	516.64	DMSO	Anionic	494.5	516	15
PI	668.4	H$_2$O	Cationic	490$\rightarrow$535	617	18
diSC$_3$(5)	546.53	DMSO	Cationic	640-652	670	19–21

To check whether the spectroscopic properties of the selected dyes were changed in our experimental conditions, excitation and emission spectra of 125, 250 and 500 nM DiBAC$_4$(3) and 5, 10 and 20 μg/mL PI were first measured (***Figure 4.1.***).

As shown in ***Figure 4.1.A*** and ***4.1.B***, for DiBAC$_4$(3) the maximum excitation and emission wavelengths were 496 nm and 516 nm, respectively, in agreement with values reported by other authors (***Table 4.1.***). Moreover, the ***Figure 4.1.C*** and ***4.1.D*** showed that the maximum excitation and emission wavelengths of PI are 490 nm and 617 nm, respectively. These data are in line with values obtained by other researchers (***Table 4.1.***), but it is important to take into consideration that the maximum excitation wavelength of PI will shift from 490 nm to 535 nm in the presence of nucleic acids (***Table 4.1.***).
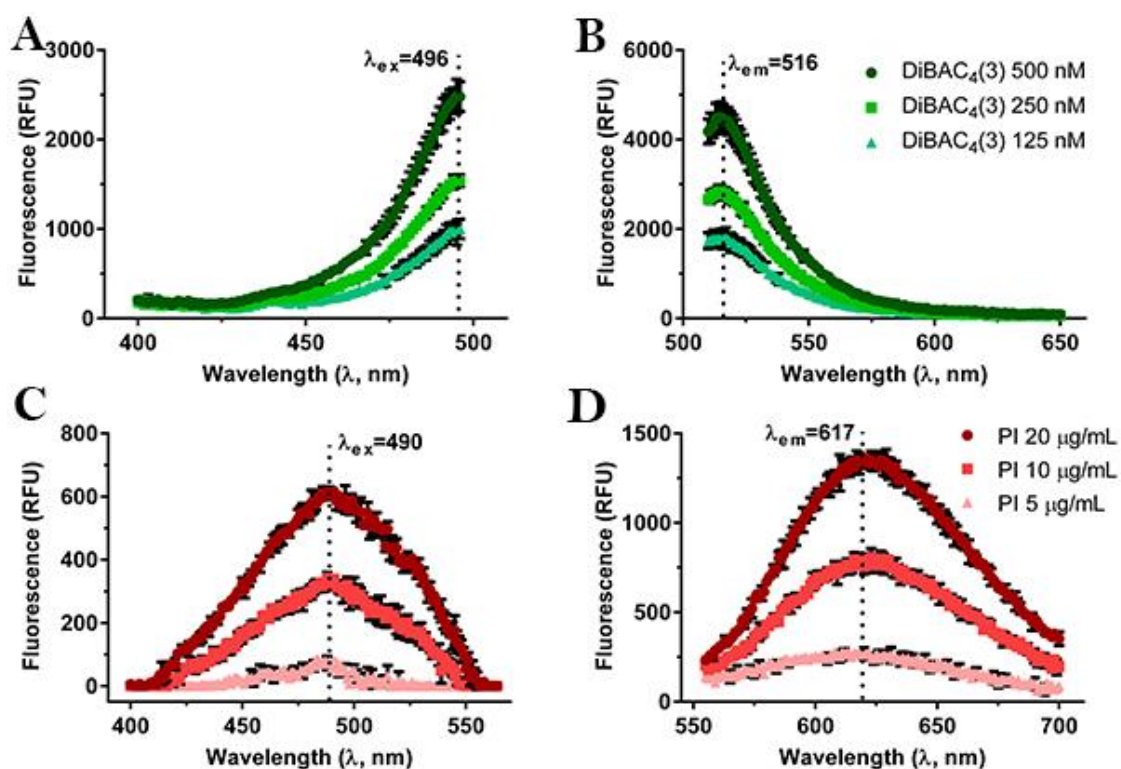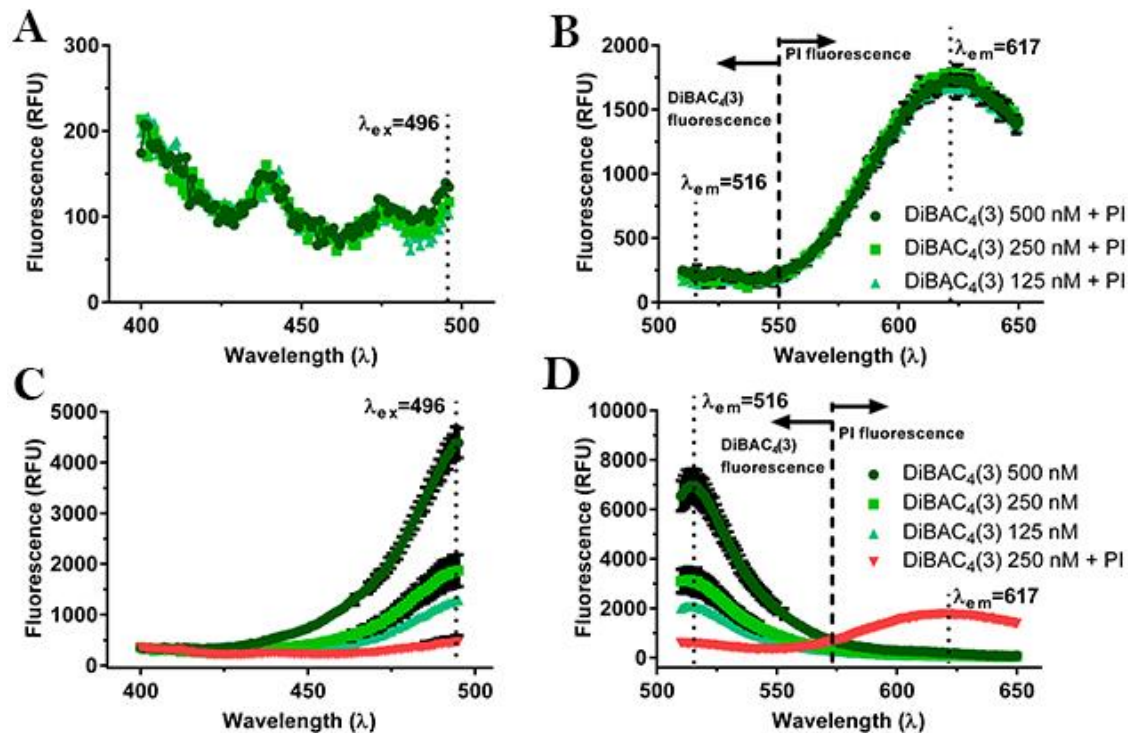
*Figure 4.1. Fluorescence Excitation (**A, C**) and Emission (**B, D**) spectra of DiBAC₄(3) (**A – B**) and PI (**C – D**). **A**, excitation spectra with 516 nm detection wavelength and **B**, emission spectra with 496 nm excitation wavelength of three different DiBAC₄(3) concentrations. **C**, excitation spectra with 617 nm detection wavelength and **D**, emission spectra with 490 nm excitation wavelength of three different PI concentrations. The maximum excitation and emission wavelengths are reported in each graph. For technical reasons due to instrument settings, spectra in **A** and **B** could not be measured at **wavelengths >496 nm and <510 nm**, respectively.*

When the spectra of DiBAC₄(3) were repeated in the presence of 10 µg/mL PI (**Figure 4.2.A – B**), the excitation spectrum was completely modified with a decrease in fluorescence at its maximum excitation wavelength (496nm) from 3000 relative fluorescence units (RFU) (**Figure 4.1.A**) to less than 200 RFU (**Figure 4.2.A**) at 500 nM DiBAC₄(3). Hence, excitation of DiBAC₄(3) in this condition was virtually absent. Also the emission spectra were remarkably changed, with a drop at its maximum emission wavelength (516nm) from ≈5000 RFU (**Figure 4.1.B**) to less than 400 RFU (**Figure 4.2.B**), at 500nM DiBAC₄(3). On the contrary, the emission of PI at 617nm was clearly evident (**Figure 4.2.B**). This means that PI strongly affected DiBAC₄(3) fluorescence.

The spectra were repeated in the presence of *S. epidermidis* (**Figure 4.2.C – D**). The excitation and emission spectra of DiBAC₄(3) (**Figure 4.2.C – D**) were very similar to those obtained without bacteria (**Figure 4.1.A – B**). When DiBAC₄(3) and PI were combined,

DiBAC$_4$(3) excitation and emission spectra were clearly modified again (***Figure 4.2.C – D***) similar to what was observed in the absence of bacteria (***Figure 4.2.A – B***).


Figure 4.2. *Fluorescence Excitation (**A, C**) and Emission (**B, D**) spectra of DiBAC$_4$(3)+PI (**A – B**), and DiBAC$_4$(3) alone, and DiBAC$_4$(3)+ PI, in the presence of bacteria (**C – D**). **A**, excitation spectra with 516 nm detection wavelength (the error bars are not shown for clarity purposes) and **B**, emission spectra with 490 nm excitation wavelength of three different DiBAC$_4$ (3) concentrations + 10 µg/ml PI. **C**, excitation spectra with 516 nm detection wavelength and **D**, emission spectra with 490 nm excitation wavelength of three different DiBAC$_4$ (3) concentrations and 250nM DiBAC$_4$(3) + 10 µg/ml PI in the presence of S. epidermidis.*

At least two hypotheses could be postulated to explain why the excitation and emission peaks of DiBAC$_4$(3) disappeared in the presence of PI.

- *Competition between dyes.* Both dyes have very similar excitation wavelengths, but PI is present at about 30-120-fold higher concentration, on a molar basis, respect to DiBAC$_4$(3). This means that PI could be preferentially excited by the light pulse, preventing light absorption by DiBAC$_4$(3) and, consequently, its excitation.

- *FRET phenomenon.* Both fluorescence dyes are excited by the light pulse, but the light emitted by DiBAC$_4$(3) (λ_{em}=516 nm) is absorbed by PI as it falls in the range of PI excitation wavelengths. So, only PI emits fluorescence.

We feel that the most realistic explanation could be a combination of both hypotheses, with a clear competition between both dyes for being excited by the light pulse and, at the same time, absorption by PI of the DiBAC$_4$(3) emission (**Figure 4.3.**). Taken together, all these results made the combination of DiBAC$_4$(3) and PI unsuitable for our purposes.
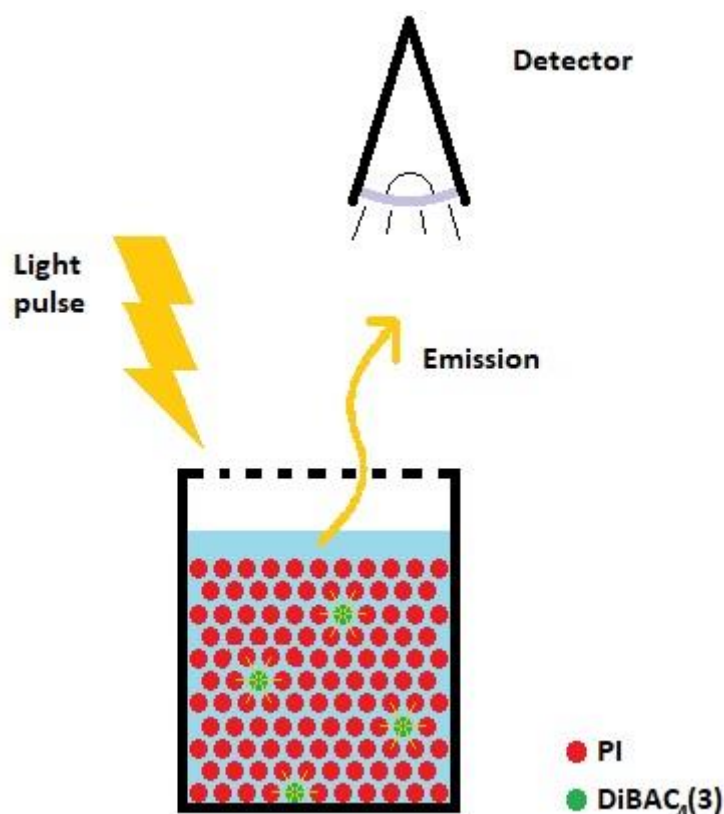
Figure 4.3. *Final hypothesis representation.*

Given the interference of the oxonol dye with PI, in the next set of experiments it was replaced by diSC$_3$(5), a cationic carbocyanine fluorescence probe with short alkyl tail (<4 carbon atoms)[20]. It is membrane-permeable and accumulates on polarized cells until a Nernstian equilibrium across the membrane is reached[22]. The strong accumulation in energized cells causes quenching of its fluorescence. Once membrane is depolarized, the dye is quickly released in the medium and, as a consequence, its fluorescence is dequenched (**Figure 4.4.**)[22].
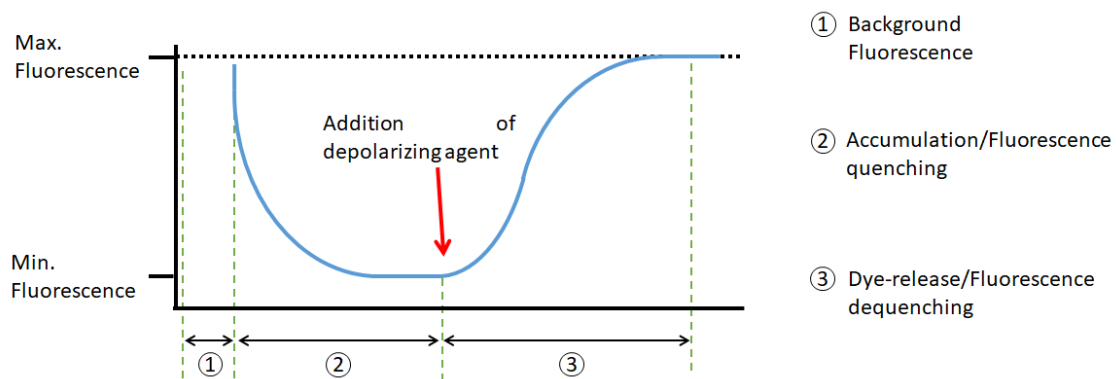
Figure 4.4. *Schematic representation of diSC$_3$(5) fluorescence kinetics following interaction with cell membrane of metabolically active cells, and subsequent addition of a depolarizing agent.*

To verify the compatibility between the two dyes in our experimental conditions, excitation and emission spectra of diSC$_3$(5) alone and in the presence of PI were first measured. As shown in **Figure 4.5.A – B**, the maximum excitation and emission wavelengths were confirmed and diSC$_3$(5) fluorescence was not affected by PI. On the other hand, it was also necessary to verify whether PI fluorescence was affected by
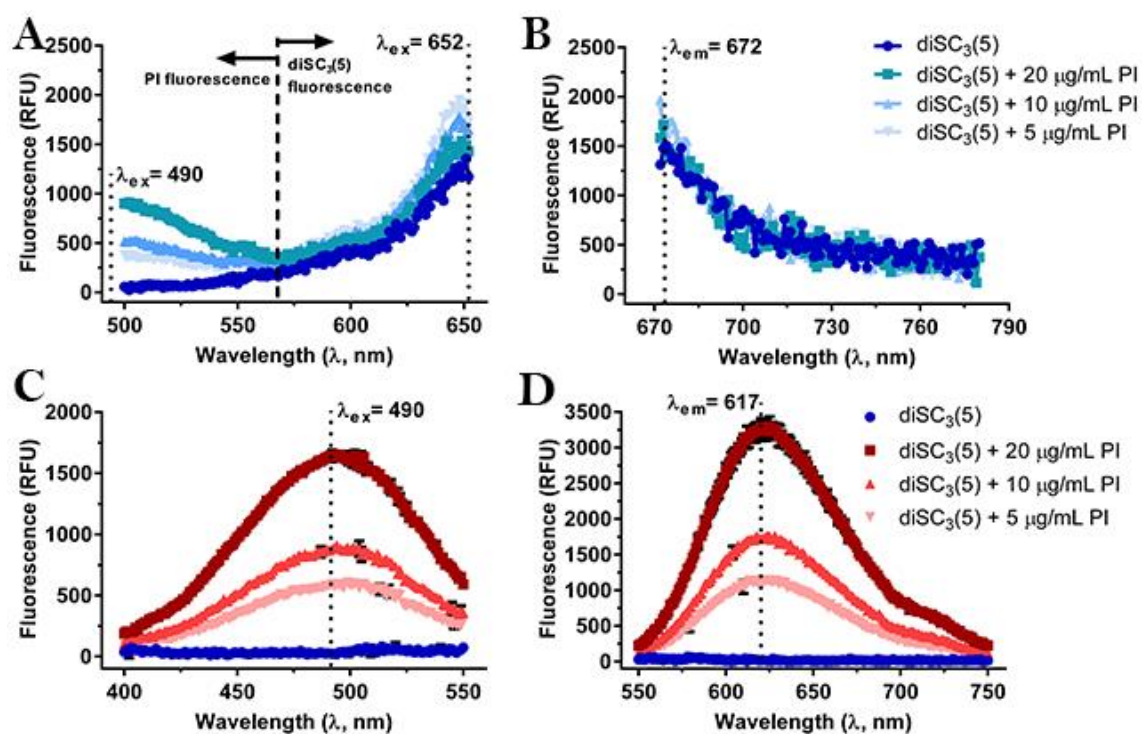
Figure 4.5. *Fluorescence Excitation (**A, C**) and Emission (**B, D**) spectra of diSC$_3$(5) and PI. **A**, excitation spectra with 672 nm detection wavelength and **B**, emission spectra with 652 nm excitation wavelength of 0.4 μM diSC$_3$ (5) + 5, 10 and 20 μg/mL PI (error bars are not shown for clarity purposes). **C**, excitation spectra with 617 nm detection wavelength and **D**, emission spectra with 490 nm excitation wavelength of 0.4 μM diSC$_3$ (5) + 5, 10 and 20 μg/mL PI. For technical reasons due to instrument settings, spectra in **A** and **B** could not be measured at **wavelengths >650 nm and <670 nm**, respectively.*

diSC$_3$(5), so measures were repeated by using the excitation and emission wavelengths reported for PI. Spectra show that there was no interference between the two dyes and that increased PI fluorescence intensities were well correlated to increased PI concentrations (***Figure 4.5.C – D***).
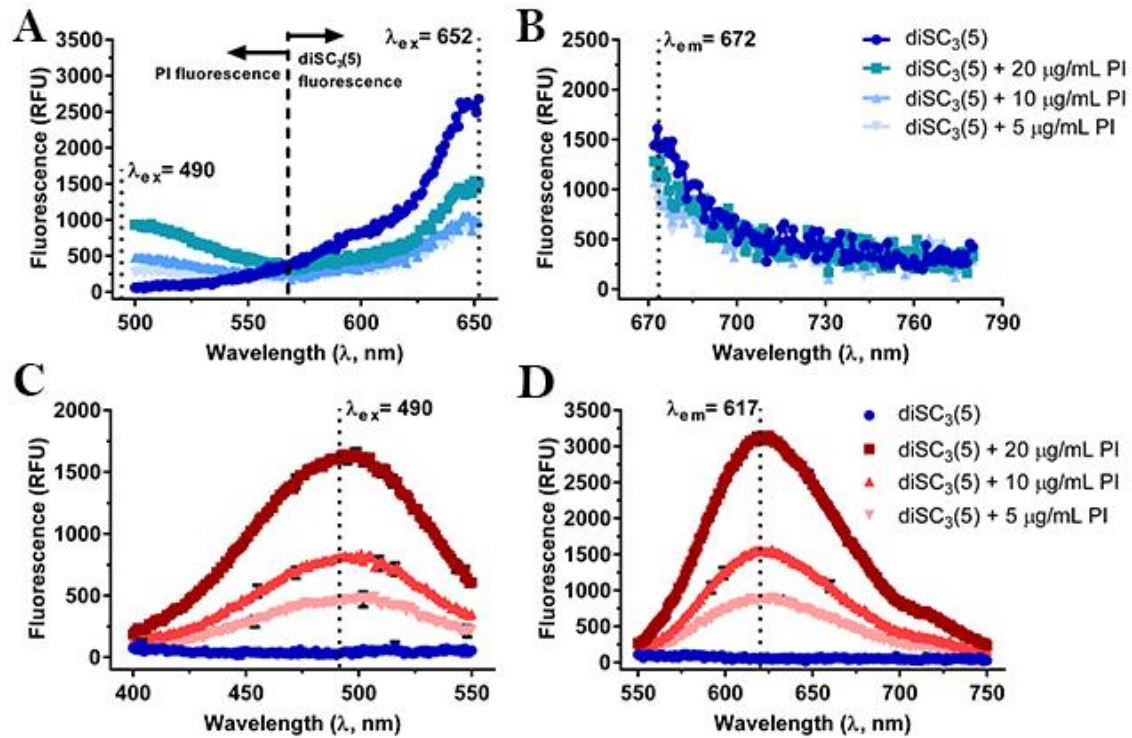
Figure 4.6. *Fluorescence Excitation (**A**, **C**) and Emission (**B**, **D**) spectra of diSC$_3$(5) with different PI concentrations in the presence of S. epidermidis. **A**, excitation spectra with 672 nm detection wavelength and **B**, emission spectra with 652 nm excitation wavelength of 0.4 μM diSC$_3$ (5) + 5, 10 and 20 μg/mL PI (error bars are not shown for clarity purposes). **C**, excitation spectra with 617 nm detection wavelength and **D**, emission spectra with 490 nm excitation wavelength of 0.4 μM diSC$_3$ (5) + 5, 10 and 20 μg/mL PI.*

Very similar spectra were measured in the presence of metabolically active *S. epidermidis* (***Figure 4.5. and 4.6.***).

Therefore, the fluorescent probes diSC$_3$(5) and PI were compatible because they did not show any interaction between them. Consequently, these dyes were suitable to function as membrane depolarization and membrane permeabilization markers in our assay.

4.2.2. Selection of membrane-active antimicrobial peptides

The next step was the selection of the antimicrobial peptide (AMPs) candidates as positive controls of membrane depolarization and membrane permeabilization events.

We selected four membrane-active AMPs based on scientific literature: Gramicidin D, Cecropin A, Magainin 2, and Melittin. Gramicidin D is a bacterial antibiotic produced by *Bacillus brevis*. It is composed by a mixture of highly similar pentadecapeptides consisting of about 85% gramicidin A. The principal structural feature of this peptide is alternating hydrophobic L- and D-amino acid residues, and their organization in the membrane environment leads to the formation of an ion channel. The insect peptide Cecropin A, the frog peptide Magainin 2, and the cytolytic peptide Melittin from bee venom, are all cationic α-helical AMPs known to permeabilize bacterial membranes. Melittin in particular is well-known as a pore-forming peptide (**Table 4.2.**).

Table 4.2. *Selected membrane-active antimicrobial peptides for the development of the fluorescence-based microplate assay.*

Peptide	Sequence	Molecular weight	Solvent	References
Cecropin A	KWKLFKKIEKVGQNIRDGIIKAGPAVAVV GQATQIAK-NH$_2$	4003.78	DMSO	[23–25]
Magainin 2	GIGKFLHSAKKFGKAFVGEIMNS-OH	2466.90	H$_2$O	[26–28]
Melittin	GIGAVLKVLTTGLPALISWIKRKRQQ-NH$_2$	2846.46	H$_2$O	[29–33]
Gramicidin D	formyl-VGALAVVVWLWLWLWG- NHCH$_2$CH$_2$OH	1880.00	DMSO	[34–37]

All these peptides are membrane-active and their antimicrobial activities are well characterized. However, it was necessary to verify their active concentrations in our experimental conditions. To this aim, the peptides were first tested against representative Gram-positive and Gram-negative reference strains in a standard broth microdilution assay.

Table 4.3.

Table 4.3. Antimicrobial activities of selected AMPs against reference Gram-positive and Gram-negative strains.

|	Cecropin A	Melittin	Magainin 2	Gramicidin D
	MIC (MBC) (μM)[a,b]			
S. epidermidis ATCC 35984	> 128	0.5 (0.5)	> 128	2 (4)
S. aureus ATCC 25923	> 128	0.5 (1)	64 (128)	4 (8)
E. coli ATCC 25922	0.75 (0.75)	1 (1)	8 (16)	>32
P. aeruginosa ATCC 27853	1 (2)	1 (2)	64 (64)	>32

[a] Determined in MH broth at $5 \cdot 10^5$ CFU/mL.

[b] Data are means of at least 2 independent experiments.

Results in **Table 4.3.** show that only melittin and gramicidin D displayed activities against the Gram-positive *S. aureus* and *S. epidermidis*, which are the principal target of the present thesis.

These results have been confirmed in the "adapted" assay conditions, i.e. with a higher inoculum (10^7 CFU/mL) and 30 min incubation in phosphate buffered saline (PBS) supplemented with 25 mM glucose (PBS-glc) (see paragraph 4. Experimental procedures). Based on their activity against *S. aureus* and *S. epidermidis*, melittin and gramicidin D were selected for further experiments.

4.2.3. Interference of uncouplers and peptides with the fluorescent dyes

To test whether the selected peptides display any interference with diSC$_3$(5) or with PI, the fluorescence of both probes mixed together in the same wells was monitored kinetically at their specific excitation and emission wavelengths before and after the addition of the AMPs, without bacteria. The uncouplers Carbonyl cyanide 3-chlorophenylhydrazone (CCCP) and Carbonyl cyanide 4-(trifluoromethoxy)phenylhydrazone (FCCP), as well as the solvent dimethyl sulfoxide (DMSO), were also included in these experiments (**Figure 4.7.**).
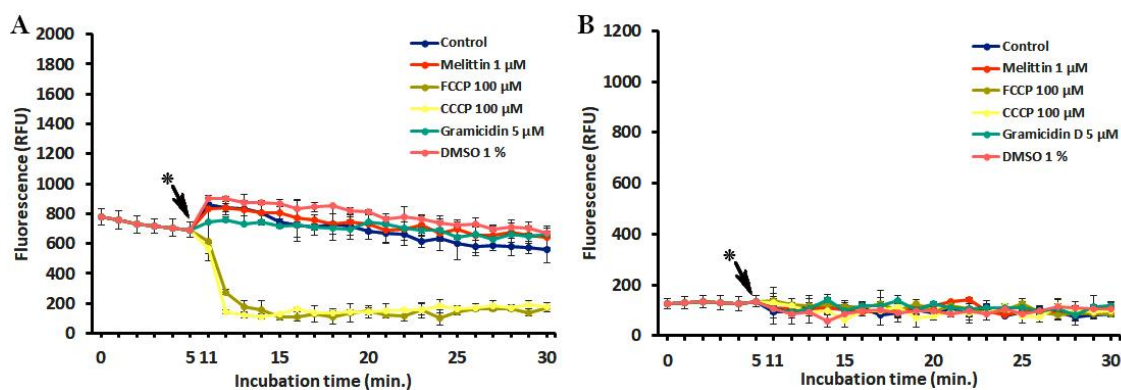
Figure 4.7. *Interference of uncouplers and peptides with the fluorescent dyes. The kinetics of (A) diSC₃(5)* $(\lambda_{ex} = 652\ nm,\ \lambda_{em} = 672\ nm)$ *and (B) PI* $(\lambda_{ex} = 535\ nm,\ \lambda_{em} = 617\ nm)$ *are shown in separate graphs for clarity purposes. The time necessary for the addition of peptides and uncouplers (indicated by an *) was about 6 minutes.*

It was observed that, at difference with both uncouplers which decrease diSC₃(5) fluorescence, the peptides and the negative control (1% DMSO) display the same kinetics meaning that they have no interference (**Figure 4.7.A**). Likewise, no interference between PI and the added molecules was recorded (**Figure 4.7.B**). Unfortunately, the interference of the uncouplers with diSC₃(5) fluorescence precluded their use in this assay.

4.2.4. Correlation of membrane alterations with bacterial killing

The interactions of membrane-active AMPs with target membranes have been extensively studied in artificial systems. Hence, in the present study our goal was to monitor the peptide-induced changes in membrane permeability in whole bacterial cells. By using membrane-targeting AMPs with well characterized mode of action, we wanted to monitor the phenomena of membrane depolarization and membrane permeabilization simultaneously, thanks to the combination of diSC₃(5) and PI. The experiments were performed by incubating *S. epidermidis* ATCC 35984 and *S. aureus* ATCC 25923 with the ion channel forming gramicidin D and with the pore-forming melittin in PBS-glc containing 0.4 µM diSC₃(5) and 5 µg/mL PI at 37 °C in low binding 96-well black microtiter plates. Fluorescence was monitored throughout the assay and, at 30 min incubation, aliquots were taken to determine bacterial viability by CFU counts.

As shown in **Figure 4.8.**, gramicidin D induced in both *Staphylococcus* spp. a significant increase of diSC₃(5) (**Figure 4.8.A and 4.8.D**), but not of PI fluorescence (**Figure 4.8.B and 4.8.E**). The increase was rapid at bactericidal concentrations (i.e. >92%

killing), while it slowed down at descending peptide concentrations that also produced lower killing. Hence, there was a clear correlation between gramicidin D concentrations, bacterial killing, and diSC₃(5) fluorescence kinetics, whereas in none of the cases PI fluorescence increased. This means that gramicidin D killed *S. epidermidis* and *S. aureus* by membrane depolarization without formation of larger pores that could enable PI uptake.
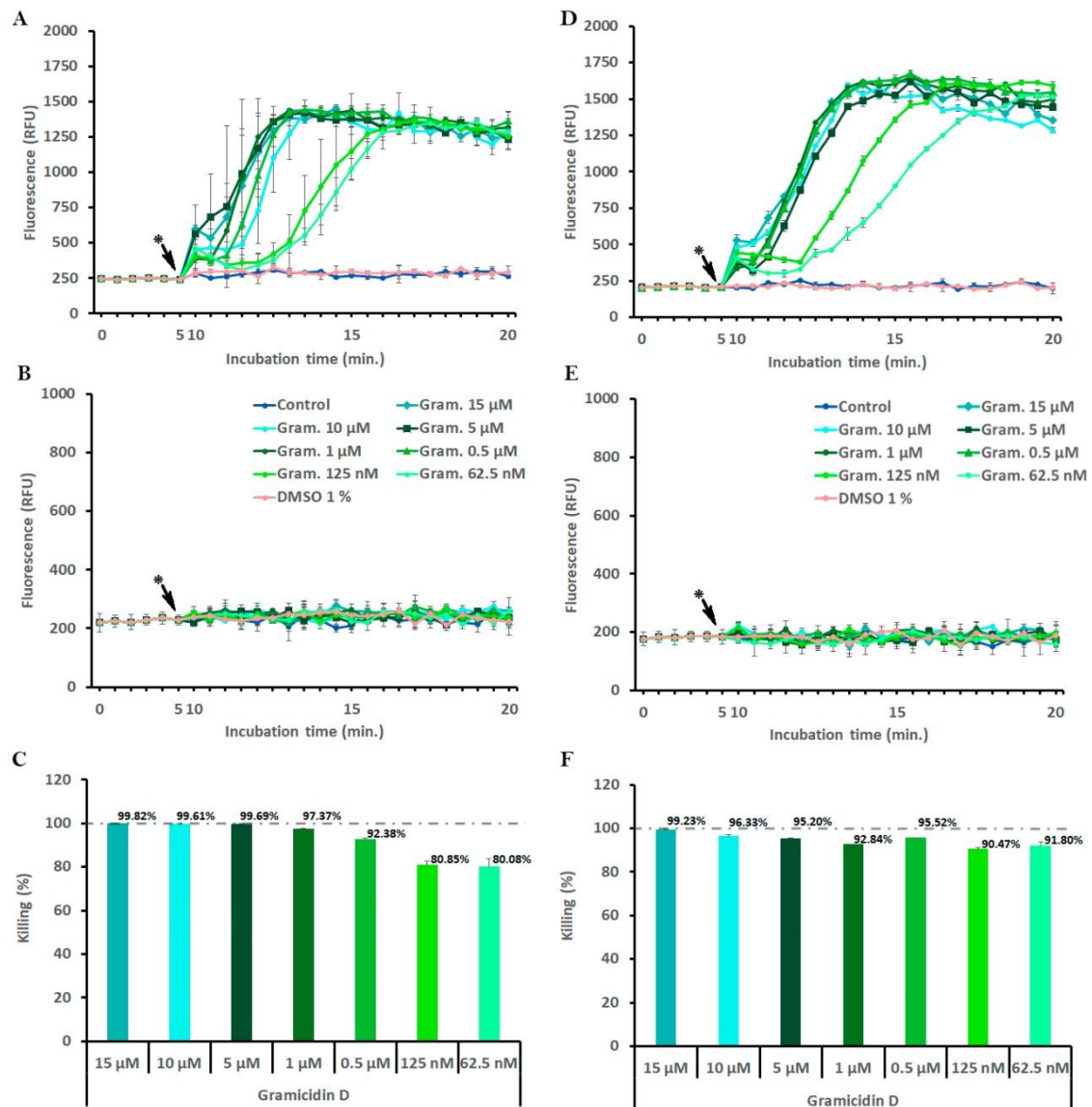
Figure 4.8. *Membrane depolarization (diSC₃ (5)) **(A, D)**, Permeabilization (PI) **(B, E)** and Killing percentage **(C, F)** of S. epidermidis **(A – C)** and S. aureus **(D – F)** caused by gramicidin D. Experiments were performed with 10^8 CFU/mL of the indicated strains in PBS-glc with 0.4 μM diSC₃(5) (λ_{ex} = 652 nm, λ_{em} = 672 nm) and 5 μg/mL PI (λ_{ex} = 535 nm, λ_{em} = 617 nm) at 37 ˚C. CFU counts were determined at 30 min incubation. diSC₃(5) and PI kinetics are in separate graphs and only the initial 20' are shown for clarity purposes. (*) peptide addition.*

Moreover, it is important to note that diSC$_3$(5) and PI *per se* were not toxic to bacteria because neither of the two probes showed an increase of fluorescence, or caused a decrease of CFUs.

Our data are in line with those reported in the literature which reveal that gramicidin D causes a rapid and full dissipation of membrane potential by forming small cation specific channels[34,36] and for this reason, many authors used this peptide as a positive control of membrane depolarization[38–40]. However, it is important to note that the diameter of gramicidin D-induced channels is estimated to measure about 4 Å, which is sufficient to accommodate the passage of monovalent cations[34], but not the uptake of larger molecules such as PI (MW=668.4). As a consequence, interaction of PI with nucleic acids is precluded despite bacteria are dying[18].

The results obtained with melittin (***Figure 4.9.***) showed a completely different picture. This pore forming peptide caused a remarkable increase of PI fluorescence, with slower kinetics at sub-MIC and more rapid kinetics at bactericidal concentrations (killing>95%). Interestingly, diSC$_3$(5) fluorescence increased only at bactericidal melittin concentrations. This means that the increase of diSC$_3$(5) fluorescence did not indicate membrane depolarization as a primary event but was rather a consequence of irreversible membrane permeabilization, which appears as the key event in the case of melittin, it was for that reason that many authors use melittin as a positive control of the membrane permeabilization phenomenon[41–43].

Taking into consideration that melittin induced pores with a diameter of 25-30 Å [44] are large enough to accommodate the passage of large molecules such as PI (***Figure 4.9.***), one can reasonably expect that ion leakage may also occur. So, in principle melittin has the ability to alter the membrane potential. It is interesting to note, however, that melittin at sub-MIC concentrations induced slower PI uptake, correlated with lower killing activity, but no increase of diSC$_3$(5) fluorescence (***Figure 4.9.***). This observation would suggest a limited membrane damage, probably caused by formation of transient pores, as reported in the literature[33], and that bacteria could recover to some extent.
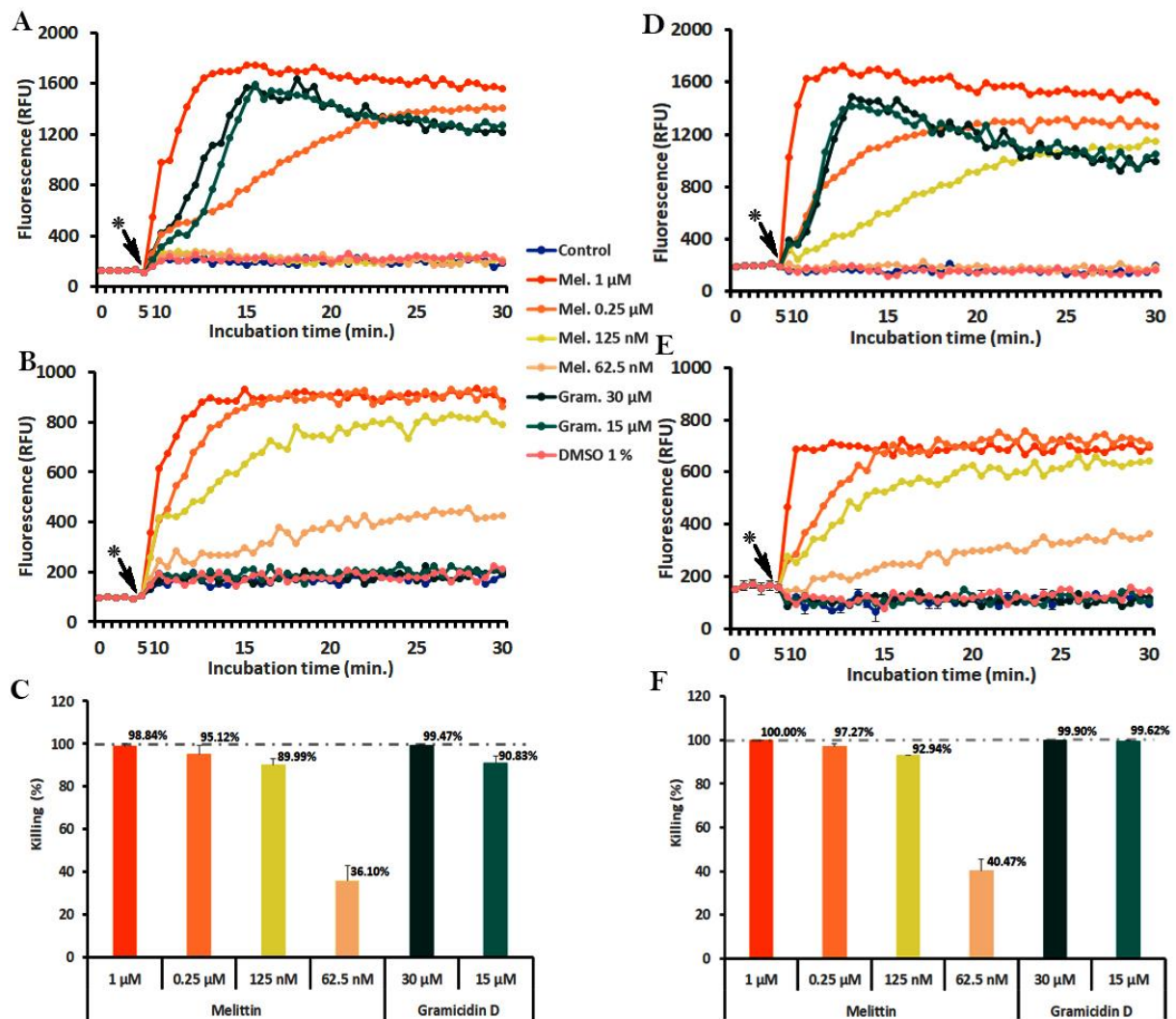
Figure 4.9. *Membrane depolarization (diSC₃ (5))* ***(A, D)****, Permeabilization (PI)* ***(B, E)*** *and Killing percentage* ***(C, F)*** *of S. epidermidis* ***(A-C)*** *and S. aureus* ***(D-F)*** *caused by melittin and gramicidin D. Experiments were performed with 10^8 CFU/mL of the indicated strains in PBS-glc containing 0.4 μM diSC₃ (5) ($λ_{ex}$ = 652 nm, $λ_{em}$ = 672 nm) and 5 μg/mL PI ($λ_{ex}$ = 535 nm, $λ_{em}$ = 617 nm) at 37 ˚C. CFU counts were determined at 30 min incubation . The kinetics of diSC₃(5) and PI are displayed in separate graphs, and error bars are not shown for clarity purposes. (*) peptide addition.*

The findings observed thanks to the combination of both fluorescent dyes have important implications for the advancement of our knowledge concerning the mode of action of gramicidin D and melittin. If for instance the assay would have been performed by using diSC₃(5) only, we would conclude that both peptides, gramicidin D and melittin, caused membrane depolarization (***Figure 4.8. A, D*** and ***Figure 4.9.A, D***) and in this case, the result obtained with melittin would be a false positive. On the contrary, if we had used only PI, the result of gramicidin D would be a false negative (***Figure 4.8. B, E*** and ***Figure 4.9.B, E***). We would speculate that gramicidin D, at difference with melittin, did

not cause membrane permeabilization and, perhaps it killed bacteria by acting on some internal target(s).

Conversely, by using the combination of diSC$_3$(5) and PI we measured the phenomena of membrane depolarization and permeabilization on the same bacterial population simultaneously. This assay thus enables to distinguish between these two phenomena and contributes to shed light on the mode of action of membrane-active agents such as the AMPs. This study confirmed that gramicidin D causes membrane depolarization and melittin induces membrane permeabilization. We also provide an additional evidence that melittin at low concentrations probably creates transient pores, which cause a membrane permeabilization which is reversible to some extent.

With the aim to better understand the phenomena induced by melittin and gramicidin on *S. epidermidis*, at the end of fluorescence kinetics (30 min incubation) bacteria were processed for analysis by Field Emission Scanning Electron Microscopy (FE-SEM) (*Figures 4.10.1. – 4.10.3.*).

Images of untreated bacterial cells, reported in *Figure 4.10.1.*, show the normal, round and smooth appearance of vital and growing staphylococcal cells, similar to those observed in *Chapters 3* and *5*.
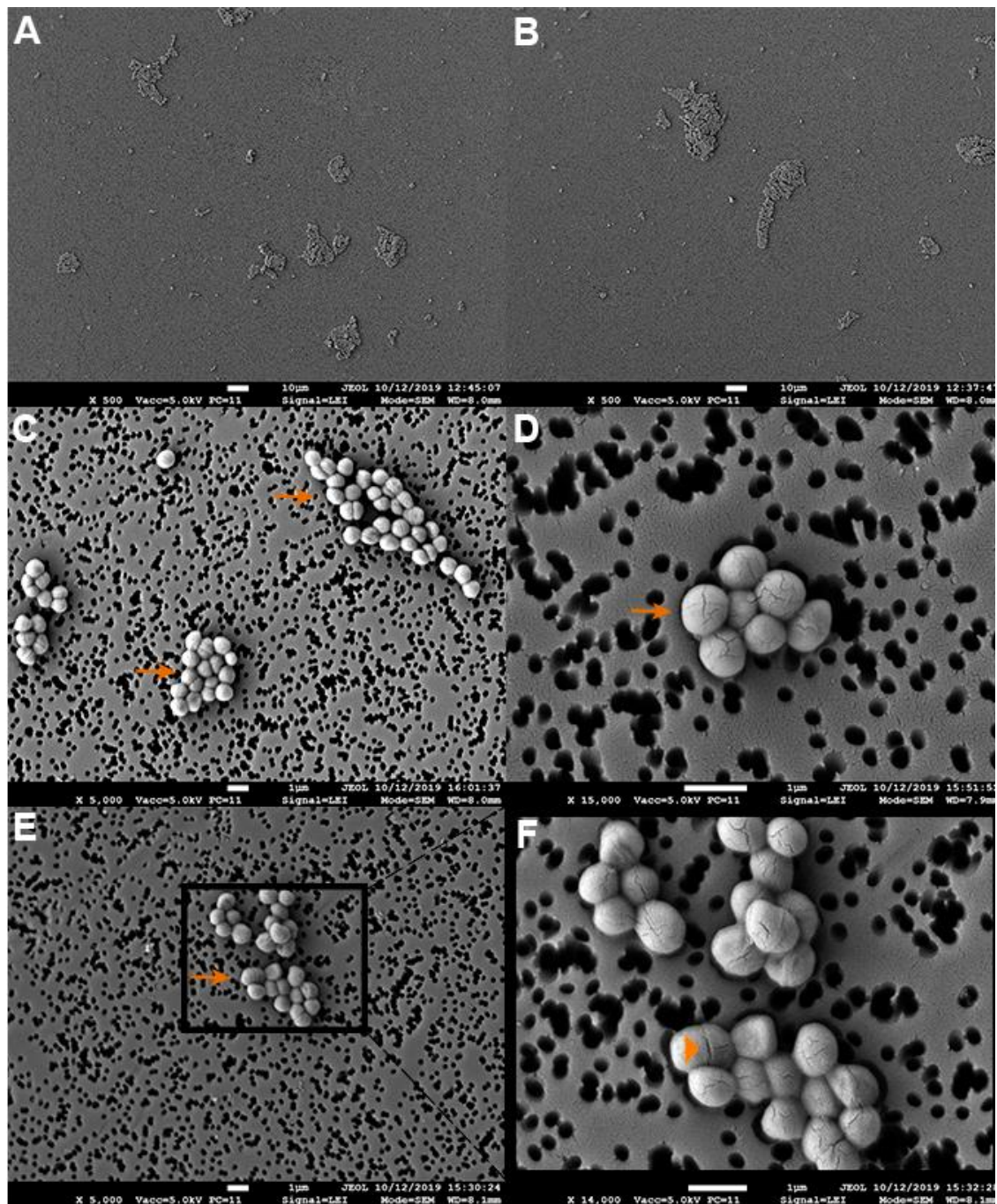
Figure 4.10.1. Morphology of S. epidermidis on polycarbonate filters analysed by FE-SEM (Panels A – F).

Arrows indicate, respectively, division septa (▶), bacterial aggregates (↑). Representative images from two experiments performed in duplicate are shown.

On the contrary, filters containing melittin treated *S. epidermidis* displayed a lower number of bacteria which presented clearly affected morphology in many cases (***Figure 4.10.2.***). Dead bacteria had increased size, lost their division septa (***Figure 4.10.2.B*** and ***4.10.2.D***), their surface lost the smooth appearance, and many of them have some protrusions similar to blebs (***Figure 4.10.2.B***). These results are in agreement with the

fluorescence data and with the literature demonstrating that melittin causes a huge membrane damage[42,45–47].
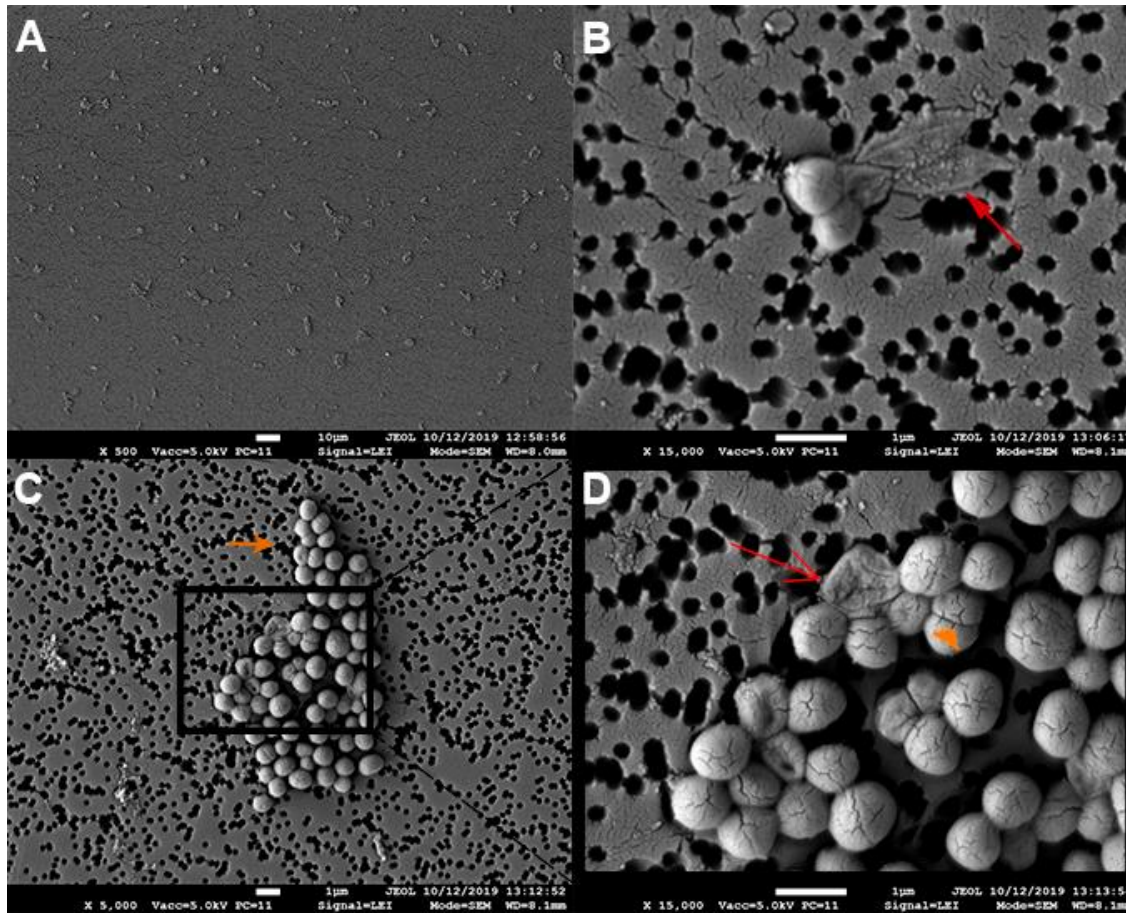

Figure 4.10.2. *Morphology of S. epidermidis treated with 1 µM melittin analysed by FE-SEM (Panels A – D). Arrows indicate, respectively, division septa (▶), bacterial aggregates (↑), collapsed bacteria (↑) and deflated bag (↑). Representative images from two experiments performed in duplicate are shown.*

The bacteria treated with gramicidin D, besides a lower number of bacteria on filter surface, also showed clearly affected morphology (***Figure 4.10.3.***). In addition, many bacteria were collapsed (***Figure 4.10.3.C – D***), some bacterial clusters presented extrusion of cytoplasmic material (***Figure 4.10.3.B – C***) and in many cases the "deflated bag" morphology was observed, suggesting impaired microbial cell growth as well as the cell division process, similar to what observed for Gramicidin S[48].
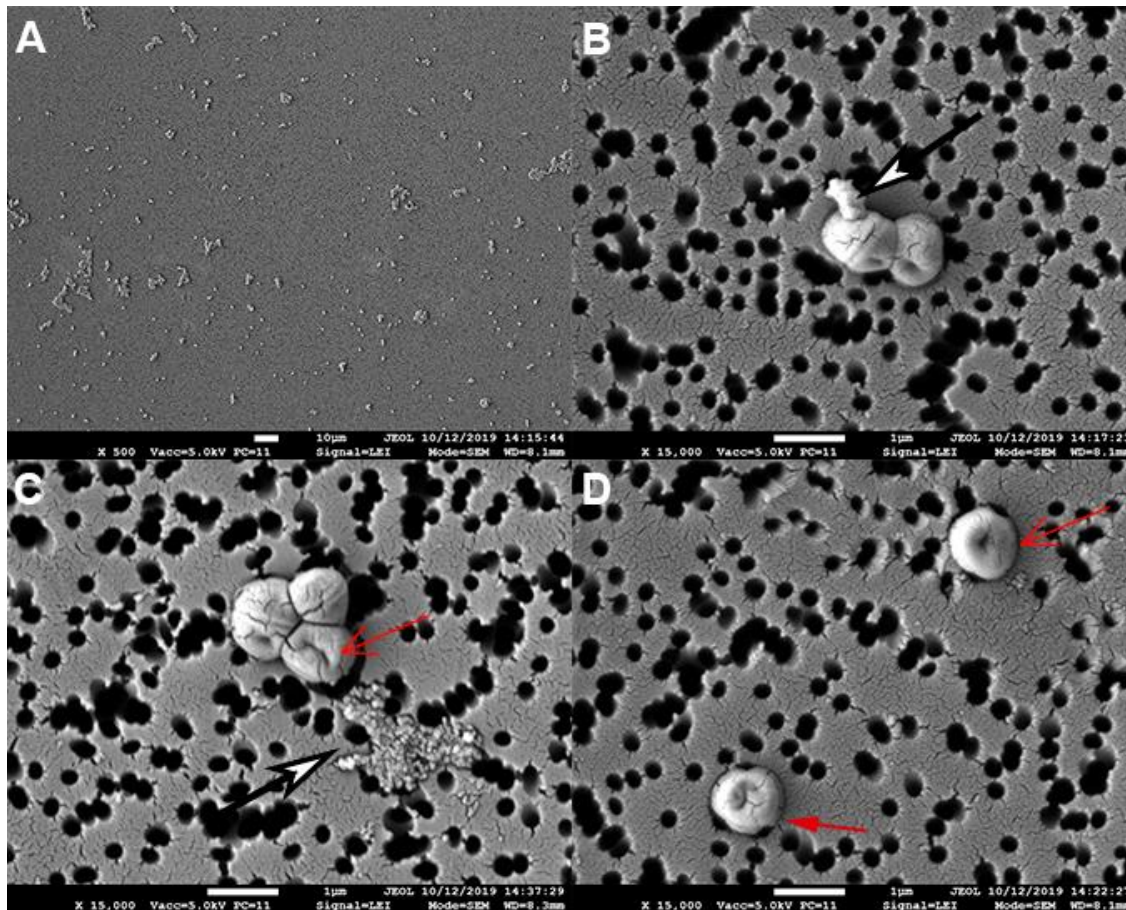
Figure 4.10.3. *Morphology of S. epidermidis treated with 30 µM Gramicidin D analysed by FE-SEM (Panels A – D). Arrows indicate, respectively, extruded cytoplasmic material (↑), collapsed bacteria (↑) and deflated bag (↑). Representative images from two experiments performed in duplicate are shown.*

4.2.5. Adaptation of the assay to lower bacterial loads

Once the experimental conditions for the membrane depolarization and permeabilization assay were established, we wanted to adapt the assay to lower bacterial concentrations with the aim to make the assay more sensitive. In order to assess which of the fluorescent probes was more sensitive, the membrane depolarization and permeabilization events were analysed by using each probe with gramicidin D or melittin, in the presence of decreasing concentrations of *S. epidermidis.*

Membrane depolarization kinetics of 10^8, 10^7, $5 \cdot 10^6$, 10^6 CFU/mL *S. epidermidis,* treated with gramicidin D, were monitored by using 0.4 µM diSC$_3$(5), with killing activity performed in parallel (***Figure 4.11.***). As shown in ***Figure 4.11.A – B and 4.11.C – D***, with 10^8 and 10^7 CFU/mL, respectively, the membrane depolarization phenomenon in *S. epidermidis,* induced by a bactericidal concentration of gramicidin D, was clearly

evident. It was still evident at 5·10^6 CFU/mL (***Figure 4.11.E – F***), although with a less clear accumulation phase (see ***Figure 4.4.***). Finally, with further lowering to 10^6 CFU/mL, the membrane depolarization event was far less evident with only a small increment in fluorescence respect to higher (***Figure 4.11.G***) bacterial concentrations (***Figure 4.11.A,C and E***). In this latter condition the duration of the accumulation phase almost doubled because it was difficult to establish when the potentiometric dye reached an equilibrium prior to adding the depolarizing agent. So we can conclude that membrane depolarization of *S. epidermidis* can be monitored with 0.4 µM diSC$_3$(5) at 10^8, 10^7, and 5·10^6 CFU/mL. All these experiments presented a clear correlation between membrane depolarization and killing activity (***Figure 4.11.B, D, F*** *and **H***).
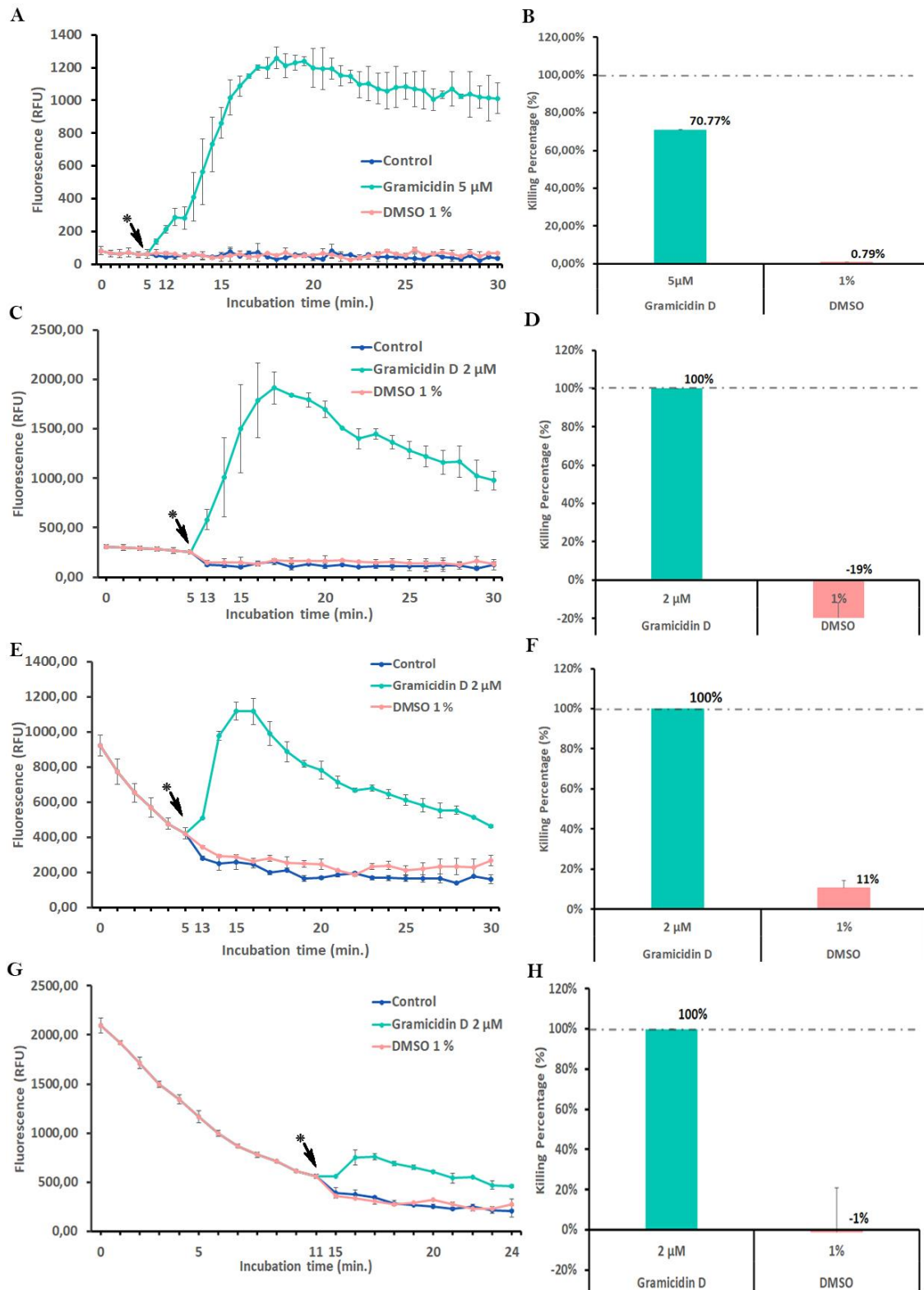
Figure 4.11. Membrane depolarization (A, C, E, G) and Killing percentage (B, D, F, H) of S. epidermidis by gramicidin D. Experiments were performed with (A-B) 10^8, (C-D) 10^7, (E-F) $5 \cdot 10^6$ and (G-H) 10^6 CFU/mL of the indicated strain in PBS-glc using 0.4 μM diSC_3 (5) (λex = 652 nm, λem = 672 nm) at 37 °C. At 30 min incubation aliquots were taken to determine bacterial viability by CFU counts. The time necessary for the addition of molecules (indicated by an *) was about 5-8 minutes.

To test PI sensitivity, the fluorescence kinetics was studied at 5 and 10 μg/mL PI and 10^8 and 10^7 CFU/mL *S. epidermidis*, treated with a bactericidal concentration of melittin. As reported in ***Figure 4.12.A*** and ***4.13.A***, with bacteria at 10^8 CFU/mL melittin addition induced an increment of PI fluorescence at both PI concentrations, in good correlation with bacterial killing (***Figure 4.12.B*** and ***4.13.B***), whereas at 10^7 CFU/mL, it was
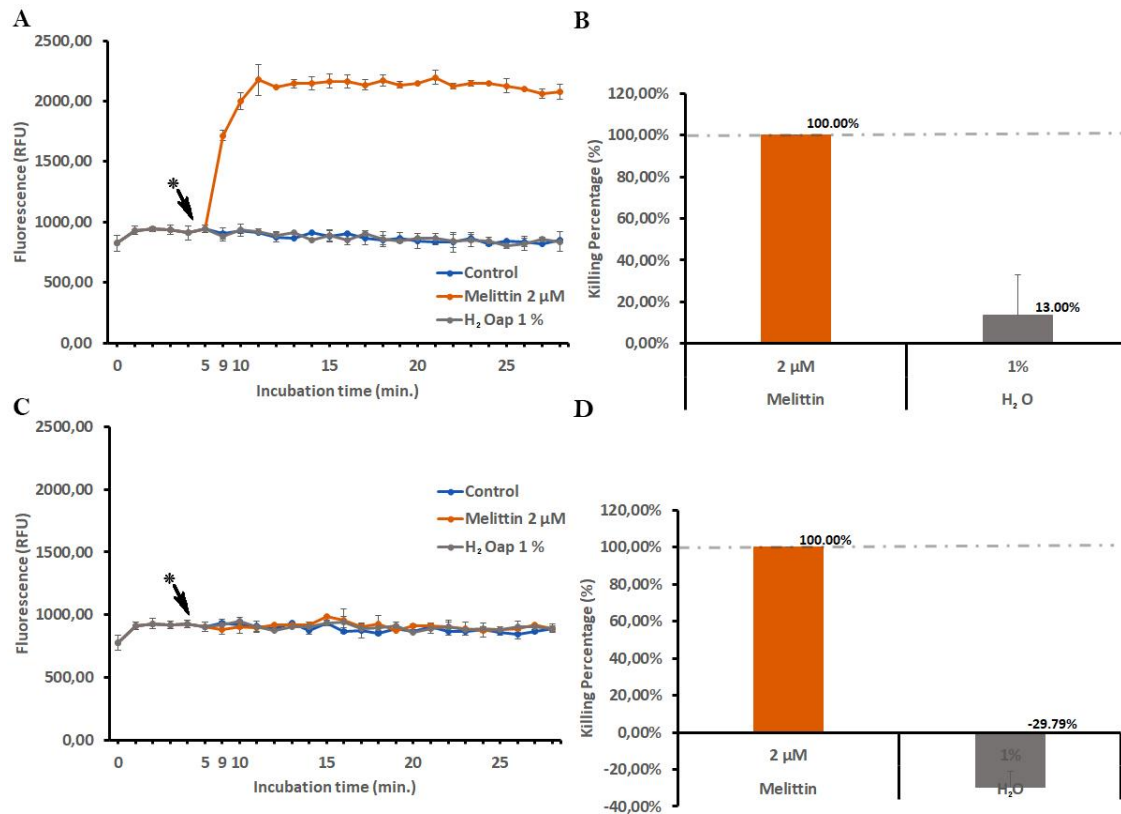
Figure 4.12. *Membrane permeabilization (**A, C**) and Killing percentage (**B, D**) of S. epidermidis by melittin. The experiment was performed with (**A-B**) 10^8, (**C-D**) 10^7 CFU/mL of the indicated strain in PBS-glc using 5 μg/mL PI (λ_{ex} = 535 nm, λ_{em} = 617 nm) at 37 ˚C. At 30 min incubation aliquots were taken to determine bacterial viability by CFU counts. The time necessary for the addition of molecules (indicated by an *) was about 4 minutes.*

impossible to measure membrane permeabilization (***Figure 4.12C*** and ***4.13C***) despite 100% killing (***Figure 4.12.D*** and ***4.13.D***). This happened at both PI concentrations (***Figure 4.12.*** and ***4.13.***), thus indicating that the limiting factor is not PI concentration but the number of bacteria, or better, their nucleic acid content. As PI emits fluorescence only upon binding to DNA, fluorescence intensity will depend on the concentration of PI-DNA complexes. These will in turn reach a detectable concentration only with a sufficiently high inoculum. These considerations are of course limited to the instrument we selected to detect fluorescence because in flow cytometry[49], for example, it was possible to

detect PI uptake with a lower bacterial suspension even in the case of staphylococci which are notoriously small. However, in the present thesis my attention was focused on the possibility to analyse fluorescence kinetics in multiple samples simultaneously, and this is possible to achieve with a multiplate reader.

Figure 4.13. Membrane permeabilization (**A, C**) and Killing percentage (**B, D**) of S. epidermidis by melittin. The experiment was performed with (**A-B**) 10^8, (**C-D**) 10^7 CFU/mL of the indicated strain mid log phase in PBS-glc using 10 µg/mL PI ($\lambda_{ex} = 535$ nm, $\lambda_{em} = 617$ nm) at 37 °C in 96 low binding black well plate. At 30 min incubation aliquots were taken to determine bacterial viability by CFU counts. The time necessary for the addition of molecules (indicated by an *) was about 4 minutes.

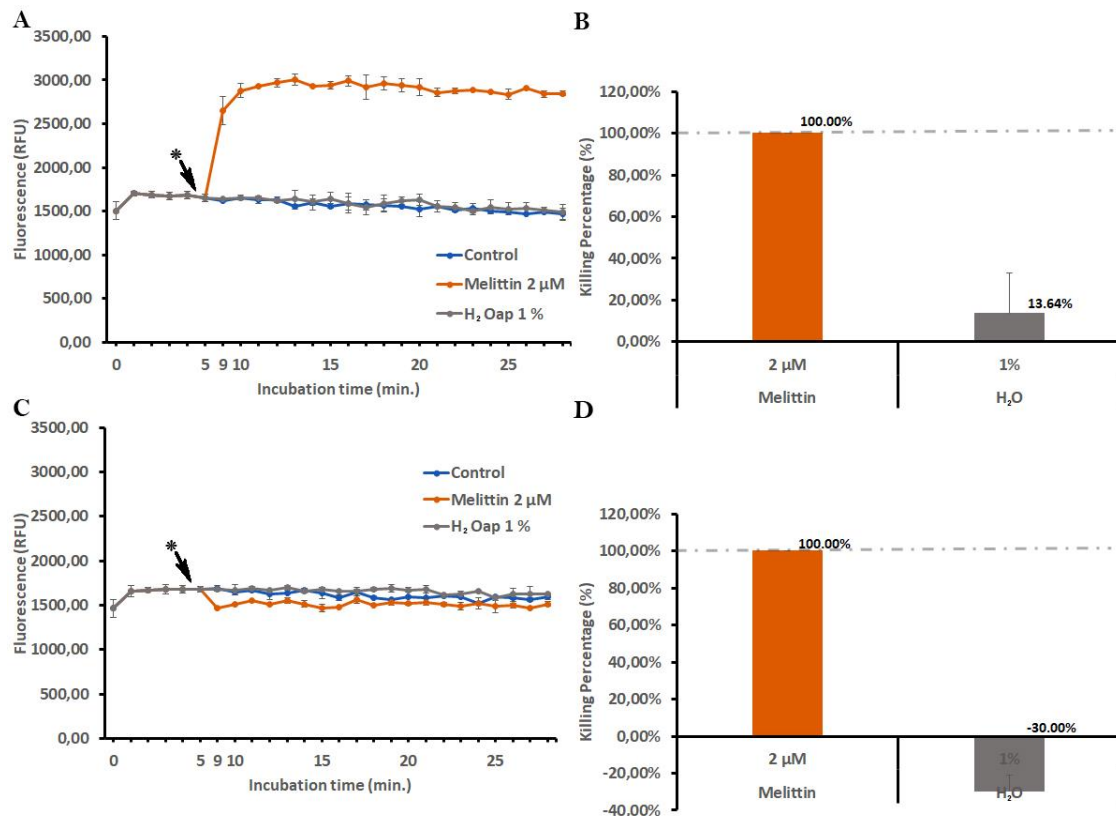## 4.3. Conclusions

- By combining the potential-sensitive dye $diSC_3(5)$ and the DNA staining dye PI, it was possible to discriminate between membrane depolarization and membrane permeabilization in whole Gram-positive bacteria.

- Concerning sensitivity, a limiting factor using a microplate reader is the concentration of PI-DNA complexes which is correlated to bacterial density. Nevertheless, $diSC_3(5)$ allows to detect membrane depolarization at lower bacterial concentrations. This fact suggests that concerning membrane perturbation, $diSC_3(5)$ is a more sensitive tool for fluorescence-based assays using a microplate reader.

- The use of microtiter plates allows the simultaneous evaluation of several membrane active antimicrobial agents.

- Concerning timing, one limiting factor of a multiplate kinetic assay could be the time needed to add several agents simultaneously. This could be a problem with very fast acting antimicrobial agents.

- FE-SEM analysis of melittin- and gramicidin-treated *S. epidermidis* confirmed different effects on bacterial morphology.

- The assay was validated with soluble peptides. It would need further optimization for applications to surface immobilized peptides.

4.4. Experimental procedure
4.4.1. Peptides and Uncouplers

The selected membrane-active peptides Gramicidin D, Cecropin A, Magainin 2, and Melittin were purchased from Sigma-Aldrich® (USA). Cecropin A and Gramicidin D were dissolved in DMSO, and Magainin 2 and Melittin were dissolved in pyrogenic water. The stock solutions were kept at -20 ˚C.

4.4.2. Bacteria and bacterial cultures

Two Gram-positive, *Staphylococcus epidermidis* ATCC 35984 and *Staphylococcus aureus* ATCC 25923, and two Gram-negative, *Escherichia coli* ATCC 25922 and *Pseudomonas aeruginosa* ATCC 27853 reference strains were obtained from American Type Culture Collection (ATCC; Manassas, VA). Bacteria were maintained on Mueller-Hinton (MH) agar plates. For antimicrobial assays, bacteria were cultured in liquid Brain Heath Infusion (BHI) overnight, 1:50-diluted in fresh medium and allowed to grow in orbital shaker at 37 ˚C. Mid-log phase bacteria were harvested after 10 min centrifugation at 1000 x g and resuspended in PBS to optimal density assessed by turbidity at 600 nm, with reference to previously determined standards. For fluorescence kinetics, mid-log phase bacteria were collected by centrifugation at 1000 x g, washed two times with PBS (pH 7.4), and finally resuspended in PBS supplemented with 25 mM glucose (PBS-glc) at the desired density assessed by turbidity at 600 nm, with reference to previously determined standards

4.4.3. Determination of the standard Minimum Inhibitory Concentration (MIC) and Minimum Bactericidal Concentration (MBC)

The minimum inhibitory concentration (MIC) of selected peptides was determined by a broth microdilution assay in 96-well microtiter plates, using MH broth with logarithmic-phase microorganisms at 5×10^5 CFU/mL, as previously reported[50], following CLSI guidelines. The minimum bactericidal concentration (MBC) was determined seeding aliquots from wells showing no visible growth on solid medium to allow colony counts.

4.4.4. Reagent preparation

Stock solutions were prepared as follows: 400 µM diSC$_3$(5) in 100% DMSO, 50 µM DiBAC$_4$(3) in 100% DMSO, and 1 mg/mL PI in $_{dd}$H$_2$O (PI would precipitate in a more concentrated solution). All stocks, protected from light by aluminium foil, are stable at -20 ˚C for at least 6 months.

4.4.5. Compatibility between fluorescence dyes

The fluorometric measurements using membrane potential-sensitive fluorescent distributional probes (Bis-(1,3-Dibutylbarbituric Acid)Trimethine Oxonol (DiBAC$_4$(3)) [15] (*Figure 4.13.A*) and 3,3'-Dipropylthiadicarbocyanine Iodide (diSC$_3$(5)) [17]) (*Figure 4.13.B*), and the membrane impermeable fluorescencent dye Propidium Iodide (PI) [10] (*Figure 4.13.C*) were performed with a Multimode Plate Reader (EnSpireTM 2300, PerkinElmer, Waltham, MA, USA) by using low-binding surface 96-black polystyrene microtiter plates (PerkinElmer), in order to prevent unspecific binding of the molecules used in the study to polystyrene surface of conventional plates.
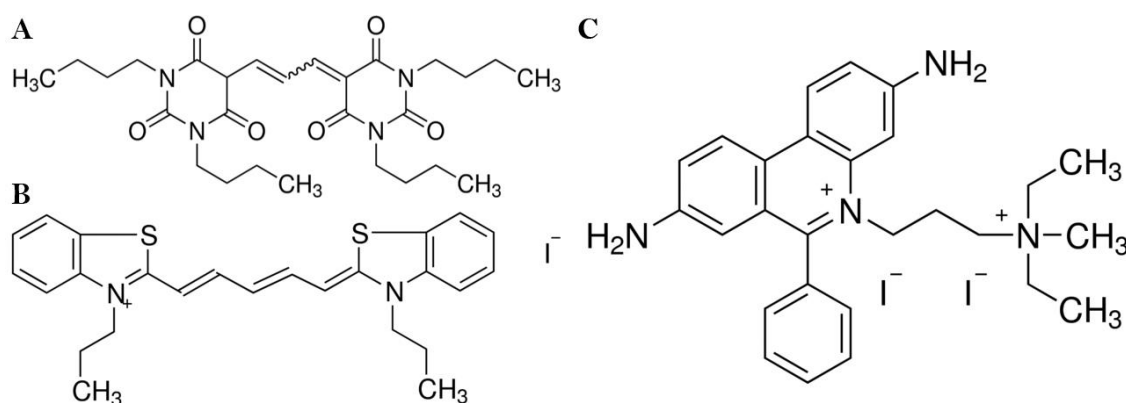
Figure 4.13. Chemical structures of (A) DiBAC$_4$(3), (B) diSC$_3$(5) and (C) PI.

4.4.6. Excitation and Emission spectra

To verify the correct excitation and emission wavelengths of each fluorescent dye, their excitation and emission spectra were measured in our assay conditions. DiBAC$_4$(3) was studied at 125, 250 and 500 nM (λ_{ex}=490 nm, λ_{em}=516 nm), and PI at 5, 10 and 20 µg/mL (λ_{ex}=535 nm, λ_{em}=617 nm) in PBS supplemented with 25 mM glucose (PBS-glc). Moreover, the excitation and emission spectra of DiBAC$_4$(3) were recorded in the presence of 10 µg/mL PI, with and without *S. epidermidis,* in PBS-glc. Furthermore, the excitation and emission spectra of 0.4 µM diSC$_3$(5) alone (λ_{ex}=652 nm, λ_{em}=672 nm) and

0.4 μM diSC$_3$(5) plus 5, 10 and 20 μg/mL PI (λ_{ex}=652 and 490 nm, λ_{em}=617 and 672 nm), were measured in PBS-glc, in the presence and in the absence of *S. epidermidis*.

4.4.7. Interference of uncouplers and peptides with the fluorescent dyes

To evaluate if the uncouplers [Carbonyl cyanide 3-chlorophenylhydrazone (CCCP) and Carbonyl cyanide 4-(trifluoromethoxy)phenylhydrazone (FCCP)], the solvent (dimethylsulfoxide (DMSO)) and the selected peptides (melittin and gramicidin D) have any interference with diSC$_3$(5) or with PI, both fluorescent dyes combined together in the same wells [black-wellplate (Optiplate)] were monitored kinetically for 30 minutes at 37 °C in PBS-glc (diSC$_3$(5); λ_{ex}=652, λ_{em}= 672 nm and PI; λ_{ex}= 490, λ_{em}=617 nm).

4.4.8. Kinetic fluorescence measurements to detect membrane depolarization and permeabilization

Mid-log phase *S. epidermidis* and *S. aureus*, resuspended at $1 \cdot 10^8$ CFU/mL in PBS-glc were incubated in the orbital shaker at 37 °C for 15 min. Therefter, diSC$_3$(5) and PI were added at final concentrations of 0.4 μM and 5 μg/mL, respectively. The solution was mixed by short vortexing and 200 μL were added in duplicate to the wells of a black 96-well plate (Optiplate, PerkinElmer). The samples were preincubated at 37 °C with fluorescence measurements every minute for 5-10 min, or until readings were stabilized (Accumulation phase). After this time, the plate was ejected. Depolarizing agents were added to their respective wells to the final concentrations of 15 - 30 μM gramicidin D, 62.5 nM - 1 μM Melittin, 1% DMSO. The plate was placed back into the reader as quickly as possible to continue monitoring diSC$_3$(5) and PI, every 0.5 minutes for around 10 – 20 min. At the end of incubation (around 30 min), aliquots were withdrawn from each well, serially diluted and plated on MH agar to allow CFU determination.

4.4.9. Field Emission Scanning Electron Microscopy (SEM) of *S. epidermidis* on Polycarbonate membrane filters

The morphology of *S. epidermidis,* deposited on polycarbonate filters was studied by Field Emission Scanning Electron Microscopy (FE-SEM) (JEOL model JSM-7610FPlus) operated in secondary electron detection mode. The working distance was adjusted in order to obtain the suitable magnification; the accelerating voltage was set to 5 keV. SEM was performed in duplicate for each sample. Briefly, upon 30 min incubation as

described above, all samples were collected by centrifugation at 1000 x g for 10 min and fixed with 5% (v/v) glutaraldehyde in PBS for 2h at room temperature. Fixed bacteria were deposited on 0.2 µm Isopore polycarbonate membrane filters (Merck Millipore), extensively rinsed with filtered sterile PBS and dehydrated in graded series of ethanol solutions (20 min each). Immediately prior to SEM analysis, samples were sputter-coated with a thin gold layer.

4.5.   References

1.   Hancock, R. E. W. & Sahl, H.-G. Antimicrobial and host-defense peptides as new anti-infective therapeutic strategies. *Nat. Biotechnol.* **24**, 1551–7 (2006).

2.   Hurdle, J. ., O'Neill, A. . & Lee, R. . Targeting bacterial membrane function: an underexploited mechanism for treating persistent infections. *Nat. Rev. Microbiol.* **9**, 62–75 (2012).

3.   Nguyen, L. T., Haney, E. F. & Vogel, H. J. The expanding scope of antimicrobial peptide structures and their modes of action. *Trends Biotechnol.* **29**, 464–472 (2011).

4.   Huang, H. W. & Charron, N. E. Understanding membrane-active antimicrobial peptides. *Q. Rev. Biophys.* **50**, e10 (2017).

5.   Oren, Z. & Shai, Y. Mode of action of linear amphipathic α-helical antimicrobial peptides. *Biopolymers* **47**, 451–463 (1998).

6.   Strahl, H. & Errington, J. Bacterial Membranes: Structure, Domains, and Function. *Annu. Rev. Microbiol.* **71**, 519–538 (2017).

7.   Brogden, K. A. Antimicrobial peptides: pore formers or metabolic inhibitors in bacteria? *Nat. Rev. Microbiol.* **3**, 238–250 (2005).

8.   Wimley, W. C. & Hristova, K. Antimicrobial Peptides: Successes, Challenges and Unanswered Questions. *J. Membr. Biol.* **239**, 27–34 (2011).

9.   Yeaman, M. R. & Yount, N. Y. Mechanisms of Antimicrobial Peptide Action and Resistance. *Pharmacol. Rev.* **55**, 27–55 (2003).

10.   Sträuber, H. & Müller, S. Viability states of bacteria-Specific mechanisms of selected probes. *Cytom. Part A* **77A**, 623–634 (2010).

11.   Roth, B. L., Poot, M., Yue, S. T. & Millard, P. J. Bacterial viability and antibiotic susceptibility testing with SYTOX green nucleic acid stain. *Appl. Environ. Microbiol.* **63**, 2421–31 (1997).

12.   Stiefel, P., Schmidt-Emrich, S., Maniura-Weber, K. & Ren, Q. Critical aspects of

using bacterial cell viability assays with the fluorophores SYTO9 and propidium iodide. *BMC Microbiol.* **15**, 36 (2015).

13. Sochacki, K. A., Barns, K. J., Bucki, R. & Weisshaar, J. C. Real-time attack on single *Escherichia coli* cells by the human antimicrobial peptide LL-37. *Proc. Natl. Acad. Sci.* **108**, E77–E81 (2011).

14. Wenzel, M. *et al.* Proteomic Response of *Bacillus subtilis* to Lantibiotics Reflects Differences in Interaction with the Cytoplasmic Membrane. *Antimicrob. Agents Chemother.* **56**, 5749–5757 (2012).

15. Epps, D. E., Wolfe, M. L. & Groppi, V. Characterization of the steady-state and dynamic fluorescence properties of the potential-sensitive dye bis-(1,3-dibutylbarbituric acid)trimethine oxonol (Dibac4(3)) in model systems and cells. *Chem. Phys. Lipids* **69**, 137–150 (1994).

16. Shapiro, H. M. Chapter 8 Cell Membrane Potential Analysis. in *Methods in Cell Biology* **41**, 121–133 (1994).

17. Wu, M., Maier, E., Benz, R. & Hancock, R. E. W. Mechanism of Interaction of Different Classes of Cationic Antimicrobial Peptides with Planar Bilayers and with the Cytoplasmic Membrane of *Escherichia coli* †. *Biochemistry* **38**, 7235–7242 (1999).

18. Arndt-Jovin, D. J. & Jovin, T. M. Chapter 16 Fluorescence Labeling and Microscopy of DNA. in *Methods in Cell Biology* **30**, 417–448 (1989).

19. Sims, P. J., Waggoner, A. S., Wang, C.-H. & Hoffman, J. F. Studies on the Mechanism by which cyanine dyes measure membrane potential in red blood cells and phosphatidylcholine vesicles. *Biochemistry* **13**, 3315–3330 (1974).

20. Veldhuizen, E. J. A. *et al.* Antimicrobial and Immunomodulatory Activities of PR-39 Derived Peptides. *PLoS One* **9**, e95939 (2014).

21. Chapter 22 - Probes for Membrane Potential. in *The Molecular Probes handbook. A guide to fluorescent probes and labeling technologies* (eds. Johnson, I. & T.Z. Spence, M.) **76**, 923–936 (Thermo Fisher Scientific, 2010).

22. Waggoner, A. Optical probes of membrane potential. *J. Membr. Biol.* **27**, 317–334 (1976).

23. Lee, E., Shin, A. & Kim, Y. Anti-Inflammatory Activities of Cecropin A and its Mechanism of Action. *Arch. Insect Biochem. Physiol.* **88**, 31–44 (2015).

24. Cerón, J. M. *et al.* The antimicrobial peptide cecropin A induces caspase-independent cell death in human promyelocytic leukemia cells. *Peptides* **31**, 1494–1503 (2010).

25. Silvestro, L., Weiser, J. N. & Axelsen, P. H. Antibacterial and Antimembrane Activities of Cecropin A in Escherichia coli. *Antimicrob. Agents Chemother.* **44**, 602–607 (2000).

26. Imura, Y., Choda, N. & Matsuzaki, K. Magainin 2 in Action: Distinct Modes of Membrane Permeabilization in Living Bacterial and Mammalian Cells. *Biophys. J.* **95**, 5757–5765 (2008).

27. Lee, W. & Lee, D. G. Magainin 2 Induces Bacterial Cell Death Showing Apoptotic Properties. *Curr. Microbiol.* **69**, 794–801 (2014).

28. Matsuzaki, K. Magainins as paradigm for the mode of action of pore forming polypeptides. *Biochim. Biophys. Acta - Rev. Biomembr.* **1376**, 391–400 (1998).

29. Alonezi, S. *et al.* Metabolomic Profiling of the Effects of Melittin on Cisplatin Resistant and Cisplatin Sensitive Ovarian Cancer Cells Using Mass Spectrometry and Biolog Microarray Technology. *Metabolites* **6**, 35 (2016).

30. Steiner, M. R., Bomalaski, J. S. & Clark, M. A. Responses of purified phospholipases A2 to phospholipase A2 activating protein (PLAP) and melittin. *Biochim. Biophys. Acta - Lipids Lipid Metab.* **1166**, 124–130 (1993).

31. Faust, J. E., Yang, P.-Y. & Huang, H. W. Action of Antimicrobial Peptides on Bacterial and Lipid Membranes: A Direct Comparison. *Biophys. J.* **112**, 1663–1672 (2017).

32. Raghuraman, H. & Chattopadhyay, A. Melittin: a Membrane-active Peptide with Diverse Functions. *Biosci. Rep.* **27**, 189–223 (2007).

33. Gee, M. L. *et al.* Imaging the action of antimicrobial peptides on living bacterial cells. *Sci. Rep.* **3**, 1557 (2013).

34. Kelkar, D. A. & Chattopadhyay, A. The gramicidin ion channel: A model membrane protein. *Biochim. Biophys. Acta - Biomembr.* **1768**, 2011–2025 (2007).

35. Pavithrra, G. & Rajasekaran, R. Gramicidin Peptide to Combat Antibiotic Resistance: A Review. *Int. J. Pept. Res. Ther.* **0**, 0 (2019).

36. Smart, O. S., Goodfellow, J. M. & Wallace, B. A. The pore dimensions of gramicidin A. *Biophys. J.* **65**, 2455–2460 (1993).

37. Burkhart, B. M. *et al.* Gramicidin D conformation, dynamics and membrane ion transport. *Biopolymers* **51**, 129–144 (1999).

38. te Winkel, J. D., Gray, D. A., Seistrup, K. H., Hamoen, L. W. & Strahl, H. Analysis of Antimicrobial-Triggered Membrane Depolarization Using Voltage Sensitive Dyes. *Front. Cell Dev. Biol.* **4**, 1–10 (2016).

39. Lee, E. K., Kim, Y.-C., Nan, Y. H. & Shin, S. Y. Cell selectivity, mechanism of action and LPS-neutralizing activity of bovine myeloid antimicrobial peptide-18 (BMAP-18) and its analogs. *Peptides* **32**, 1123–1130 (2011).

40. Shang, D. *et al.* Membrane interaction and antibacterial properties of chensinin-1, an antimicrobial peptide with atypical structural features from the skin of *Rana chensinensis*. *Appl. Microbiol. Biotechnol.* **96**, 1551–1560 (2012).

41. Rončević, T. *et al.* Antibacterial Activity Affected by the Conformational Flexibility in Glycine–Lysine Based α-Helical Antimicrobial Peptides. *J. Med. Chem.* **61**, 2924–2936 (2018).

42. Akbari, R. *et al.* Action mechanism of melittin-derived antimicrobial peptides, MDP1 and MDP2, de novo designed against multidrug resistant bacteria. *Amino Acids* **50**, 1231–1243 (2018).

43. Rončević, T. *et al.* Membrane-active antimicrobial peptide identified in *Rana arvalis* by targeted DNA sequencing. *Biochim. Biophys. Acta - Biomembr.* **1861**, 651–659 (2019).

44. Ladokhin, A. S., Selsted, M. E. & White, S. H. Sizing membrane pores in lipid vesicles by leakage of co-encapsulated markers: pore formation by melittin. *Biophys. J.* **72**, 1762–1766 (1997).

45. Bardbari, A. M. *et al.* Highly synergistic activity of melittin with imipenem and colistin in biofilm inhibition against multidrug-resistant strong biofilm producer strains of Acinetobacter baumannii. *Eur. J. Clin. Microbiol. Infect. Dis.* **37**, 443–454 (2018).

46. Park, S.-C. *et al.* Investigation of toroidal pore and oligomerization by melittin using transmission electron microscopy. *Biochem. Biophys. Res. Commun.* **343**, 222–228 (2006).

47. Wang, G., Na, J., Pan, L., Xing, Z. & Fang, H. Ultrastructural observation on sterilization of melittin. *Sci. China Life Sci.* **54**, 166–170 (2011).

48. Hartmann, M. *et al.* Damage of the Bacterial Cell Envelope by Antimicrobial Peptides Gramicidin S and PGLa as Revealed by Transmission and Scanning Electron Microscopy. *Antimicrob. Agents Chemother.* **54**, 3132–3142 (2010).

49. D'Este, F. *et al.* Antimicrobial and host cell-directed activities of Gly/Ser-rich peptides from salmonid cathelicidins. *Fish Shellfish Immunol.* **59**, 456–468 (2016).

50. D'Este, F., Oro, D., Boix-Lemonche, G., Tossi, A. & Skerlavaj, B. Evaluation of free or anchored antimicrobial peptides as candidates for the prevention of orthopaedic device-related infections. *J. Pept. Sci.* **23**, 777–789 (2017).

Chapter 5 – Mode of action of AMPs in the immobilized state

5.1. Introduction

To obtain effective antimicrobial coatings with AMPs, it is crucial not to compromise their functionality upon immobilization. Several studies addressed these aspects by investigating the coupling chemistry, the role of spacer length or site of peptide anchoring, or peptide orientation on immobilized peptide activity[1,2]. Among these, some studies demonstrated ability of anchored peptides to permeabilize artificial lipid vesicles[3–5], and Gabriel *et al.* demonstrated that N-terminally conjugated LL-37 was capable to permeabilize *E. coli*[6]. However, it is not clear how can membrane-active peptides, covalently anchored to a solid support, interact with the cytoplasmic membrane of whole bacteria, causing membrane permeabilization. This is particularly difficult to understand in the case of Gram-positive microorganisms, which are wrapped by a thick peptidoglycan layer[7]. Some authors suggest that an electrostatic imbalance on bacterial surface would affect the Donnan potential across the membrane, which would in turn activate lethal cellular events such as the activation of autolytic enzymes, or disruption of electrostatic balance of internal layers[8]. Although the exact molecular mechanism has not yet been unravelled, Hilpert *et al.* demonstrated by using the membrane potential-sensitive fluorescent distributional probe 3,3'-Dipropylthiadicarbocyanine Iodide (diSC$_3$(5)), that the immobilized peptides were able to destabilize the cell envelope of Gram-positive bacteria[8].

In this chapter we investigated the mode of action of surface-anchored B27(1-18). First we studied how peptide orientation, i.e. N-terminal or C-terminal immobilization, influences peptide behaviour on titanium. This was accomplished by comparing the antimicrobial efficacy of titanium samples functionalized with the cysteinylated derivatives B27(1-18)^{Cys} and ^{Cys}B27(1-18), against *S. epidermidis*. Additional mechanistic insights were obtained by applying the fluorescence-based assay, developed in the

previous chapter (***chapter 4***), to resin-bound analogues of B27(1-18). By using this approach it was possible to determine how antimicrobial activity was affected by orientation and to compare peptide efficacy and mode of action of free and anchored peptide derivatives.

5.2. Results and Discussion

As continuation and deepening of the study described in ***chapter 3***, in collaboration with Biomaterials, Biomechanics & Tissue Engineering research group (BiBiTE) from Polytechnic University of Catalonia (Barcelona, Catalonia, Spain), we decided to investigate the influence of peptide orientation on the antimicrobial performance of titanium functionalized with BMAP27(1-18)[9]. Similar to what reported in ***chapter 3***, the amino acid sequence was modified at the N-terminus or C-terminus by addition of three 6-aminohexanoic acid (Ahx) units as a spacer and one cysteine residue as anchoring moiety. The derivatives BMAP27(1-18)-(Ahx)$_3$-Cys and Cys-(Ahx)$_3$-BMAP27(1-18) are hereafter referred to as B27(1-18)^{Cys} and ^{Cys}B27(1-18). In order to verify whether the antimicrobial properties have been affected by this modification, their minimum inhibitory concentrations (MICs) against two Gram-positive bacterial species were determined in a standard MIC assay (***Table 5.1.***). Although the two cysteinylated derivatives displayed slightly lower MIC values (one well difference) against both strains compared to the original BMAP27(1-18), the differences are too small to be considered significant. Most important, the two derivatives did not display any difference in activity.

Table 5.1. *Antimicrobial activity of soluble cysteinylated peptides against two Gram-positive reference strains.*

	BMAP27(1-18)	B27(1-18)^{Cys}	^{Cys}B27(1-18)
	MIC (μM)[a,b]		
S. epidermidis ATCC 35984	2	1	1
S. aureus ATCC 25923	4	2	2

[a] Determined in MH broth.

[b] Data are means of at least 3 independent experiments.

For peptide coupling to titanium the same strategy described in ***chapter 3*** was applied (***Figure 5.1.***).
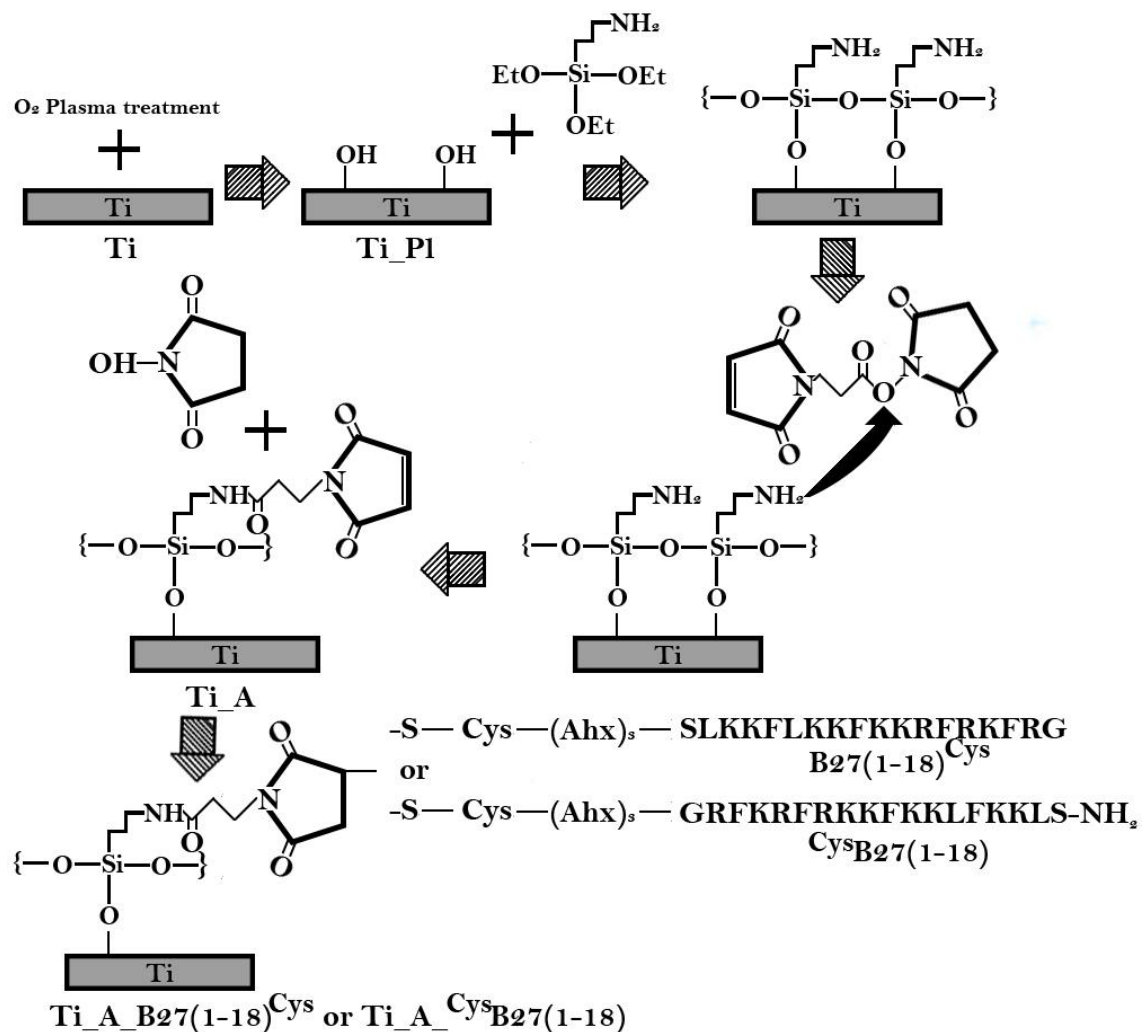
Figure 5.1. *Schematic representation of covalent anchoring of* B27(1-18)[Cys] *or* [Cys]B27(1-18) *to titanium by maleimide-thiol chemistry. NB: the amino acid sequence of* B27(1-18)[Cys] *is written backwards and it does not represent a retro analogue.*

5.2.1. Physicochemical characterization of titanium samples

To verify whether Ti functionalization occurred properly, Ti samples were characterized by static contact angle (CA) measurements and XPS essentially as described in *chapter 3*. CA analysis revealed considerable modifications in wettability as a result of each treatment (Ti_Pl *vs.* Ti; Ti_A *vs.* Ti_Pl; Ti_A *vs.* Ti_A_B27(1-18)[Cys] and Ti_A *vs* Ti_A_[Cys]B27(1-18)) (*Figure 5.2.*). Based on these findings, which are in line with previous reports[10,11], we can reasonably deduce that the expected modifications have taken place. In addition, another important observation was the absence of any significant difference in wettability between Ti samples functionalized with B27(1-18)[Cys] and [Cys]B27(1-18).
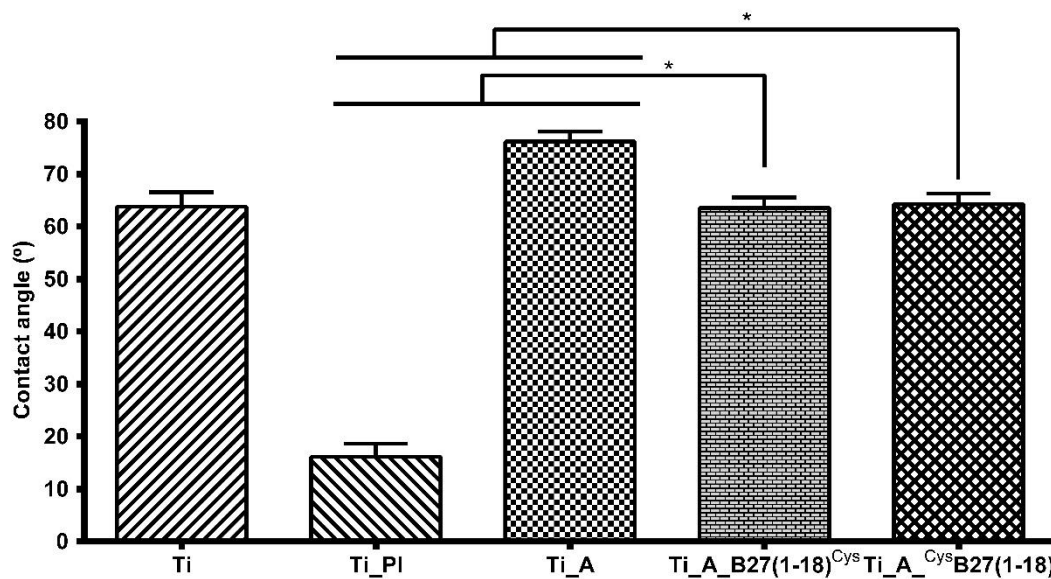
Figure 5.2. *Average values of contact angles of the indicated Ti samples in duplicate. The experiment was performed two times. Asterisks denote statistically significant differences between the indicated samples (P < 0.05).*

The XPS spectra (data not shown) gave similar results, with an equal increment in carbon (C 1s) and nitrogen (N 1s) contents, along with reduction of oxygen (O 1s) and titanium (Ti 2p) percentages in Ti_A_B27(1-18)^{Cys} and Ti_A_^{Cys}B27(1-18) respect to Ti_A and Ti samples, indicating stable binding of peptide molecules to titanium.

5.2.2. Analysis of antimicrobial properties of titanium samples

The antimicrobial efficacy was analysed as explained in **chapter 3**, testing first the inhibition of bacterial adhesion. Ti samples were immersed in a suspension of *S. epidermidis* for 2 h at 37°C, then planktonic cells were rinsed away and adherent bacteria recovered by vortexing and plating on solid medium. The colony forming units (CFU) of *S. epidermidis* on Ti_A_B27(1-18)^{Cys} and Ti_A_^{Cys}B27(1-18) disks were remarkably less than those recovered from bare Ti, and also respect to Ti_A, without significant difference between N- or C-terminally immobilized peptides (**Figure 5.3.**). These results would suggest that bacteria have been killed upon contact with the bio-functionalized titanium, regardless of peptide orientation.
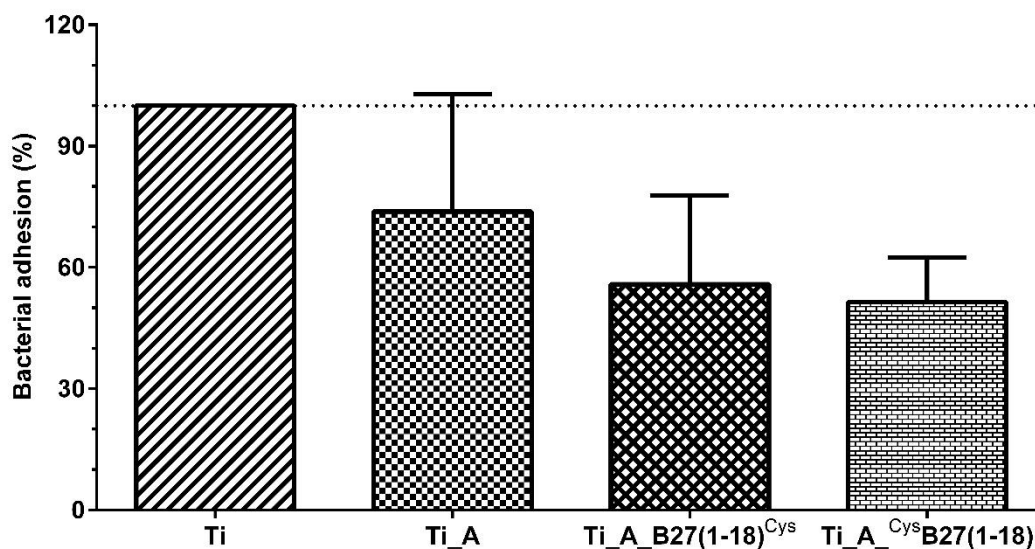
Figure 5.3. *Adhesion of S. epidermidis to the indicated Ti samples. Following 2 h incubation at 37 °C, the CFUs of adherent microorganisms were recovered by a vortexing procedure, serial dilutions and plating on solid medium. Results are expressed as percent CFU respect to CFU recovered from bare titanium (Ti) and are the means ± SD of at least three independent experiments performed in triplicate.*

To better understand the events occurring during staphylococcal adhesion, in parallel to CFU determination, the morphology of adhered bacteria was studied by SEM. This analysis revealed remarkable differences in the morphology of *S. epidermidis* cells on the different substrata (***Figures 5.4.1. – 5.4.2.***).

S. epidermidis cells on Ti and Ti_A samples had normal round shape, with smooth surface and evident division septa (***Figure 5.4.1.F***). Microorganisms in division phase were frequently observed, often forming multilayer agglomerates (***Figure 5.4.1.A, B***), covered by a dense and grey layer resembling a blanket (***Figure 5.4.1.C – E***). In these clusters bacteria were tightly connected by junctions (***Figure 5.4.1.C, 5.4.1.E and 5.4.1.F***). At the contact interface between bacterial and Ti surface a halo (***Figure 5.4.1.D***) and fimbriae-like surface appendages were observed (***Figure 5.4.1.E – F***). These structures, likely representing extracellular matrix components, together with the formation of multilayers with tightly interconnected individual cells firmly attached to titanium surface by adhesion structures, indicate early biofilm formation[12–14]. Taking into consideration the well-known biofilm properties of *S. epidermidis* ATCC 35984, a recognized heavy matrix producer[15,16], the morphological characteristics of titanium attached bacteria observed by SEM are in line with the literature. The morphological differences between *S. epidermidis* attached to bare Ti (***Figure 5.4.1.A, 5.4.1.C and***

5.4.1.E*)** and those attached to silanized Ti disks were not significant (Figure 5.4.1.B,***
5.4.1.D *and **5.4.1.F***).
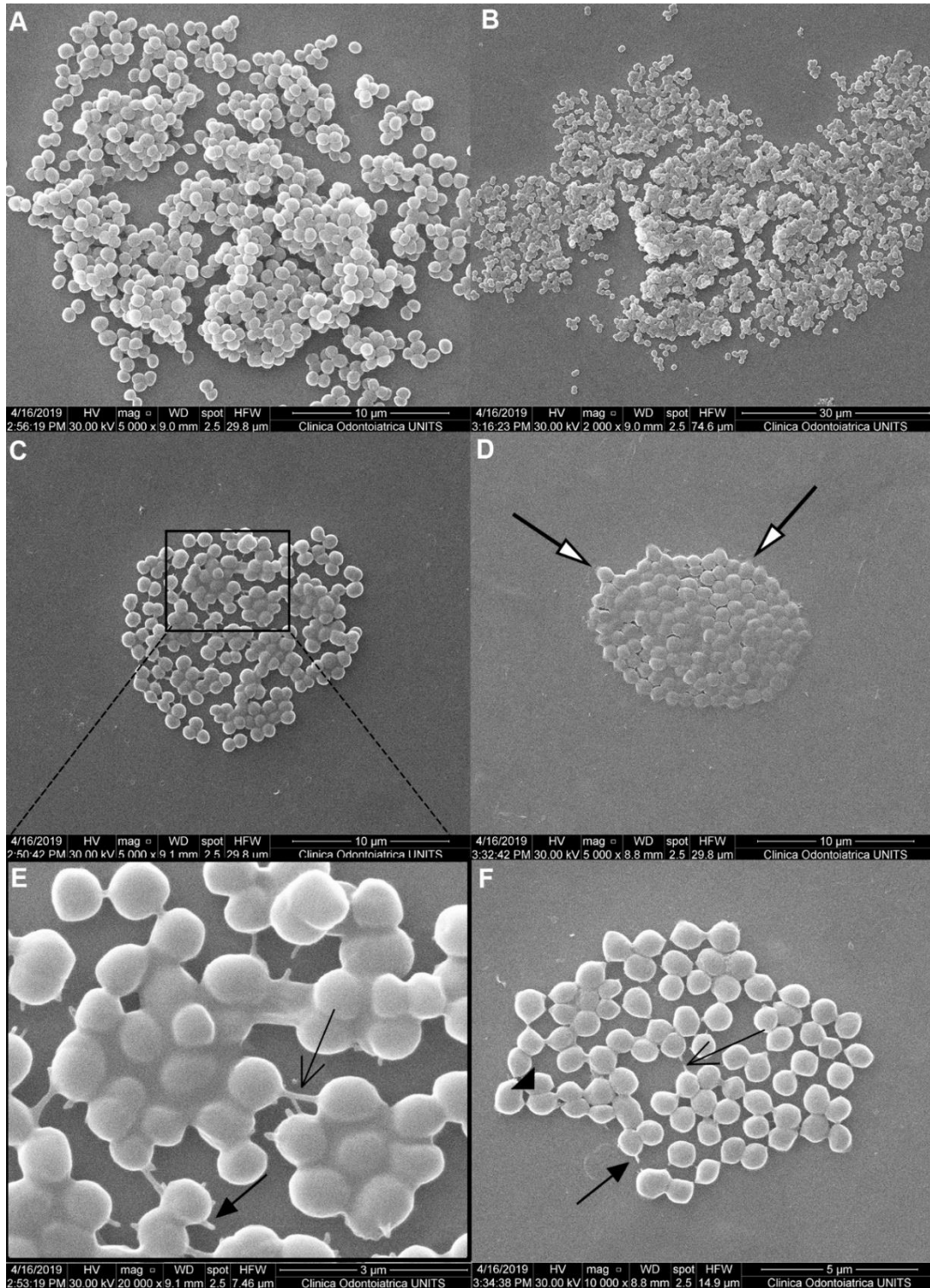
Figure 5.4.1. *Morphology of S. epidermidis on Ti (Panels A, C, E) and Ti_A (Panels B, D, F) samples*
analysed by SEM. Upon 2 h incubation all samples were rinsed, fixed and processed for SEM analysis.
Panel E is a higher magnification of the image presented in Panel C. Arrows indicate division septa (▲),
halos (⇑), contact junctions (↑), pseudopod-like structures (↑). Representative images from two
experiments performed in duplicate are shown.

On the contrary, a lower number of intact *S. epidermidis* cells were attached to Ti_A_B27(1-18)[Cys] and Ti_A_[Cys]B27(1-18) samples (***Figure 5.4.2.***). Instead of typical biofilm structures, remains of dead cells were observed on both types of peptide-functionalized titanium samples (***Figure 5.4.2.B – D***). On Ti_A_[Cys]B27(1-18) samples it was also possible to note structures with ragged surface, probably extruded cytoplasmic material from dead cells, near intact bacterial cells (***Figure 5.4.2.E***), and in other fields, dead *S. epidermidis* cells appeared collapsed, with dramatically affected morphology (***Figure 5.4.2.F***).

Collectively, based on SEM analysis and CFU counts we can reasonably deduce that immobilized BMAP27(1-18), regardless of its orientation on metal surfaces, was able to kill *S. epidermidis*, although SEM images do not add a clear-cut information on possible different effects between the two analogues. Concerning contact killing, our observations are in line with previous findings reported in ***chapter 3***, while concerning orientation-dependent activity, the lack of a significant difference between the N- and C-terminally immobilized peptides appears in contrast with the literature[3,8,17–19]. Some authors suggest that the antimicrobial efficacy of tethered peptides could be affected by the position of cationic and hydrophobic residues[8,20,21]. In particular, in a study involving the sheep cathelicidin SMAP-29, an alfa-helical peptide highly similar to BMAP-27 [22], Soares *et al.* registered remarkably better antimicrobial activity with the peptide immobilized *via* its C-terminus[19]. A comparative analysis of the amino acid sequences of BMAP27(1-18) and of the AMPs studied by others can help explain these apparent discrepancies. In comparison to SMAP-29, BMAP27(1-18) lacks the C-terminal hydrophobic tail[23], and the 1-18 segment of BMAP-27, containing 10 cationic residues (3 Arg and 7 Lys), results in a highly cationic sequence. Moreover, the first amino acid of SMAP-29 is an Arginine, followed by a Glycine residue, whereas the same amino acids are present at inverted positions (GR instead of RG)[22,23] in BMAP-27, as well as in BMAP27(1-18). This could at least partly explain why masking of the N-terminal Arg upon tethering of SMAP-29 *via* its N-terminus resulted in decreased activity, whereas killing ability of BMAP27(1-18) seemed not much affected by tethering orientation. An additional evidence that antimicrobial activity of BMAP-27 is relatively independent on anchoring position was provided by Rapsch *et al.*[24]. In that study the full length BMAP-

27 was randomly immobilized on glass surface by utilizing various chemistries exploiting its amino groups, without any spacer, and the immobilized peptide was active against *E. coli.* In this respect it is important to note that in our hands, N-terminally biotinylated BMAP-27 and BMAP27(1-18), immobilized on streptavidin resin beads, proved bactericidal to a similar extent against two *Staphylococcus* spp[9]. In comparison with melittin[3] or with Dhvar5 peptide[17], the cationic groups of BMAP27(1-18) are evenly distributed along the peptide sequence, being cationic residues regularly interspersed with hydrophobic ones. Hence, its amphipathicity is conformation-dependent, at difference with melittin and Dhvar5, both characterized by sequence-dependent amphipathicity with hydrophobic and cationic residues segregated at the N-terminus and the C-terminus, respectively. In both cases tethering orientation affected the activity of the immobilized peptides, but with opposite results. C-terminally immobilized melittin was more active respect to the N-terminally anchored peptide[3], whereas C-terminally immobilized Dhvar5 was less effective than the N-terminally linked analogue[17]. This means that besides structural features such as amino acid sequence, conformation, and amphipaticity, there are other variables to be considered when analysing the peptide efficacy in the immobilized state. In this respect, researchers of the field agree on the necessity to elucidate the antimicrobial mode of action of surface immobilized AMPs.
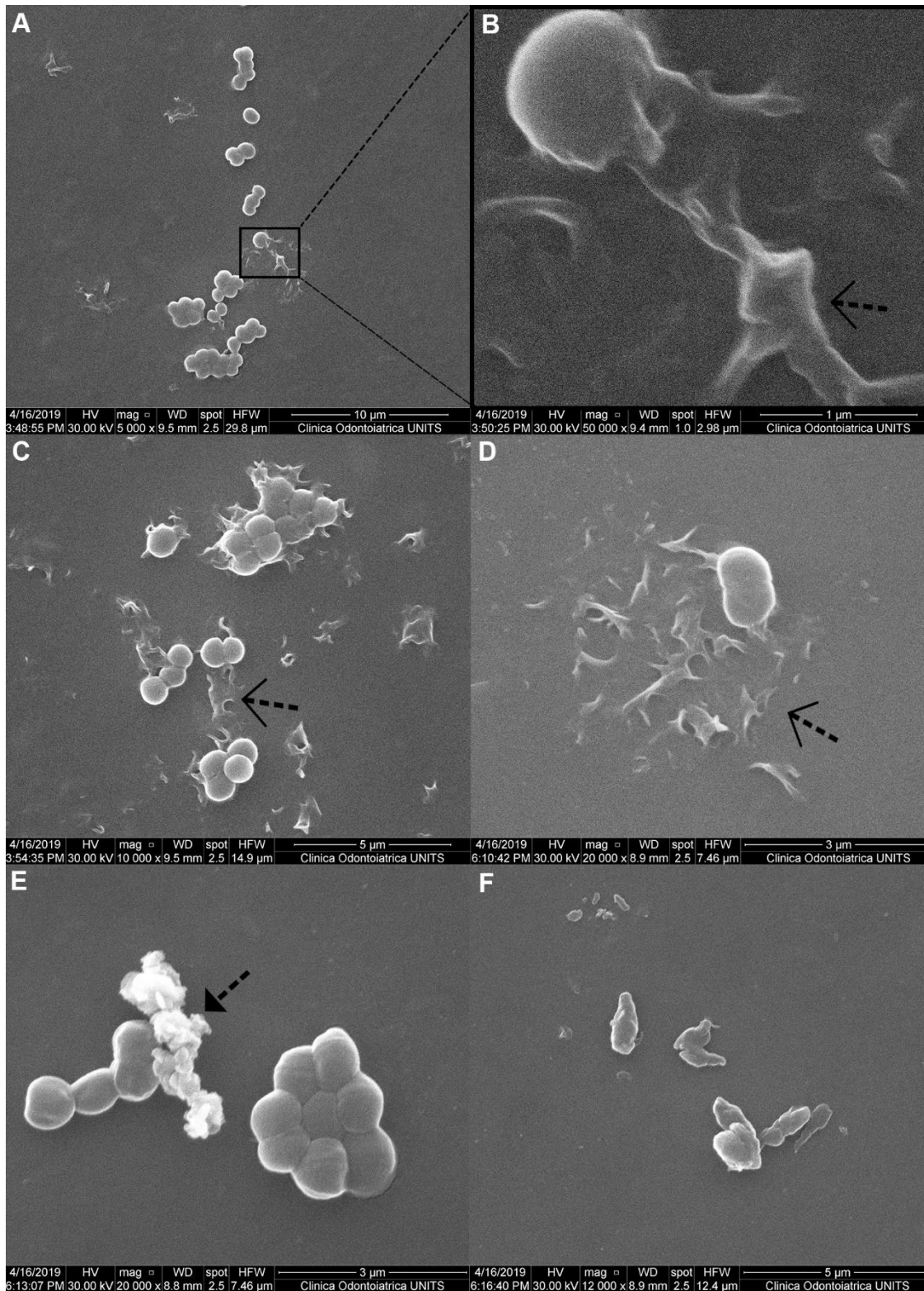
Figure 5.4.2. *Morphology of S. epidermidis on Ti_A_B27(1-18)* [Cys] *(Panels A-C) and Ti_A_* [Cys] *B27(1-18) (Panels D-F) samples analysed by SEM. Upon 2 h incubation all samples were rinsed, fixed and processed for SEM analysis. Panel B is a higher magnification of the image presented in Panel A. Arrows indicate extruded cytoplasmic material (↑), dead bacteria residues (↑). Representative images from two experiments performed in duplicate are shown.*

5.2.3. Mode of action studies of free and anchored B27(1-18)

To address this issue we applied the fluorescence-based assay developed in **Chapter 4**. We were interested in particular whether a membrane-active peptide such as BMAP27(1-18), when immobilized on solid support, retained its capacity to interact with the cytoplasmic membrane of target microorganisms. In order to compare the membrane-perturbing ability of free and anchored BMAP27(1-18), we needed to keep both peptide forms in solution and to know their respective concentrations. To meet both requirements we decided to use a streptavidin/biotin-based anchoring method applied to an agarose-based commercial resin.
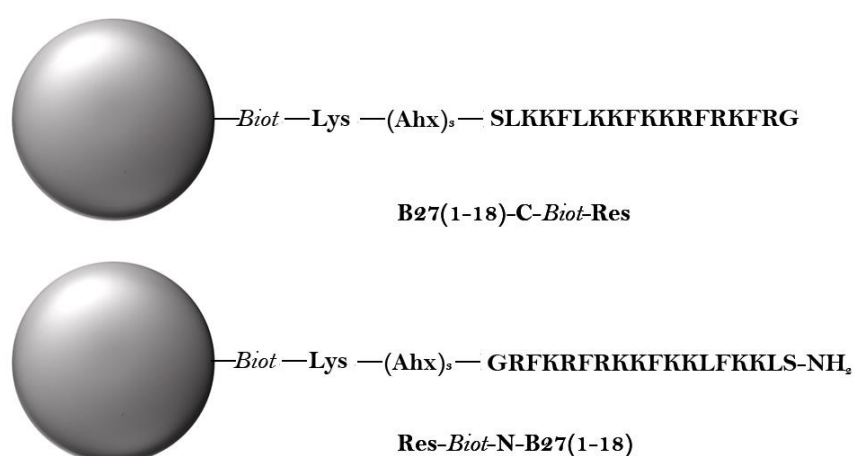
Figure 5.5. Coupling of B27(1-18)-C-Biot and Biot-N-B27(1-18) to Streptavidin resin beads. NB: the amino acid sequence of B27(1-18)^{Lys} is written backwards and it does not represent a retro analogue.

We synthesized two biotinylated derivatives of BMAP27(1-18) by following exactly the same scheme as for titanium bound cysteinylated peptides, with the only difference that the C- or N-terminal Cysteine was replaced by a Lysine residue for the subsequent biotinylation. These biotinylated peptides are referred to as B27(1-18)-C-*Biot* and *Biot*-N-B27(1-18) (**Figure 5.5.**). Prior to coupling to streptavidin-resin beads, the antimicrobial properties of these new derivatives have been checked against *S. aureus* and *S. epidermidis* in a standard MIC assay (**Table 5.2.**).

Table 5.2. Antimicrobial activity of soluble biotinylated peptides against two Gram-positive reference strains.

|	BMAP27(1-18)	B27(1-18)-C-Biot	Biot-N-B27(1-18)
	MIC (µM)[a,b]		
S. epidermidis ATCC 35984	2	2	2
S. aureus ATCC 25923	4	1	1

[a] Determined in MH broth.

[b] Data are means of at least 3 independent experiments.

B27(1-18)-C-*Biot* and *Biot*-N-B27(1-18) peptides maintained and slightly improved efficacy against *S. epidermidis* and *S. aureus*, respectively (**Table 5.2.**), but without differences in MIC values between them.

The two derivatives were then coupled to streptavidin-resin beads to mimic an immobilized condition but in a fluid state, suitable for the microplate fluorescence assay. In order to make quantitative pairwise comparisons between the free and anchored peptides, and between the N-terminally and C-terminally resin-coupled peptides, it was mandatory to determine peptide concentration of all samples by using the same method. To this aim, the resin-bound peptides were eluted and their concentration determined by UV absorbance at 257 nm. This information was used to normalize the concentration of anchored and free peptides in the following assays by adjusting resin volumes accordingly.

5.2.4. Interference of free and resin-bound peptides with the fluorescent dyes

To test whether the two biotinylated peptides, both free and bound to streptavidin resin beads display any interference with diSC$_3$(5) or with PI, the fluorescence of both probes, mixed together in the same wells, was monitored kinetically at their specific excitation and emission wavelengths before and after the addition of the AMPs or resins, without bacteria. The kinetics in **Figure 5.6.** show that there is no interference between dyes and peptides or resins.
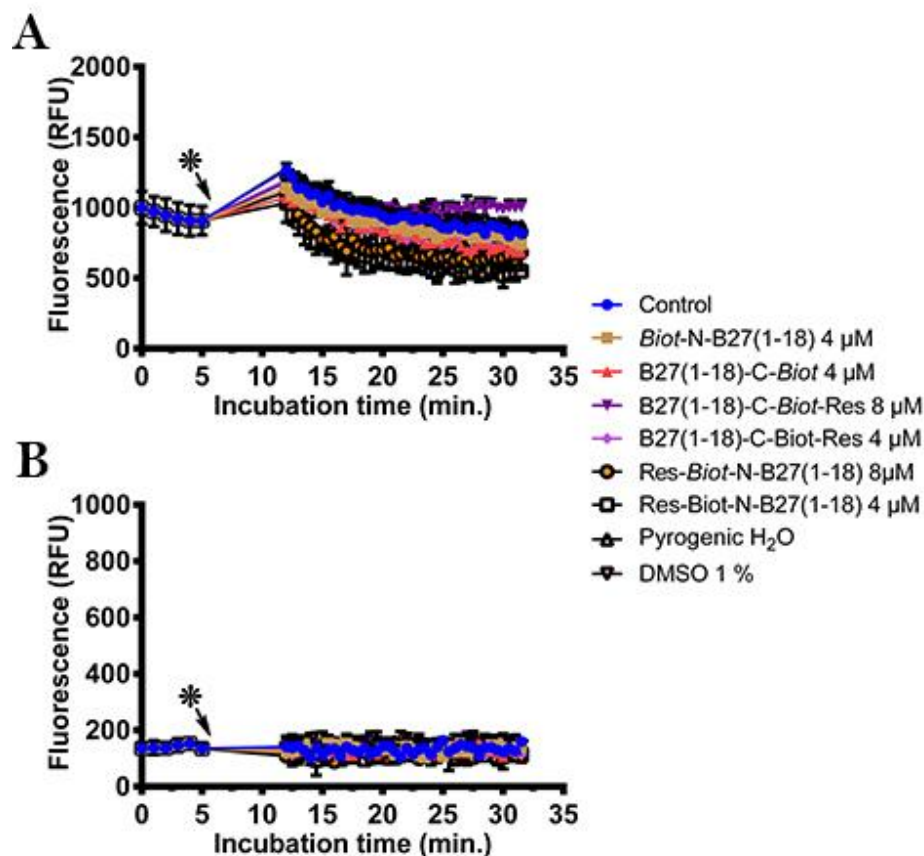
Figure 5.6. *Interference of peptides with the fluorescent dyes. The kinetics of (A) diSC$_3$(5) (λ_{ex} = 652 nm, λ_{em} = 672 nm) and (B) PI (λ_{ex} = 535 nm, λ_{em} = 617 nm) are shown in separate graphs for clarity purposes. The time necessary for the addition (indicated by an *) of peptides and resins was about 7 minutes.*

5.2.5. Correlation of membrane alterations with bactericidal activity of free peptides

In this part of my thesis, I had the dual goal to verify the membrane-perturbing ability of soluble biotinylated peptides, and to compare it with possibly different effects of C- and N-terminally anchored AMPs on whole bacteria by using the combination of the fluorescent dyes diSC$_3$(5) and PI. The experiments were first performed by incubating *S. epidermidis* ATCC 35984 with free peptides in PBS-glc containing 0.4 μM diSC$_3$(5) and 5 μg/mL PI at 37 ˚C in a low binding 96-well black microtiter plate. The fluorescence of both probes was monitored kinetically and at 30 min incubation, aliquots were taken to determine bacterial viability by CFU counts. The ion channel forming Gramicidin D was used as positive control (100% depolarization).

As expected, Gramicidin D induced increase of diSC$_3$(5), but not of PI fluorescence (**Figure 5.7.**), in line with the results reported in **chapter 4.2.4.**. On the contrary, both

free peptides (B27(1-18)-C-*Biot* and *Biot*-N-B27(1-18)) showed a picture more similar to the effects of melittin (***chapter 4.2.4.***). In fact, both peptides caused a rapid increase of both, diSC$_3$(5) and PI fluorescence, at their bactericidal concentrations (1 – 8 µM, i.e. those causing >90% killing), while at lower peptide concentrations (125 – 250 nM), that also produced lower killing, only PI showed an increment, whereas the fluorescence of diSC$_3$(5) remained at baseline level (***Figure 5.7.***). This means that the increase of diSC$_3$(5) fluorescence was rather a consequence of irreversible membrane permeabilization, which appears as the key event in the case of both peptides, and did not indicate a mechanism primarily based on membrane depolarization.
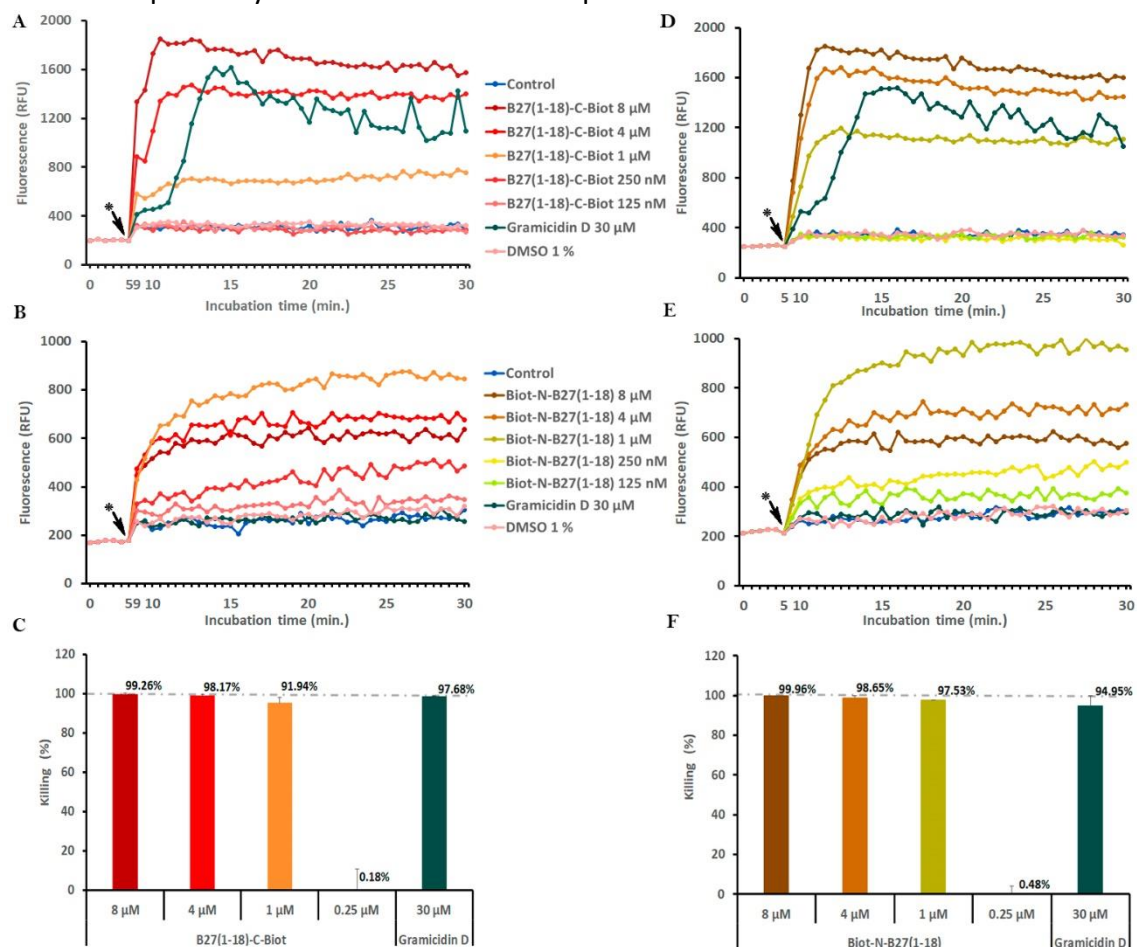
Figure 5.7. *Membrane depolarization (**A, D**), permeabilization (**B, E**) and killing (**C, F**) of S. epidermidis by B27(1-18)-C-Biot (**A – C**) and Biot-N-B27(1-18) (**D – F**). The experiments were performed with 10^8 CFU/mL in PBS-glc containing 0.4 µM diSC$_3$ (5) (λ$_{ex}$ = 652 nm, λ$_{em}$ = 672 nm) and 5 µg/mL PI (λ$_{ex}$ = 535 nm, λ$_{em}$ = 617 nm) at 37 ˚C. At 30 min incubation aliquots were taken to determine bacterial viability by CFU counts. The kinetics of diSC$_3$(5) and PI are displayed in separate graphs, and error bars are not shown for clarity purposes. (*) peptide addition.*

These results are in line with previous findings, although obtained with a different experimental approach using as target *E. coli* ML35[23], and in partial contrast with the

findings by Lee et al[25] which used the same potentiometric dye with *S. aureus* as target. According to their experiments, at difference with the full length BMAP-27, BMAP27(1-18) would not cause calcein release from large unilamellar vesicles, whereas both peptides would be equally able to depolarize whole *S. aureus*[25]. Hence, the authors concluded that BMAP27(1-18) did not act by membrane permeabilization but by membrane depolarization. Based on the findings reported in this thesis we can conclude that the increase of diSC$_3$(5) fluorescence observed by Lee et al was a consequence of bacterial membrane permeabilization induced by BMAP27(1-18). As the molecular weights of calcein (MW 622.53) and PI (MW 668.4) are very similar, it is not clear why this phenomenon could not be detected by calcein release, but we cannot exclude that for some reason BMAP27(1-18) was less able to interact with the LUVs that were used in the cited study[25].

Another interesting observation was the lack of proportionality between PI fluorescence and bactericidal peptide concentrations. At difference with melittin that caused a dose-dependent increase of PI uptake (see previous chapter), 1 μM BMAP27(1-18) produced higher increment of PI fluorescence than 4 μM and 8 μM, while the increase of diSC$_3$(5) fluorescence observed at these peptide concentrations was dose-dependent. As all these concentrations were highly bactericidal, one can argue that when membrane damage is extensive, highly cationic peptide molecules bind to bacterial DNA thus displacing PI.

Notably, by investigating the membrane-perturbing ability of BMAP-27-derived peptides we validated the fluorescence-based microplate assay, developed in ***chapter 4,*** that allowed us to obtain some mechanistic insights concerning the interaction of these peptides with whole bacterial cells.

5.2.6. Correlation of membrane alterations with bactericidal activity of resin-bound peptides

Due to relatively low peptide loading on resin, the fluorescence assay developed in the previous chapter was adapted to a lower bacterial concentration, i.e. 10^7 CFU/mL instead of 10^8 CFU/mL. As reported in ***chapter 4***, this bacterial density, though not sufficient to detect PI uptake, is still sufficient to detect fluorescence of diSC$_3$(5).

Knowing from the previous paragraph that the fluorescence of diSC$_3$(5) increased in a dose-dependent manner at bactericidal peptide concentrations, we were confident that the assay was suitable for resin-bound peptides. To study the mode of action of immobilized B27(1-18)-C-*Biot* and *Biot*-N-B27(1-18), the assay was performed by adding free peptides or their corresponding resin equivalents to 10^7 CFU/mL *S. epidermidis* in PBS-glc containing 0.4 µM diSC$_3$(5) in a black microtiter plate. Gramicidin D was the positive control (***Figure 5.8***). Aliquots were withdrawn at 30 min incubation to determine bacterial viability.
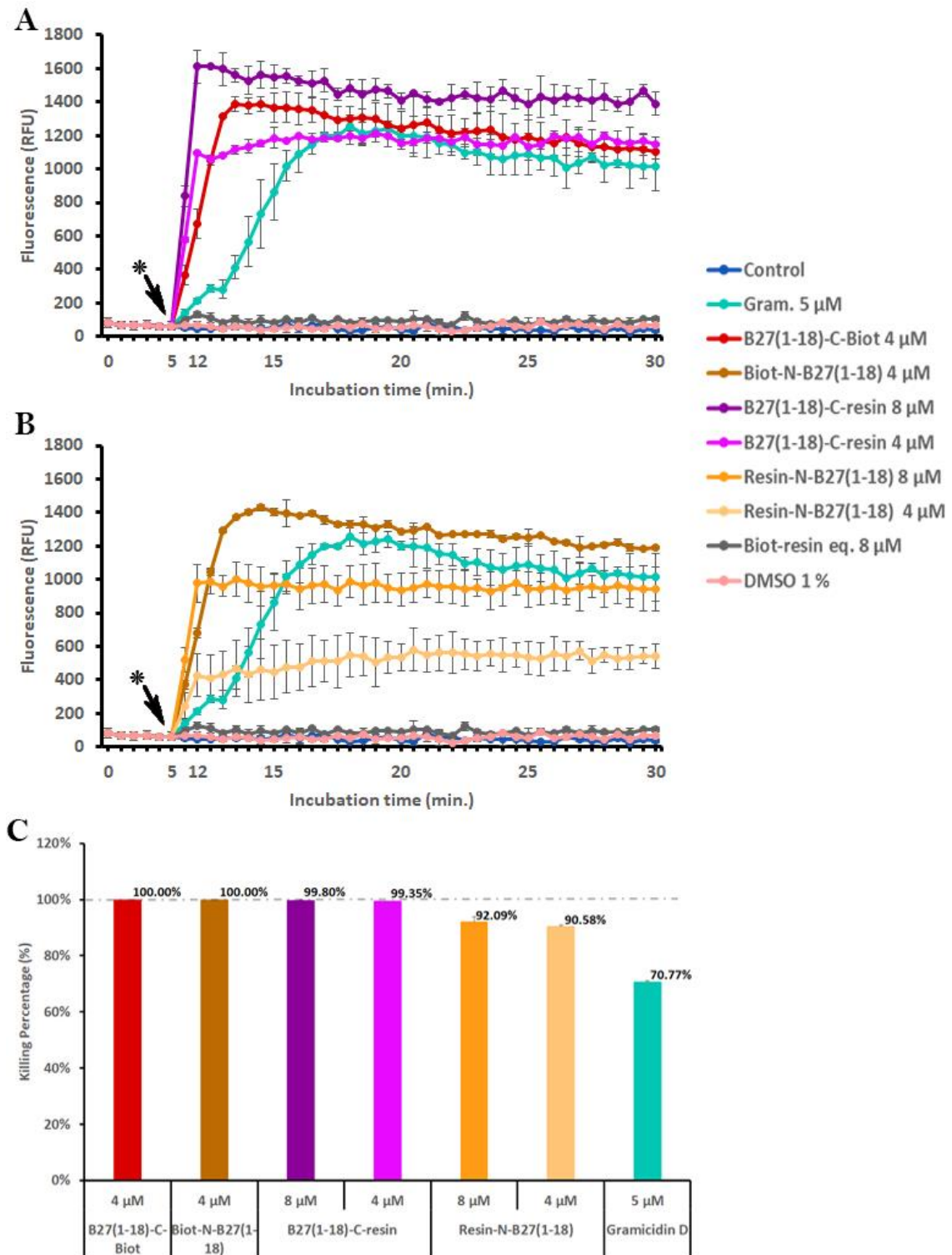
*Figure 5.8. Membrane depolarization (**A, B**) and Killing (**C**) of S. epidermidis caused by free and resin-bound B27(1-18)-C-Biot and Biot-N-B27(1-18). The experiments were performed with 10^7 CFU/mL in PBS-glc containing 0.4 µM diSC$_3$ (5) (λ_{ex} = 652 nm, λ_{em} = 672 nm) at 37 ˚C. At 30 min incubation aliquots were taken to determine bacterial viability by CFU counts. The membrane depolarization caused by each of the two peptides is displayed in separate graphs (**A** and **B**) for clarity purposes. (*) peptide or resin addition.*

As expected, 4 µM free B27(1-18)-C-*Biot* and *Biot*-N-B27(1-18) showed the same behaviour by promoting a rapid increase of diSC$_3$(5), correlated to 100% killing (***Figure 5.8.***). On the contrary, at an equivalent peptide concentration the resin-bound peptides showed a distinct behaviour with the C-terminally immobilized peptide more active than the N-terminal counterpart. This difference was even more evident when the resin amounts were increased to 8 µM peptide concentration equivalents. In fact, B27(1-18)-C-resin, at concentrations equivalent to 4 and 8 µM free peptide, promoted a dose-related increase of diSC$_3$(5) fluorescence, correlated to a killing activity higher than 99% (***Figure 5.8.A, C***). On the other hand, both resin-N-B27(1-18) concentrations (corresponding to the same 4 and 8 µM free peptide), caused a remarkably lower diSC$_3$(5) fluorescence, which was nevertheless associated with >90% killing (***Figure 5.8.B, C***).

Interestingly, both peptides coupled to resin beads showed kinetics of diSC$_3$(5) release similar to those caused by melittin (***chapter 4, Figure 4.9.***), where at low concentrations the diSC$_3$(5) increment reached approximately ≈20% of the maximum fluorescence. This type of kinetics was completely different from that observed with Gramicidin D where, at all concentrations, the diSC$_3$(5) fluorescence always reached the maximum, although with less steep curves (***chapter 4, Figure 4.8.***). Hence, we can deduce that both peptides in the anchored state acted by permeabilization of the bacterial cell membrane, like the free B27(1-18)-C-*Biot* and *Biot*-N-B27(1-18) peptides. It remains to be established why the N-terminally bound peptide was less efficient than the C-terminal one.

5.2.7. SEM analysis of membrane alterations induced by free and resin-bound peptides

To shed light on the events that took place at the staphylococcal surface during mode of action studies, the bacteria morphology was analysed by SEM. We were curious to see possible differences in the morphology of *S. epidermidis* upon treatment with free and resin-bound peptides (***Figures 5.9.1. – 5.9.6.***). Biotinylated streptavidin-resin beads were used as negative controls (***Figure 5.9.1.***).

Untreated *S. epidermidis* cells and those put in contact with the control resin had normal appearance. Bacteria were opaque, round in shape, with smooth surface and

with clearly evident division septa (*Figure 5.9.1.B − C* and *F*). Bacteria exhibited the expected size, with an average diameter value around 0.8 µm, clearly and easily distinguishable from resin beads. Bacteria formed clusters throughout the filter extension, also on the surface of biotinylated streptavidin resin beads (*Figure 5.9.1.*). As dividing bacteria were frequently observed, this means that bacteria were viable and growing (*Figure 5.9.1.*). Of course, as the assay was performed in solution, typical biofilm structures (as those visualized in *chapter 3*) were not observed.
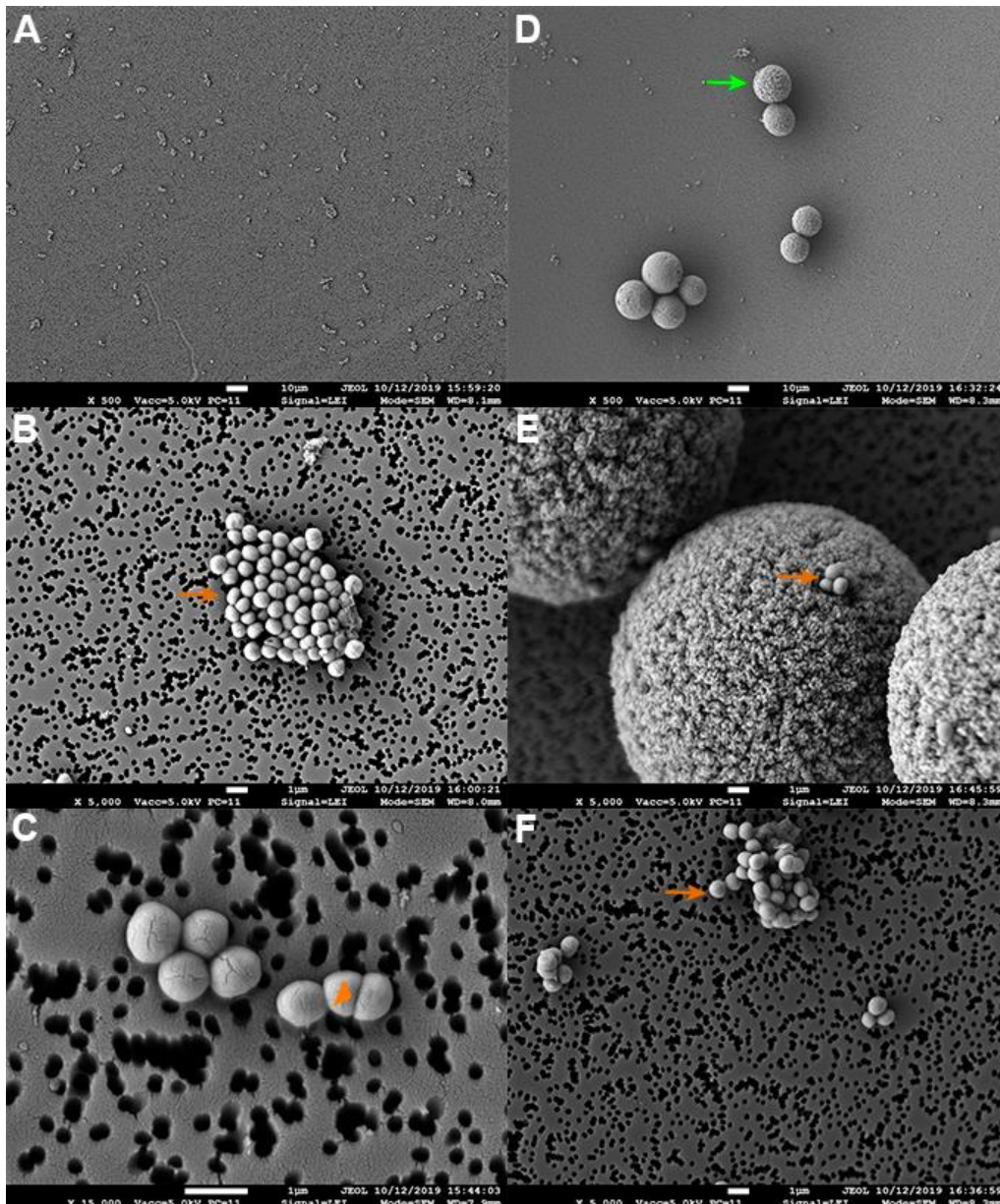
Figure 5.9.1. Morphology of untreated S. epidermidis on polycarbonate filters analysed by SEM in the absence (Panels A − C) and in the presence of biotinylated streptavidin resin beads (Panels D − F). Arrows indicate, respectively, resin beads ( ), division septa ( ), bacterial aggregates ( ). Representative images from two experiments performed in duplicate are shown.

In contrast, the filters containing *S. epidermidis* treated with free biotinylated peptides presented a lower number of bacteria with some agglomerates and many *S. epidermidis* cells were dramatically affected (***Figure 5.9.2. and 5.9.3.***). In some cases dead bacteria appeared swelled, without division septa, and in others were collapsed, deflated and appeared to merge into the filter (***Figure 5.9.2.D – F and I***). In numerous cases, a mix of live and dead bacteria in the same cluster were observed, appearing as a big amorphous mass deposited on filter (***Figure 5.9.2.C***). Moreover, some bacteria appeared collapsed with extrusion of cytoplasmic material out of the cell (***Figure 5.9.2.G – H***).
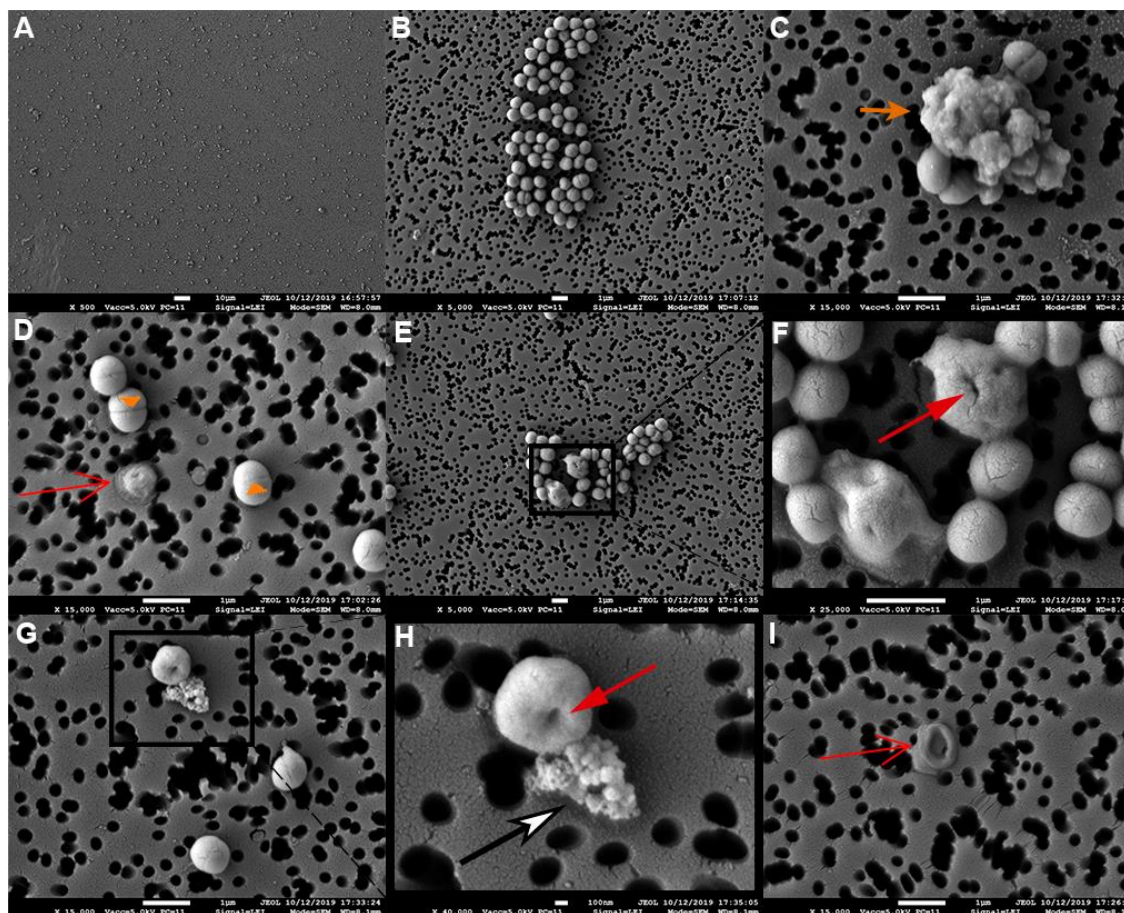
Figure 5.9.2. *Morphology of S. epidermidis treated with B27(1-18)-C-Biot on polycarbonate filters analysed by SEM (Panels A – I). Panels F and H show a higher magnification of images presented in Panels E and G, respectively. Arrows indicate, respectively, division septa (▸), bacterial aggregates (↑), extruded cytoplasmic material (↑), collapsed bacteria (↑), deflated bag (↑). Representative images from two experiments performed in duplicate are shown.*

On the filters presenting *S. epidermidis* treated with *Biot*-N-B27(1-18) peptide, bacteria with their division septa (***Figure 5.9.3.D***), and sometimes microorganisms with

a perfect appearance near a big mass of extruded cytoplasmic material were visualized (***Figure 5.9.3.D***). Moreover, a high number of agglomerates containing live bacteria and residues of bacterial cell membranes (***Figure 5.9.3.C***), and in many cases dead elongated bacteria (***Figure 5.9.3.E − F***) were observed, surrounded by an amorphous material (***Figure 5.9.3.E***), probably extruded cytoplasmic content. These modifications in morphology went in parallel with the reduction in CFUs and, together with the increment of PI fluorescence also at low peptide concentrations, demonstrate that BMAP27(1-18) in solution induces membrane permeabilization of bacteria in a similar way to melittin. Moreover, there are some differences that may be important to emphasize: *S. epidermidis* treated with B27(1-18)-C-*Biot* showed many bacteria collapsed with extrusion of cytoplasmic material; bacteria treated with *Biot*-N-B27(1-18) displayed numerous dead elongated bacteria which in some cases were surrounded by an amorphous material.
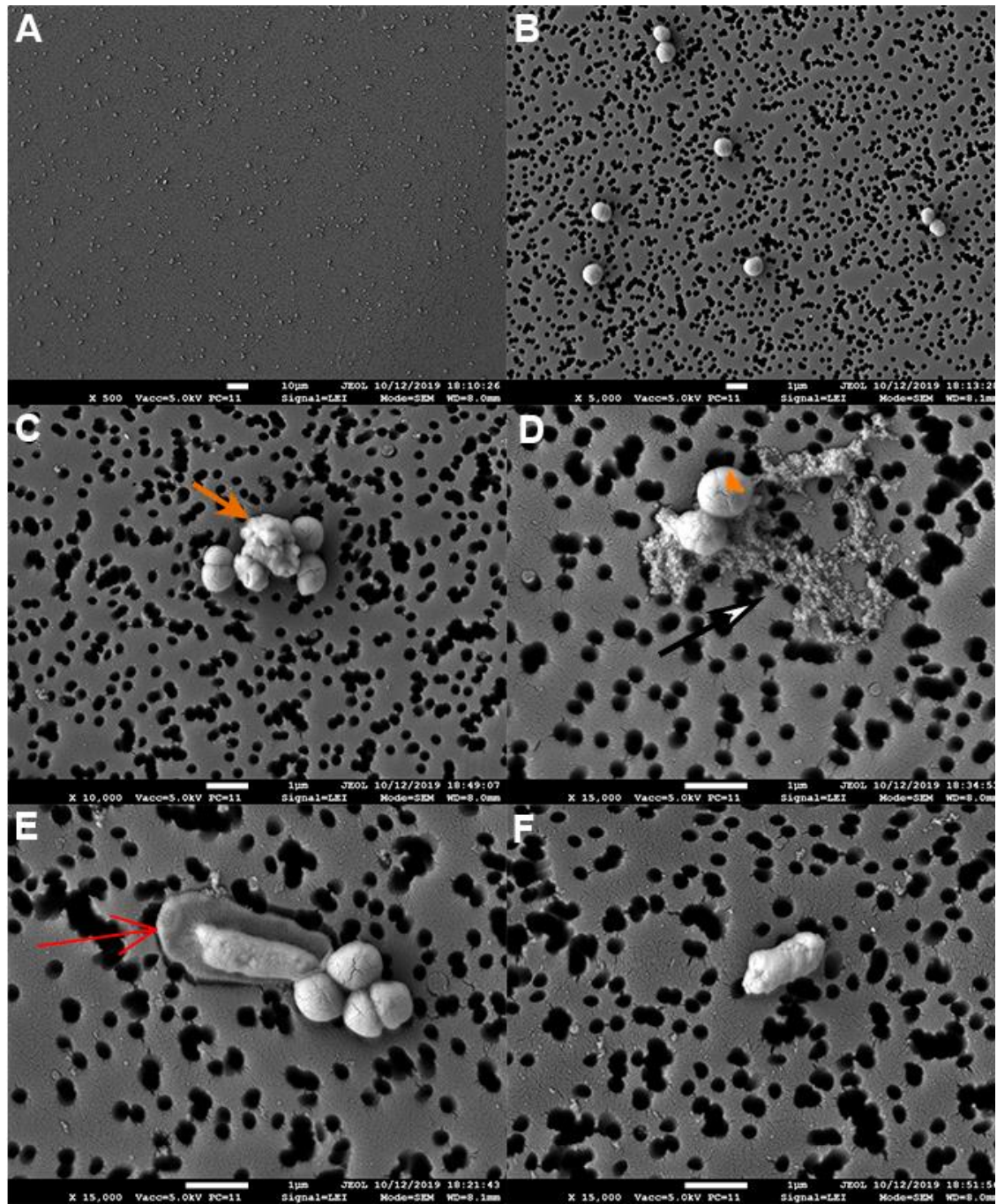
Figure 5.9.3. Morphology of S. epidermidis treated with Biot-N-B27(1-18) on polycarbonate filters analysed by SEM (Panels A – F). Arrows indicate, respectively, division septa (▶), bacterial aggregates (↑), extruded cytoplasmic material (↑), collapsed bacteria (↑). Representative images from two experiments performed in duplicate are shown.

On the other hand, when both peptides (B27(1-18)-C-*Biot* and *Biot*-N-B27(1-18)) were attached to streptavidin resin beads, a reduced number of *S. epidermidis* cells with some clusters and many morphologically modified bacteria were observed (**Figure 5.9.4. and 5.9.5.**). On the filters containing bacteria treated with B27(1-18)-C-*Biot*-Res, a

cluster of big balls corresponding to resin were observed (**Figure 5.9.4.A**), some of them carried on surface a mix of live and dead bacterial aggregates (**Figure 5.9.4.D**) and collapsed bacteria (**Figure 5.9.4.G**). Near to these beads, accumulation of *S. epidermidis* residues and dead elongated bacteria surrounded by an amorphous material were observed (**Figure 5.9.4.E – F**) similar to the deflated bag observed by *Biot*-N-B27(1-18) peptide treatment (**Figure 5.9.3.E – F**). However, in most of the cases *S. epidermidis* appeared collapsed on resin surface (**Figure 5.9.4.G**) and on the filters (**Figure 5.9.4.H – I**), with extrusion of cytoplasmic material out of the cell (**Figure 5.9.4.I**).
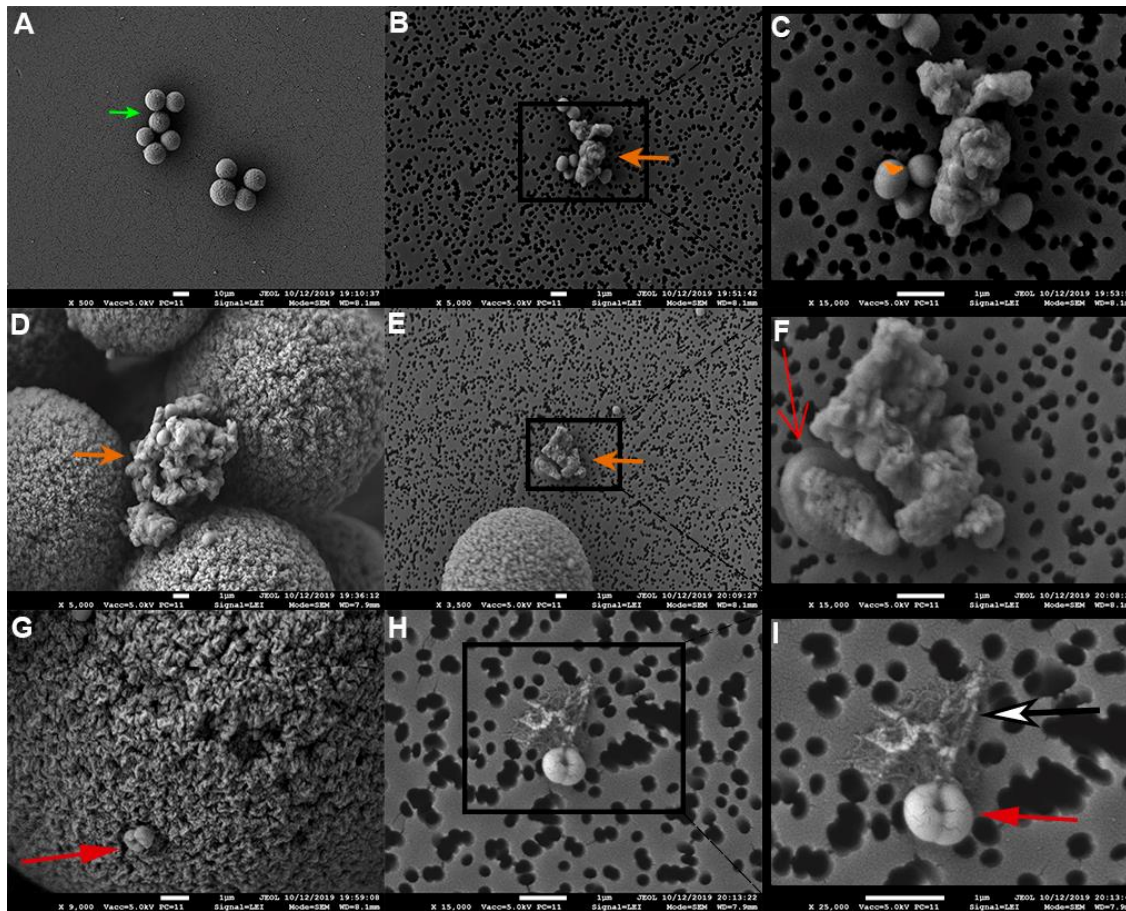
Figure 5.9.4. Morphology of S. epidermidis treated with B27(1-18)-C-Biot-Res on polycarbonate filters analysed by SEM (Panels A – I). Panels C, F and I show a higher magnification of images presented in Panels B, E and H, respectively. Arrows indicate, respectively, resin beads ($\uparrow$), division septa ($\blacktriangleright$), bacterial aggregates ($\uparrow$), collapsed bacteria ($\uparrow$), extruded cytoplasmic material ($\uparrow$), collapsed bacteria 2 ($\uparrow$). Representative images from two experiments performed in duplicate are shown.

The filters containing bacteria treated with Res-N-*Biot*-B27(1-18) also presented many clusters of big balls corresponding to resin beads (***Figure 5.9.5.A***). Besides bacteria with normal morphology with well-defined division septa, some agglomerates of collapsed bacteria or with cytoplasmic material were visible (***Figure 5.9.5.B***). In addition,
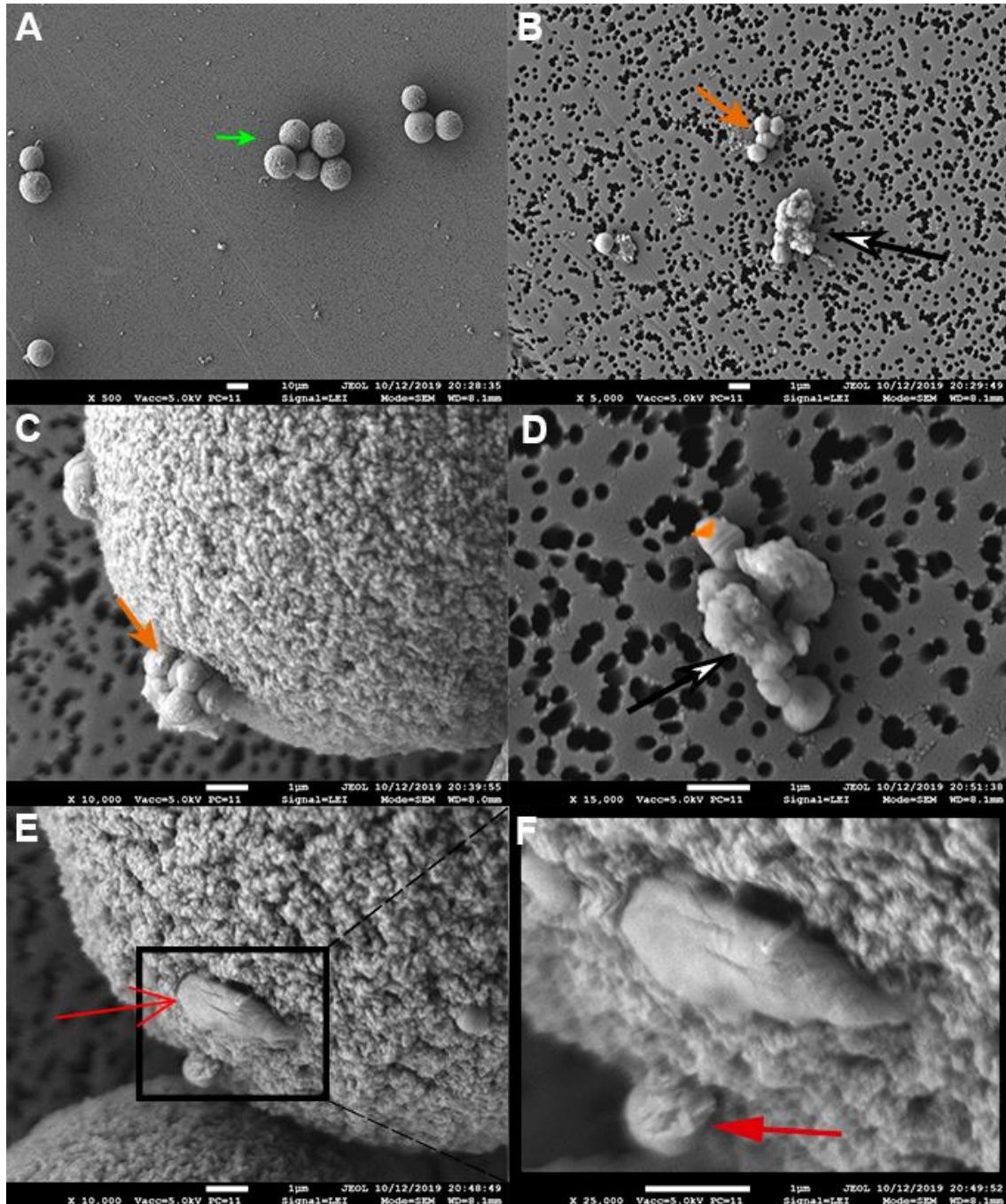
Figure 5.9.5. *Morphology of S. epidermidis treated with Res-Biot-N-B27(1-18) on polycarbonate filters analysed by SEM (Panels A – F). Panel F is a higher magnification of the image presented in Panel E. Arrows indicate, respectively, resin beads (↑), division septa (▶), bacterial aggregates (↑), extruded cytoplasmic material (⇑), deflated bag (↑) and collapsed bacteria (↑). Representative images from two experiments performed in duplicate are shown.*

the surface of many resin beads brought bacterial aggregates with blebs (*Figure 5.9.5.C*) and dead elongated bacteria (*Figure 5.9.5.E – F*). Close to these beads, accumulation of bacterial residues (*Figure 5.9.5.B*) and aggregates of live and dead bacteria were observed (*Figure 5.9.5.D*).

These marked changes in bacterial morphology indicated that *S. epidermidis* viability was strongly affected. However, the "deflated bag" morphology, in the absence of visible surface damage as for example blebs or holes[22], would suggests the digestion of *S. epidermidis* content occurred from inside, probably upon activation of autolytic enzymes[26].

5.3. Conclusions

- The antimicrobial assays showed that the adhesion of *S. epidermidis* to peptide-functionalized titanium samples was remarkably inhibited respect to bare titanium, suggesting effective coupling of B27(1-18)^{Cys} and ^{Cys}B27(1-18) on to the metal surface.

- The antimicrobial efficacy of titanium-immobilized B27(1-18)^{Cys} or ^{Cys}B27(1-18) was very similar. This is probably due to the uniform charge distribution along the peptide sequence, with cationic residues regularly interspersed with those hydrophobic.

- Titanium attached peptides induced remarkable modifications in bacterial morphology, as observed by SEM, supporting a contact-killing action by the immobilized AMP and opening the question concerning its mode of action in the immobilized state.

- To address the mode of action issue, biotinylated peptide derivatives were coupled to streptavidin resin beads as a model support. The biotin-streptavidin bond, though not covalent, is strong and stable for months if the resins are kept at 4 °C in sterile condition.

- As assessed by the fluorescence measurements, the mode of action of free B27(1-18)-C-*Biot* and *Biot*-N-B27(1-18) peptides is implemented by membrane permeabilization similar to what observed with melittin.

- Both resin-immobilized peptides killed *S. epidermidis* by membrane permeabilization similar to what observed with their free counterparts, with the C-terminally immobilized peptide showing better efficacy respect to the N-terminal analogue.

- SEM analysis revealed remarkable changes in morphology of bacteria treated with the biotinylated peptides free in solution and attached to streptavidin resin beads.

5.4. Experimental procedure

5.4.1. Peptide synthesis and characterization

The peptides (B27(1-18)^{Cys} and ^{Cys}B27(1-18)) used for coating of titanium were purchased from NovoPro (Shangai, China). The two biotinylated peptides were synthesized on a Biotage Initiator+ microwave-assisted automated peptide synthesizer using Fmoc-chemistry, essentially as described in **Chapter 3**. All the corresponding amino acid sequences are illustrated in **Table 5.3**. The sequence of BMAP27(1-18) was modified either at the C-terminus or at the N-terminus by addition of three units of 6-aminohexanoic acid (Ahx), similar to what described in **Chapter 3**, and a Cysteine residue to introduce an –SH anchoring group, or a Lysine residue for biotinylation (**Table 5.3.**).

Table 5.3. *Peptide sequences of the AMP derivatives used in this study.*

Peptide	Sequence
B27(1-18)^{Cys}	GRFKRFRKKFKKLFKKLS-(Ahx)$_3$-Cys
^{Cys}B27(1-18)	Cys-(Ahx)$_3$-GRFKRFRKKFKKLFKKLS-NH$_2$
B27(1-18)^{Lys}	GRFKRFRKKFKKLFKKLS-(Ahx)$_3$-Lys
^{Lys}B27(1-18)	Lys-(Ahx)$_3$-GRFKRFRKKFKKLFKKLS-NH$_2$

Biotinylation was performed off-line by coupling 5 equivalents of D(+)-biotin to the fully protected resin-bound peptides in the presence of equimolar 2-(1H-benzotriazole-1-yl)-1,1,3,3-tetramethylaminium tetrafluoroborate (TBTU) and 1H-hydroxybenzotriazole (HOBt) in N,N-dimethylformamide (DMF) containing 0.6 N N-methylmorpholine for 4h at room temperature. The reaction completion was monitored by the Kaiser test[27]. After cleavage and deprotection, the peptides have been purified by reverse phase high performance liquid chromatography (RP-HPLC) on a C18 Delta-Pak column (Waters; USA) and confirmed by mass spectrometry using a Q-STAR hybrid quadrupole time-of-flight mass spectrometer (Applied Biosystems/MDS Sciex, Concord, ON, Canada) equipped with an electrospray ion source. The biotinylated peptides are referred to as B27(1-18)-C-*Biot* and *Biot*-N-B27(1-18). Peptide concentration was determined as described in **Chapter 3**.

5.4.2. Peptide Immobilization on titanium disks

The cysteinylated B27(1-18) derivatives were coupled to titanium disks by applying exactly the same procedure used in *Chapter 3*.

5.4.3. Physicochemical Characterization of the Biofunctionalized Titanium Surfaces

This was done by Static Contact Angle Measurements and X-ray photoelectron spectroscopy as described in *Chapter 3.*

5.4.4. Immobilization of peptide onto resin beads

To this purpose, the high performance streptavidin-Sepharose® resin (GE Healthcare Life Sciences) was used. It is composed of highly cross-linked agarose beads with a mean diameter of about 30 μm, functionalized with streptavidin. It is designed for purification of biotinylated molecules and is supposed to have high binding capacity, as stated by the manufacturer. Prior to peptide immobilization, 400 μL resin aliquots were transferred in Eppendorf tubes and extensively washed three times with 1.6 mL sterile PBS by 5 min centrifugation at 300 g at room temperature, to remove the ethanol solution used for resin storage. Biotinylated peptides (*Biot*-N-B27(1-18) and B27(1-18)-C-*Biot*) were dissolved in sterile PBS at 1 mM concentration. 400 μL of each peptide solution were added to the same volume of washed resin samples and allowed to react overnight at 4˚C under agitation. As a control, a resin sample was coupled in parallel with biotin. Samples were then allowed to re-equilibrate at room temperature, centrifuged, and rinsed 5 times with 1.6 mL of PBS. The UV absorbance at 257 nm of the resin supernatants was monitored throughout the coupling procedure. Washings stopped when the absorbance reached the baseline level. All the procedures were performed under sterile conditions. Derivatised resins were kept at 4 °C.

5.4.5. Determination of resin loading

To estimate the amount of resin-bound peptides, their concentration was determined by measuring the absorbance at 257 nm of resin supernatants containing eluted peptides. First, 400 μL aliquots of each resin, including that coupled with biotin used as reference, were washed three times with 1.6 mL of sterile water by centrifugation, to remove the salts present in PBS. Thereafter, peptides were eluted

from the resins by addition of 1.6 mL 0.05% TFA. The elution was repeated twice, the obtained supernatants were combined and freeze-dried. After lyophilization, peptides were dissolved in 400 µL water and their concentration determined by UV absorbance.

5.4.6. Bacteria and antimicrobial activity assays

The reference strains *Staphylococcus epidermidis* ATCC 35984 and *Staphylococcus aureus* ATCC 25923 were cultured as described in **Chapters 3** and **4**.

5.4.6.1. Determination of the Minimum Inhibitory Concentration (MIC)

The MIC of B27(1-18)^{Cys}, ^{Cys}B27(1-18), B27(1-18)^{Lys} and ^{Lys}B27(1-18) peptides in solution was determined by the standard broth microdilution assay as described in **Chapter 3**.

5.4.6.2. Evaluation of bacterial adhesion to titanium surface

Adhesion of *S. epidermidis* ATCC 35984 to titanium samples was investigated as in **chapter 3.4.4.2.**. All experiments were performed in triplicate for each type of surface.

5.4.6.3. Scanning Electron Microscopy (SEM) of *S. epidermidis* on Ti samples

SEM of titanium samples was performed on duplicate samples by applying the same procedure used in **Chapter 3**.

5.4.7. Kinetic fluorescence measurements to detect membrane depolarization and permeabilization

The procedure developed in **Chapter 4** was applied. Mid-log phase *S. epidermidis,* resuspended at $1 \cdot 10^7$ CFU/mL or $1 \cdot 10^8$ CFU/mL in PBS-glc were incubated in the orbital shaker at 37 ˚C for 15 min. Therefter, diSC$_3$ (5) alone, or diSC$_3$(5) and PI together were added at final concentrations of 0.4 µM and 5 µg/mL, respectively. The solution was mixed by short vortexing and 200 µL were added in duplicate to the wells of a black 96-well plate (Optiplate, PerkinElmer). The plate was preincubated at 37 °C for 5 - 10 min until readings were stabilized. After this time, the plate was ejected for addition of free and resin-bound peptides. The plate was placed back into the reader and fluorescence monitored for additional 10 - 20 minutes. At the end of incubation (around 30 min), aliquots were withdrawn from each well, serially diluted and plated on MH agar to allow CFU determination.

5.4.7.1. Field Emission Scanning Electron Microscopy (SEM) of *S. epidermidis* on Polycarbonate membrane filters

The morphology of *S. epidermidis,* treated with free and anchored peptides, and deposited on polycarbonate filters, was studied by Field Emission Scanning Electron Microscopy (FE-SEM) (JEOL model JSM-7610FPlus) as described in **Chapter 4**, on duplicate samples.

5.4.8. Statistical analysis

Data, presented as mean values ± standard deviations, have been analysed by a non-parametric U Mann-Whitney test (IBM SPSS Statistics 20 software, Armonk, NY, USA). Statistical significance was set at *P* value <0.05.

5.5. References

1. Costa, F., Carvalho, I. F., Montelaro, R. C., Gomes, P. & Martins, M. C. L. Covalent immobilization of antimicrobial peptides (AMPs) onto biomaterial surfaces. *Acta Biomater.* **7**, 1431–1440 (2011).

2. Onaizi, S. A. & Leong, S. S. J. Tethering antimicrobial peptides: Current status and potential challenges. *Biotechnol. Adv.* **29**, 67–74 (2011).

3. Bagheri, M., Beyermann, M. & Dathe, M. Mode of action of cationic antimicrobial peptides defines the tethering position and the efficacy of biocidal surfaces. *Bioconjug. Chem.* **23**, 66–74 (2012).

4. Bagheri, M., Beyermann, M. & Dathe, M. Immobilization Reduces the Activity of Surface-Bound Cationic Antimicrobial Peptides with No Influence upon the Activity Spectrum. *Antimicrob. Agents Chemother.* **53**, 1132–1141 (2009).

5. Gao, G. *et al.* Biomembrane Interactions Reveal the Mechanism of Action of Surface-Immobilized Host Defense IDR-1010 Peptide. *Chem. Biol.* **19**, 199–209 (2012).

6. Gabriel, M., Nazmi, K., Veerman, E. C., Nieuw Amerongen, A. V. & Zentner, A. Preparation of LL-37-Grafted Titanium Surfaces with Bactericidal Activity. *Bioconjug. Chem.* **17**, 548–550 (2006).

7. Malanovic, N. & Lohner, K. Antimicrobial Peptides Targeting Gram-Positive Bacteria. *Pharmaceuticals* **9**, 59 (2016).

8. Hilpert, K. *et al.* Screening and Characterization of Surface-Tethered Cationic Peptides for Antimicrobial Activity. *Chem. Biol.* **16**, 58–69 (2009).

9. D'Este, F., Oro, D., Boix-Lemonche, G., Tossi, A. & Skerlavaj, B. Evaluation of free or anchored antimicrobial peptides as candidates for the prevention of orthopaedic device-related infections. *J. Pept. Sci.* **23**, 777–789 (2017).

10. Godoy-Gallardo, M. *et al.* Antibacterial properties of hLf1-11 peptide onto titanium surfaces: A comparison study between silanization and surface initiated polymerization. *Biomacromolecules* **16**, 483–496 (2015).

11. Mas-Moruno, C., Garrido, B., Rodriguez, D., Ruperez, E. & Gil, F. J. Biofunctionalization strategies on tantalum-based materials for osseointegrative applications. *J. Mater. Sci. Mater. Med.* **26**, 1–12 (2015).

12. Williams, D. L. & Bloebaum, R. D. Observing the Biofilm Matrix of *Staphylococcus epidermidis* ATCC 35984 Grown Using the CDC Biofilm Reactor. *Microsc. Microanal.* **16**, 143–152 (2010).

13. Valdez-Salas, B. *et al.* In Vitro Assessment of Early Bacterial Activity on Micro/Nanostructured Ti6Al4V Surfaces. *Molecules* **22**, 832 (2017).

14. Cao, P. *et al.* Coupling Plant-Derived Cyclotides to Metal Surfaces: An Antibacterial and Antibiofilm Study. *Int. J. Mol. Sci.* **19**, 793 (2018).

15. Sabaté Brescó, M. *et al.* Pathogenic Mechanisms and Host Interactions in *Staphylococcus epidermidis* Device-Related Infection. *Front. Microbiol.* **8**, (2017).

16. Fey, P. D. & Olson, M. E. Current concepts in biofilm formation of *Staphylococcus epidermidis*. *Future Microbiol.* **5**, 917–33 (2010).

17. Costa, F. M. T. A., Maia, S. R., Gomes, P. A. C. & Martins, M. C. L. Dhvar5 antimicrobial peptide (AMP) chemoselective covalent immobilization results on higher antiadherence effect than simple physical adsorption. *Biomaterials* **52**, 531–538 (2015).

18. Masurier, N. *et al.* Site-specific grafting on titanium surfaces with hybrid temporin antibacterial peptides. *J. Mater. Chem. B* **6**, 1782–1790 (2018).

19. Soares, J. W., Kirby, R., Doherty, L. A., Meehan, A. & Arcidiacono, S. Immobilization and orientation-dependent activity of a naturally occurring antimicrobial peptide. *J. Pept. Sci.* **21**, 669–679 (2015).

20. Vidlak, D. & Kielian, T. Infectious Dose Dictates the Host Response during *Staphylococcus aureus* Orthopedic-Implant Biofilm Infection. *Infect. Immun.* **84**, 1957–1965 (2016).

21. Chen, R. *et al.* Characterization of chemoselective surface attachment of the cationic peptide melimine and its effects on antimicrobial activity. *Acta Biomater.*

8, 4371–4379 (2012).

22. Skerlavaj, B., Benincasa, M., Risso, A., Zanetti, M. & Gennaro, R. SMAP-29: a potent antibacterial and antifungal peptide from sheep leukocytes. *FEBS Lett.* **463**, 58–62 (1999).

23. Skerlavaj, B. *et al.* Biological Characterization of Two Novel Cathelicidin-derived Peptides and Identification of Structural Requirements for Their Antimicrobial and Cell Lytic Activities. *J. Biol. Chem.* **271**, 28375–28381 (1996).

24. Rapsch, K., Bier, F. F., Tadros, M. & von Nickisch-Rosenegk, M. Identification of Antimicrobial Peptides and Immobilization Strategy Suitable for a Covalent Surface Coating with Biocompatible Properties. *Bioconjug. Chem.* **25**, 308–319 (2014).

25. Lee, E. K., Kim, Y.-C., Nan, Y. H. & Shin, S. Y. Cell selectivity, mechanism of action and LPS-neutralizing activity of bovine myeloid antimicrobial peptide-18 (BMAP-18) and its analogs. *Peptides* **32**, 1123–1130 (2011).

26. Wilmes, M. *et al.* Killing of Staphylococci by θ-Defensins Involves Membrane Impairment and Activation of Autolytic Enzymes. *Antibiotics* **3**, 617–631 (2014).

27. Kaiser, E., Colescott, R. L., Bossinger, C. D. & Cook, P. I. Color test for detection of free terminal amino groups in the solid-phase synthesis of peptides. *Anal. Biochem.* **34**, 595–598 (1970).

Chapter 6 – Osteoblasts compatibility of peptide-functionalized titanium samples and the "Race for the surface" concept

6.1. Introduction

As already mentioned, it is crucial to adopt strategies for the prevention of bacterial adhesion to and biofilm formation on the prosthetic surfaces, not only by enhancing the perioperative preventative measures but also by developing biomaterials resistant to bacterial infection and compatible with osteoblasts cells. A complex dynamics of events occurring during and after implantation, like the osteoblasts attachment, growth and differentiation, should be considered to reach a complete implant integration. In fact, the events that follow prostheses implantation can be regarded as a "race for the surface": if it is won by host tissue cells, the implant surface is covered by tissue and becomes less susceptible to bacterial colonization. However, if the race is won by bacteria, then biofilm formation on the implant surface reduces the likeliness of tissue integration[1–3].

In this chapter we investigated the compatibility of titanium samples functionalized with BMAP27(1-18) to osteoblast cells. Moreover, to address the "race for the surface" issue, peptide-grafted titanium samples were tested in bacteria-osteoblasts co-culture experiments. In addition, the influence of peptide orientation was also studied in these experiments. Titanium samples prepared and analysed for antimicrobial properties in *Chapters 3* and *5* were used.

6.2. Results and Discussion

6.2.1. Evaluation of compatibility of titanium samples to osteoblast cells

The biocompatibility of our Ti samples to osteoblasts cells was addressed by incubating Ti samples with the osteosarcoma-derived MG-63 cells, used as a model, in a 48-well plate. After 4 h incubation, the metabolic activity of the attached cells was evaluated by a PrestoBlue® metabolic assay. The viability of cells attached to Ti_A and Ti_A_B27(1-18)^{SH} samples was comparable to cell viability on bare titanium, which is known for its biocompatibility (***Figure 6.1.A***). Highly similar results were obtained with a different batch of samples, including Ti_A_B27(1-18)^{Cys} and Ti_A_^{Cys}B27(1-18), and
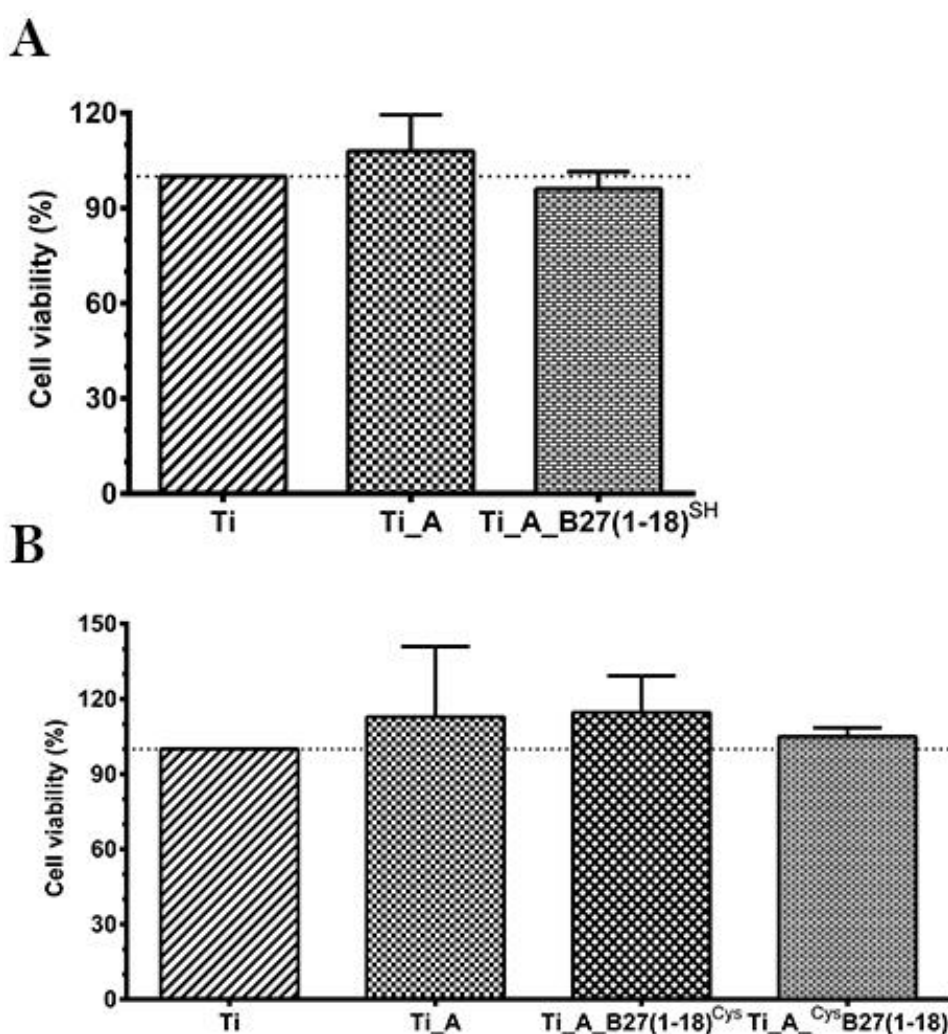
Figure 6.1. *MG-63 osteoblast viability upon adhesion to functionalized Ti samples using the metabolic dye PrestoBlue®. Results are expressed as percent cell viability respect to cells seeded on bare titanium and are the means ± SD of at least three independent experiments performed in triplicate. Differences between samples did not reach statistical significance. Panels A and B refer to titanium samples described in **Chapters 3** and **5**, respectively.*

their respective controls (***Figure 6.1.B***). These data indicate that cells were vital and able to adhere to different substrata without significant toxic effects neither by the peptide, regardless of its orientation, nor by the other organic molecules present on Ti (e.g. Ti_A). This observation adds to previous studies reporting absence of cytotoxic effects of BMAP27(1-18) against several host cell types both in solution[4–6], and upon immobilization[7].

Taking into consideration the cytocompatibility of the functionalized Ti samples, we next investigated their antimicrobial efficacy in a more sophisticated context by addressing the issue of "race for the surface". This concept derives from the observation that the surface of an ideal prosthesis should be resistant to bacterial invasion and at the same time prone to colonization by host tissue cells[1,3,8].

In order to analyse if the colonizing capacity of osteoblast cells could be hampered by bacteria attached on Ti itself, a co-culture experiment of MG-63 cells and bacteria was performed. Prior to seeding osteoblasts on Ti samples, Ti samples were incubated with *S. epidermidis* for 2 h at 37 °C, similar to the antimicrobial assays described in ***chapter 3***. After withdrawal of planktonic bacteria and washings, the bacteria-contaminated Ti samples were seeded with freshly resuspended MG-63 cells in antibiotic-free DMEM medium supplemented with 2% MH, and incubated for additional 6 h and 24 h. These time points were selected to follow cell adhesion (6 h) and early proliferation (24 h). Thereafter, Ti disks were processed and analysed by confocal fluorescence microscopy in order to evaluate MG-63 cell number, size and morphology.
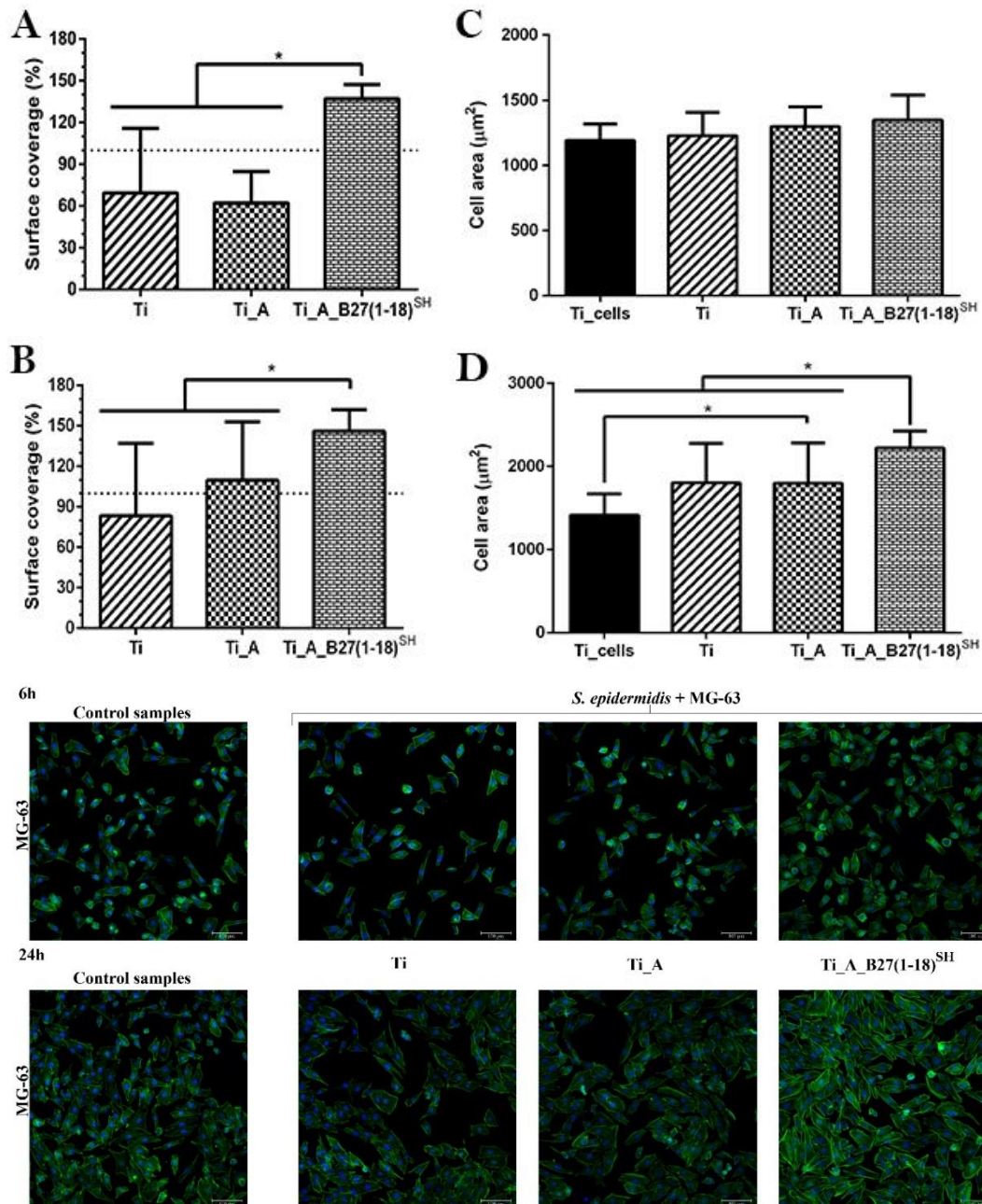
Figure 6.2. Osteoblast adhesion to the indicated Ti samples in a cell-bacteria co-culture experiment. MG-63 cells were seeded on functionalized Ti disks, previously incubated with S. epidermidis, and co-cultured in antibiotic-free medium for additional 6 h (**A, C**) and 24 h (**B, D**). At these time points, samples were fixed and stained with Alexa Fluor 488-phalloidin and Hoechst. Osteoblast cell number and morphology were evaluated by CLSM with a Leica TCS SP8 X microscope followed by quantification with the ImageJ software. Five optical fields were analysed for each condition on duplicate samples. **A, B**: percent cell surface coverage in the presence of bacteria respect to bacteria free controls. **C, D**: mean cell area values in the presence (Ti, Ti_A, Ti_A_B27(1-18)^{SH}) and in the absence (Ti_cells) of bacteria. Asterisks denote statistically significant differences between the indicated samples (P < 0.05). Representative images for each condition are shown in the lower part of the figure. Scale bar = 100 μm. Results refer to titanium samples described in **Chapter 3**.

The results and their representative CSLM images are displayed in *Figure 6.2.*. Data refer to titanium samples described in *Chapter 3* and were calculated as percent cell surface coverage respect to bacteria-free Ti controls (*Figure 6.2.A, B*), and mean cell area (*Figure 6.2.C, D*). It is obvious that the presence of *S. epidermidis* affected cell adhesion and spreading on distinct Ti samples to different extents. In *Figure 6.2.A* (6-h time point), osteoblast adhesion to Ti and Ti_A samples was 40% inhibited, but MG-63 cell adhesion to Ti_A_B27(1-18)[SH] samples was not impaired but rather enhanced. Moreover, as at this time point osteoblast size (*Figure 6.2.C*) and morphology (*Figure 6.2.*, images in the upper row) were on average highly comparable, the increment of surface coverage on Ti_A_B27(1-18)[SH] samples could be reasonably attributed to a higher number of adhered MG-63 cells. This data would indicate that the bactericidal action exerted by peptide-functionalized Ti, as observed by SEM (*Chapter 3, Figure 3.6.3.*) and confirmed by CFU counts (*Chapter 3, Figure 3.5.*), was effective to enable displacement of *S. epidermidis* by osteoblasts cells, which could thus predominate and spread onto the Ti surface. This idea seems further supported by the increase of surface coverage (*Figure 6.2.B*), and mean cell area (*Figure 6.2.D*) observed after 24 h co-incubation on BMAP27(1-18)-functionalized samples. However, this explanation does not take into consideration possible specific effects of the Ti-anchored peptide on osteoblasts cells. This question was not addressed in these experiments because in a previous study[7] BMAP27(1-18) proved neutral with respect to MG-63 cell growth and differentiation. Interpretation of results is additionally complicated by the intriguing observation that at 24-h time point a slight improvement of osteoblast adhesion and spreading compared to bacteria-free control was found in Ti and Ti_A samples, which were devoid of antimicrobial properties (*Chapter 3, Figure 3.5. – 3.7.*). This would suggest that bacterial killing may not be the only explanation and also other phenomena in the complex network of multiple interactions between bacteria, implant surfaces, and relevant tissue cells[1,9,10], should be considered.
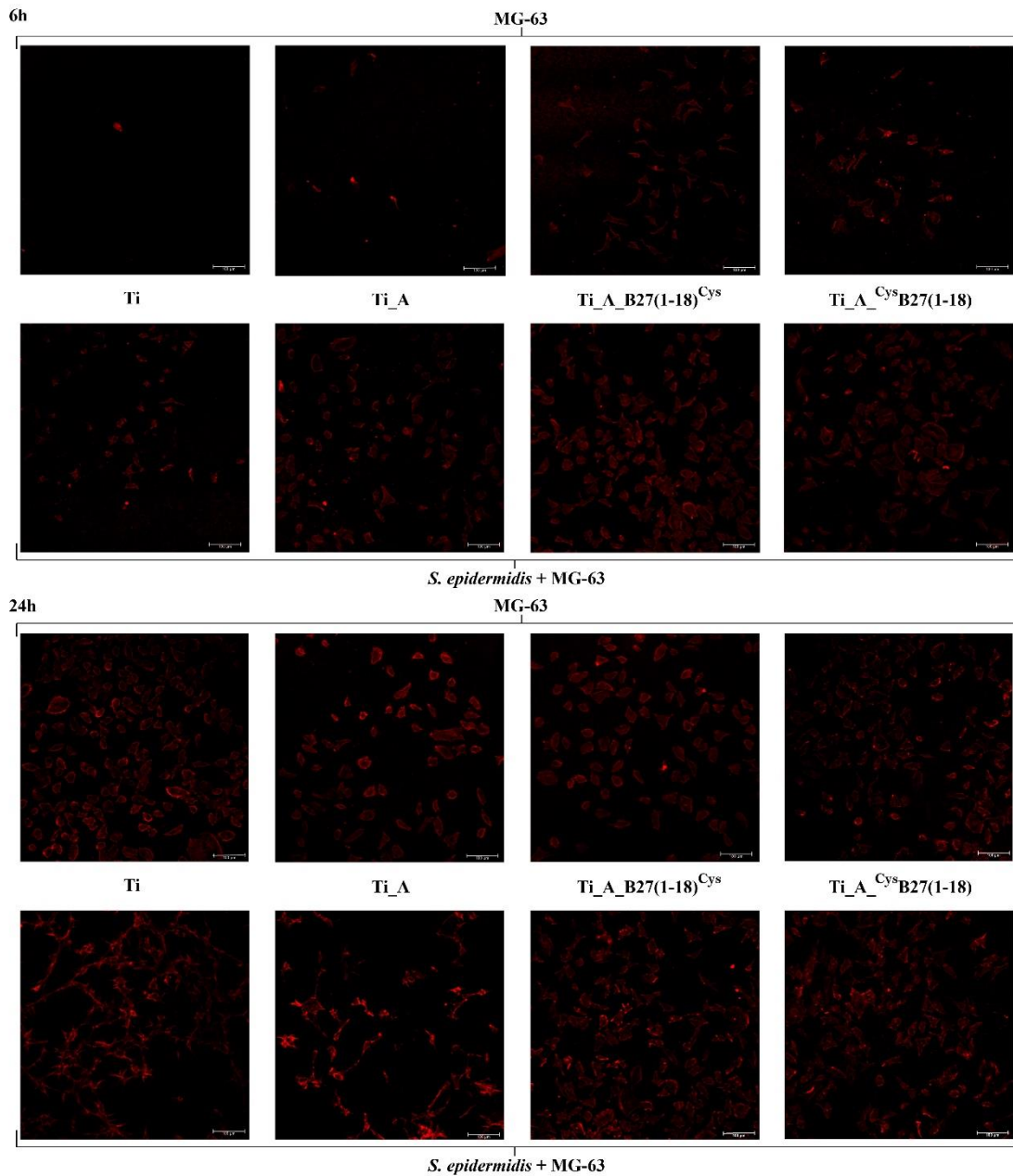
Figure 6.3. *Representative images of osteoblast cells adhered to Ti, Ti_A, Ti_A_B27(1-18)^{Cys} and Ti_A_^{Cys}B27(1-18) at 6 h and 24 h in the absence and in the presence of bacteria. At these time points, samples were fixed and stained with Alexa Fluor 546-phalloidin and Hoechst. Images were taken by CLSM with a Leica TCS SP8 X microscope. Only red stained cells (Alexa Fluor 546-phalloidin) are shown. Scale bar = 100 μm. Results refer to titanium samples described in **Chapter 5**.*

To go deeper into these aspects, we performed a more detailed analysis of osteoblast cells on Ti samples by following essentially the same experimental protocol, with a lower initial cell number (1×10^4/mL instead of 4×10^4/mL), and the difference that each type of sample was incubated with cells in the presence and in the absence of bacteria. In this way we wanted to distinguish between results due to direct antimicrobial activity, and other possible effects of Ti-anchored peptides on cell adhesion and spreading. We also wanted to understand whether these variables could be affected by peptide orientation. Specifically, in these experiments Ti, Ti_A, Ti_A_B27(1-18)^{Cys} and Ti_A_^{Cys}B27(1-18) samples (described in **Chapter 5**) were incubated in the absence and in the presence of *S. epidermidis* ATCC 35984, and after 2 h were washed and seeded with osteoblast cells in antibiotic-free DMEM medium supplemented with 2% MH. Samples were then fixed and processed for CLSM at 6 h and 24 h incubation as described previously. Representative images are shown in **Figure 6.3.**. Images were analysed by ImageJ software as in the previous experiments, but the pairwise combination of samples enabled us to improve data analysis. We first focused on the spreading ability of osteoblast cells on different substrata by analysing mean cell area values (**Figure 6.4.**).
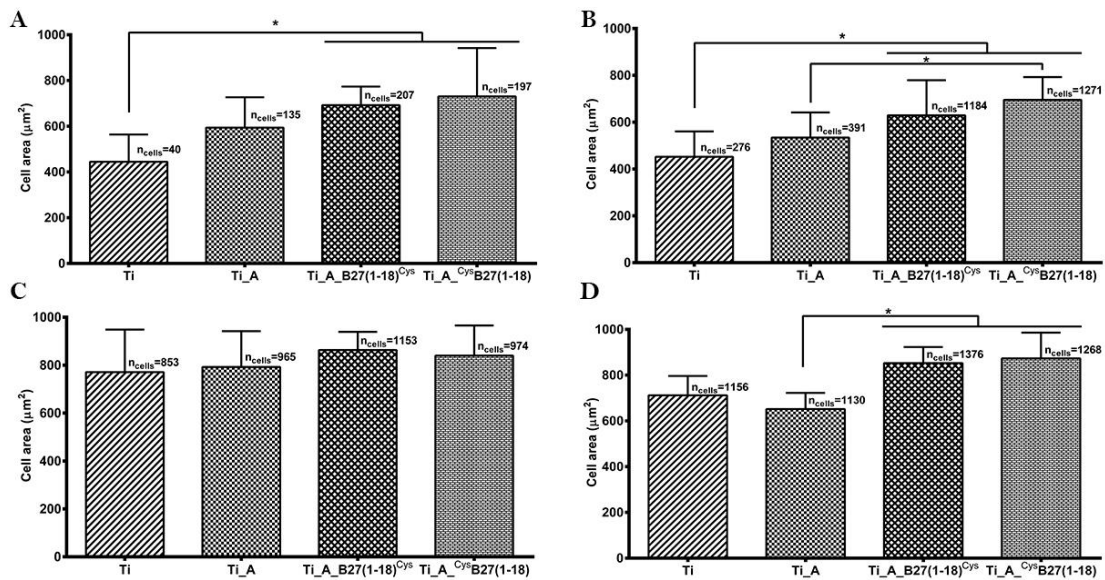

Figure 6.4. MG-63 mean cell area values on Ti, Ti_A, Ti_A_B27(1-18)^{Cys} and Ti_A_^{Cys}B27(1-18) at 6 h (**A, B**) and 24 h (**C, D**) in the absence (**A, C**) and in the presence (**B, D**) of bacteria. Osteoblast cell number (**Table 6.1.**) and morphology were evaluated by CLSM with a Leica TCS SP8 X microscope followed by quantification with the ImageJ software. Nine optical fields were analysed for each condition on duplicate samples. Asterisks denote statistically significant differences between the indicated samples (P < 0.05).

At 6 h incubation, these values were increasingly higher going from Ti to Ti_A to Ti_A_B27(1-18)^{Cys} and Ti_A_^{Cys}B27(1-18), incubated without bacteria (with statistically significant difference respect to Ti controls) (**Figure 6.4.A**). Similar results were also observed for titanium samples pre-incubated in the presence of *S. epidermidis* (**Figure 6.4.B**). Remarkably, at the same time point the osteoblast numbers on Ti_A_B27(1-18)^{Cys} and Ti_A_^{Cys}B27(1-18) samples were around 5 times higher than on bare Ti (**Figure 6.4.A** and **Table 6.1**), and similarly higher osteoblast numbers (around 4-5 times more than on Ti disks) were also detected on peptide-functionalized titanium samples that were pre-incubated with bacteria (**Figure 6.4.B** and **Table 6.1**). Apparently, comparing data presented in panels **A** and **B** of **Figure 6.4.** (i.e. presence *vs*. absence of bacteria), one would say that mean cell area values of cells adhered to different substrata have exactly the same increasing trend, regardless of the presence of bacteria, suggesting some cell adhesion-promoting effects of the anchored peptides. It is important to note, however, that in all titanium samples that have been pre-incubated with bacteria, total cell numbers were significantly higher respect to their bacteria-free counterparts (**Table 6.1**). This observation is intriguing because it suggests that bacteria themselves could in some way affect cell adhesion[11]. Taking into account what has been reported for the oral environment[12,13], currently we cannot rule out possible stimulating effects of bacteria on tissue cell expression of adhesion molecules that would in turn improve cell adhesion and spreading.

Table 6.1. Total number of MG-63 cells and MG-63/field obtained from 9 fields on duplicate samples for each Ti condition using Confocal Laser Scanning Microscopy.

|	6 hours				24 hours			
	MG-63		S. ep.+MG-63		MG-63		S. ep.+MG-63	
	Total cells	Cells field	Total cells	Cells field	Total cells	Cells field	Total cells	Cells field
Ti	40	2.2	276	15.3	853	47.4	1156	64.2
Ti_A	135	7.5	391	21.7	965	53.6	1130	62.8
Ti_A_B27(1-18)^{Cys}	207	11.5	1184	65.7	1153	64.1	1376	76.4
Ti_A_^{Cys}B27(1-18)	197	10.9	1271	70.6	974	54.1	1268	70.4

On the other hand, at 24-h time point osteoblast spreading was highly comparable on diverse Ti substrates (*Figure 6.4.C*), with values between 750 - 1000 μm^2, and with globally higher cell numbers respect to those detected at 6 h (*Table 6.1.*), suggesting that in the absence of bacteria cells were able to proliferate on all substrates. In general, this holds true also for cells on samples pre-incubated with *S. epidermidis,* but it is important to note that in this case, mean cell area values of cells on Ti_A_B27(1-18)^{Cys} and Ti_A_^{Cys}B27(1-18) were significantly higher respect to Ti_A samples (*Figure 6.4.D*). However, total cell numbers on all bacteria pre-incubated samples at 24 h, though increased respect to their bacteria-free counterparts at the same time point, show a notable difference between samples, functionalized with peptides, and controls (*Table 6.1*). In fact, comparing cell numbers registered on bacteria-preincubated samples at 6 and 24 h, there was a higher increase of total cells in Ti and Ti_A than in each peptide-grafted titanium (*Table 6.1*). This apparent discrepancy (respect to data reported in
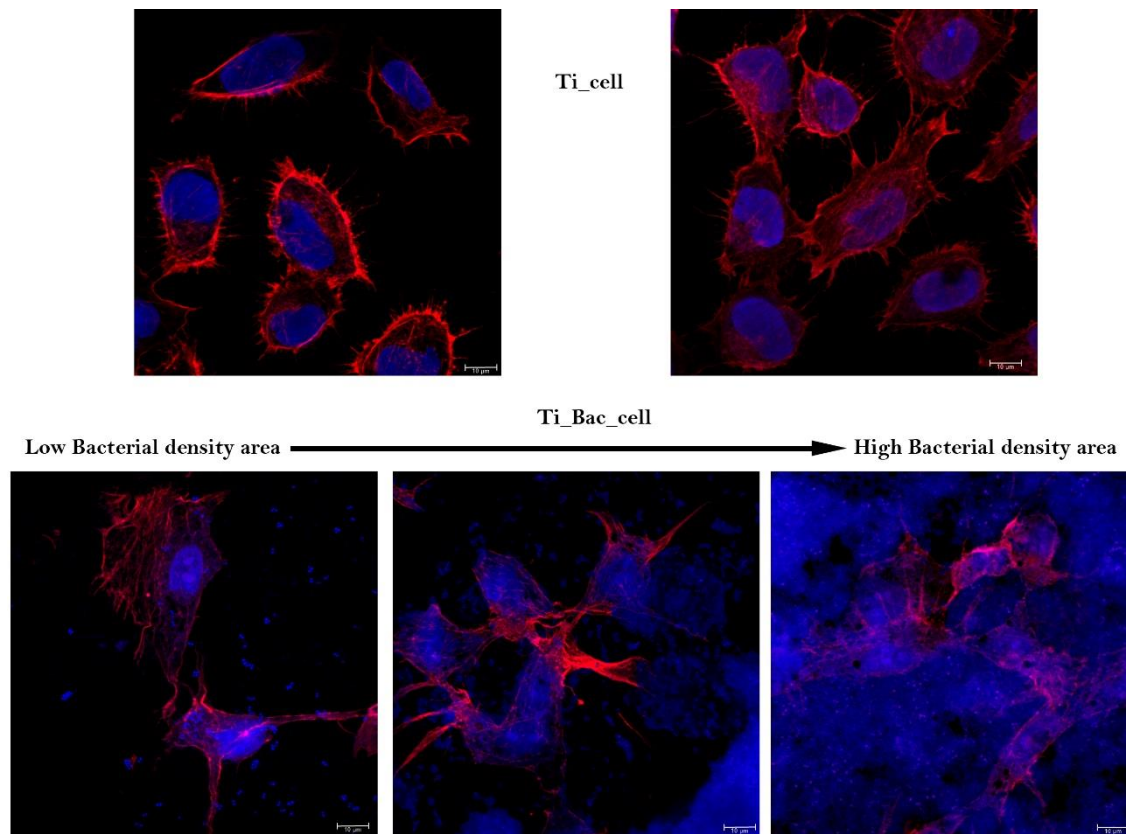
Figure 6.5. *Representative images of MG-63 cell morphology in the absence and in the presence of S. epidermidis. Samples were fixed and stained with Alexa Fluor 546-phalloidin and Hoechst as above and observed by CLSM with a Leica TCS SP8 X microscope. Both colours (Alexa Fluor 546-phalloidin and Hoechst) are shown. The diffused blue layer in the lower right picture indicates bacterial biofilm on the sample. Scale bar = 10 μm.*

Figure 6.4.D) could be explained by the observation that MG-63 cells on contaminated Ti samples were apparently smaller with obvious modifications in morphology as a consequence of biofilm formation, which was clearly evident in some areas (*Figure 6.5.*) and which was not observed on peptide-functionalized samples. Another possible explanation could be that cells simply reached a plateau at this time point.

By analysing CLSM images, it was possible to calculate percent cell surface coverage on Ti_A, Ti_A_B27(1-18)^{Cys} and Ti_A_^{Cys}B27(1-18) samples both in the absence and in the presence of *S. epidermidis* ATCC 35984, at 6 h and 24 h, by taking as 100% their corresponding Ti controls. As shown in *Figure 6.6*, at 6 h incubation this analysis revealed significant differences between silanized and peptide-functionalized samples in both conditions, i.e. in the absence and in the presence of bacteria (*Figure 6.6.A – B*), which were not unexpected given the number of cells observed on these samples (*Table 6.1.*). On the contrary, the differences between samples were not significant at the early proliferation point (24 h), regardless the presence of bacteria (*Figure 6.6.C* and *Figure 6.6.D*), although the mean values appeared different between silanized and peptide-functionalized samples.
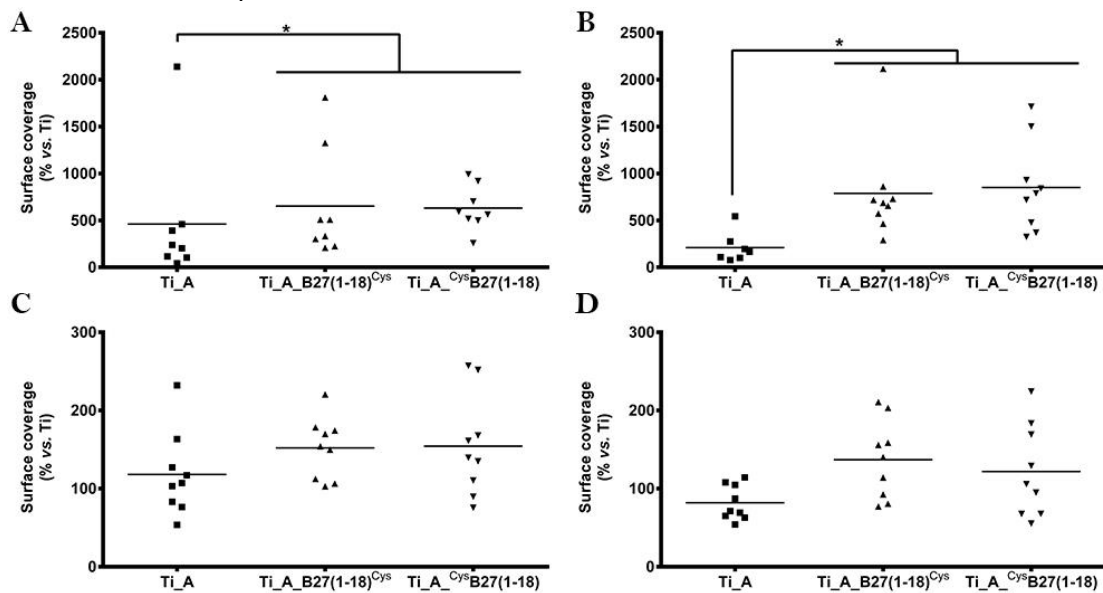
Figure 6.6. MG-63 surface coverage percentages on Ti_A, Ti_A_B27(1-18)^{Cys} and Ti_A_^{Cys}B27(1-18) respect to Ti at 6 h (*A, B*) and 24 h (*C, D*) in the absence (*A, C*) and in the presence (*B, D*) of bacteria. Data were obtained by analysing CLSM images with the ImageJ software. Nine optical fields were analysed for each condition on duplicate samples. Asterisks denote statistically significant differences between the indicated samples (P < 0.05).

For a more proper understanding of the differences in surface coverage upon pre-incubation of samples with bacteria, we calculated the osteoblasts surface coverage on each titanium sample, pre-incubated with *S. epidermidis*, taking as 100% the corresponding sample, incubated with cells only. These data, reported in **Figure 6.7.** for the 6-h time point, indicate that osteoblast surface coverage was in general incremented on all samples, with slightly higher values on peptide-functionalized titanium. Concerning bacteria, as mentioned before the presence of *S. epidermidis* on titanium surface could have some influence on cell adhesion. In this respect, it has been reported that dead *S. aureus* enhances osteoblast adhesion and differentiation to bone-associated biomaterials[11].
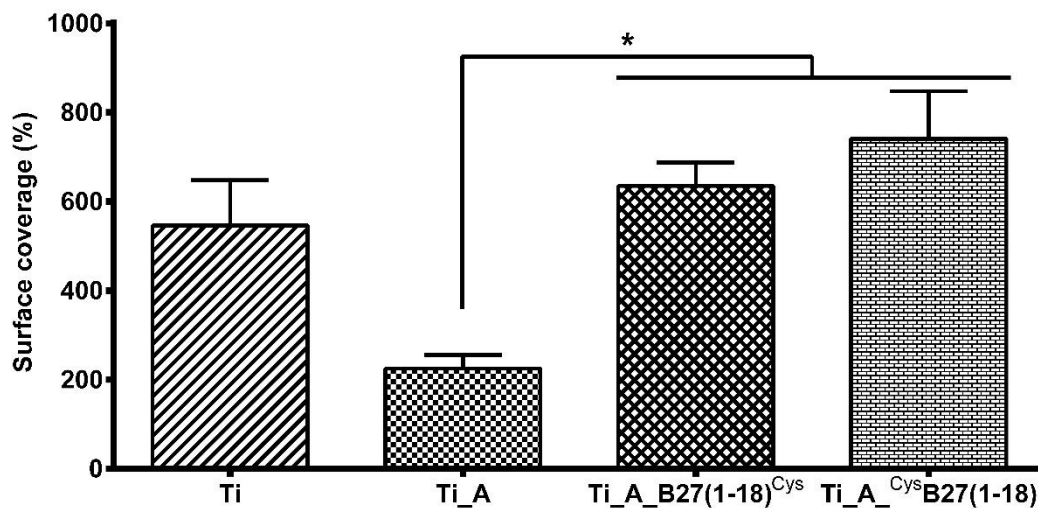
Figure 6.7. MG-63 surface coverage percentages on Ti, Ti_A, Ti_A_B27(1-18)^{Cys} and Ti_A_^{Cys}B27(1-18) samples in the presence of S. epidermidis respect to Ti, Ti_A, Ti_A_B27(1-18)^{Cys} and Ti_A_^{Cys}B27(1-18) samples without bacteria. Data were obtained by analysing CLSM images with the ImageJ software. Nine optical fields were analysed for each condition on duplicate samples. Asterisks denote statistically significant differences between the indicated samples (P < 0.05).

Concerning the peptide BMAP27(1-18), all the analyses presented in this chapter indicate improved osteoblast adhesion on peptide-grafted titanium. This could be explained by its antimicrobial activity when considering bacteria-contaminated samples. Moreover, increased osteoblast surface coverage on Ti_A_B27(1-18)^{Cys} and Ti_A_^{Cys}B27(1-18) samples in the absence of bacteria would suggest possible effects of the anchored peptide on osteoblast adhesion and spreading. It is important to note in

this respect that antimicrobial peptides free in solution, e.g. LL-37 and β-defensins, have been reported to promote various processes implicated in bone repair[14–17].

Finally, as already observed for the antimicrobial properties of the tethered peptides (see **Chapter 5**), none of the analyses reported in this chapter revealed significant differences between the two peptide analogues, immobilized via their N- or C-termini. A lack of influence of peptide orientation would mean that the protective effects towards osteoblasts cells are probably mediated by a direct antimicrobial effect (i.e. killing), rather than by a more sophisticated cell-mediated mechanism. This reasoning is based on several studies demonstrating equal if not better antibacterial efficacy of diastereomers, retroanalogs and all-D enantiomers of AMPs[18–20], thus indicating that the effects of AMPs on bacteria do not require a stereospecific or sequence-dependent recognition by bacterial components. Nevertheless, many effects elicited by AMPs on host tissue cells are not canonical receptor-mediated phenomena[21].

6.3. Conclusions

- The immobilized peptide did not produce any cytotoxic effect on osteoblast-like cells regardless of its orientation.

- MG-63 cells adhered and spread better on peptide-functionalized Ti than on bare and silanized titanium. This would mean that the immobilized peptide promotes cell adhesion in some way.

- It seems that *S. epidermidis* promotes osteoblast cells adhesion with an unknown mechanism.

- Osteoblast-like cells adhered and spread better on functionalized Ti when co-cultured with bacteria compared to non-coated surfaces. This could be the combined result of peptide-mediated killing and of dead-bacteria mediated stimulation of cell adhesion.

6.4. Experimental procedure

6.4.1. Cell culture

The purpose of the cell culture is to determine if cells are able to adhere, remain viable and able to compete for the surface in a prosthetic device for bone applications. Usually, the cells implicated in bone formation are osteoblasts and mesenchymal stem cells. In this study, the human osteoblast-like MG-63 cell line was employed as a model. This bone osteosarcoma cell line could represent a realistic way to understand the events that take place when a prosthetic device is implanted in the body. MG-63 cell line was obtained from ATCC (Manassas, VA, USA).

MG-63 cells were maintained in complete Dulbecco's Modified Eagle Medium (DMEM) supplemented with 10 % (v/v) heat inactivated FBS, 2 mM L-glutamine, 100 units/mL penicillin and 100 µg/mL streptomycin., in a humidified incubator at 37 °C and 5 % CO_2 atmosphere. Culture medium was changed every 2 days to conserve the appropriate levels of nutrients, growth factors and hormones for cell growth as well as for the pH and the osmotic pressure of the culture. MG-63 cells were maintained at optimal density for continued growth and to stimulate further proliferation. When cells decrease or stop their proliferation, they reach confluence, and were detached and seeded in a new flask.

6.4.2. Cell adhesion and viability assay

The biocompatibility of titanium samples was evaluated by measuring viability of the MG-63 cell line by using the metabolic dye PrestoBlue®. Cells were seeded onto titanium samples in a 48-well plate at a density of 4 x 10^4 cells/well in complete medium and allowed to adhere for 4 h at 37 °C. Next, the medium was aspirated, cells were washed with sterile PBS and incubated at 37 °C for 90 min in fresh complete medium containing 10 % (v/v) PrestoBlue®. Cell metabolic activity was measured fluorometrically according to PrestoBlue® manufacturer's instructions by using a Multimode Plate Reader (EnSpire™ 2300, PerkinElmer, Waltham, MA, USA). All experiments were performed in triplicate for each type of surface.

6.4.3. Cell-bacteria co-culture

This assay was performed according to previously reported studies[3,9]. Titanium samples were incubated with 1 mL of *S. epidermidis* (6×10^4 CFU/mL) in a 48-well plate for 2 h at 37 °C as described above. The medium was then removed and the samples were rinsed three times in sterile PBS. Afterwards, MG-63 cells, freshly re-suspended in DMEM medium without Penicillin and Streptomycin, supplemented with 2% MH broth, were seeded on bacteria-covered surfaces at a density of 4×10^4 cells/well in the batch of Ti samples with B27(1-18)[SH] and at density of 1×10^4 cells/well in the batch of Ti samples with B27(1-18)[Cys] and [Cys]B27(1-18) peptides. Bacteria and MG-63 cells were incubated at 37 °C in humidified 5% CO_2 for 6 and 24 h. At these time points, samples were fixed in 3% Paraformaldehyde, stained with Alexa Fluor 488 or 546-phalloidin and Hoechst 33342 and examined by Confocal Laser Scanning Microscopy (CLSM) with a Leica TCS SP8 microscope (Leica Microsystems GmbH, Wetzlar, Germany). Images were analysed using ImageJ 1.51w software (NIH, Bethesda, MD, USA) to determine cell area and surface coverage. All experiments were performed in duplicate for each type of surface.

6.4.4. Statistical analysis

Data, presented as mean values ± standard deviations, have been analysed by a post-hoc HSD tukey non-parametric U Mann-Whitney test (IBM SPSS Statistics 20 software, Armonk, NY, USA). Statistical significance was set at *P* value <0.05.

6.5. References

1.   Gristina, A. Biomaterial-centered infection: microbial adhesion versus tissue integration. *Science (80-.).* **237**, 1588–1595 (1987).

2.   Subbiahdoss, G., Kuijer, R., Grijpma, D. W., van der Mei, H. C. & Busscher, H. J. Microbial biofilm growth *vs.* tissue integration: "The race for the surface" experimentally studied. *Acta Biomater.* **5**, 1399–1404 (2009).

3.   Godoy-Gallardo, M. *et al.* Anhydride-functional silane immobilized onto titanium surfaces induces osteoblast cell differentiation and reduces bacterial adhesion and biofilm formation. *Mater. Sci. Eng. C* **59**, 524–532 (2016).

4.   Skerlavaj, B. *et al.* Biological Characterization of Two Novel Cathelicidin-derived Peptides and Identification of Structural Requirements for Their Antimicrobial and Cell Lytic Activities. *J. Biol. Chem.* **271**, 28375–28381 (1996).

5.   Benincasa, M., Skerlavaj, B., Gennaro, R., Pellegrini, A. & Zanetti, M. In vitro and in vivo antimicrobial activity of two α-helical cathelicidin peptides and of their synthetic analogs. *Peptides* **24**, 1723–1731 (2003).

6.   Lee, E. K., Kim, Y.-C., Nan, Y. H. & Shin, S. Y. Cell selectivity, mechanism of action and LPS-neutralizing activity of bovine myeloid antimicrobial peptide-18 (BMAP-18) and its analogs. *Peptides* **32**, 1123–1130 (2011).

7.   D'Este, F., Oro, D., Boix-Lemonche, G., Tossi, A. & Skerlavaj, B. Evaluation of free or anchored antimicrobial peptides as candidates for the prevention of orthopaedic device-related infections. *J. Pept. Sci.* **23**, 777–789 (2017).

8.   Pham, V. T. H. *et al.* "Race for the Surface": Eukaryotic Cells Can Win. *ACS Appl. Mater. Interfaces* **8**, 22025–22031 (2016).

9.   Zhao, B. *et al.* Soft tissue integration versus early biofilm formation on different dental implant materials. *Dent. Mater.* **30**, 716–727 (2014).

10.   Neoh, K. G., Hu, X., Zheng, D. & Kang, E. T. Balancing osteoblast functions and bacterial adhesion on functionalized titanium surfaces. *Biomaterials* **33**, 2813–2822 (2012).

11. Somayaji, S. N., Huet, Y. M., Gruber, H. E. & Hudson, M. C. UV-killed *Staphylococcus aureus* enhances adhesion and differentiation of osteoblasts on bone-associated biomaterials. *J. Biomed. Mater. Res. Part A* **95A**, 574–579 (2010).

12. Engels-Deutsch, M., Rizk, S. & Haïkel, Y. Streptococcus mutans antigen I/II binds to α5β1 integrins via its A-domain and increases β1 integrins expression on periodontal ligament fibroblast cells. *Arch. Oral Biol.* **56**, 22–28 (2011).

13. Kramer, P. R., JanikKeith, A., Cai, Z., Ma, S. & Watanabe, I. Integrin mediated attachment of periodontal ligament to titanium surfaces. *Dent. Mater.* **25**, 877–883 (2009).

14. Kittaka, M. *et al.* The antimicrobial peptide LL37 promotes bone regeneration in a rat calvarial bone defect. *Peptides* **46**, 136–142 (2013).

15. Zhang, Z. & Shively, J. E. Generation of Novel Bone Forming Cells (Monoosteophils) from the Cathelicidin-Derived Peptide LL-37 Treated Monocytes. *PLoS One* **5**, e13985 (2010).

16. Zhang, Z. & Shively, J. E. Acceleration of Bone Repair in NOD/SCID Mice by Human Monoosteophils, Novel LL-37-Activated Monocytes. *PLoS One* **8**, e67649 (2013).

17. Kraus, D. *et al.* Human β-defensins differently affect proliferation, differentiation, and mineralization of osteoblast-like MG63 cells. *J. Cell. Physiol.* **227**, 994–1003 (2012).

18. Di Grazia, A. *et al.* d-Amino acids incorporation in the frog skin-derived peptide esculentin-1a(1-21)NH2 is beneficial for its multiple functions. *Amino Acids* **47**, 2505–2519 (2015).

19. Kindrachuk, J. *et al.* Stability, toxicity, and biological activity of host defense peptide BMAP28 and its inversed and retro-inversed isomers. *Biopolymers* **96**, 14–24 (2011).

20. Mardirossian, M. *et al.* D-BMAP18 antimicrobial peptide is active *In Vitro*, resists to pulmonary proteases but loses its activity in a murine model of *Pseudomonas aeruginosa* lung infection. *Front. Chem.* **5**, 1–9 (2017).

21.   Xhindoli, D. *et al.* The human cathelicidin LL-37 — A pore-forming antibacterial peptide and host-cell modulator. *Biochim. Biophys. Acta - Biomembr.* **1858**, 546–566 (2016).

Chapter 7 – General conclusions and future outlook

In order to obtain titanium with anti-infective surface, in the present thesis Ti samples were successfully functionalized with the cathelicidin α-helical peptide B27(1-18)^{SH}, as assessed by contact angle, XPS, and QCM-D analyses. The attempt to rise the peptide concentration in the coupling solution did not increase surface coverage. To improve functionalization, I would need to modify the coupling strategy substantially. This could be done at various levels. One could for example modify the molecule to be immobilized, for instance by synthesizing more complex derivatives (i.e. dendrimers) carrying multiple copies of antimicrobial sequences, or by synthesizing constructs containing multiple (e.g. antimicrobial and cell-adhesive) functionalities. Another level where it would be possible to introduce modifications would be on titanium surface, for example by applying a chemistry producing polymer brushes, which would increase the number of anchoring points for the AMPs.

Adhesion of *S. epidermidis* to peptide-functionalized titanium disks was remarkably inhibited respect to bare titanium, suggesting effective coupling of B27(1-18)^{SH}, B27(1-18)^{Cys} and ^{Cys}B27(1-18) to the metal surface in a form that preserves their activity. The antimicrobial efficacy of B27(1-18)^{Cys} or ^{Cys}B27(1-18) was comparable, probably as a consequence of a uniform charge distribution along the peptide sequence, with cationic residues regularly interspersed with those hydrophobic. The altered bacterial morphology on peptide-functionalized Ti samples, as assessed by SEM, indicate a contact killing effect of the attached peptide and suggests a diverse mode of action respect to that displayed in solution.

Surface immobilized BMAP-27(1-18), regardless of its orientation, displayed good compatibility to osteoblast-like cells and favoured their adhesion and spreading in co-culture with bacteria, presumably by virtue of a direct, microbicidal effect. In addition, MG-63 cells adhered and spread better on peptide-functionalized Ti than on Ti controls

also in the absence of bacteria. This could indicate that the immobilized BMAP27(1-18) promoted cell adhesion with an as yet unknown mechanism. Hence, further studies to analyse these findings more in depth are required. Another interesting aspect that arose from co-culture experiments, though not related to AMPs, was the unexplained effect of bacteria on osteoblast cells. It would be very interesting to understand whether live or dead bacteria, or their components, elicit specific effects on osteoblast cells, promoting their adhesion and spreading.

By applying the developed microplate assay based on the combination of a potential-sensitive dye with a nucleic acid stain, we were able to distinguish membrane depolarization and permeabilization on whole bacteria. The phenomena of membrane depolarization, due to ion movements across the membrane, and membrane permeabilization, due to pore formation, were monitored by using gramicidin D and melittin, two peptides with well-known mechanism of action, on *Staphylococcus* species. To increment the sensitivity of this microplate assay, in order to use it with lower concentrations of bacteria, one possibility could be the replacement of PI by another nucleic acid stain with higher fluorescence emission upon binding to DNA.

By using the fluorescence assay we were able to demonstrate that B27(1-18)-C-*Biot* and *Biot*-N-B27(1-18) peptides in solution displayed a mode of action where membrane permeabilization was the key event. Furthermore, the assay was feasible also for the resin-anchored peptides. Both immobilised B27(1-18)-C-*Biot* and *Biot*-N-B27(1-18) peptides eliminated *S. epidermidis via* permeabilization of the bacterial membranes similar to both free peptides in solution. In addition, in the fluorescence assay the C-terminal immobilized peptide showed better efficacy respect to the N-terminal analogue. The subsequent analysis by SEM highlighted significant alterations of bacterial morphology treated with free and immobilized peptides. These data suggest that membrane permeabilization is only one of the phenomena caused by these molecules while alternative/additional mechanisms could be implicated for the anchored peptide. These alternative mechanisms could be related to activation of autolytic enzymes. This hypothesis could be verified using a *S. epidermidis* mutant with a reduced content of WTA/LTA, and in turn a reduced capacity to activate autolysins.

For further development in perspective of orthopaedic applications, it would be valuable studying the stability/efficacy of Ti-attached peptide in the presence of human serum and/or other relevant biological components such as hyaluronic acid, or in the presence of proteases. Although these aspects have not been addressed yet, data collected in the present thesis are promising, highlighting the potential of BMAP27(1-18) for the development of biomaterials refractory to microbial contamination.

Annex
List of publications and Communications

PUBLICATIONS

2020   Colloids and Surfaces B: Biointerfaces, 185, 110586 (DOI: 10.1016/j.colsurfb.2019.110586)

Boix-Lemonche, G., Guillem-Marti, J., D'Este, F., Manero, J. M. & Skerlavaj, B.

Covalent grafting of titanium with a cathelicidin peptide produces an osteoblast compatible surface with antistaphylococcal activity

2017   Journal of Peptide Science, 23, 777–789 (DOI: 10.1002/psc.3026)

D'Este, F., Oro, D., Boix-Lemonche, G., Tossi, A. & Skerlavaj, B.

Evaluation of free or anchored antimicrobial peptides as candidates for the prevention of orthopaedic device-related infections

COMMUNICATIONS

28-30/08/2019   The 9th International Meeting on Antimicrobial Peptides (IMAP 2019) – Utrecht, The Netherlands

Poster 1: Boix-Lemonche, G., D'Este, F. & Skerlavaj, B.

A Rapid Fluorescence-based Microplate Assay to Obtain Mechanistic Insights on the Interaction of Membrane Active Peptides with whole Bacterial Cells

Poster 2: Boix-Lemonche, G., Guillem-Marti, J., D'Este, F., Manero, J. M. & Skerlavaj, B.

Killing of S. epidermidis by a Membrane Active Peptide in Solution and upon Surface Anchoring: insights on mode of action

25-27/08/2017   The 7th International Meeting on Antimicrobial Peptides (IMAP 2017)

– Copenhagen, Denmark

Poster: <u>Boix-Lemonche, G.</u>, Guillem-Marti, J., D'Este, F., Manero, J. M.

& Skerlavaj, B.

Covalent Anchoring of an α-helical Cathelicidin Peptide to Reduce

Staphylococcal Adhesion to Titanium Surface

A Rapid Fluorescence-based Microplate Assay to Obtain Mechanistic Insights on the Interaction of Membrane Active Peptides with whole Bacterial Cells

Gerard Boix-Lemonche; Francesca D'Este; Barbara Skerlavaj

Department of Medicine (DAME); University of Udine (UNIUD); Udine; Italy.

Introduction

For development of novel antimicrobials, an interesting target is represented by bacterial cytoplasmic membrane where vital processes take place[1]. Membrane interactions of Antimicrobial Peptides (AMPs) were extensively investigated by using model membrane systems[2, 4]. However interactions of AMPs with whole bacteria could be different due to complexity of living microbial membranes[5].

Aim of the study

The aim of the present study was to develop a rapid fluorescence-based microplate assay to get mechanistic and kinetic insights on interaction of membrane active peptides with cytoplasmic membranes of whole bacteria.

How have we done it?

We wanted to distinguish between membrane depolarization due to ion movements across the membrane, and membrane permeabilization due to pore formation, in *Staphylococcus* species. To monitor both phenomena simultaneously, bacteria were incubated with a combination of the potential-sensitive dye 3,3'-Dipropylthiadicarbocyanine Iodide (diSC$_3$(5))[6] and the DNA staining dye Propidium Iodide (PI)[7].
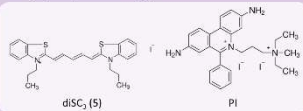
The study was performed by using bactericidal and sub-inhibitory concentrations of the ion channel forming peptide gramicidin D[8], and the pore forming peptide melittin[4].

MIC (MBC)

The minimum inhibitory (MIC) and bactericidal (MBC) concentrations of the membrane active peptides were determined by a broth microdilution assay following Clinical and Laboratory Standards Institute (CLSI) guidelines.

Table 1: Antimicrobial activities against reference strains.

	Melittin	Gramicidin D
	MIC (MBC) (μM)[a, b]	
S. epidermidis ATCC 35984	0.5 (0.5)	2 (4)
S. aureus ATCC 25923	0.5 (1)	4 (8)
E. coli ATCC 25922	1 (1)	>32
P. aeruginosa ATCC 27853	1 (2)	>32

[a] Determined in MH broth at 5-10^5 CFU/mL.
[b] Data are means of at least 2 independent experiments.

Fluorescence dyes have any interference?

The experiment was performed in phosphate buffered saline (PBS) supplemented with 25mM glucose (PBS-glc), using 0.4μM diSC$_3$(5) (λ_{ex}=652nm; λ_{em}=672nm) and 5 μg/mL PI (λ_{ex}=535nm; λ_{em}=617nm) in 96-black well plate. We did not observe any interference between diSC$_3$(5) and PI. *= molecules addition.
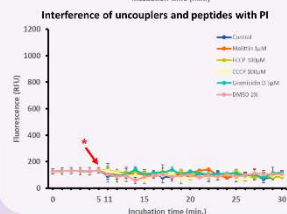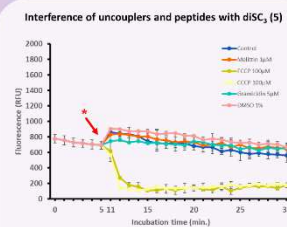

What happens when we use Melittin?

The experiment was performed with 10^8 CFU/mL of the indicated strains (mid-log phase) in PBS-glc, using 0.4μM diSC$_3$(5) and 5 μg/mL PI at 37°C in 96-black well plate. At 30 min. incubation, aliquots were taken to determine bacterial viability by CFU counts. *= molecules addition.
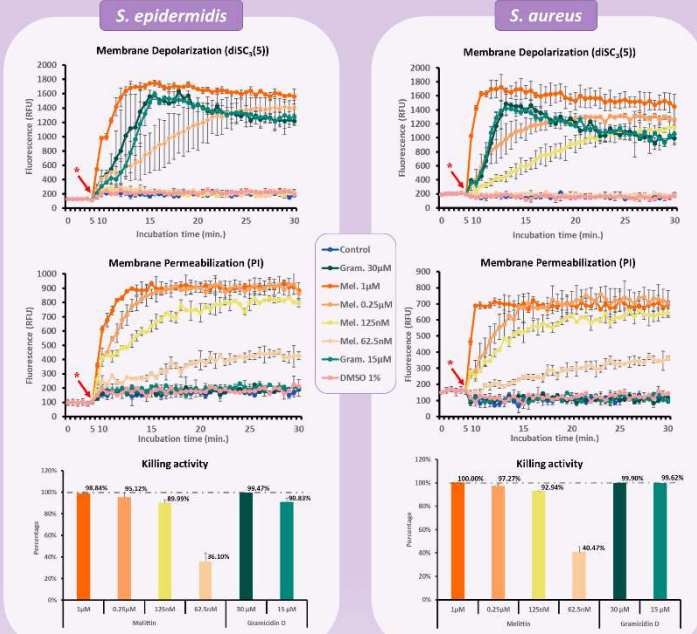
The pore forming peptide melittin, at sub-MIC and bactericidal concentrations caused, respectively, increase in PI fluorescence only or of both dyes simultaneously, suggesting membrane permeabilization as key event.

What happens when we use Gramicidin D?

The experiment was performed with 10^8 CFU/mL of *S. epidermidis* (mid-log phase) in the same conditions as above. *= molecules addition
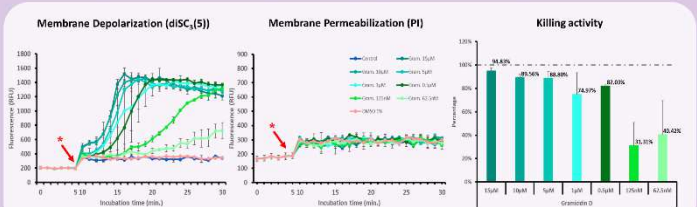
Gramicidin D induced rapid increase in diSC$_3$(5), but not PI fluorescence, with slower kinetics at descending peptide concentrations. In this case bacterial death is related to formation of ion channels causing membrane depolarization.

Conclusions

By combining the potential-sensitive dye diSC$_3$(5) and the DNA staining dye PI, it was possible to discriminate between membrane depolarization and membrane permeabilization in whole gram-positive bacteria. Moreover, the use of microtiter plates allows the simultaneous evaluation of several membrane active antimicrobial agents. We believe that this assay could be applied in mode of action studies of other membrane active AMPs.

Acknowledgments

Contact information

gerardboixlemonche@gmail.com
ORCID: 0000-0002-9093-0695

LinkedIn Profile

ResearchGate Profile

Key Bibliography

[1] J. . Hurdle, A. . O'Neill, R. . Lee, Nat. Rev. Microbiol. 2012, 9, 62.
[2] L. T. Nguyen, E. F. Haney, H. J. Vogel, Trends Biotechnol. 2011, 29, 464.
[3] H. W. Huang, N. E. Charron, Q. Rev. Biophys. 2017, 50, e10.
[4] Z. Oren, Y. Shai, Biopolymers 1998, 47, 451.
[5] H. Strahl, J. Errington, Annu. Rev. Microbiol. 2017, 71, 519.
[6] M. Wu, E. Maier, R. Benz, R. E. W. Hancock, Biochemistry 1999, 38, 7235.
[7] H. Sträuber, S. Müller, Cytom. Part A 2010, 77A, 623.
[8] D. A. Kelkar, A. Chattopadhyay, Biochim. Biophys. Acta - Biomembr. 2007, 1768, 2011.

Killing of *S. epidermidis* by a Membrane Active Peptide in Solution and upon Surface Anchoring: insights on mode of action

Boix-Lemonche, Gerard[1]; Guillem-Marti, Jordi[2,3]; D'Este, Francesca[1]; Manero, Jose María[2]; Skerlavaj, Barbara[1]

1. Department of Medicine (DAME); University of Udine (UNIUD); Udine; Italy.
2. Biomaterials, Biomechanics and Tissue Engineering Group, Department of Materials Science and Metallurgy; Polytechnic Catalonia University (UPC); Barcelona; Spain.
3. Barcelona Research Center in Multiscale Science and Engineering-UPC; Barcelona; Spain.

Introduction

The development of biomaterials coated with antimicrobial peptides could represent an effective strategy to prevent bacterial colonization of implants[1,2]. The design of such coatings could be improved by deeper understanding of the mode of action of immobilized molecules[3].

Aim of the study

The aim of the present study was to investigate the mode of action of a membrane active peptide, free and surface-anchored, against *Staphylococcus epidermidis* ATCC 35984, a microorganism with known adhesive and biofilm forming properties[4].

Experimental approach

The cathelicidin peptide BMAP27(1-18)[5] was evaluated for its membrane perturbing and bactericidal activities in a fluorescence-based microplate assay by using the potential-sensitive dye 3,3'-Dipropylthiadicarbocyanine Iodide (diSC3(5))[6] and CFU counts. The assay can be applied to free peptides in solution and to peptides immobilized on solid support, provided that the latter do not interfere with the assay. We found that streptavidin-functionalized agarose resin was suitable for this purpose[5].
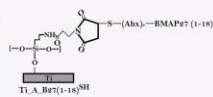
The cathelicidin derived peptide BMAP27(1-18):

GRFKRFRKKFKKLFKKLS

was slightly modified and biotinylated at the N- or C-terminus:

and bound to streptavidin resin beads to evaluate the effect of peptide orientation on its activity.
In addition, to mimic orthopaedic settings, a BMAP27(1-18) derivative was immobilized on titanium disks:

MIC (MBC)

The minimum inhibitory (MIC) and bactericidal (MBC) concentrations of BMAP27(1-18) derivatives were determined by a broth microdilution assay following Clinical and Laboratory Standards Institute (CLSI) guidelines.

Table 1: Antimicrobial activities against reference strains

	BMAP27(1-18)	B27 (1-18)[H]	B18Nb	B18Cb
	MIC (µM)[a,b]			
S. epidermidis ATCC 35984	2	1	2	2
S. aureus ACTCC 25923	4	4	4	2
E. coli ATCC 25822	2	4	8	2
P. aeruginosa ATCC 27853	2	4	8	0.5

[a] Determined in MH broth at 5·10⁵ CFU/mL.
[b] Data are means of at least 3 independent experiments.

What happens with BMAP27(1-18) in solution?

The experiment was performed with 10⁸ CFU/mL *S. epidermidis* (mid-log phase) in PBS supplemented with 25mM glucose, using 0.4µM diSC3(5) and 5 µg/mL PI at 37°C in 96-black well plate. At 30 min. incubation, aliquots were taken to determine bacterial viability by CFU counts. Only results with B18Nb are shown. *= molecules addition.
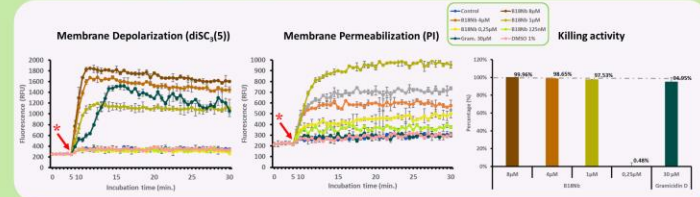
At difference with the channel forming gramicidin D, B18Nb and B18Cb at bactericidal concentrations induced rapid increase of both fluorescence dyes simultaneously, confirming that the mode of action is based on the membrane permeabilizing ability of this type of peptides. In this case, membrane depolarization appears as a obvious consequence of this ability and monitoring diSC3(5) and PI fluorescence is equivalent.

What happens with BMAP27 (1-18) attached to resin beads?

The experiment was performed in the same conditions as above with 10⁷ CFU/mL *S. epidermidis* (mid-log phase) without PI. *= molecules addition.
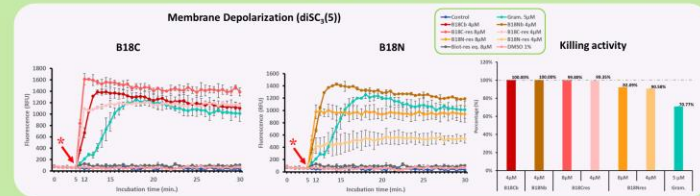
Similar to peptides in solution those immobilized, at concentrations causing 90-99% killing, induced rapid increase in diSC3(5) fluorescence, but with different efficacy between B18Cb and B18Nb. These variations could be attributed to different antimicrobial efficacy in the immobilized state or to different peptide accessibility on the resin. Anyway, data indicate ability of the immobilized peptides to interact with bacterial cytoplasmic membrane causing bacterial death.

Morphological analysis

To get closer to orthopaedic settings, the anti-staphylococcal efficacy was investigated upon peptide tethering to titanium. Morphology of *S. epidermidis* adhered to peptide-functionalized metal disks upon 2h. incubation was analysed by Scanning Electron Microscopy.

S. epidermidis adhered to peptide-functionalized titanium revealed marked morphological modifications (elongated shape, absence of division septa, extrusion of cytoplasmic material) that correlated with the drop in CFU counts (60-65% respect to bare titanium) indicate a bactericidal effect of the immobilized peptide.

Conclusions

The simultaneous increase of both dyes fluorescence upon incubation of bacteria with BMAP27(1-18) in solution indicates that the bactericidal action is caused by irreversible gross membrane perturbation. The increase in diSC3(5) fluorescence seems a consequence of membrane permeabilization.
The peptide immobilized on streptavidin resin beads is able to kill bacteria by membrane perturbation, although with lower efficacy respect to the soluble form, depending also on peptide orientation.
SEM analysis of *S.epidermidis* adhered to peptide-functionalized titanium showed marked alterations in morphology, indicating ability of the titanium bound peptide to exert bactericidal activity. It remains to elucidate whether this effect is mediated by membrane permeabilization or whether alternative/additional mechanisms should be postulated.

Key Bibliography
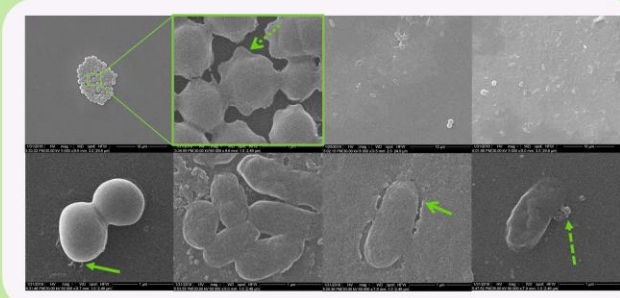
[1] D. Campoccia, L. Montanaro, C. R. Arciola, Biomaterials 2013, 34, 8533.
[2] A. Andrea, N. Molchanova, H. Jenssen, Biomolecules 2018, 8, 27.
[3] K. Hilpert, M. Elliott, H. Jenssen, J. Kindrachuk, C. D. Fjell, J. Körner, D. F. H. Winkler, L. Weaver; P. Henklein, A. S. Ulrich, et al., Chem. Biol. 2009, 16, 58.
[4] M. Sabaté Brescó, L. G. Harris, K. Thompson, B. Stanic, M. Morgenstern, L. O'Mahony, R. G. Richards, T. F. Moriarty, Front. Microbiol. 2017, 8, DOI 10.3389/fmicb.2017.01401.
[5] F. D'Este, D. Oro, G. Boix-Lemonche, A. Tossi, B. Skerlavaj, J. Pept. Sci. 2017, 23, 777.
[6] M. Wu, E. Maier, R. Benz, R. E. W. Hancock, Biochemistry 1999, 38, 7235.

Contact information

LinkedIn Profile

ResearchGate Profile

gerardboixlemonche@gmail.com
ORCID: 0000-0002-9093-0695

Covalent Anchoring of an α-helical Cathelicidin Peptide to Reduce Staphylococcal Adhesion to Titanium Surfaces

Boix-Lemonche, Gerard[1]; Guillem-Marti, Jordi[2,3]; D'Este, Francesca[1]; Manero, Jose María[2]; Skerlavaj, Barbara[1]

1. Department of Medicine (DAME); University of Udine (UNIUD); Udine; Italy.

2. Biomaterials, Biomechanics and Tissue Engineering Group, Department of Materials Science and Metallurgy; Polytechnic Catalonia University (UPC); Barcelona; Spain.

3. Barcelona Research Center in Multiscale Science and Engineering-UPC; Barcelona; Spain.

Introduction

The clinical use of titanium implants is routine in orthopaedic surgery. However, several causes such as poor bone-implant integration, incorrect prosthesis design or bacterial infection may lead to implant failure[1].

Infection of orthopaedic implants is difficult to treat due to formation of biofilm which protects bacteria from the immune system and decreases susceptibility to antibiotics[1]. *Staphylococcus aureus* and *Staphylococcus epidermidis* are among the most common Gram-positive causative agents[2]. The development of biomaterials coated with antimicrobial peptides could represent a valuable strategy to prevent bacterial colonization of implants[3].

Aim of the study

The aim of the present work was to covalently immobilize BMAP27(1-18), an α-helical cathelicidin derived peptide, onto Titanium surfaces, in order to inhibit bacterial colonization and enhance osseointegration of implants.

Why BMAP27 (1-18)?

The antimicrobial peptide BMAP27 (1-18) was selected because it is effective against prosthetic joint pathogens, including clinical isolates; it is active in the presence of human serum, hyaluronic acid and synovial fluid; it is not cytotoxic to osteoblast cells at microbicidal concentrations and maintains activity upon immobilization on solid support[4].

Which coupling strategy has been used?

Titanium disks (1cm diameter) were pretreated with Oxygen plasma, silanized with (3-Aminopropyl)triethoxysilane (APTES) and the bifunctional crosslinker 3-(maleimide)propionic acid N-hydroxysuccinimide ester was then added to the silanized surface. The last step was the coupling of the BMAP27 (1-18) derivative that was synthesized with a free thiol bearing spacer at the N-terminus in order to react with the maleimide groups.
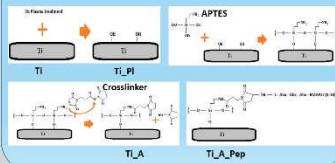
Characterization of functionalized surfaces

The functionalized surfaces have been characterized in terms of wettability, surface mass density and chemical composition by contact angle, Quartz Crystal Microbalance with dissipation monitoring (QCM-D) and X-ray Photoelectron Spectroscopy (XPS) respectively.

QCM-D

QCM-D is a reliable and sensitive method to measure very small masses in the order of ng/cm². In this technique a piezoelectric quartz sensor undergoes oscillation upon application of an alternating electric field across the crystal. If a mass is adsorbed on the crystal, the resonant frequency decreases proportionally to the mass of the peptide. The contribution of water to the mass of the adsorbed layer can be estimated from the dissipation factor.

In this assay a TiO₂ crystal sensor was activated as described above (Ti_A), afterwards BMAP27(1-18) derivative was added (100µM in PBS, pH 6.5) and changes in resonant frequency and dissipation at 25ºC were monitored for 22 hours, using Qtools software (Q-sense).

Frequency and dissipation curves were fitted to a Voigt viscoelastic model to yield the adsorbed mass and thickness of the peptide layer, as well as kinetic information.

Table 1: Features of the peptide functionalized surface.

	Thickness increase (nm)	Surface mass density (ng/cm²)	Viscosity (kg/ms)	Shear elastic modulus (Mpa)
Peptide	2,870±0,010	344,220±1,401	0,001±0,000	0,103±0,000

Chemical composition

The XPS analysis was performed with an XR50 Mg anode source operating at 150W and a Pholbos 150 MCD-9 detector (D8 advance, SPECS Surface Nano Analysis GmbH, Germany). High-resolution spectra were recorded with pass energy of 25eV at 0.1eV steps at a pressure below 7.5 · 10⁻⁹mbar.

Silanization of Ti samples was deduced by the presence of silicon (Si 2p) in Ti_A and Ti_A_Pep samples. Moreover, an increase in the percentages of carbon (C 1s) and nitrogen (N 1s), and a reduction in the percentages of oxygen (O 1s) and titanium (Ti 2p), were observed in Ti_A and Ti_A_Pep samples compared to controls (Ti). The covalent attachment of peptide was supported by an increase in nitrogen and a decrease in silicon (Si 2p) and oxygen (O 1s) contents in Ti_A_Pep compared to Ti_A samples.

Table 2: Chemical composition (atomic %) and Si/Ti relative atomic ratio.

|	C1s	N1s	O1s	Si 2p	S 2p	Ti 2p	Si/Ti
Ti	18.08±0.32	0.89±0.03	47.16±0.86	0.70±0.16	1.53±0.10	31.65±0.24	0.02±0.00
Ti_A	24.77±0.18	3.54±0.03	37.75±0.15	12.18±0.34	0.90±0.02	20.86±0.05	0.58±0.01
Ti_A_Pep	26.85±0.87	4.82±0.35	34.68±2.97	10.49±0.85	0.95±0.34	22.23±0.57	0.47±0.03

Wettability

To define the wettability, contact angle measurements were performed with the sessile drop method with ultrapure distilled water and the apolar liquid diiodomethane. Surface free energy was then calculated using the following equation according to Owens, Wendt, Rabel and Kaelble (OWRK) method:

$$\gamma_L(1 + \cos\theta) = 2\left[\left(\gamma_L^d \gamma_S^d\right)^{-2} + \left(\gamma_L^p \gamma_S^p\right)^{-2}\right]$$

where γ_L^d is the dispersive part and γ_L^p is the polar part, respectively, of the liquid surface tension (γ,). θ is the contact angle of the liquid (L) and solid (S).

Ti_A_Pep samples displayed significantly different contact angle values (non-parametric Mann-Whitney U-test, p<0.05) in comparison with those of Ti_PI and Ti_A samples.
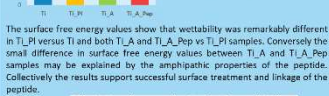
The surface free energy values show that wettability was remarkably different in Ti_PI versus Ti and both Ti_A and Ti_A_Pep vs Ti_PI samples. Conversely the small difference in surface free energy values between Ti_A and Ti_A_Pep samples may be explained by the amphipathic properties of the peptide. Collectively the results support successful surface treatment and linkage of the peptide.

Table 3: Values of contact angles obtained with water (Θ₂(H₂O)) and diiodomethane (Θ (diiod.)); polar (γᵖ) and dispersive (γᵈ) components and surface free energy (γ).

|	Θ₂ (H₂O)°	Θ (diiod.)°	γᵖ (mJ/m²)	γᵈ (mJ/m²)	γᵗ (mJ/m²)
Ti	70.38±0.51	44.97±0.34	8.03±0.26	37.02±0.18	45.05±0.23
Ti_PI	7.49±0.17	23.93±0.31	32.39±0.06	46.52±0.11	78.91±0.05
Ti_A	62.74±0.85	45.28±0.89	12.03±0.46	36.84±0.48	48.87±0.61
Ti_A_Pep	68.29±0.86	42.27±0.96	8.62±0.42	38.42±0.49	47.04±0.56

Bacterial adhesion

Antimicrobial efficacy was evaluated by measuring adhesion of the reference strain *S. epidermidis* ATCC 35984 (1·10⁷CFU/mL inoculum) to Ti samples upon 2 hour incubation in Müller-Hinton broth. The Ti samples have been previously sterilized by soaking in 70% ethanol for 30min, washed 2 times with sterile PBS and put in triplicate in a 24-well plate. After incubation, planktonic bacteria were removed, Ti samples were washed 2 times with sterile PBS and viability of Ti-adhered bacteria was determined by CFU counts after detachment from Ti disks by a vortexing step.

In the presence of BMAP27 (1-18) a significant reduction (64.41%) of *S. epidermidis* adhesion respect to bare titanium was observed.
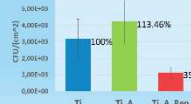
Biofilm formation

To evaluate the capacity of the functionalized surfaces to inhibit the initial stages of biofilm formation, *S. epidermidis* ATCC 35984 (6·10⁷CFU/mL inoculum) was allowed to adhere to Ti samples for 2 hours in Müller-Hinton broth. The Ti samples have been sterilized as described previously and put in triplicate in a 48-well plate. After adhesion, planktonic bacteria were removed, Ti samples were washed 2 times with sterile PBS and allowed to grow in Müller-Hinton broth at 37ºC for additional 20h. Biofilm development was followed by using the metabolic dye Presto-Blue® according to the manufacturers instructions.
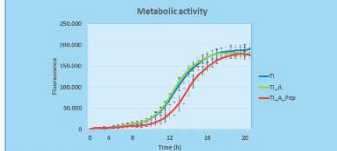
After 20h, an early biofilm has developed. The apparent delay (1h 30min) of growth curve on Ti_A_Pep samples was presumably due to inhibition of the initial bacterial adhesion.

Osteoblast Viability

The biocompatibility of the functionalized Ti samples was evaluated by measuring viability of the human osteosarcoma-derived MG-63 cell line by using the metabolic dye Presto-blue®. MG63 cells (4·10⁴cell/well) were seeded in complete DMEM medium on Ti samples, previously sterilized as described, in triplicate in a 48-well plate. After 4hours of adhesion at 37ºC, cell medium was removed, samples were washed with sterile PBS 2 times and incubated 90 min in complete DMEM containing Presto-blue® at 37ºC.

Metabolic activity of the cells was determined by measuring fluorescence at λ=560-590nm, and reported as percent cell viability with respect to untreated surfaces(Ti).

Results indicate good compatibility of peptide-functionalized Ti samples with osteoblast cells.

Conclusions and future work

- Collectively the results obtained with contact angle, XPS and QCM-D analyses indicate successful attachment of BMAP27 (1-18) to titanium surface.
- Furthermore, the adhesion of *S. epidermidis* to peptide-functionalized titanium disks was remarkably inhibited respect to bare titanium, suggesting effective coupling of BMAP27(1-18) to the metal surface.
- The results of osteoblasts viability assays indicate good compatibility of peptide-functionalized Ti samples with osteoblast cells.

Future work:
- Additional immobilization experiments are currently underway aimed at increasing peptide surface coverage to further improve antimicrobial efficacy of peptide-functionalized titanium.

Key Bibliography

[1] A. J. Tande and R. Patel, *Clin. Microbiol. Rev.*, vol. 27, no. 2, pp. 302–345, 2014.

[2] P. C. Matthews, *et al.*, *BMJ*, vol. 338, no. June, p. b1773, 2009.

[3] M. Godoy-Gallardo, *et al.*, *Acta Biomater.*, vol. 10, no. 8, pp. 3522–3534, 2014.

[4] F. D'Este, *et al.*, *J. Pep. Sci.*, 2017. (published online, Article DOI: 10.1002/psc.3026)

Acknowledgments

USING e-ANNOTATION TOOLS FOR ELECTRONIC PROOF CORRECTION

Required software to e-Annotate PDFs: Adobe Acrobat Professional or Adobe Reader (version 8.0 or above). (Note that this document uses screenshots from Adobe Reader DC.)
The latest version of Acrobat Reader can be downloaded for free at: http://get.adobe.com/reader/

Once you have Acrobat Reader open on your computer, click on the Comment tab (right-hand panel or under the Tools menu).

This will open up a ribbon panel at the top of the document. Using a tool will place a comment in the right-hand panel. The tools you will use for annotating your proof are shown below:
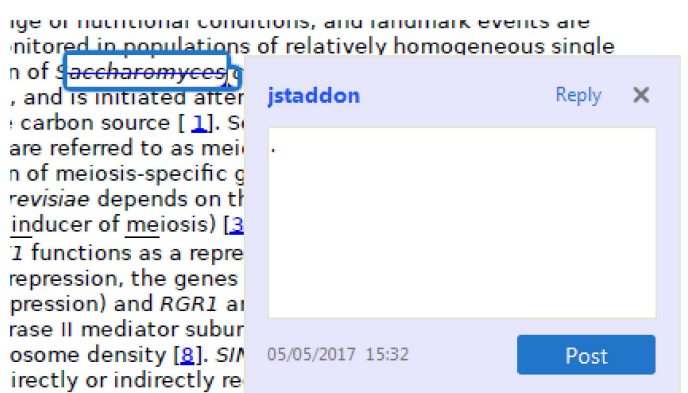
---
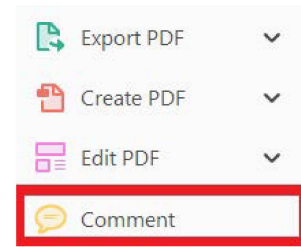
1. Replace (Ins) Tool – for replacing text.

Strikes a line through text and opens up a text box where replacement text can be entered.

How to use it:

- Highlight a word or sentence.

- Click on the Replace (Ins) icon.

- Type the replacement text into the blue box that appears.

(Example annotation screenshot: text about populations of relatively homogeneous single cells of Saccharomyces, with jstaddon comment box dated 05/05/2017 15:32, "Post" button.)

2. Strikethrough (Del) Tool – for deleting text.

Strikes a red line through text that is to be deleted.

How to use it:
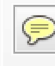
- Highlight a word or sentence.

- Click on the Strikethrough (Del) icon.

- The text will be struck out in red.
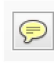
experimental data if available. For ORFs to be had to meet all of the following criteria:
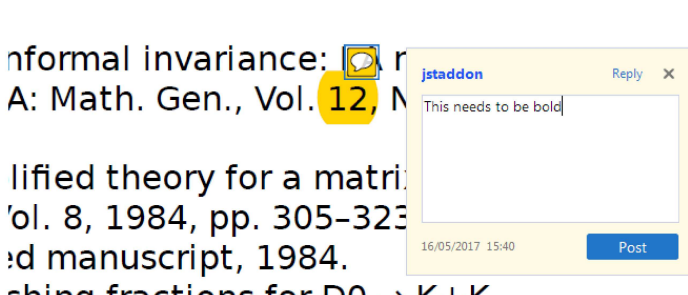
1. Small size (35–250 amino acids).
2. Absence of similarity to known proteins.
3. Absence of functional data which could n the real overlapping gene.
4. Greater than 25% overlap at the N-termin terminus with another coding feature; ove both ends; or ORF containing a tRNA.

---

3. Commenting Tool – for highlighting a section to be changed to bold or italic or for general comments.

Use these 2 tools to highlight the text where a comment is then made.

How to use it:

- Click on the Commenting icon.

- Click and drag over the text you need to highlight for the comment you will add.

- Click on the comment icon.

- Click close to the text you just highlighted.

- Type any instructions regarding the text to be altered into the box that appears.
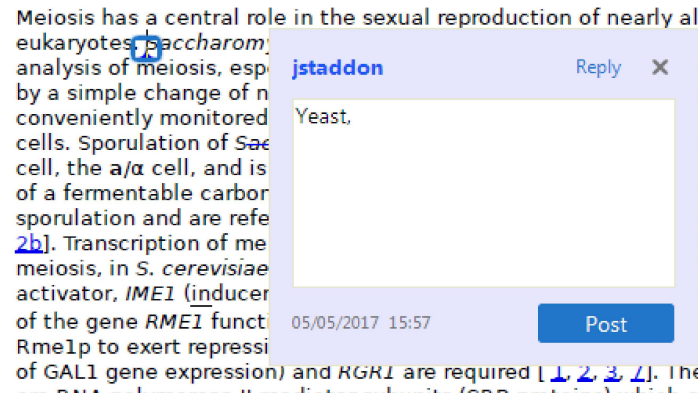
(Example annotation screenshot: "nformal invariance: A: Math. Gen., Vol. 12, N ... lified theory for a matri ol. 8, 1984, pp. 305–323 ed manuscript, 1984. ching fractions for D0 → K+K olation in D0 decays', Phys" with jstaddon comment box "This needs to be bold" dated 16/05/2017 15:40.)
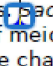
4. Insert Tool – for inserting missing text at specific points in the text.

Marks an insertion point in the text and opens up a text box where comments can be entered.

How to use it:

- Click on the Insert icon.

- Click at the point in the proof where the comment should be inserted.

- Type the comment into the box that appears.

Meiosis has a central role in the sexual reproduction of nearly all eukaryotes ... analysis of meiosis, esp ... by a simple change of ... conveniently monitored ... cells. Sporulation of Sae ... cell, the a/α cell, and is ... of a fermentable carbon ... sporulation and are refe ... 2b]. Transcription of me ... meiosis, in *S. cerevisiae* ... activator, *IME1* (inducer ... of the gene *RME1* functi ... Rme1p to exert repressi ... of GAL1 gene expression) and *RGR1* are required [1, 2, 3, 2]. These ge

(jstaddon comment box "Yeast," dated 05/05/2017 15:57, "Post" button.)

5. **Attach File** **Tool – for inserting large amounts of text or replacement figures.**

Inserts an icon linking to the attached file in the appropriate place in the text.

How to use it:

- Click on .

- Click on the proof to where you'd like the attached file to be linked.
- Select the file to be attached from your computer or network.
- Select the colour and type of icon that will appear in the proof. Click OK.

    The attachment appears in the right-hand panel.

chondrial preparatior
ative damage injury
e extent of membra
, malondialdehyde (
(TBARS) formation.
ured by high perform

6. **Add stamp** **Tool – for approving a proof if no corrections are required.**

Inserts a selected stamp onto an appropriate place in the proof.

How to use it:

- Click on .

- Select the stamp you want to use. (The Approved stamp is usually available directly in the menu that appears. Others are shown under *Dynamic*, *Sign Here*, *Standard Business*).

- Fill in any details and then click on the proof where you'd like the stamp to appear. (Where a proof is to be approved as it is, this would normally be on the first page).

or the business cycle, starting with the
. on perfect competition, constant ret
production. In this environment goods
extra
he
etermined by the model. The New-Key
otaki (1987), has introduced produc
general equilibrium models with nomin

APPROVED

7. **Drawing Markups** **Tools – for drawing shapes, lines, and freeform annotations on proofs and commenting on these marks.**
Allows shapes, lines, and freeform annotations to be drawn on proofs and for comments to be made on these marks.

Drawing tools available on comment ribbon

Line
Arrow
Rectangle
Oval
Text Callout
Polygon
Cloud
Connected Lines
Expand Drawing Tools
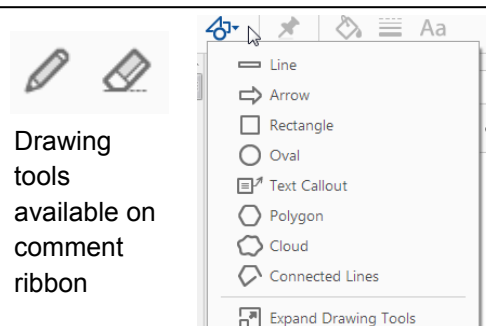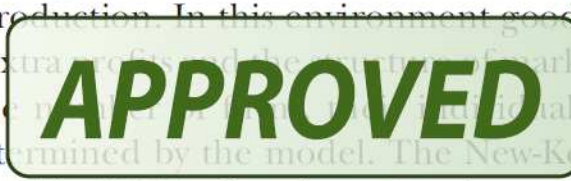
How to use it:

- Click on one of the shapes in the Drawing Markups section.
- Click on the proof at the relevant point and draw the selected shape with the cursor.
- To add a comment to the drawn shape, right-click on shape and select *Open Pop-up Note.*
- Type any text in the red box that appears.

jstaddon   Reply X
08/05/2017 09:52   Post

jstaddon
Please rearrange so these are in
the correct order
08/05/2017 09:49

For further information on how to annotate proofs, click on the Help menu to reveal a list of further options:
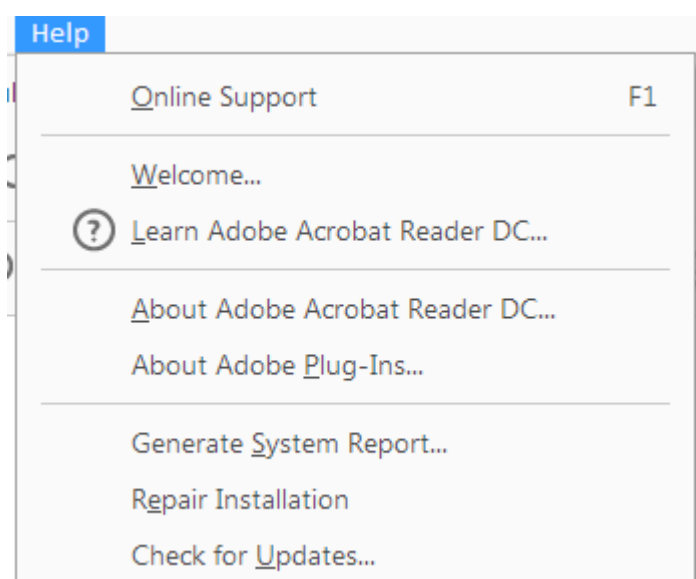
Help

Online Support   F1

Welcome...

(?) Learn Adobe Acrobat Reader DC...

About Adobe Acrobat Reader DC...

About Adobe Plug-Ins...

Generate System Report...

Repair Installation

Check for Updates...

Research Article

Evaluation of free or anchored antimicrobial peptides as candidates for the prevention of orthopaedic device-related infections

Francesca D'Este,[a†] Debora Oro,[a†] Gerard Boix-Lemonche,[a] Alessandro Tossi[b] and Barbara Skerlavaj[a*] [ORCID]

The prevention of implant-associated infection, one the most feared complications in orthopaedic surgery, remains a major clinical challenge and urges development of effective methods to prevent bacterial colonization of implanted devices. Alpha-helical antimicrobial peptides (AMPs) may be promising candidates in this respect due to their potent and broad-spectrum antimicrobial activity, their low tendency to elicit resistance and possible retention of efficacy in the immobilized state.

The aim of this study was to evaluate the potential of five different helical AMPs, the cathelicidins BMAP-27 and BMAP-28, their (1–18) fragments and the rationally designed, artificial P19(9/G7) peptide, for the prevention of orthopaedic implant infections. Peptides were effective at micromolar concentrations against 22 *Staphylococcus* and *Streptococcus* isolates from orthopaedic infections, while only BMAP-28 and to a lesser extent BMAP-27 were active against *Enterococcus faecalis*. Peptides in solution showed activities comparable to those of cefazolin and linezolid, on a molar basis, and also a variable capacity to neutralize bacterial lipopolysaccharide, while devoid of adverse effects on MG-63 osteoblast cells at concentrations corresponding to the MIC. The (1–18) BMAP fragments and P19(9/G7) were selected for further examination, based on better selectivity indices, and showed effectiveness in the presence of hyaluronic acid and in synovial fluid, while human serum affected their activity to variable extents, with BMAP-27(1–18) best retaining activity. This peptide was immobilized on streptavidin–resin beads and retained activity against reference *Staphylococcus epidermidis* and *Staphylococcus aureus* strains, with negligible toxicity towards osteoblasts, underlining its potential for the development of infection-resistant biomaterials for orthopaedic application. Copyright © 2017 European Peptide Society and John Wiley & Sons, Ltd.

Keywords: α-helical antimicrobial peptide; prosthetic joint pathogens; *Staphylococcus*; human serum; hyaluronic acid; peptide immobilization

Introduction

Implant-associated infection is a major challenge in orthopaedic surgery. Although it occurs in only a small proportion of cases, infection of prosthetic joints is a feared and devastating complication of arthroplasty procedures and is associated with substantial morbidity and a huge economic burden [1–3]. The incidence of infection can be much higher following trauma surgery, such as fracture fixation [4]. More than half of infections are caused by Gram-positive cocci, the most common being coagulase-negative *Staphylococcus* spp. and *Staphylococcus aureus*, followed by *Streptococcus* and *Enterococcus* spp. A relevant proportion of these is polymicrobial, often involving methicillin-resistant *S. aureus* (MRSA). Gram-negative bacilli, anaerobes and fungi are less frequent causative agents [1,3]. Treatment of infections associated with orthopaedic devices is challenging as bacteria tend to grow in biofilms, which reduces antibiotic efficacy, added to which is the growing incidence of antibiotic resistance also in orthopaedic settings [1,3,5]. The prevention of initial bacterial colonization of the implant surface thus remains a priority.

In this respect, natural antimicrobial peptides (AMPs) may represent a valuable reservoir of lead compounds for the development of novel anti-infective agents. AMPs comprise structurally diverse molecules endowed with potent microbicidal properties, acting as relevant components of the immune system in a wide range of living organisms [6]. Unlike conventional antibiotics, which act on specific bacterial targets, the mode of action of AMPs in most cases

* Correspondence to: Barbara Skerlavaj, Department of Medicine, University of Udine, P.le Kolbe 4, 33100 Udine, Italy. E-mail: barbara.skerlavaj@uniud.it

Abbreviations: ALP, alkaline phosphatase; AMP, antimicrobial peptide; BHI, brain–heart infusion; CFU, colony-forming unit; CLSI, Clinical and Laboratory Standards Institute; DEG, diethylene glycol; DMEM, Dulbecco's Modified Eagle's Medium; DMF, N,N-dimethylformamide; DXM, dexamethasone; FBS, foetal bovine serum; HA, hyaluronic acid; HBSS, Hanks' Balanced Salt Solution; HPLC, high performance liquid chromatography; HS, human serum; HSA, human serum albumin; LDH, lactate dehydrogenase; LPS, lipopolysaccharide; MBC, minimum bactericidal concentration; MH, Mueller-Hinton; MIC, minimum inhibitory concentration; MRSA, methicillin-resistant Staphylococcus aureus; MRSE, methicillin-resistant Staphylococcus epidermidis; NO, nitric oxide; OM, osteogenic medium; PBS, phosphate buffered saline; RPMI, Roswell Park Memorial Institute; SF, synovial fluid; SD, standard deviation; TFA, trifluoroacetic acid.

† These authors contributed equally to this work.

a   Department of Medicine, University of Udine, P.le Kolbe 4, 33100, Udine, Italy

b   Department of Life Sciences, University of Trieste, Via Giorgieri 5, 34127, Trieste, Italy

relies on their capacity to selectively perturb bacterial membranes, owing to their cationic and amphipathic nature [6,7]. This mechanism accounts for their broad spectrum of activity and efficacy also against antibiotic-resistant strains, as well as for their low propensity to promote bacterial resistance [7]. Additionally, in several instances, AMPs have exhibited immunomodulatory properties due to their ability to interact with host cells and modulate their functions, without damaging them [8,9]. Several natural or artificial AMPs are currently under preclinical or clinical development as novel anti-infectives [6,9,10]. Moreover, an emerging approach focuses on exploiting these molecules for the fabrication of infection-resistant biomaterials for medical use [10–12].

Among the diverse structural classes of AMPs, linear peptides adopting an α-helical conformation appear to possess the most robust antimicrobial activities, with lower susceptibility to medium conditions [13,14]. In addition to broad-spectrum activity, they can bind and neutralize proinflammatory bacterial components such as lipopolysaccharide (LPS) [9,15]. Given their abundance in nature and their relatively easy chemical production with respect to other structural classes, native peptide sequences have been exploited as templates for numerous synthetic helical AMPs with optimized structural parameters to enhance antimicrobial potency and selectivity [16,17]. As their killing mechanism does not require internalization by target bacteria, α-helical AMPs may retain activity upon immobilization, which may render them suitable for the development of antimicrobial surfaces [18–20].

In the present study, five cationic α-helical AMPs, i.e. two bovine members of the cathelicidin AMP family [21], two shorter derivatives [22] and a rationally designed artificial AMP [17], have been evaluated for potential applications in the prevention of orthopaedic device-related infections. Antimicrobial efficacy of peptide candidates has been assayed against bacterial isolates from clinical cases of orthopaedic infection, in comparison with two conventional antibiotics. The peptides were also evaluated for LPS-neutralizing capacity and for potential effects on osteoblast viability and differentiation. Based on their more favourable selectivity indices, the study was then narrowed to the three shorter peptide candidates, which were examined for antimicrobial efficacy under conditions more closely resembling those encountered *in vivo* in arthroplasty settings. The peptide with the best activity overall was then tethered to resin beads via streptavidin–biotin technology to obtain a proof-of-concept demonstration of antimicrobial efficacy upon immobilization.

Materials and Methods

Media and Reagents

Derivatized polyethylene glycol–polystyrene (PEG-PS) resins, coupling reagents for peptide synthesis and 9-fluorenylmethoxy carbonyl (Fmoc)-amino acids were purchased from Applied Biosystems/Thermo Fisher Scientific (Waltham, MA, USA), Novabiochem (Laufelfingel, Switzerland) and ChemImpex (Wood Dale, IL, USA). Peptide synthesis-grade *N,N*-dimethylformamide (DMF), dichloromethane, piperidine and HPLC-grade acetonitrile were from Biosolve (Valkenswaard, The Netherlands). Trifluoroacetic acid (TFA), trifluoroethanol and N-methylmorpholine were from Acros Chimica (Beerse, Belgium). The biotinylating reagents D(+)-Biotin and O-(N-Biotinyl-3-aminopropyl)-O′-(N-glutaryl-3-aminopropyl)-diethyleneglycol (N-Biotinyl-NH-PEG₂-COOH) were obtained from Calbiochem (La Jolla, CA, USA) and Novabiochem, respectively. High-performance Streptavidin-

Sepharose™ resin was purchased from GE Healthcare Life Sciences (Little Chalfont, Buckinghamshire, UK).

Dehydrated media for microbiological assays were obtained from Difco laboratories (Detroit, MI, USA) and Oxoid/Thermo Fisher Scientific. Cefazolin sodium salt, linezolid, LPS from *E. coli* O111:B4, dexamethasone (DXM), hyaluronic acid sodium salt (HA) and normal human serum (HS) were from Sigma-Aldrich (St. Louis, MO, USA). Media and supplements for cell culture were from Sigma-Aldrich with the exception of foetal bovine serum (FBS) (Euroclone, Pero, Italy). Unless otherwise specified, FBS and HS were inactivated at 56 °C for 30 min prior to use. Synovial fluid (SF) samples were obtained with informed consent at Udine University Hospital (Udine, Italy); samples were centrifuged, aliquoted and stored at −80 °C.

The Griess and PrestoBlue® reagents were from Molecular Probes/Thermo Fisher Scientific and Invitrogen/Thermo Fisher Scientific, respectively. The CytoTox 96® Non-Radioactive Cytotoxicity Assay kit was from Promega (Madison, WI, USA). All other reagents, including p-Nitrophenyl Phosphate Liquid Substrate System, were from Sigma-Aldrich. Buffers were prepared in double glass-distilled water.

Peptide Synthesis and Characterization

Peptides (Table 1) were synthesized in the solid phase using the Fmoc-chemistry. Difficult coupling steps were handled as described previously [14,23]. BMAP-27 and BMAP-27(1–18) were biotinylated by coupling 5 equivalents of D(+)-Biotin to the N-terminus of resin-bound peptides in the presence of equimolar 2-(1H-benzotriazole-1-yl)-1,1,3,3-tetramethyluronium tetrafluoro-borate (TBTU) and 1H-hydroxybenzotriazole (HOBt) in DMF containing 0.6 N N-methylmorpholine for 4 h at room temperature. BMAP-27(1–18) was alternatively biotinylated with N-Biotinyl-NH-PEG₂-COOH using the same procedure. The biotinylated peptides are referred to as biot-B27, biot-B27(1–18) and biot-DEG-B27(1–18) in the following sections. After cleavage and deprotection, the peptides were HPLC-purified and confirmed by mass spectrometry using a Q-STAR hybrid quadrupole time-of-flight mass spectrometer (Applied Biosystems/MDS Sciex, Concord, ON, Canada) equipped with an electrospray ion source. Peptide concentrations were determined in aqueous solution by measuring the absorbance at 257 nm (Phe residues) for BMAP-27 and BMAP-27(1–18), and at 280 nm (Tyr and Trp residues) for BMAP-28, BMAP-28(1–18) and P19(9/G7) [14,23].

Peptide Immobilization on Streptavidin-Sepharose Resin

Two-hundred fifty microlitres of 1 mM solutions of the biotinylated peptides [i.e. biot-B17, biot-B27(1–18) and biot-DEG-B27(1–18)] in

Table 1.	Peptide sequences and molecular characteristics				
Peptide	Sequence[a]	MW	Length	q[b]	%H[c]
BMAP-27	GRFKRFRKKFKKLFKKLSPVIPLLHL	3225	26	+12	42
BMAP-28	GGLRSLGRKILRAWKKYGPIIVPIIRI	3074	27	+8	48
BMAP-27(1–18)	GRFKRFRKKFKKLFKKLS	2342	18	+11	33
BMAP-28(1–18)	GGLRSLGRKILRAWKKYG	2058	18	+7	39
P19(9/G7)	GLLKKIGKKAKKALKKLGY	2085	19	+9	42

[a]The C-terminus of all peptides is amidated.
[b]q, net charge.
[c]%H, percent hydrophobic residues (sum of A, F, I, L, Y and W residues divided by number of residues).

PBS were mixed with an equal volume of high performance Streptavidin-Sepharose resin (previously washed free of the storage buffer) resuspended in PBS, and allowed to react overnight at 4 °C under gentle agitation. One resin sample was coupled in parallel with D(+)-Biotin for use as a reference control. Samples were then allowed to re-equilibrate at room temperature, centrifuged and washed extensively with PBS until the absorbance at 257 nm of the resin supernatants reached the baseline level. Resin samples were then resuspended in PBS and either tested immediately, or stored at 4 °C for up to 1 month before use.

The amount of immobilized peptide was estimated after peptide elution from a resin aliquot by 15-min treatment with 0.05% (v/v) TFA and lyophilization. The lyophilized eluates were redissolved in water and assayed using the Bradford reagent with reference to standard curves generated by serial dilutions of the corresponding soluble peptides.

Bacteria and Culture Conditions

The reference strains were *Staphylococcus epidermidis* ATCC 12228 and ATCC 35984, *S. aureus* ATCC 25923, *Escherichia coli* ATCC 25922 and *Pseudomonas aeruginosa* ATCC 27853. Clinical bacterial isolates were collected from hip revision and other orthopaedic surgery at the Valdoltra Orthopaedic Hospital (Ankaran, Slovenia) and the Udine University Hospital (Udine, Italy), and included eight strains of *S. epidermidis*, eight strains of *S. aureus*, one strain each of *Staphylococcus capitis*, *Staphylococcus hominis* and *Staphylococcus caprae*, two strains of *Streptococcus agalactiae*, one group G *Streptococcus* and two isolates of *Enterococcus faecalis*. Bacteria were maintained on Mueller-Hinton (MH) agar plates. One isolate of *S. epidermidis* from the Udine hospital was methicillin-resistant as assessed according to the guidelines and interpretative tables of the Clinical and Laboratory Standards Institute (CLSI). Bacteria were cultured in either liquid Brain Hearth Infusion (BHI) (*Staphylococcus*, *Streptococcus* and *Enterococcus* strains) or MH broth (*E. coli* and *P. aeruginosa*) for 18 h, 1:50-diluted in fresh medium and allowed to grow in an orbital shaker at 37 °C. Mid-log phase bacteria were harvested after 10-min centrifugation at 1000 g and resuspended in MH broth to an optimal density before use in antimicrobial assays. Bacterial density was assessed by turbidity at 600 nm, with reference to previously determined standards. For biofilm experiments, the bacterial inoculum was prepared essentially according to Pompilio *et al.* [24], by direct suspension of colonies grown overnight on MH plates in liquid medium.

Antimicrobial Assays

The minimum inhibitory concentration (MIC) of the peptides in solution was determined by a broth microdilution assay in 96-well microtiter plates, using MH broth with logarithmic-phase microorganisms at 2.5×10^5 CFU/ml, as previously reported [14], following CLSI guidelines. The clinically used antibiotics cefazolin and linezolid were tested in parallel for comparison. The minimum bactericidal concentration (MBC) was determined by plating aliquots from wells showing no visible growth on solid medium to allow colony counts.

Assays for Inhibition of Biofilm Formation

Fifty microlitres of a *S. epidermidis* ATCC 35984 suspension (2×10^6 CFU/ml in MH broth), prepared as described above, was dispensed into flat-bottomed 96-well microtiter plates containing 50 µl in MH of each test agent, at 2× the final dose. Plates were then incubated for 24 h at 37 °C, followed by removal of non-adherent bacteria by aspiration and rinsing with PBS. Fresh MH broth was then added, and adherent cells were quantified using the PrestoBlue cell viability reagent according to the manufacturer's specifications.

Bacterial Growth Kinetics Analysis

Serial dilutions of peptides, at 2× the final concentration, were prepared in 50-µl PBS alone or in PBS supplemented either with 1 or 6 mg/ml hyaluronic acid (HA) (leading to 0.5 and 3 mg/ml final HA concentrations, respectively), or with 50% HS (25% final concentration), or with 40% synovial fluid (SF, 20% final concentration) in U-bottom 96-well plates. Fifty microlitres of adjusted suspensions of *S. epidermidis* ATCC 35984 or *S. aureus* ATCC 25923 in MH broth was added to each well to achieve the final density of 1×10^7 CFU/ml. Plates were then sealed with optically clear plastic films to avoid evaporation, and bacterial growth was monitored at 600 nm for 6 h at 37 °C, with 10-s shaking steps at 15-min intervals. Bacteria grown in each medium in the absence of peptides served as growth controls. In some experiments, peptide dilutions in the selected media were pre-incubated for 3 h at 37 °C prior to the addition of bacteria. Data are reported either as growth curves, or as the calculated percent growth inhibition at 6 h with respect to bacteria incubated in corresponding media in the absence of peptides.

Antibacterial Activity of Immobilized Peptides

Ten-microlitre aliquots of peptide-functionalized Streptavidin-Sepharose resins (5% v/v final resin concentration), or the corresponding supernatants, were diluted in PBS to a final volume of 100 µl in microcentrifuge tubes and supplemented with 100 µl of a 2×10^7 CFU/ml suspension of *S. epidermidis* ATCC 35984 or *S. aureus* ATCC 25923 in MH broth. Bacterial viability was assessed after 1-h incubation at 37 °C on a rotating wheel by the PrestoBlue assay and CFU counts.

Cell Culture and Stimulation

The murine macrophage-like RAW 264.7 and the human osteoblast-like MG-63 cell lines were obtained from ATCC (Manassas, VA, USA) and maintained in RPMI-1640 and DMEM medium, respectively, in a humidified incubator at 37 °C and 5% CO_2 atmosphere. Both media were supplemented with 10% (v/v) FBS, 2 mM L-glutamine, 100 units/ml penicillin and 100 µg/ml streptomycin (complete media).

To analyse the effects on LPS-induced nitric oxide (NO) production, RAW 264.7 cells were seeded in 24-well plates at a density of 9×10^5 cells/well, cultured overnight and treated for 24 h with 100 ng/ml LPS in the absence and presence of peptides at the indicated concentrations, in complete RPMI.

MG-63 cells used for cell viability and cytotoxicity assays were seeded in 96-well plates at a density of 7500/well and grown for 24 h in complete DMEM before being incubated with increasing peptide concentrations in complete medium, or, alternatively, in DMEM supplemented with 10% (v/v) HS, or in HBSS supplemented with 10% HS in the absence and presence of 0.5 mg/ml HA. Peptide-functionalized resins were tested at 5% (v/v) in complete medium. Incubation times were 1 h and 24 h for lactate dehydrogenase (LDH) release and cell viability assays, respectively.

For osteoblast differentiation experiments, MG-63 cells were seeded in 24-well plates at a density of 3×10^5/well in complete medium, grown to 80% confluence and incubated for 7 days in serum-free DMEM supplemented with 10 mM β-glycerophosphate and 50 μg/ml L-ascorbic acid (osteogenic medium, OM) in the absence or presence of 2-μM peptides, of 100-nM dexamethasone (DXM, positive control) or a combination of peptides and DXM. During the incubation period, medium was replaced twice with fresh OM supplemented with the stimuli.

Nitric Oxide (NO) Determination

The amount of NO released by LPS- and peptide-treated RAW 264.7 cells was estimated by spectrophotometric quantification of the stable NO metabolite nitrite in the cell culture supernatants using the Griess reagent. Data were expressed as percent of nitrite produced in response to LPS in the absence of peptides.

Cytotoxicity and Cell Viability Assays

Membrane damage to MG-63 cells was evaluated as leakage of the cytosolic enzyme lactate dehydrogenase (LDH). LDH activity was quantified in both cell-free supernatants and cell lysates using the CytoTox 96 Non-Radioactive Cytotoxicity Assay kit. Data were calculated as percentage of total cellular LDH activity. Cell viability was assessed using the resazurin-based PrestoBlue metabolic dye according to the manufacturer's instructions.

Measurement of Alkaline Phosphatase (ALP) Activity

MG-63 cells, incubated in OM with peptides and DXM as described above, were harvested by trypsinization, resuspended in water and sonicated. Lysate proteins were quantified by the Bradford assay. ALP activity was assessed spectrophotometrically from the transformation of p-nitrophenyl phosphate to p-nitrophenol at 37 °C. Briefly, 10-μg protein aliquots of cell lysates were diluted in water in microtiter plates to a final volume of 50 μl, mixed with 150 μl of p-Nitrophenyl Phosphate Liquid Substrate System and incubated for 80 min at 37 °C. Absorbance was read at 405 nm and compared to a p-nitrophenol standard curve. Data were calculated as nmoles/mg/min and expressed as fold-increase with respect to basal ALP activity, or as percent of ALP activity induced by DXM alone.

Results

Design and Selection of Candidate Peptides

The peptides used in this study (Table 1) were selected on the basis of their reported broad antimicrobial activity spectra that covered Gramme-positive cocci [17,22,23,25]. BMAP-27 and BMAP-28 are amphipathic α-helical bovine cathelicidins that were previously shown to exert potent bactericidal activity based on rapid membrane permeabilization [22,25]. The two shorter derivatives, BMAP-27(1–18) and BMAP-28(1–18) (hereafter referred to as B27(1–18) and B28(1–18)), were synthetically more accessible and showed improved selectivity with respect to prokaryotic cells [22]. The peptide P19(9/G7) (hereafter P19) was rationally designed based on a consensus sequence derived from a panel of over 100 of natural helical AMPs of invertebrate, anuran and mammalian origin [17,23]. This peptide is based on an amidated, 18-residue

sequence, like the BMAP fragments, with an added C-terminal Tyr residue to improve quantification accuracy.

Antimicrobial Activity against Orthopaedic Pathogens

The MIC and MBC values of the peptides towards representative reference strains of Gramme-positive *S. epidermidis* and *S. aureus* and Gramme-negative *E. coli* and *P. aeruginosa* are reported in Table 2. Based on the frequent presence of Gramme-positive micro-organisms among the causative agents of orthopaedic device-related infections [1,3], the peptides were assayed against a panel of Gramme-positive clinical isolates from such infections, including *Staphylococcus*, *Streptococcus* and *Enterococcus* species (Table 3). All peptides proved effective at low micromolar concentrations against most strains, with MBC values very close to the MICs, with the exception of *E. faecalis*, which was susceptible only to BMAP-28 and to a lesser extent to BMAP-27. On a molar basis, their potency was comparable to cefazolin and linezolid, two conventional antibiotics used in orthopaedic practice [26,27]. Considering *S. aureus* and *S. epidermidis* species, susceptibility of clinical isolates and corresponding reference strains to the AMPs was similar. Among the peptides, the rationally designed P19 was overall somewhat less effective against *S. aureus*, while its activity against the other *Staphylococcus* strains was comparable to that of the BMAP peptides. In general, peptides were highly active against *S. epidermidis*, whereas somewhat higher MIC values were observed against *S. aureus* isolates. In addition, all peptides prevented the formation of *S. epidermidis* ATCC 35984 biofilm at their MIC values, as shown in Figure 1a. Cefazolin and linezolid, tested in parallel, resulted in complete biofilm inhibition at 16 μM (fourfold MIC) and 6 μM (MIC), respectively (Figure 1b and data not shown).

Neutralization of Bacterial Lipopolysaccharide

Peptides were next evaluated for their ability to neutralize the effects of bacterial LPS, an activity common to several amphipathic helical AMPs [15] that could be advantageous in the context of orthopaedic biomaterials [28–30]. This was tested by inhibition of LPS-induced nitric oxide (NO) release from RAW 264.7 macrophage-like cells co-stimulated with peptides and LPS. BMAP-27 and -28 completely abolished the NO response at concentrations as low as 0.5–1 μM (Figure 2), consistent with previous reports on their direct LPS-binding properties [31–33]. Among the three shorter peptides, B28(1–18) virtually abolished the LPS-induced response at 2 μM, while B27(1–18) and P19, respectively, caused 80% and 66% inhibition at 8 μM (Figure 2). These results could not be ascribed to cytotoxic effects on the RAW cells, as cell

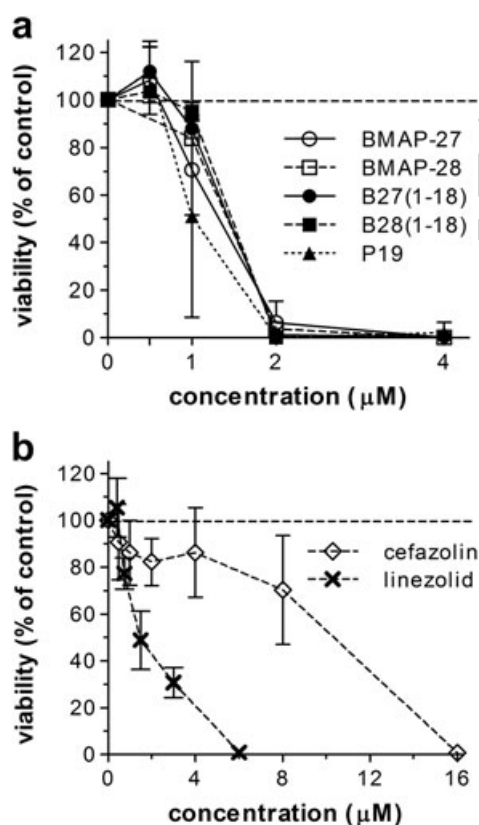| Table 2.	Antimicrobial activities against reference strains				
Organism	BMAP-27	BMAP-28	B27 (1–18)	B28 (1–18)	P19
	MIC (MBC) (μM)[a,b]				
S. epidermidis ATCC 12228	1 (1)	1 (1)	1 (1)	1 (1)	1 (1)
S. epidermidis ATCC 35984	2 (2)	2 (2)	2 (2)	2 (2)	4 (4)
S. aureus ATCC 25923	2 (4)	2 (2)	4 (8)	2 (4)	16 (32)
E. coli ATCC 25922	1 (1)	2 (2)	2 (2)	1 (1)	2 (2)
P. aeruginosa ATCC 27853	2 (4)	4 (16)	2 (4)	2 (4)	2 (2)

[a]Determined in MH broth.
[b]Data are means of at least three independent experiments.

Table 3. Antimicrobial activities against bacterial isolates obtained from clinical cases of orthopaedic infections

Organism (no. of isolates)	BMAP-27	BMAP-28	B27(1–18)	B28(1–18)	P19	Cefazolin	Linezolid
	MIC range (μM)[a,b]						
S. epidermidis (8)	0.5–2 (1[c])	1–2 (2[c])	0.5–4 (1[c])	1–2 (1[c])	0.5–32 (1[c])	0.5–16 (>16[c])	<0.4 – >95 (3[c])
S. aureus (8)	2–4	1–4	2–16	2–8	16 – >64	0.5–2	6
other Staphylococcus spp. (3)	0.5–1	1–2	0.5–1	0.5–1	0.5–1	0.5–4	3
E. faecalis (2)	8–32	4	>64	64	>128	>16	6
Streptococcus spp. (3)	1–2	0.5–4	1–2	1–2	0.5–2	0.25	1.5–3
—	MBC range (μM)[a,b]						
S. epidermidis (8)	1–2 (1[c])	1–2 (2[c])	0.5–4 (1[c])	0.5–4 (1[c])	0.5–64 (0.5[c])	0.5–16 (>16[c])	n.d.
S. aureus (8)	2–4	1–4	2–16	2–8	16 – >64	1–4	n.d.
other Staphylococcus spp. (3)	0.5–1	1–2	0.5–1	0.5–1	0.5–1	1 – >16	n.d.
E. faecalis (2)	8 – >32	4	>64	>64	>128	>16	n.d.
Streptococcus spp. (3)	1–2	2–4	1–2	1–2	0.5–2	1	n.d.
—	MIC_{50} (MIC_{90}) (μM)[a,b,c]						
S. epidermidis (8)	1 (1)	2 (2)	1 (1)	1 (1)	1 (2)	2 (8)	3 (6)
S. aureus (8)	2 (2)	2 (2)	4 (8)	4 (4)	16 (32)	1 (2)	6 (6)

n.d., not determinable.
[a]Determined in MH broth.
[b]Data are means of at least three independent experiments.
[c]Methicillin-resistant strain.
[d]MIC_{50} and MIC_{90}: concentrations that inhibited 50% and 90%, respectively, of the strains.

viability was not impaired under the experimental conditions used (resazurin-based metabolic assays, data not shown).

Effects on Osteoblast Viability and Differentiation

To assess their safety for orthopaedic applications, the effects of peptides on osteoblast cells were investigated using the human osteosarcoma-derived MG-63 cell line, as a well-established *in vitro* osteoblast model [34,35]. Potential short- and long-term effects were assessed in terms of membrane damage, cell viability and cell differentiation. Figure 3a shows the percentage of lactate dehydrogenase (LDH) release by cells incubated with the peptides for 1 h in standard cell culture medium, as an indicator of impaired plasma membrane integrity. None of the peptides caused detectable LDH release at concentrations in each peptide's MIC range (cf.

Figure 1. Inhibition of *S. epidermidis* biofilm formation. *S. epidermidis* ATCC 35984 (1 × 10^{6} CFU/ml in MH broth) was seeded into flat-bottom 96-well polystyrene microtiter plates in the absence and presence of the indicated concentrations of peptides (a) or antibiotics (b). Adherent bacterial cells were quantified after 24-h incubation by the Prestoblue metabolic assay. Results are expressed as percent viability compared to untreated bacteria and are the means ± SD of three independent experiments performed at least in triplicate.

Figure 2. Lipopolysaccharide (LPS) neutralization. RAW 264.7 cells were stimulated with 100 ng/ml *E. coli* O111:B4 LPS in complete RPMI, in the absence and presence of peptides at the indicated concentrations. Nitrite values were determined in the culture supernatants after 24-h incubation using the Griess reagent. Data were calculated as percent of nitrite produced in response to LPS in the absence of peptides and are the means ± SD of three independent experiments.
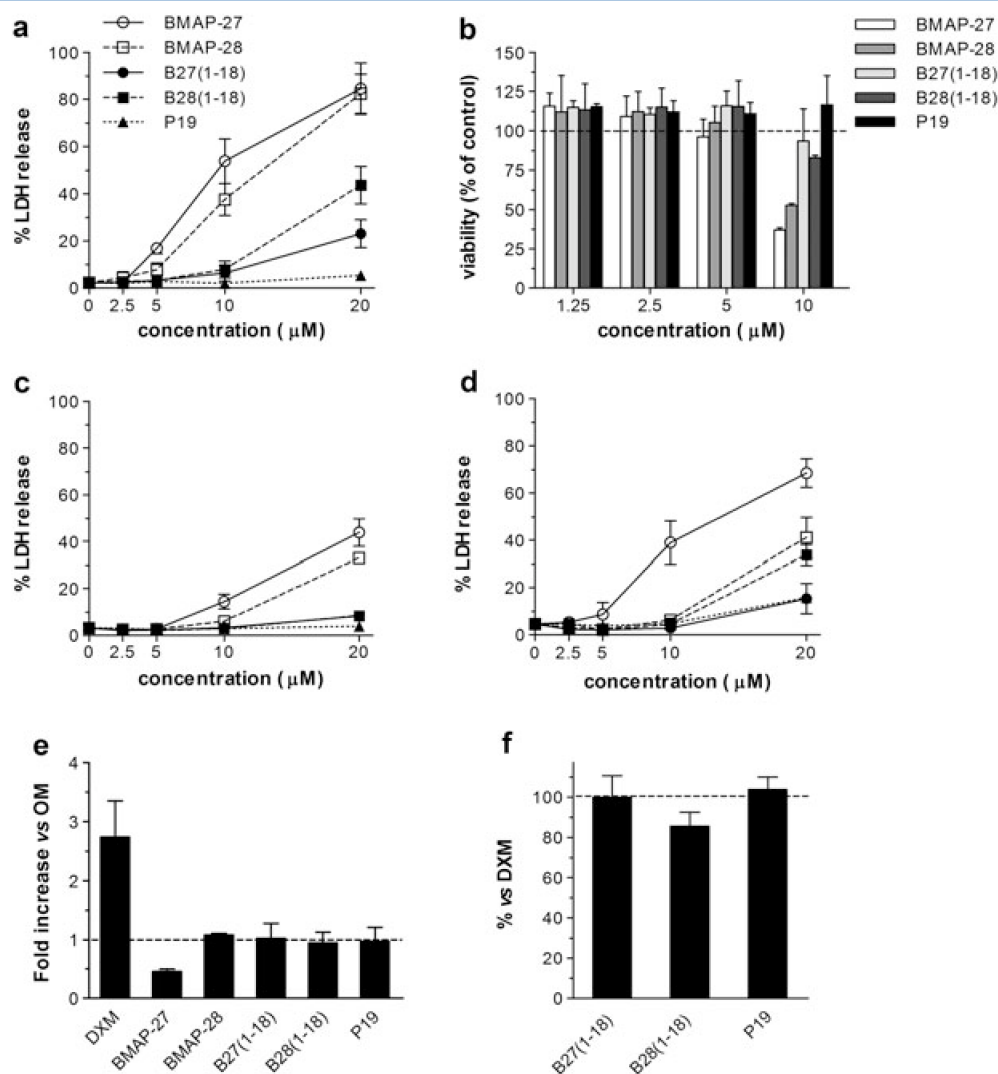
Figure 3. Effects on osteoblast viability and differentiation. a, c, d) MG-63 osteoblast cells were incubated in the absence and presence of the indicated peptide concentrations under the following medium conditions: a) DMEM supplemented with 10% FBS (complete medium); c) DMEM supplemented with 10% human serum (HS); d) HBSS supplemented with 10% HS and 0.5 mg/ml hyaluronic acid (HA). LDH activity was measured in the culture supernatants after 1-h incubation and expressed as percentage of total cellular LDH activity. b) Cells were incubated with peptides for 24 h in complete medium. Cell viability was evaluated by the Prestoblue metabolic assay and is reported as percentage of untreated cells. e, f) Cells were incubated in osteogenic medium (OM) in the absence and presence of 2-μM peptides or 100-nM dexamethasone (DXM) (e), or a combination of peptides and DXM (f). Alkaline phosphatase (ALP) activity was measured in cell lysates after 7 days of incubation and expressed as fold-increase with respect to basal ALP activity (e) or as percent of ALP activity induced by DXM alone (f). Data are the means ± SD of three independent experiments.

Figure 3a and Table 3). The shorter BMAP derivatives were safe up to 10 μM, while the parent peptides caused 38–54% LDH release at this concentration. P19 did not cause detectable effects up to at least 20 μM (Figure 3a). Remarkably, the toxicity of full-length and truncated BMAPs was clearly reduced when using human rather than standard foetal bovine serum in the cell culture medium (Figure 3c), indicating that the range of safe concentrations under conditions relevant to *in vivo* settings could actually be wider. To mimic the joint environment, peptides were assayed in Hanks' Balanced Salt Solution (HBSS) supplemented with HS and hyaluronic acid (HA) at 0.5 mg/ml, a concentration reflecting those found in periprosthetic synovial fluid [36]. Under these conditions, peptides were safe up to 10 μM with the exception of BMAP-27, which caused approximately 40% and 68% LDH release at 10 and 20 μM, respectively (Figure 3d). The three shorter peptides, and in particular P19 and B27(1–18), showed lower overall toxicity. This was also confirmed in terms of cell viability after 24-h incubation

with 1.25 to 10-μM peptides in standard culture medium, which indicated the impairment of cell viability only on treatment with the full-length BMAPs at the highest tested concentration (Figure 3b). Long-term effects on osteoblast cells were also addressed by measuring alkaline phosphatase (ALP) activity as a differentiation marker for these cells [37]. Peptides were evaluated in comparison with dexamethasone (DXM) as a reference osteogenic stimulus [37]. MG-63 cells incubated for 7 days with 2μM peptides in osteogenic medium showed comparable ALP activity as control cells except after treatment with BMAP-27, which caused an approximately 50% reduction in activity (Figure 3e). A 2.7-fold increase in ALP activity was detected in DXM-treated cells (Figure 3e). The three shorter peptides were further investigated in combination with the latter stimulus, showing no significant effects on the DXM-induced response (Figure 3f), suggesting they would not be detrimental to the osseointegration processes.

Antimicrobial Activity in the Presence of Hyaluronic Acid, Synovial Fluid and Blood Serum

Given their compatibility with osteoblast cells, the (1–18) BMAP derivatives and P19 were subjected to further investigation. Their antimicrobial efficacy against *S. epidermidis* ATCC 35984 and *S. aureus* ATCC 25923 was assayed in the presence of HA (as it could interact electrostatically with the cationic peptides due to its negative charge), used at 0.5 and 3 mg/ml to mimic periprosthetic and normal synovial fluid concentrations, respectively [36,38]. Figure 4 shows growth kinetic analyses in the presence of increasing peptide concentrations, expressed as percent growth inhibition after 6-h incubation in each media. HA *per se* did not significantly affect bacterial growth (data not shown). Remarkably, all of the peptides retained full activity against both *Staphylococcus* species under these conditions. Furthermore, full peptide efficacy was retained even after 3 h pre-incubation of peptides with HA (6 mg/ml) before the addition of the bacterial suspension (data not shown), suggesting that peptides should retain efficacy in the joint environment, where HA is a relevant component. This was further supported by growth kinetics analysis of *S. aureus* ATCC 25923 incubated with the peptides in the presence of a clinical sample of synovial fluid (SF, 20%) (Figure 5). A limited number of SF samples were available, showing a rather variable intrinsic inhibition of bacterial growth (data not shown); the one that was chosen for the reported experiment allowed an appreciable *S. aureus* growth within the 6-h experimental time frame. Peptides, tested at 2 μM in its presence, instead completely prevented bacterial growth (Figure 5).

The applicative potential of the peptides was next assessed by antimicrobial assays performed in the presence of HS, based on reported evidence of inhibitory effects of serum components on AMP activity [14,39–41]. Figure 6 shows the percentage of growth
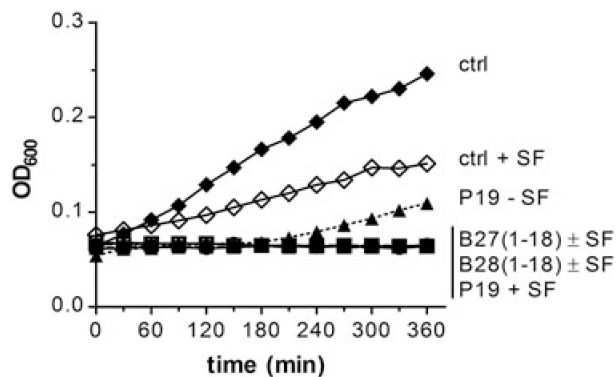
Figure 5. Effects on *S. aureus* growth in the presence of synovial fluid (SF). *S. aureus* ATCC 25923 was incubated at 1×10^7 CFU/ml in 50% MH broth in the absence (closed symbols) and presence (open symbols) of 20% synovial fluid and of 2 μM of the indicated peptides. OD readings at 600 nm (OD_{600}) at 30-min intervals are reported.

inhibition of *S. epidermidis* and *S. aureus* incubated for 6 h with increasing peptide concentrations in the absence and presence of commercial pooled HS at 25%. HS *per se* did not impair growth of either strain (data not shown), while affecting the peptides' inhibitory activity to variable extents. Complete inhibition of *S. epidermidis* growth in the presence of HS was achieved at the same B27(1–18) concentrations as those effective in its absence, and only slightly higher B28(1–18) and P19 concentrations (Figure 6a, b). In the case of *S. aureus*, B27(1–18) and P19 showed a two-fold increase and B28(1–18) a four-fold increase in the concentrations necessary to obtain complete bacterial inhibition (Figure 6d, e). Notably, when peptides were pre-incubated with 50% HS for 3 h prior to addition of the bacterial suspension, all of the peptides were similarly
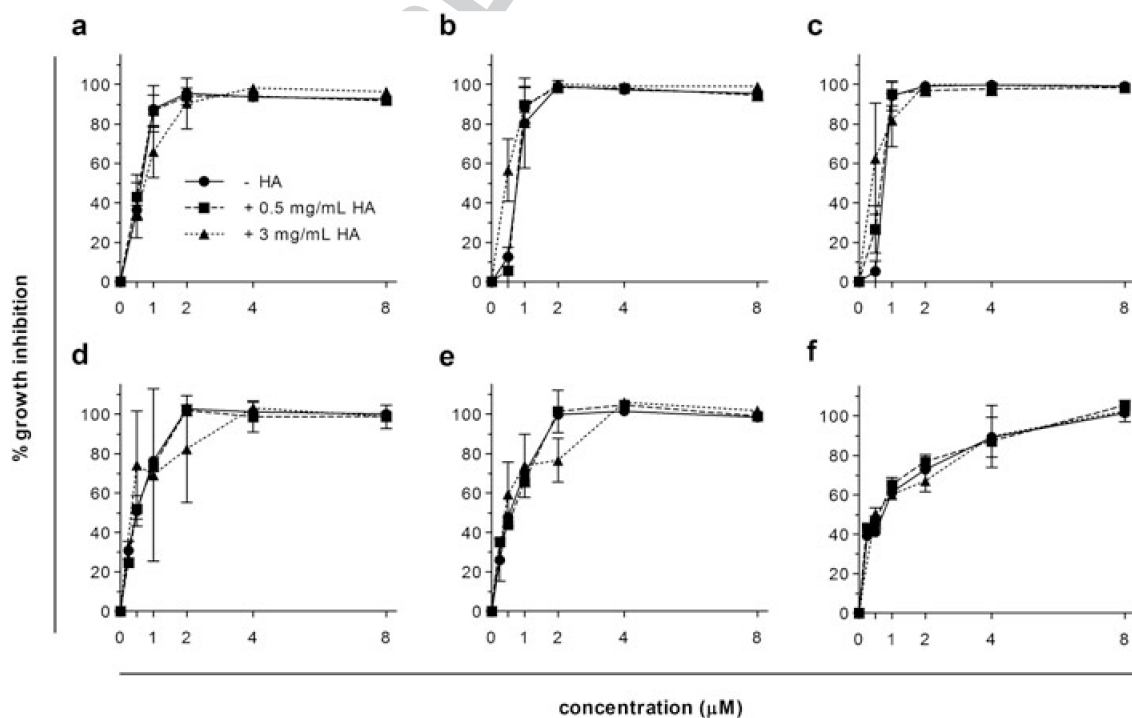
Figure 4. Peptide effects on bacterial growth in the presence of hyaluronic acid (HA). *S. epidermidis* ATCC 35984 (a–c) and *S. aureus* ATCC 25923 (d–f) (1×10^7 CFU/ml in 50% MH broth) were incubated with the indicated concentrations of B27(1–18) (a, d), B28(1–18) (b, e) or P19 (c, f) in the absence (circles, solid lines) and presence of 0.5 mg/ml (squares, dashed lines) and 3 mg/ml (triangles, dotted lines) HA. Bacterial growth was monitored for 6 h by optical density (OD) at 600 nm. Data were calculated as percentage of growth inhibition at the 6-h time point with respect to bacteria incubated in corresponding media in the absence of peptides. The means ± SD of three independent experiments are reported.
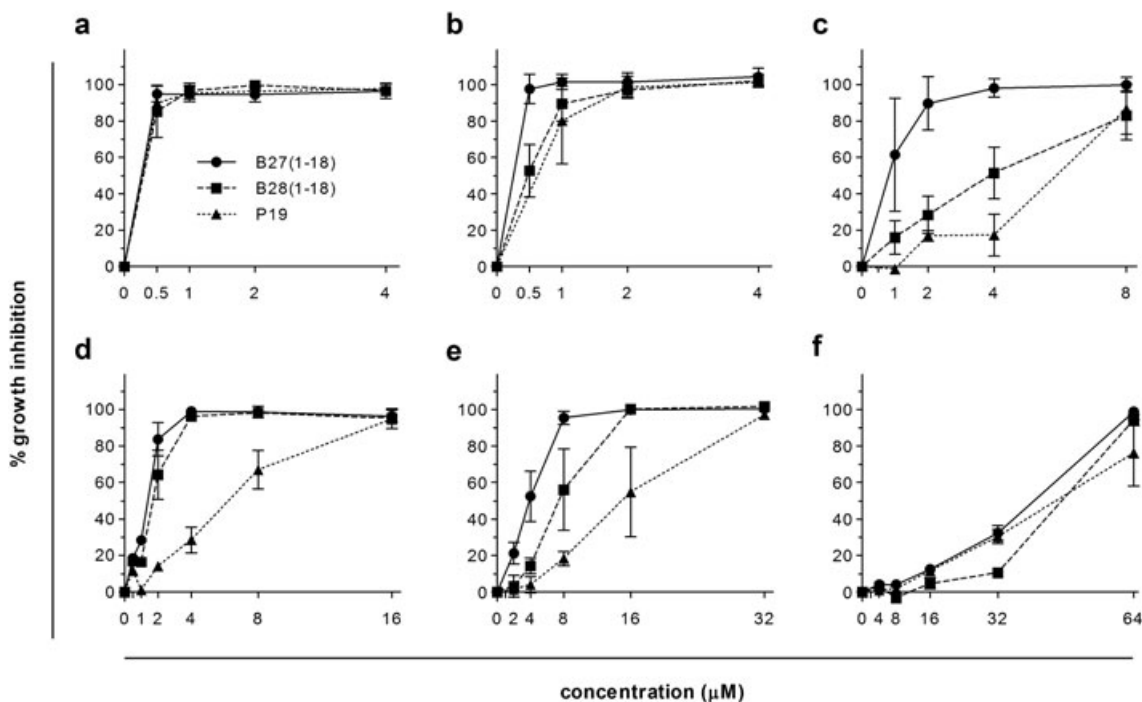
Figure 6. **Effects on bacterial growth in the presence of human serum (HS).** *S. epidermidis* ATCC 35984 (a–c) and *S. aureus* ATCC 25923 (d–f) (1×10^7 CFU/ml) were grown in 50% MH broth in the absence (a, d) and presence (b, c, e, f) of 25% human serum (HS) and of peptides at the indicated concentrations. Bacteria were added immediately after the preparation of peptide dilutions in PBS (a, d) or HS-containing PBS (b, e) or, alternatively, were dispensed to the wells after 3 h pre-incubation of the peptides at 37 °C in the presence of HS (c, f). Bacterial growth was monitored for 6 h by OD_{600} determinations at 30-min intervals. Data were calculated as percentage of growth inhibition at 6 h with respect to corresponding controls incubated in the absence of peptides, and are the means ± SD of three independent experiments.

affected, with the concentration required for complete inhibition of *S. aureus* growth increasing to 64 μM (Figure 6f). With respect to *S. epidermidis* growth inhibition under these conditions, B27(1–18) clearly retained the best activity [complete inhibition at 2–4 μM vs > 8 μM for B28(1–18) and P19] (Figure 6c). When B27(1–18) efficacy against *S. epidermidis* was tested in the presence of heat-inactivated HS (as in the experiments described thus far) or in the presence of HS not subjected to heat inactivation, results were overlapping (data not shown).
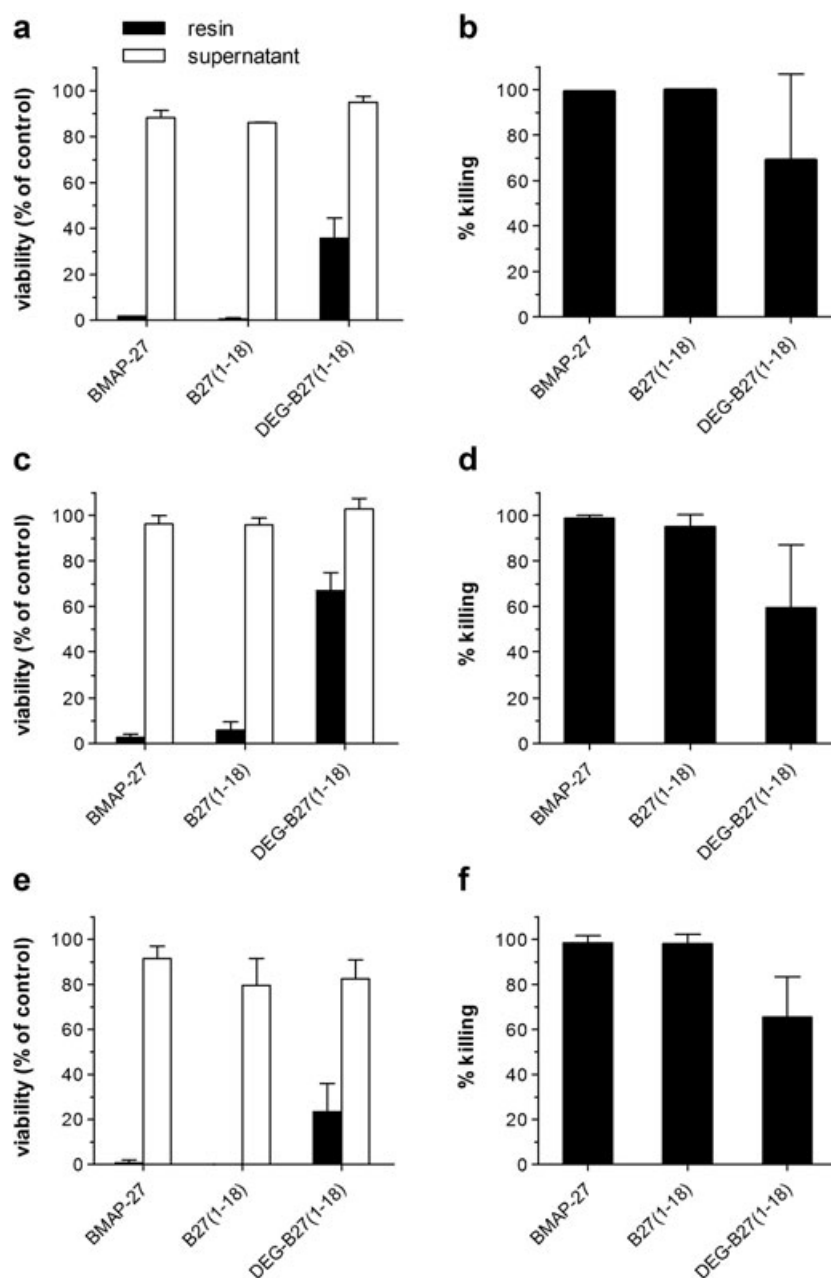
Antimicrobial Efficacy in the Immobilized State

Considering the overall results obtained thus far, the functional analysis of peptide candidates narrowed the choice to B27(1–18) for further evaluation of efficacy upon immobilization. Its parental BMAP-27 was previously reported to retain activity when covalently linked to a solid surface [19], so it was tested in parallel for comparison. Peptides were N-terminally biotinylated and conjugated to a commercial agarose resin functionalized with streptavidin. B27(1–18) was also derivatized with a biotinylated diethylene glycol (DEG) spacer to favour peptide mobility. In solution, the biotinylated derivatives showed comparable MIC values to the corresponding non-biotinylated peptides against reference *S. epidermidis* and *S. aureus* strains (data not shown), indicating that this modification did not alter activity. Peptide-functionalized resin samples were incubated with *S. epidermidis* ATCC 35984 and *S. aureus* ATCC 25923 suspensions for 1 h under agitation. Antibacterial effects were evaluated by the resazurin-based metabolic assay and colony counts. As reported in Figure 7a and c, total bacterial inactivation was achieved upon exposure to BMAP-27 and B27(1–18)-derivatized resins, while with the DEG-B27(1–18)-functionalized sample, 65%

and 33% inhibition of *S. epidermidis* and *S. aureus* was, respectively, observed. Consistent with this, CFU counts revealed complete killing in the case of immobilized BMAP-27 and B27(1–18), and a partial effect with DEG-B27(1–18) (Figure 7b, d). It is important to note that the control resin, derivatized with biotin only, and the supernatants from peptide-derivatized resin samples did not affect bacterial viability (Figure 7a, c). To verify the stability of the functionalized resins, their activity against *S. epidermidis* ATCC 35984 was also measured after 1-month storage at 4 °C and, as shown in Figure 7 e and f, it was fully retained, indicating that the peptide–resin coupling is quite stable. This was also supported by the lack of activity of supernatants from 1-month-old resin samples (Figure 7e). Finally, LDH release assays on MG-63 cells incubated for 1 h with 5% resin suspensions did not reveal any impairment of cell membrane integrity (Table 4) supporting compatibility of functionalized resins with osteoblast cells.

Discussion

Surface modifications to render implants refractory to bacterial colonization are among the main strategies currently pursued to prevent orthopaedic implant-associated infection [42,43]. The antimicrobial peptides of innate immunity are receiving increasing attention as novel anti-infective agents also in the field of medical devices [8–11]. The aim of the present study was to identify a peptide candidate active against relevant orthopaedic implant pathogens under conditions resembling *in vivo* settings and suitable to be immobilized onto solid supports in view of future development of peptide-based infection-resistant biomaterials for orthopaedic applications.

Figure 7. Antimicrobial efficacy of biotinylated peptides immobilized on Streptavidin-Sepharose resin. Streptavidin-Sepharose resin beads functionalized with biotinylated derivatives of BMAP-27 and B27(1–18) as described in the method section were assayed for antimicrobial efficacy either immediately after completion of the coupling procedure (a–d) or upon 1-month storage at 4 °C (e, f). *S. epidermidis* ATCC 35984 (a, b, e, f) and *S. aureus* ATCC 25923 (c, d) (1×10^7 CFU/ml in 50% MH broth) were incubated for 1 h with 5% of the indicated resins (closed bars) or their respective supernatants (open bars) under gentle agitation. a, c, e) Bacterial viability was determined by the Prestoblue metabolic assay and expressed as percent relative to bacteria incubated with the control resin functionalized with biotin only, or the corresponding supernatant. b, d, f) Bacterial killing in resin-treated samples was determined based on colony counts, and expressed relative to the control resin. The means ± SD of three independent experiments are reported.

Five α-helical peptide candidates were compared for their *in vitro* efficacy against clinically relevant Gram-positive bacterial strains isolated from orthopaedic infections. In keeping with previous reports, the BMAP peptides displayed similar low micromolar MIC values against most of the tested strains under standard conditions [14,25,44–46]. The comparable, or only slightly decreased potency of the (1–18) BMAP fragments confirms that antimicrobial activity is mainly mediated by the N-terminal segment predicted to adopt the amphipathic helical conformation [22,25,33]. In this regard, peptide modifications on parental or truncated BMAPs not subverting the overall helical fold

were shown to be irrelevant to peptide activity [33,39,47,48], supporting a relatively non-specific mode of peptide interaction with bacterial membranes that accounts for broad-spectrum permeabilizing effects.

While showing comparable efficacy to the BMAPs on other tested bacterial species, P19 displayed a clearly decreased activity against *S. aureus* strains. This suggests a partially different mode of action. Indeed, peptides of the P19 series have been proposed to act on *Staphylococcus* strains by a mechanism dependent on interference with functional processes at membrane level rather than on direct permeabilization [49].

Table 4. Effects of immobilized peptides on cell membrane integrity in osteoblast cells

Treatment[a]	% LDH release[b]
Control	3.6 ± 0.8
Resin-biotin	1.7 ± 2.1
Resin-B27	4.9 ± 1.9
Resin-B27(1–18)	3.0 ± 0.3
Resin-DEG-B27(1–18)	2.7 ± 0.3

[a]1-h exposure of MG-63 cells to 5% resins in complete medium.
[b]Data were calculated as percentage of total cellular LDH activity, and are the means ± SD of three separate experiments.

With the exception of BMAP-28, the peptides under investigation showed lower efficacy against the clinical isolates of *E. faecalis* with P19 being the least effective. Concerning the BMAPs and derivatives, despite the limited number of strains tested, the observed MICs and the differences in potency are on the whole in line with a previous study assaying their activity against ten *E. faecalis* isolates, including vancomycin-resistant strains [25].

In general, the peptides under study showed a comparable efficacy to conventional antibiotics on a molar basis and moreover proved effective against a methicillin-resistant clinical isolate of *S. epidermidis* (MRSE). This adds to previous reports on the efficacy of BMAPs and their derivatives, as well as of P19, on antibiotic-resistant Gramme-positives, including MRSA [23,25,44,50]. Moreover, peptides prevented *S. epidermidis* biofilm formation at microbicidal concentrations, with an all-or-nothing effect overall, likely due to rapid killing of bacteria before their deposition/attachment to the surface of microplate wells. At variance with the AMPs, both cefazolin and linezolid displayed a gradual inhibition of biofilm formation, consistent with a mode of action not directly targeting the bacterial membrane [51,52]. Furthermore, while linezolid was effective at preventing biofilm formation also at sub-MIC concentrations, cefazolin showed complete inhibition only at fourfold its MIC. Comparing the efficacy of the peptides to cefazolin, the antibiotic of choice in perioperative orthopaedic prophylaxis [26], the selected AMPs appear to be suitable candidates for the prevention of bacterial colonization of implanted devices.

A distinctive feature of cationic AMPs is their capacity to neutralize proinflammatory bacterial components such as LPS (endotoxin) [15]. This property may be advantageous for applications in the field of orthopaedic biomaterials because endotoxin contamination may be responsible for adverse tissue reactions and can negatively affect the osseointegration process [28–30,53]. Indeed, the murine cathelicidin CRAMP, another α-helical cathelicidin that is paralogous to BMAPs, has been shown to inhibit LPS- and flagellin-induced osteoclastogenesis by direct neutralization of these bacterial components and accordingly has been proposed to act as a protector of bone resorption induced by bacterial infection in mice [54]. In the present study, in comparison to the complete LPS-neutralizing activity of the full length BMAPs, the three shorter peptides displayed a lower but appreciable effect. With respect to (1–18) BMAP peptides, this residual but still appreciable LPS-neutralizing effect, as already reported by Lee *et al.* [33], is in line with that also reported for the rabbit paralog CAP18, and sheep BMAP ortholog SMAP-29 [55]. These latter peptides have been proposed to bear LPS-binding sites, located both at the N- and C-terminal ends, that function cooperatively [55]. The lack of the equivalent to one of these sites in the (1–18) BMAP fragments could

explain their somewhat lower LPS-binding capacity compared to the parental molecules. Nevertheless, the residual activity might still be relevant in an *in-vivo* setting, where LPS levels are expected to be significantly lower than those normally used in *in-vitro* assays [56].

One of the major drawbacks in the clinical development of AMPs are cytotoxic effects on host cells [8,9], which offsets several beneficial activities on host cell functions, in addition to their direct microbicidal properties [8,9]. In this respect, the human cathelicidin LL-37, while exerting some toxic effects on osteoblasts [57], has been shown to promote bone regeneration *in vivo* by distinct mechanisms involving stimulation of other cell types [58–60]. In addition, LL-37 has been shown to inhibit osteoclastogenesis *in vitro* [61]. Moreover, the toxic effects of this peptide may be counteracted *in vivo* by endogenous factors [62,63]. Another class of human AMPs, the beta-defensins, are reported to display stimulatory effects on osteoblast proliferation and differentiation [64]. In the present study, all candidate peptides proved safe to osteoblast cells in their MIC value range, with BMAP fragments and P19 clearly displaying a wider selectivity index. This was observed both in standard media and in the presence of HS and hyaluronic acid as relevant factors in view of an orthopaedic application. Our data confirm the improved selectivity of BMAP truncated analogs against prokaryotic *versus* mammalian cells with respect to the parent peptides [22,33]. Moreover, these fragments as well as P19 did not affect osteoblast differentiation *per se*, nor impaired the effect of a recognized osteogenic stimulus [37], which bolsters their suitability for applications on orthopaedic devices.

Although in contrast with several reports on AMP activity being inhibited by anionic polysaccharides [65–68], in the present study, the activity of B27(1–18), B28(1–18) and P19 against *S. epidermidis* and *S. aureus* was fully retained in the presence of HA at concentrations representative of those found in periprosthetic and normal synovial fluid [36,38]. The potential for peptide efficacy in the skeletal joint environment was further supported by potent activity in the presence of a clinical synovial fluid sample, selected among a limited number of available samples due to its compatibility with *S. aureus* growth. Notably, expression of several AMPs was reported in both healthy and inflamed synovial membranes and joint fluid [69–71], and this may reasonably contribute to the inhibitory effects of joint fluid on microbial growth [72]. In an applicative perspective, the presence of endogenous AMPs could be advantageous because they may synergize with exogenously introduced AMPs.

Influence of blood components, e.g. serum albumin and lipoproteins [41,73,74], on AMP activity represents a crucial issue to be addressed in view of potential therapeutic applications. In fact, both BMAP-27 and BMAP-28 have been shown in previous studies to retain antimicrobial properties in the presence of heat-inactivated bovine serum, although at higher peptide concentrations [14,39]. In our growth kinetics assays, the AMPs were effective against both *Staphylococcus* species in serum coincubation experiments, at concentrations comparable or only slightly higher than those in serum-free medium (see Figure 6b, e). Peptides showed a more evident decrease in potency upon pre-incubation with serum (Figure 6c, f), but it was interesting to note that while a decrease in activity against *S. aureus* was observed for all the tested AMPs, B27(1–18) was the least affected in the case of *S. epidermidis*. The inhibitory effect of serum on peptide activity likely depends on peptide sequestration by serum components, as supported by overlapping activity of B27(1–18) against *S. epidermidis* in the presence of active and heat-inactivated HS, suggesting a minimal contribution of enzymatic degradation. In this respect, the different behaviour of

Copyright © 2017 European Peptide Society and John Wiley & Sons, Ltd.

10

B27(1–18) towards two *Staphylococcus* species was rather unexpected, because peptide binding to serum proteins would be expected to comparably affect peptide activity regardless of the target microorganism. It is widely accepted that membrane-active AMPs exert their microbicidal action through both electrostatic and hydrophobic interactions with bacterial membrane surfaces [6,7], while binding to serum seems preponderantly of a hydrophobic nature [74–76]. As B27(1–18) is the least hydrophobic and most cationic of the three shorter AMPs (see Table 1), hydrophobic interactions with serum factors may be relatively weaker and electrostatic attractions with the bacterial surface play a more dominant role. One could thus reasonably speculate that in the presence of a sufficiently anionic bacterial surface, peptide–bacteria interaction would be favoured even in the presence of serum.

According to published reports, *S. epidermidis* has a more anionic surface than *S. aureus* [77,78], which might explain the generally higher activity observed for the three short AMPs against *S. epidermidis* strains as compared to *S. aureus* (Tables 2 and 3). Moreover, for the same reason, *S. epidermidis* could be less prone to shielding by serum, and this is particularly evident for the less hydrophobic and more cationic B27(1–18). The competition of serum and bacterial surface for this AMP is evidently finely balanced, as the less anionic *S. aureus* has a more serum-sensitive susceptibility to this peptide. A similar hypothesis has been proposed by Huang *et al.* [73], to explain the different susceptibilities of selected bacterial species to a cationic α-helical AMP in the presence of human serum albumin (HSA). Notably, in this latter study, *S. epidermidis* was the only microorganism whose susceptibility to the peptide was not affected by HSA [73], again indicating competitive binding to AMPs of this structural class.

Due to its better performance under *in vivo*-mimicking conditions, B27(1–18) was the best candidate for further studies with immobilized peptide. Like the parent BMAP-27, reported to maintain activity on surface tethering [19], B27(1–18) was bactericidal to both *S. epidermidis* and *S. aureus* when bound to resin beads. The streptavidin/biotin-based anchoring method, which approaches the strength of a covalent bond [79], was selected as being a facile and straightforward procedure, suitable for obtaining a proof-of-concept demonstration of peptide efficacy on immobilization [80]. In our study, peptides were tethered via the N-terminus as this facilitated the biotinylation procedure, also given the reported efficacy of several N-terminally immobilized α-helical AMPs [11,18,20]. In our hands, immobilization of biotinylated peptides on streptavidin-functionalized resin beads led to a highly stable conjugate, as bactericidal activity from free peptide was not detected in the resin supernatants, even after a month of storage.

Comparison between full length surface-linked BMAP-27, surface-linked B27(1–18) and also a derivative of the latter with a diethylene glycole spacer [DEG-B27(1–18)] indicated similar activity of BMAP-27 and B27(1–18) on both tested strains, whereas DEG-B27(1–18) showed a somewhat lower efficacy. This however may be due to a lower peptide-loading on the resin, as assessed by peptide quantification upon elution from resin samples. For the DEG-modified peptide, resin loading was assessed to be only 25% that of unmodified B27(1–18) (data not shown). In fact, a fivefold increase in DEG-B27(1–18) resin (from 5 to 25%) led to complete inhibition of *S. epidermidis* and an almost 80% reduction of *S. aureus* viability (data not shown). The reason for including a flexible spacer is that it could be relevant to the efficacy of surface-immobilized AMPs [11,12], but in our system activity appeared to be retained also in its absence, in keeping with the findings of Rapsch *et al.* on directly immobilized α-helical AMPs, including BMAP-27 [19].

In that study, immobilized BMAP-27 was significantly less cytotoxic than the soluble counterpart and was proposed to act via bacterial membrane depolarization [19]. Notably, in our study also, none of the anchored peptides induced appreciable membrane damage to osteoblast cells. In view of a potential application of these peptides in the prevention of orthopaedic device-related infections, surface-immobilized full-length BMAP-27 and the synthetically more accessible B27(1–18) fragment appear to have equivalent antimicrobial efficacy and host-cell compatibility, so that issues related to chemical synthesis procedures and production costs would obviously play in favour of the shorter analog.

Conclusions

Collectively, the results of this study highlight the potential of the α-helical peptide B27(1–18) for the prevention of orthopaedic implant-related infections. It effectively killed bacterial species responsible for orthopaedic infections and prevented staphylococcal biofilm formation. Moreover, it attenuated an LPS-induced inflammatory response and was devoid of adverse effects on osteoblast cells. Its antimicrobial efficacy was comparable to that of cefazolin, widely used in orthopaedic perioperative prophylaxis, and was retained in the presence of relevant biological fluids and components. The proof-of-concept demonstration of its efficacy upon immobilization, obtained with B27(1–18)-functionalized resin beads, encourages further efforts aimed at tethering this peptide onto supports relevant for orthopaedic medical devices, such as titanium or ceramic, in view of the development of peptide-based infection-resistant biomaterials for prostheses.

References

1 Matthews PC, Berendt AR, McNally MA, Byren I. Diagnosis and management of prosthetic joint infection. *BMJ* 2009; **338**: b1773.
2 Sadoghi P, Liebensteiner M, Agreiter M, Leithner A, Bohler N, Labek G. Revision surgery after total joint arthroplasty: a complication-based analysis using worldwide arthroplasty registers. *J. Arthroplast.* 2013; **28**: 1329.
3 Tande AJ, Patel R. Prosthetic joint infection. *Clin. Microbiol. Rev.* 2014; **27**: 302.
4 Metsemakers WJ, Kuehl R, Moriarty TF, Richards RG, Verhofstad MH, Borens O, Kates S, Morgenstern M. Infection after fracture fixation: current surgical and microbiological concepts. *Injury* 2016.
5 ECDC. European Centre for Disease Prevention and Control. *Surveillance of Surgical Site Infections in Europe 2010–2011*. ECDC: Stockholm, 2013.
6 Hancock RE, Sahl HG. Antimicrobial and host-defense peptides as new anti-infective therapeutic strategies. *Nat. Biotechnol.* 2006; **24**: 1551.

7   Nguyen LT, Haney EF, Vogel HJ. The expanding scope of antimicrobial peptide structures and their modes of action. *Trends Biotechnol.* 2011; **29**: 464.

8   Mansour SC, Pena OM, Hancock RE. Host defense peptides: front-line immunomodulators. *Trends Immunol.* 2014; **35**: 443.

9   Yeung AT, Gellatly SL, Hancock RE. Multifunctional cationic host defence peptides and their clinical applications. *Cell. Mol. Life Sci.* 2011; **68**: 2161.

10 Wang G, Mishra B, Lau K, Lushnikova T, Golla R, Wang X. Antimicrobial peptides in 2014. *Pharmaceuticals (Basel)* 2015; **8**: 123.

11 Costa F, Carvalho IF, Montelaro RC, Gomes P, Martins MC. Covalent immobilization of antimicrobial peptides (AMPs) onto biomaterial surfaces. *Acta Biomater.* 2011; **7**: 1431.

12 Onaizi SA, Leong SS. Tethering antimicrobial peptides: current status and potential challenges. *Biotechnol. Adv.* 2011; **29**: 67.

13 Nagaoka I, Hirota S, Yomogida S, Ohwada A, Hirata M. Synergistic actions of antibacterial neutrophil defensins and cathelicidins. *Inflamm. Res.* 2000; **49**: 73.

14 Tomasinsig L, De Conti G, Skerlavaj B, Piccinini R, Mazzilli M, D'Este F, Tossi A, Zanetti M. Broad-spectrum activity against bacterial mastitis pathogens and activation of mammary epithelial cells support a protective role of neutrophil cathelicidins in bovine mastitis. *Infect. Immun.* 2010; **78**: 1781.

15 Rosenfeld Y, Papo N, Shai Y. Endotoxin (lipopolysaccharide) neutralization by innate immunity host-defense peptides. Peptide properties and plausible modes of action. *J. Biol. Chem.* 2006; **281**: 1636.

16 Ong ZY, Wiradharma N, Yang YY. Strategies employed in the design and optimization of synthetic antimicrobial peptide amphiphiles with enhanced therapeutic potentials. *Adv. Drug Deliv. Rev.* 2014; **78**: 28.

17 Zelezetsky I, Tossi A. Alpha-helical antimicrobial peptides – using a sequence template to guide structure–activity relationship studies. *Biochim. Biophys. Acta* 2006; **1758**: 1436.

18 Gabriel M, Nazmi K, Veerman EC, Nieuw Amerongen AV, Zentner A. Preparation of LL-37-grafted titanium surfaces with bactericidal activity. *Bioconjug. Chem.* 2006; **17**: 548.

19 Rapsch K, Bier FF, Tadros M, von Nickisch-Rosenegk M. Identification of antimicrobial peptides and immobilization strategy suitable for a covalent surface coating with biocompatible properties. *Bioconjug. Chem.* 2014; **25**: 308.

20 Soares JW, Kirby R, Doherty LA, Meehan A, Arcidiacono S. Immobilization and orientation-dependent activity of a naturally occurring antimicrobial peptide. *J. Pept. Sci.* 2015; **21**: 669.

21 Zanetti M. Cathelicidins, multifunctional peptides of the innate immunity. *J. Leukoc. Biol.* 2004; **75**: 39.

22 Skerlavaj B, Gennaro R, Bagella L, Merluzzi L, Risso A, Zanetti M. Biological characterization of two novel cathelicidin-derived peptides and identification of structural requirements for their antimicrobial and cell lytic activities. *J. Biol. Chem.* 1996; **271**: 28375.

23 Zelezetsky I, Pag U, Sahl HG, Tossi A. Tuning the biological properties of amphipathic alpha-helical antimicrobial peptides: rational use of minimal amino acid substitutions. *Peptides* 2005; **26**: 2368.

24 Pompilio A, Scocchi M, Pomponio S, Guida F, Di Primio A, Fiscarelli E, Gennaro R, Di Bonaventura G. Antibacterial and anti-biofilm effects of cathelicidin peptides against pathogens isolated from cystic fibrosis patients. *Peptides* 2011; **32**: 1807.

25 Benincasa M, Skerlavaj B, Gennaro R, Pellegrini A, Zanetti M. In vitro and in vivo antimicrobial activity of two alpha-helical cathelicidin peptides and of their synthetic analogs. *Peptides* 2003; **24**: 1723.

26 Bratzler DW, Dellinger EP, Olsen KM, Perl TM, Auwaerter PG, Bolon MK, Fish DN, Napolitano LM, Sawyer RG, Slain D, Steinberg JP, Weinstein RA. Clinical practice guidelines for antimicrobial prophylaxis in surgery. *Am. J. Health Syst. Pharm.* 2013; **70**: 195.

27 Osmon DR, Berbari EF, Berendt AR, Lew D, Zimmerli W, Steckelberg JM, Rao N, Hanssen A, Wilson WR. Diagnosis and management of prosthetic joint infection: clinical practice guidelines by the Infectious Diseases Society of America. *Clin. Infect. Dis.* 2013; **56**: e1.

28 Bonsignore LA, Anderson JR, Lee Z, Goldberg VM, Greenfield EM. Adherent lipopolysaccharide inhibits the osseointegration of orthopedic implants by impairing osteoblast differentiation. *Bone* 2013; **52**: 93.

29 Bonsignore LA, Colbrunn RW, Tatro JM, Messerschmitt PJ, Hernandez CJ, Goldberg VM, Stewart MC, Greenfield EM. Surface contaminants inhibit osseointegration in a novel murine model. *Bone* 2011; **49**: 923.

30 Lieder R, Petersen PH, Sigurjonsson OE. Endotoxins – the invisible companion in biomaterials research. *Tissue Eng Part B Rev* 2013; **19**: 391.

31 D'Este F, Tomasinsig L, Skerlavaj B, Zanetti M. Modulation of cytokine gene expression by cathelicidin BMAP-28 in LPS-stimulated and -unstimulated macrophages. *Immunobiology* 2012; **217**: 962.

32 Ghiselli R, Cirioni O, Giacometti A, Mocchegiani F, Orlando F, Bergnach C, Skerlavaj B, Silvestri C, Vittoria AD, Zanetti M, Rocchi M, Scalise G, Saba V. Effects of the antimicrobial peptide BMAP-27 in a mouse model of obstructive jaundice stimulated by lipopolysaccharide. *Peptides* 2006; **27**: 2592.

33 Lee EK, Kim YC, Nan YH, Shin SY. Cell selectivity, mechanism of action and LPS-neutralizing activity of bovine myeloid antimicrobial peptide-18 (BMAP-18) and its analogs. *Peptides* 2011; **32**: 1123.

34 Luo X, Chen J, Song WX, Tang N, Luo J, Deng ZL, Sharff KA, He G, Bi Y, He BC, Bennett E, Huang J, Kang Q, Jiang W, Su Y, Zhu GH, Yin H, He Y, Wang Y, Souris JS, Chen L, Zuo GW, Montag AG, Reid RR, Haydon RC, Luu HH, He TC. Osteogenic BMPs promote tumor growth of human osteosarcomas that harbor differentiation defects. *Lab. Investig.* 2008; **88**: 1264.

35 Pautke C, Schieker M, Tischer T, Kolk A, Neth P, Mutschler W, Milz S. Characterization of osteosarcoma cell lines MG-63, Saos-2 and U-2 OS in comparison to human osteoblasts. *Anticancer Res.* 2004; **24**: 3743.

36 Guenther LE, Pyle BW, Turgeon TR, Bohm ER, Wyss UP, Schmidt TA, Brandt JM. Biochemical analyses of human osteoarthritic and periprosthetic synovial fluid. *Proc Inst Mech Eng H* 2014; **228**: 127.

37 Xiong Y, Yang HJ, Feng J, Shi ZL, Wu LD. Effects of alendronate on the proliferation and osteogenic differentiation of MG-63 cells. *J Int Med Res* 2009; **37**: 407.

38 Tercic D, Bozic B. The basis of the synovial fluid analysis. *Clin. Chem. Lab. Med.* 2001; **39**: 1221.

39 Ahmad A, Azmi S, Srivastava RM, Srivastava S, Pandey BK, Saxena R, Bajpai VK, Ghosh JK. Design of nontoxic analogues of cathelicidin-derived bovine antimicrobial peptide BMAP-27: the role of leucine as well as phenylalanine zipper sequences in determining its toxicity. *Biochemistry* 2009; **48**: 10905.

40 Johansson J, Gudmundsson GH, Rottenberg ME, Berndt KD, Agerberth B. Conformation-dependent antibacterial activity of the naturally occurring human peptide LL-37. *J. Biol. Chem.* 1998; **273**: 3718.

41 Wang Y, Agerberth B, Lothgren A, Almstedt A, Johansson J. Apolipoprotein A-I binds and inhibits the human antibacterial/cytotoxic peptide LL-37. *J. Biol. Chem.* 1998; **273**: 33115.

42 Campoccia D, Montanaro L, Arciola CR. A review of the biomaterials technologies for infection-resistant surfaces. *Biomaterials* 2013; **34**: 8533.

43 Swartjes JJ, Sharma PK, van Kooten TG, van der Mei HC, Mahmoudi M, Busscher HJ, Rochford ET. Current developments in antimicrobial surface coatings for biomedical applications. *Curr. Med. Chem.* 2015; **22**: 2116.

44 Blodkamp S, Kadlec K, Gutsmann T, Naim HY, von Kockritz-Blickwede M, Schwarz S. In vitro activity of human and animal cathelicidins against livestock-associated methicillin-resistant *Staphylococcus aureus*. *Vet. Microbiol.* 2016; **194**: 107.

45 Mardirossian M, Pompilio A, Crocetta V, De Nicola S, Guida F, Degasperi M, Gennaro R, Di Bonaventura G, Scocchi M. In vitro and in vivo evaluation of BMAP-derived peptides for the treatment of cystic fibrosis-related pulmonary infections. *Amino Acids* 2016; **48**: 2253.

46 Pompilio A, Crocetta V, Scocchi M, Pomponio S, Di Vincenzo V, Mardirossian M, Gherardi G, Fiscarelli E, Dicuonzo G, Gennaro R, Di Bonaventura G. Potential novel therapeutic strategies in cystic fibrosis: antimicrobial and anti-biofilm activity of natural and designed alpha-helical peptides against *Staphylococcus aureus*, *Pseudomonas aeruginosa*, and *Stenotrophomonas maltophilia*. *BMC Microbiol.* 2012; **12**: 145.

47 Ahmad A, Asthana N, Azmi S, Srivastava RM, Pandey BK, Yadav V, Ghosh JK. Structure–function study of cathelicidin-derived bovine antimicrobial peptide BMAP-28: design of its cell-selective analogs by amino acid substitutions in the heptad repeat sequences. *Biochim. Biophys. Acta* 2009; **1788**: 2411.

48 Takagi S, Nishimura J, Bai L, Miyagi H, Kuroda K, Hayashi S, Yoneyama H, Ando T, Isogai H, Isogai E. Susceptibility difference between methicillin-susceptible and methicillin-resistant *Staphylococcus aureus* to a bovine myeloid antimicrobial peptide (BMAP-28). *Anim. Sci. J.* 2014; **85**: 174.

49 Pag U, Oedenkoven M, Sass V, Shai Y, Shamova O, Antcheva N, Tossi A, Sahl HG. Analysis of in vitro activities and modes of action of synthetic antimicrobial peptides derived from an alpha-helical 'sequence template'. *J. Antimicrob. Chemother.* 2008; **61**: 341.

50 Takagi S, Hayashi S, Takahashi K, Isogai H, Bai L, Yoneyama H, Ando T, Ito K, Isogai E. Antimicrobial activity of a bovine myeloid antimicrobial

peptide (BMAP-28) against methicillin-susceptible and methicillin-resistant *Staphylococcus aureus*. *Anim. Sci. J.* 2012; **83**: 482.

51 Leach KL, Brickner SJ, Noe MC, Miller PF. Linezolid, the first oxazolidinone antibacterial agent. *Ann. N. Y. Acad. Sci.* 2011; **1222**: 49.

52 Zaffiri L, Gardner J, Toledo-Pereyra LH. History of antibiotics. From salvarsan to cephalosporins. *J Invest Surg* 2012; **25**: 67.

53 Greenfield EM, Beidelschies MA, Tatro JM, Goldberg VM, Hise AG. Bacterial pathogen-associated molecular patterns stimulate biological activity of orthopaedic wear particles by activating cognate Toll-like receptors. *J. Biol. Chem.* 2010; **285**: 32378.

54 Horibe K, Nakamichi Y, Uehara S, Nakamura M, Koide M, Kobayashi Y, Takahashi N, Udagawa N. Roles of cathelicidin-related antimicrobial peptide in murine osteoclastogenesis. *Immunology* 2013; **140**: 344.

55 Tack BF, Sawai MV, Kearney WR, Robertson AD, Sherman MA, Wang W, Hong T, Boo LM, Wu H, Waring AJ, Lehrer RI. SMAP-29 has two LPS-binding sites and a central hinge. *Eur. J. Biochem.* 2002; **269**: 1181.

56 Opal SM, Scannon PJ, Vincent JL, White M, Carroll SF, Palardy JE, Parejo NA, Pribble JP, Lemke JH. Relationship between plasma levels of lipopolysaccharide (LPS) and LPS-binding protein in patients with severe sepsis and septic shock. *J Infect Dis* 1999; **180**: 1584.

57 Sall J, Carlsson M, Gidlof O, Holm A, Humlen J, Ohman J, Svensson D, Nilsson BO, Jonsson D. The antimicrobial peptide LL-37 alters human osteoblast Ca2+ handling and induces Ca2+-independent apoptosis. *J Innate Immun* 2013; **5**: 290.

58 Kittaka M, Shiba H, Kajiya M, Fujita T, Iwata T, Rathvisal K, Ouhara K, Takeda K, Komatsuzawa H, Kurihara H. The antimicrobial peptide LL37 promotes bone regeneration in a rat calvarial bone defect. *Peptides* 2013; **46**: 136.

59 Zhang Z, Shively JE. Generation of novel bone forming cells (monoosteophils) from the cathelicidin-derived peptide LL-37 treated monocytes. *PLoS One* 2010; **5**: e13985.

60 Zhang Z, Shively JE. Acceleration of bone repair in NOD/SCID mice by human monoosteophils, novel LL-37-activated monocytes. *PLoS One* 2013; **8**: e67649.

61 Supanchart C, Thawanaphong S, Makeudom A, Bolscher JG, Nazmi K, Kornak U, Krisanaprakornkit S. The antimicrobial peptide, LL-37, inhibits in vitro osteoclastogenesis. *J. Dent. Res.* 2012; **91**: 1071.

62 Svensson D, Westman J, Wickstrom C, Jonsson D, Herwald H, Nilsson BO. Human endogenous peptide p33 inhibits detrimental effects of LL-37 on osteoblast viability. *J. Periodontal Res.* 2015; **50**: 80.

63 Svensson D, Wilk L, Morgelin M, Herwald H, Nilsson BO. LL-37-induced host cell cytotoxicity depends on cellular expression of the globular C1q receptor (p33). *Biochem. J.* 2016; **473**: 87.

64 Kraus D, Deschner J, Jager A, Wenghoefer M, Bayer S, Jepsen S, Allam JP, Novak N, Meyer R, Winter J. Human beta-defensins differently affect proliferation, differentiation, and mineralization of osteoblast-like MG63 cells. *J. Cell. Physiol.* 2012; **227**: 994.

65 Benincasa M, Mattiuzzo M, Herasimenka Y, Cescutti P, Rizzo R, Gennaro R. Activity of antimicrobial peptides in the presence of polysaccharides produced by pulmonary pathogens. *J. Pept. Sci.* 2009; **15**: 595.

66 Herasimenka Y, Benincasa M, Mattiuzzo M, Cescutti P, Gennaro R, Rizzo R. Interaction of antimicrobial peptides with bacterial polysaccharides from lung pathogens. *Peptides* 2005; **26**: 1127.

67 Nelson A, Berkestedt I, Schmidtchen A, Ljunggren L, Bodelsson M. Increased levels of glycosaminoglycans during septic shock: relation to mortality and the antibacterial actions of plasma. *Shock* 2008; **30**: 623.

68 Toppazzini M, Coslovi A, Boschelle M, Marsich E, Benincasa M, Gennaro R, Paoletti S. Can the interaction between the antimicrobial peptide LL-37 and alginate be exploited for the formulation of new biomaterials with antimicrobial properties? *Carbohyd Polym* 2011; **83**: 578.

69 Gollwitzer H, Dombrowski Y, Prodinger PM, Peric M, Summer B, Hapfelmeier A, Saldamli B, Pankow F, von Eisenhart-Rothe R, Imhoff AB, Schauber J, Thomas P, Burgkart R, Banke IJ. Antimicrobial peptides and proinflammatory cytokines in periprosthetic joint infection. *J. Bone Joint Surg. Am.* 2013; **95**: 644.

70 Paulsen F, Pufe T, Conradi L, Varoga D, Tsokos M, Papendieck J, Petersen W. Antimicrobial peptides are expressed and produced in healthy and inflamed human synovial membranes. *J. Pathol.* 2002; **198**: 369.

71 Varoga D, Pufe T, Mentlein R, Kohrs S, Grohmann S, Tillmann B, Hassenpflug J, Paulsen F. Expression and regulation of antimicrobial peptides in articular joints. *Ann. Anat.* 2005; **187**: 499.

72 Gruber BF, Miller BS, Onnen J, Welling RD, Wojtys EM. Antibacterial properties of synovial fluid in the knee. *J Knee Surg* 2008; **21**: 180.

73 Huang J, Hao D, Chen Y, Xu Y, Tan J, Huang Y, Li F. Inhibitory effects and mechanisms of physiological conditions on the activity of enantiomeric forms of an alpha-helical antibacterial peptide against bacteria. *Peptides* 2011; **32**: 1488.

74 Peck-Miller KA, Darveau RP, Fell HP. Identification of serum components that inhibit the tumoricidal activity of amphiphilic alpha helical peptides. *Cancer Chemother. Pharmacol.* 1993; **32**: 109.

75 Ciornei CD, Sigurdardottir T, Schmidtchen A, Bodelsson M. Antimicrobial and chemoattractant activity, lipopolysaccharide neutralization, cytotoxicity, and inhibition by serum of analogs of human cathelicidin LL-37. *Antimicrob. Agents Chemother.* 2005; **49**: 2845.

76 Sorensen O, Bratt T, Johnsen AH, Madsen MT, Borregaard N. The human antibacterial cathelicidin, hCAP-18, is bound to lipoproteins in plasma. *J. Biol. Chem.* 1999; **274**: 22445.

77 Dickson JS, Koohmaraie M. Cell-surface charge characteristics and their relationship to bacterial attachment to meat surfaces. *Appl Environ Microb* 1989; **55**: 832.

78 Rawlinson LA, O'Gara JP, Jones DS, Brayden DJ. Resistance of *Staphylococcus aureus* to the cationic antimicrobial agent poly(2-(dimethylamino ethyl)methacrylate) (pDMAEMA) is influenced by cell-surface charge and hydrophobicity. *J. Med. Microbiol.* 2011; **60**: 968.

79 Dundas CM, Demonte D, Park S. Streptavidin–biotin technology: improvements and innovations in chemical and biological applications. *Appl. Microbiol. Biotechnol.* 2013; **97**: 9343.

80 Hilpert K, Elliott M, Jenssen H, Kindrachuk J, Fjell CD, Korner J, Winkler DF, Weaver LL, Henklein P, Ulrich AS, Chiang SH, Farmer SW, Pante N, Volkmer R, Hancock RE. Screening and characterization of surface-tethered cationic peptides for antimicrobial activity. *Chem. Biol.* 2009; **16**: 58.

Research Article

Evaluation of free or anchored antimicrobial peptides as candidates for the prevention of orthopaedic device-related infections

Francesca D'Este, Debora Oro, Gerard Boix-Lemonche, Alessandro Tossi and Barbara Skerlavaj
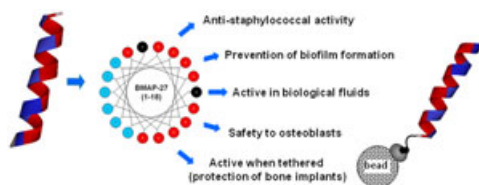
Peptide structure adapted from PDB solution structure 2KET (BMAP-27).

Author Query Form

Dear Author,

During the copyediting of your paper, the following queries arose. Please respond to these by annotating your proofs with the necessary changes/additions.
- If you intend to annotate your proof electronically, please refer to the E-annotation guidelines.
- If you intend to annotate your proof by means of hard-copy mark-up, please use the standard proofing marks. If manually writing corrections on your proof and returning it by fax, do not write too close to the edge of the paper. Please remember that illegible mark-ups may delay publication.

Whether you opt for hard-copy or electronic annotation of your proofs, we recommend that you provide additional clarification of answers to queries by entering your answers on the query sheet, in addition to the text mark-up.

Query No.	Query	Remark
Q1	AUTHOR: Please confirm that given names (red) and surnames/family names (green) have been identified correctly.	names are ok
Q2	AUTHOR: Please verify that the linked ORCID identifiers are correct for each author.	ORCID is ok
Q3	AUTHOR: Columns with blank spaces has been replaced with emdash (- -) as it can indicate many things. Please define significance of the columns with emdash (- -) replacement or leave as is if there is none.	leave as is
Q4	AUTHOR: Please provide volume number and page range for ref. 4	provided
Q5	AUTHOR: Please provide the page range for this chapter in Reference.	provided

Please confirm that the funding sponsor list below was correctly extracted from your article: that it includes all funders and that the text has been matched to the correct FundRef Registry organization names. If a name was not found in the FundRef registry, it may not be the canonical name form, it may be a program name rather than an organization name, or it may be an organization not yet included in FundRef Registry. If you know of another name form or a parent organization name for a "not found" item on this list below, please share that information.

FundRef Name	FundRef Organization Name
University of Udine, Department of Medicine	not found
European Regional Development Fund, Cross-Border Cooperation Italy-Slovenia Programme 2007-2013 (Strategic project Trans2Care - Transregional Network for Innovation and Technology Transfer to Improve Health Care)	~~not found~~ European Union (EU)
~~European Regional Development Fund~~	~~European Regional Development Fund~~

Covalent grafting of titanium with a cathelicidin peptide produces an osteoblast compatible surface with antistaphylococcal activity

Gerard Boix-Lemonche [a], Jordi Guillem-Marti [b, c], Francesca D'Este [a], José María Manero [c], Barbara Skerlavaj [a], *

[a] Department of Medicine (DAME), University of Udine, Piazzale Kolbe, 4, 33100 Udine, Italy
[b] Biomaterials, Biomechanics and Tissue Engineering Group, Department of Materials Science and Metallurgical Engineering, Universitat Politècnica de Catalunya (UPC), Av. Eduard Maristany 14, 08930, Barcelona, Spain
[c] Barcelona Research Center in Multiscale Science and Engineering-UPC, Av. Eduard Maristany 14, 08930, Barcelona, Spain

ARTICLE INFO

ABSTRACT

Bacterial infection of orthopaedic implants, often caused by Staphylococcus species, may ultimately lead to implant failure. The development of infection-resistant, osteoblast-compatible biomaterials could represent an effective strategy to prevent bacterial colonization of implants, reducing the need for antibiotics.

In this study, the widely used biomaterial titanium was functionalized with BMAP27(1–18), an α-helical cathelicidin antimicrobial peptide that retains potent staphylocidal activity when immobilized on agarose beads. A derivative bearing a short spacer with a free thiol at the N-terminus was coupled to silanized titanium disks via thiol-maleimide chemistry. Tethering was successful, as assessed by Contact angle, Quartz Crystal Microbalance with Dissipation monitoring (QCM-D), and X-ray Photoelectron Spectroscopy (XPS), with an average surface mass density of $456\,ng/cm^2$ and a layer thickness of $3\,nm$. The functionalized titanium displayed antimicrobial properties against a reference strain of Staphylococcus epidermidis with well-known biofilm forming capability. Reduction of bacterial counts and morphological alterations of adhering bacteria, upon 2 h incubation, indicate a rapid contact-killing effect. The immobilized peptide was not toxic to osteoblasts, which adhered and spread better on functionalized titanium when co-cultured with bacteria, compared to non-coated surfaces. Results suggest that functionalization of titanium with BMAP27(1–18) could be promising for prevention of bacterial colonization in bone graft applications.

1. Introduction

Infection of implanted prostheses is the most serious complication in arthroplasty procedures and it may lead to implant failure [1]. Treatment is difficult, mainly due to formation of microbial biofilm on device surfaces [1–3]. When sessile, bacteria grow encased in a self-made extracellular matrix that protects them from host defence and renders them less accessible to antibiotics [1,2,4]. Bacteria in biofilms are remarkably less susceptible to currently used antibiotics, when compared to their planktonic counterparts, so that only a few of the available antibiotics are effective against them [3,5,6]. Treatment can be additionally challenging in the case of infections caused by pathogens with acquired antibiotic-resistance [1,5]. Among the most frequent causative agents of prosthetic joint infections and orthopaedic surgical site infections are Gram-positive microorganisms [7], with

20–30 % of cases being ascribed to Staphylococcus aureus and about 20–40 % to coagulase-negative staphylococci [5]. In this respect, Staphylococcus epidermidis, which is a harmless commensal in healthy subjects, is emerging as an opportunistic pathogen in immunocompromised patients, preterm newborns, and patients with indwelling medical devices [8]. Its ability to adhere and form biofilm on device surfaces is recognized as a true virulent factor [9].

Consequently, it is crucial to adopt strategies for the prevention of bacterial adhesion to, and biofilm formation on, implant surfaces, not only by improving the perioperative preventative measures but also with the development of osteoblast-compatible biomaterials resistant to bacterial infection. In fact, events following implantation have been described as a "race for the surface". If it is won by host tissue cells, the implant surface is covered by tissue and becomes less susceptible to bacterial colonization. If, however, it is won by bacteria, then biofilm

Table 1

Antimicrobial activity of soluble peptides against reference strains.

	BMAP27(1-18)	B27(1-18)[SH]
	MIC (μM)[a,b]	
S. epidermidis ATCC 35,984	2	1
S. aureus ATCC 25923	4	4
E. coli ATCC 25,922	2	4
P. aeruginosa ATCC 27,853	2	4

[a] Determined in MH broth.

[b] Data are means of at least 3 independent experiments.

Table 2

Contact angle values and calculation of surface free energy and of its polar and dispersive components. Results are expressed as means ± SD of five measurements for each condition on duplicate samples.

	CA_w (°)	POL (mJ/ m^2)	DISP (mJ/ m^2)	SFE (mJ/ m^2)
Ti	70.4 ± 0.5	8.0 ± 0.3	37.0 ± 0.2	45.1 ± 0.2
Ti_Pl	7.5 ± 0.2 [a]	32.4 ± 0.1 [a]	46.5 ± 0.1 [a]	78.9 ± 0.1 [a]
Ti_A	62.7 ± 0.9 [a,b]	12.0 ± 0.5 [a,b]	36.8 ± 0.5 [b]	48.9 ± 0.6 [a,b]
Ti_A_B27(1-18)[SH]	68.3 ± 0.9 [b,c]	8.6 ± 0.4 [b,c]	38.4 ± 0.5 [a,b]	47.0 ± 0.6 [a,b]

CA_w: contact angle water; POL: polar component; DISP: dispersive component and SFE: surface free energy.

[a] Statistically significant differences *versus* control Ti ($P < 0.05$).

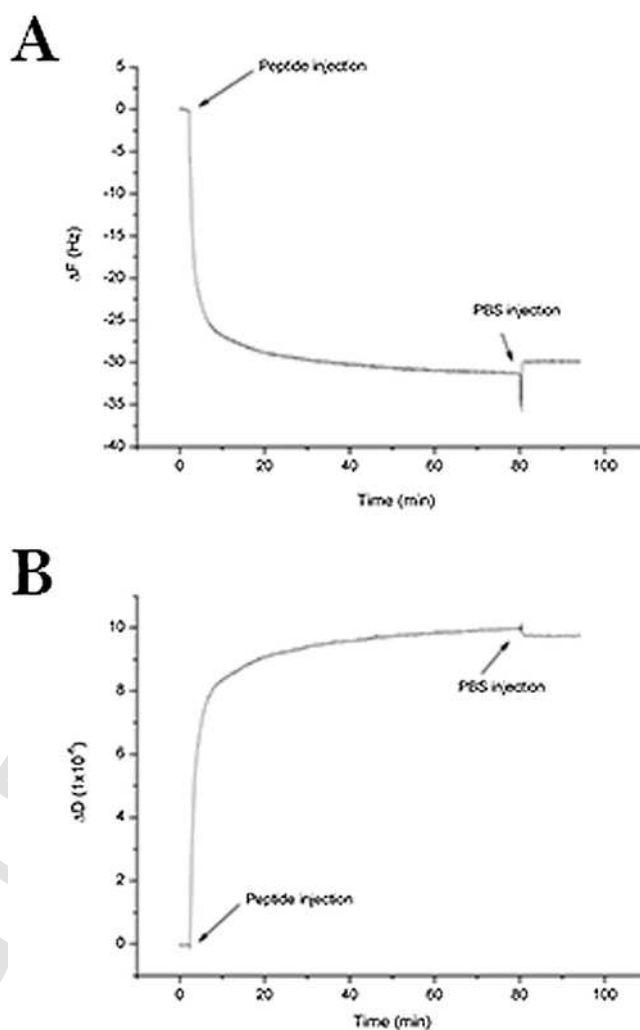[b] Statistically significant differences *vs*. Ti_Pl ($P < 0.05$).

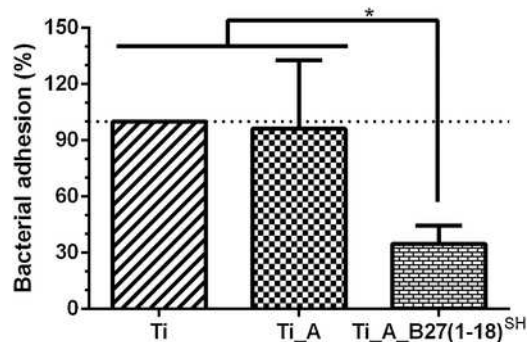[c] Statistically significant differences *vs*. Ti_A ($P < 0.05$).
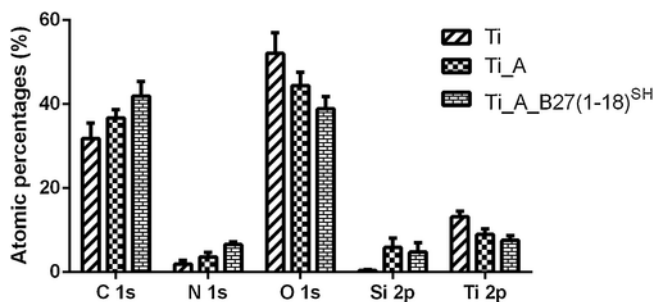
Fig. 1. Chemical composition (atomic percentage) obtained by XPS analysis of the indicated titanium surfaces. Results are the average ± SD of at least two samples for each condition.

Fig. 2. Resonance frequency (A) and dissipation (B) of a Ti crystal sensor upon addition of B27(1–18)[SH] solution in a QCM-D assay. Prior to addition of 100 μM peptide solution in PBS, the sensor has been treated as described in Materials and Methods. Data were fitted in the Voigt viscoelastic model to obtain surface mass density and thickness values.

Fig. 3. Adhesion of *S. epidermidis* to the indicated Ti samples. Following 2 h incubation at 37 °C, the CFUs of adherent microorganisms were recovered by a vortexing procedure, serial dilutions and plating on solid medium. Results are expressed as percent CFU respect to CFU recovered from bare titanium (Ti) and are the means ± SD of at least three independent experiments performed in triplicate. * Statistically significant difference *vs*. Ti and *vs*. Ti_A ($P < 0.05$).

formation on the implant surface reduces the likeliness of tissue integration [10–12].

Among the several approaches that are currently being examined for orthopaedic applications [13–15], the development of biomaterials coated with antimicrobial peptides (AMPs) could represent an effective strategy to prevent bacterial colonization of implants [16–18]. AMPs represent an untapped reservoir of natural antibacterial molecules [19,20]. Despite a remarkably high variation in size and sequence, most of these molecules are small, cationic and amphipathic, and are membrane-active [21,22]. Their mode of action, based on membrane permeabilization, has important consequences such as broad spectrum activity including antibiotic-resistant clinical isolates, efficacy also against biofilm-embedded microorganisms, and low tendency to elicit resistance [4,22–24]. These are useful properties in the light of the growing antibiotics resistance problem [25]. Furthermore, various AMPs have been shown to modulate host cell functions in a manner useful for host defence [19], and this includes the bone environment [26–28]. In this respect, several recent studies report the successful tethering of short cationic AMPs onto the surface of titanium (Ti) or other metals by using various coupling procedures [29–37]. These dif-

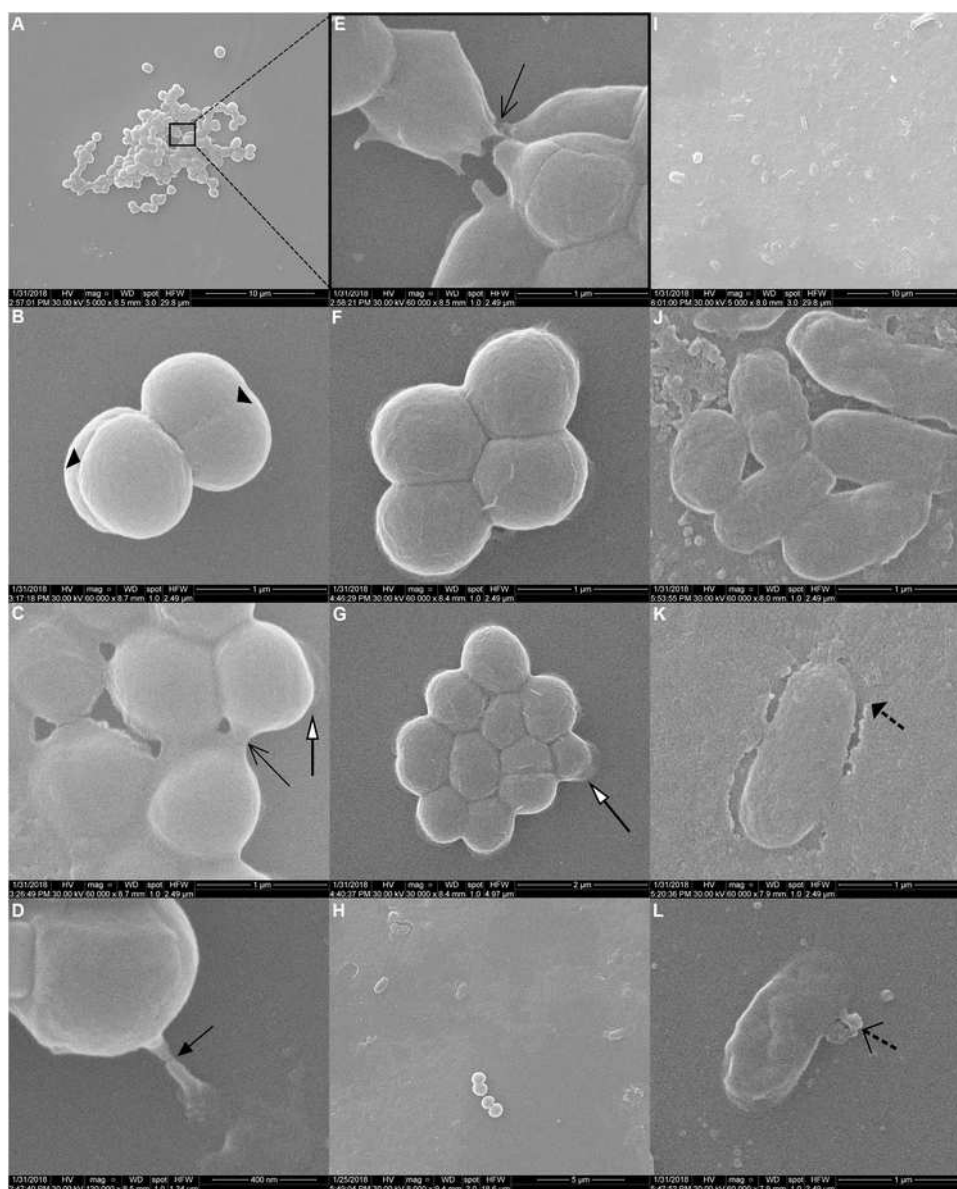fer mainly by the choice of tethering orientation (N- or C-terminal) and the nature and length of a possible spacer between the peptide and anchoring moiety [16,17,38]. However, there is a lively debate concerning what antimicrobial efficacy is retained by AMPs upon surface an-

Fig. 4. Morphology of *S. epidermidis* on distinct titanium samples analysed by SEM. Upon 2 h incubation all samples were rinsed, fixed and processed for SEM analysis. Panels A – E, Ti; panels F – G, Ti_A; panels H – L, Ti_A_B27(1–18)^{SH}. Panel E is a higher magnification of the image represented in Panel A. Arrows indicate, respectively, division septa (▲), contact junctions (↑), halos (↑̂), pseudopod-like structures (↑), empty circles (↑̂), extruded cytoplasmic material (↑̂). Representative images from two experiments performed in duplicate are shown.

choring [39–42]. Depending on several parameters related to the structural characteristics of the peptide and to the coupling strategies used for tethering, an immobilized peptide can display quite different antimicrobial properties with respect to its soluble counterpart [43–45]. With respect to covalent surface immobilization, membrane-active peptides could be suitable candidates as they would not need to penetrate into the bacterial cell to reach intracellular targets. Furthermore, assembling short, linear and therefore relatively simple peptide molecules onto a surface should have a positive impact on the production costs.

In a previous study an AMP derived from the α-helical cathelicidin BMAP27, namely the BMAP27(1–18) fragment, was selected for immobilization onto solid support [46]. In solution this peptide displayed potent bactericidal activity against Gram-positive clinical isolates including methicillin resistant *S. aureus* (MRSA) [47,48] and methicillin resistant *S. epidermidis* (MRSE) [46]. It was active also in the presence of relevant biological components such as serum, hyaluronic acid and synovial fluid, and was biocompatible to osteoblasts [46]. Moreover,

an N-biotinylated analogue tethered to streptavidin resin beads retained a potent killing capacity against *S. aureus* and *S. epidermidis* [46].

Based on these properties, in the present study a derivative of BMAP27(1–18) was covalently immobilized on the surface of titanium, which is a widely and routinely used metal for orthopaedic implants [49,50]. Functionalized Ti samples were characterized by contact angle (CA), quartz crystal microbalance with dissipation monitoring (QCM-D) and X-ray photoelectron spectroscopy (XPS). Their antimicrobial efficacy was investigated against a biofilm-forming *S. epidermidis* reference strain by colony forming unit (CFU) counts, evaluation of metabolic activity, and scanning electron microscopy (SEM). Biocompatibility was determined by measuring viability of MG-63 osteoblast-like cells upon cell adhesion to Ti samples. Finally, the capacity to promote cell adhesion also in the presence of contaminating bacteria was addressed in a cell-bacteria co-culture experiment by analysing cell number and morphology by confocal fluorescence microscopy. The aim was to assess whether Ti-immobilized BMAP27(1–18) was able to inhibit
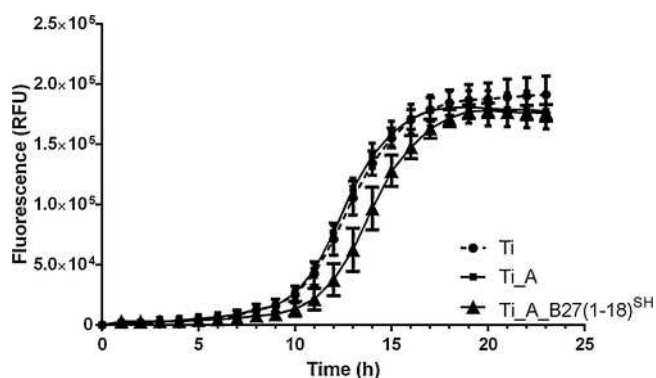
Fig. 5. Growth kinetics of *S. epidermidis* on the indicated Ti samples (Ti, circles; Ti_A, squares; Ti_A_B27(1–18)[SH], triangles). After 2h incubation and washing, fresh MH supplemented with the metabolic dye PrestoBlue® was added and adherent bacteria were allowed to grow overnight at 37 °C. Growth kinetics were monitored by measuring fluorescence emission that is directly proportional to microorganism viability. Results are reported as relative fluorescence units (RFU) and are the means ± SD of at least three independent experiments performed in triplicate.
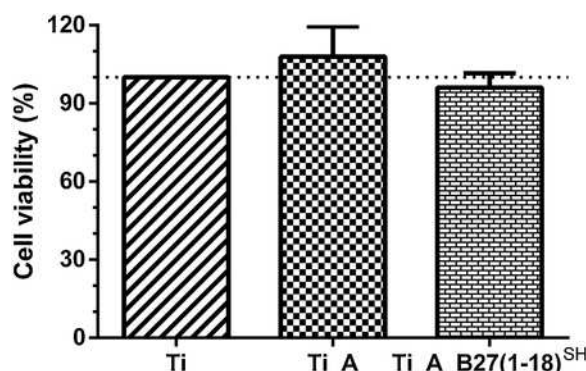

Fig. 6. Osteoblast viability upon adhesion to functionalized Ti samples. MG-63 osteoblast cells were seeded on Ti disks in a 48-well plate in complete medium. After 4h incubation samples were gently washed and viability of adherent cells quantified by the metabolic dye PrestoBlue®. Results are expressed as percent cell viability respect to cells seeded on bare titanium and are the means ± SD of at least three independent experiments performed in triplicate. Differences between samples did not reach statistical significance.

bacterial colonization while being compatible with osteoblast cells, with the final goal of exploiting this system for the production of infection-resistant titanium surfaces.

2. Materials and methods

2.1. Media and reagents

Polyethylene glycol–polystyrene (PEG-PS) resin, coupling reagents for peptide synthesis and 9-fluorenylmethoxy carbonyl (Fmoc)-amino acids were purchased from Applied Biosystems/Thermo Fisher Scientific (Waltham, MA, USA). Peptide synthesis-grade N,N-dimethylformamide (DMF), dichloromethane, piperidine and high performance liquid chromatography (HPLC)-grade acetonitrile were from Biosolve (Valkenswaard, The Netherlands). Trifluoroacetic acid (TFA) and N-methylmorpholine were from Acros Chimica (Beerse, Belgium). 6-aminohexanoic acid (Ahx) and 3-mercaptopropionic acid (MPA) were purchased from Fluorochem Ltd (Hadfield, Derbyshire, UK).

Commercially pure Ti grade II disks were obtained from Technalloy S.A. (Sant Cugat del Vallès, Spain). (3-aminopropyl)triethoxysilane (APTES) and N-succinimidyl-3-maleimidopropionate (SMP) were purchased from Sigma-Aldrich (St Louis, MO, USA). Alexa fluor 488-phalloidin, Hoechst 33,342, and PrestoBlue® reagent were from Invitrogen/Thermo Fisher Scientific. Dehydrated media for antimicrobial ac-

tivity assays were from Difco laboratories (Detroit, MI, USA), and Oxoid/Thermo Fisher Scientific, cell culture media and supplements from Sigma-Aldrich (St. Louis, MO, USA), and Fetal bovine serum (FBS) from Euroclone (Pero, Italy).

2.2. Sample preparation

Ti disks of 10 mm diameter and 2 mm height were polished with wet abrasive papers (800, 1200 and 2400 - European P-grade standard) and smoothed with a water suspension of alumina particles (1 μm and 0.05 μm particle size) on cotton cloths. Before the activation and silanization process, samples were ultrasonically rinsed with cyclohexane, isopropanol, distilled water, ethanol and acetone and finally stored dry under vacuum.

2.3. Activation and silanization of samples

Ti samples were activated by 10 min oxygen plasma treatment at 100 W power in a Standard Plasma System (FEMTO, Diener electronic GmbH, Germany). Samples were silanized with 2% (v/v) APTES in anhydrous toluene for 1 h at 70 °C under agitation and nitrogen atmosphere. Ti disks were then sonicated for 5 min and washed with toluene, isopropanol, distilled water, ethanol and acetone, and dried with nitrogen. Thereafter, aminosilanized samples were immersed in a 7.5 mM solution of the bifunctional crosslinker SMP in DMF for 1 h under agitation at room temperature. Finally, aminosilanized samples carrying the SMP group (Ti_A) were rinsed with DMF, distilled water, ethanol and acetone, and dried under nitrogen.

2.4. Peptide synthesis

The amino acid sequence of the α-helical cathelicidin derived peptide BMAP27(1–18) (GRFKRFRKKFKKLFKKLS, amidated C-terminus) [46] was modified at the N-terminus by addition of three aminohexanoic acid (Ahx) residues and one unit of 3-mercaptopropionic acid (MPA) as spacer and anchoring group, respectively. The resulting MPA-(Ahx)₃-BMAP27(1–18), hereafter referred to as B27(1–18)[SH], was synthesized on a Biotage Initiator + microwave-assisted automated peptide synthesizer in the solid phase using Fmoc-chemistry, according to published procedures [46]. After cleavage and deprotection, B27(1–18)[SH] was HPLC-purified and confirmed by mass spectrometry using a Q-STAR hybrid quadrupole time-of-flight mass spectrometer (Applied Biosystems/MDS Sciex, Concord, ON, Canada) equipped with an electrospray ion source. Peptide concentration was determined in aqueous solution by measuring the absorbance at 257 nm taking into account the molar extinction coefficient of 195.1 for each Phe residue [46].

2.5. Immobilization of peptide onto titanium samples

B27(1–18)[SH], dissolved in phosphate buffered saline (PBS) at pH 6.5 to a 100 μM concentration, was deposited onto Ti_A samples (100 μL/disk) and incubated overnight at room temperature. Thereafter, the peptide functionalized Ti samples were rinsed with PBS and dried with nitrogen. These samples are designated as Ti_A_B27(1–18)[SH].

2.6. Physicochemical characterization

2.6.1. Static contact angle measurements and surface energy calculations
The hydrophilicity of the Ti surfaces was determined by the sessile drop method using the Contact Angle System OCA15 plus (Dataphysics, Filderstadt, Germany). All measurements were done at room temperature using MilliQ ultrapure water (Merck Millipore Corporation, Bedford, MA, USA), and diiodomethane (Sigma-Aldrich, Spain) as
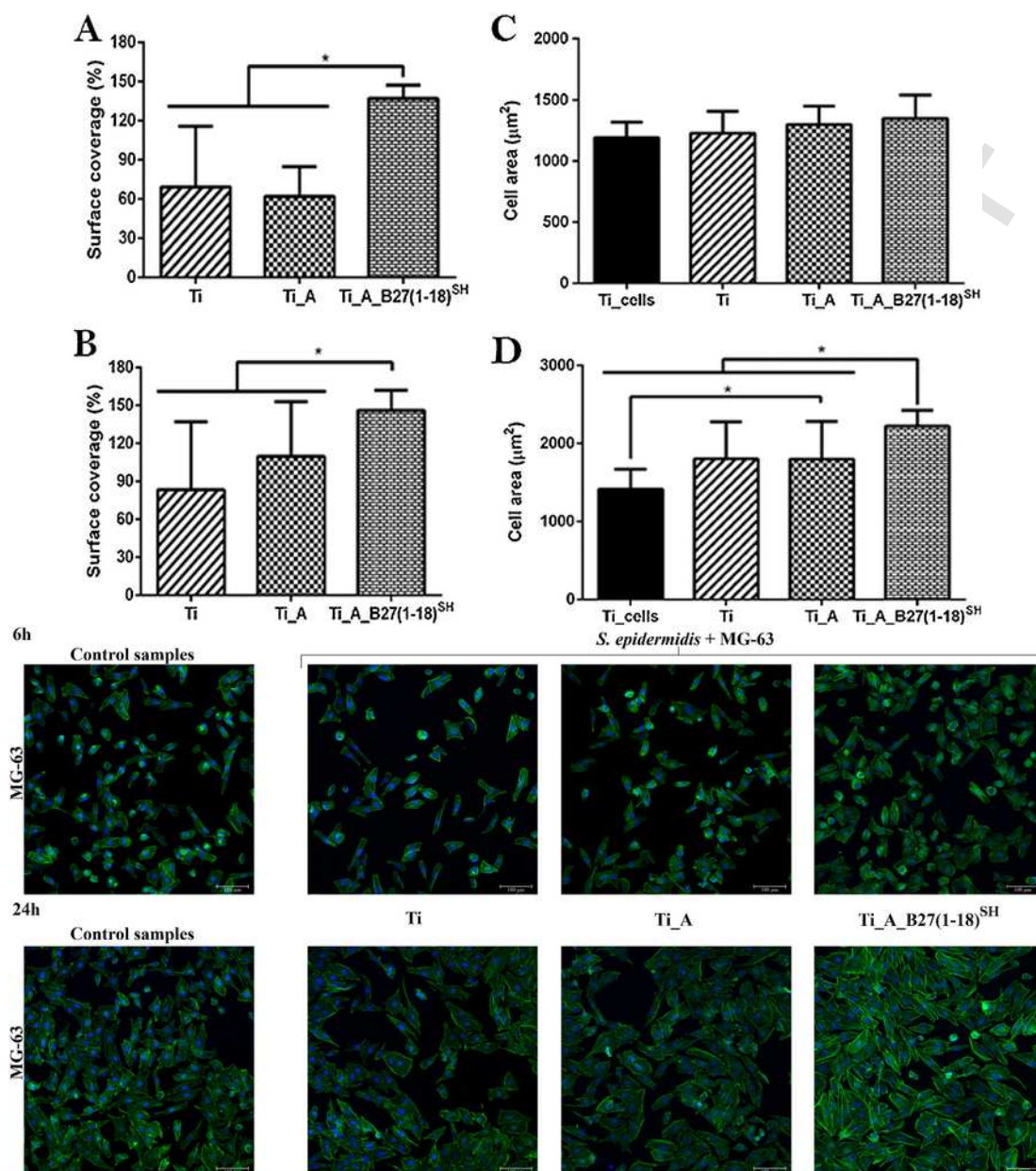
Fig. 7. Osteoblast adhesion to the indicated Ti samples in a cell-bacteria co-culture experiment. MG-63 cells were seeded on functionalized Ti disks, previously incubated with *S. epidermidis*, and co-cultured in antibiotic-free medium for additional 6 h (A, C) and 24 h (B, D). At these time points, samples were fixed and stained with Alexa Fluor 488-phalloidin and Hoechst. Osteoblast cell number and morphology were evaluated by CLSM with a Leica TCS SP8 X microscope followed by quantification with the ImageJ software. Results are expressed as means ± SD of five optical fields for each condition on duplicate samples. A, B: percent cell surface coverage in the presence of bacteria respect to bacteria free controls. C, D: mean cell area values in the presence (Ti, Ti_A, Ti_A_B27(1–18)^{SH}) and in the absence (Ti_cells) of bacteria. Asterisks denote statistically significant differences between the indicated samples ($P < 0.05$). Representative images for each condition are shown in the lower part of the figure. Scale bar = 100 μm.

wetting liquids (drop volume of 1 μL and 1 μL/min dosing rate). Static contact angles were calculated using SCA 20 software (Dataphysics). The surface energy and its dispersive and polar components were determined using the Owens, Wendt, Rabel, and Kaelble (OWRK) equation applied to both water and diiodomethane measurements [32,51]. Data are means of five measurements per disk for three sample replicates.

2.6.2. X-ray photoelectron spectroscopy (XPS)

The chemical composition of the surface of Ti samples was analysed using XPS instrument (D8 advance, SPECS Surface Nano Analysis GmbH, Germany) equipped with an XR50 Mg anode source operating at 150 W and a Phoibos 150 MCD-9 detector. High-resolution spectra

were registered with pass energy of 25 eV at 0.1 eV steps at a pressure below 7.5×10^{-9} mbar. Binding energies were referenced to the C1 s signal. Data were analysed using CasaXPS software (Version 2.3.16, Casa Software Ltd., Teignmouth, UK). Two samples were analysed for each studied condition.

2.6.3. Quartz crystal microbalance with dissipation monitoring (QCM-D)

To quantify and characterize the peptide layer attached to the surfaces, QCM-D measurements were performed on Ti crystal sensors (QSX 310, Q-Sense, Sweden) in a D-300 instrument (Q-sense, Sweden). Ti sensors, cleaned as previously described [52], were activated with O_2 plasma and subsequently treated with APTES and SMP as described above for Ti_A samples. Prior to monitoring the adsorption of

B27(1–18)[SH], the baseline was stabilized with PBS for 30–60 min. Afterwards, B27(1–18)[SH] derivative was added (100 μM in PBS, pH 6.5) and changes in resonance frequency and dissipation were monitored at 25 °C for 100 min, in real-time using a Qsoft software (Q-Sense, Sweden). Frequency and dissipation curves were fitted to a Voigt viscoelastic model [53] to yield the adsorbed mass and thickness of the peptide layer, as well as kinetic information, by using the Q-tool data analysis software (Q-Sense, Sweden).

2.7. Bacteria and antimicrobial activity assays

The reference strains *Staphylococcus epidermidis* ATCC 35,984, *Staphylococcus aureus* ATCC 25923, *Escherichia coli* ATCC 25,922 and *Pseudomonas aeruginosa* ATCC 27,853 were used in MIC assays with soluble peptides. Bacteria were cultured either in liquid Brain Hearth Infusion (BHI) (both *Staphylococcus* species) or in Mueller-Hinton (MH) (both Gram-negatives) overnight at 37 °C. *Staphylococcus epidermidis* ATCC 35,984 was used in antimicrobial assays with Ti-bound peptide. Stationary phase bacteria were harvested by 10 min centrifugation at 1000 x g and resuspended in sterile PBS (pH 7.4). Bacterial density was assessed by turbidity at 600 nm, with reference to previously determined standards. For the experiments, bacterial suspensions were prepared in MH broth at optimal density.

2.7.1. Determination of the minimum inhibitory concentration (MIC)

The minimum inhibitory concentration (MIC) of B27(1–18)[SH] in solution was determined by a broth microdilution assay in 96-well microtiter plates, using MH broth with logarithmic-phase microorganisms at 5×10^5 CFU/mL, as previously reported [46], following Clinical and Laboratory Standards Institute (CLSI) guidelines.

2.7.2. Evaluation of bacterial adhesion to titanium surface

Bacterial adhesion was studied adapting a previously described protocol [33]. Prior to use in antimicrobial assays Ti, Ti_A and Ti_A_B27(1–18)[SH] samples were sterilized by 30 min treatment with 70% ethanol, and then thoroughly rinsed with sterile PBS in order to remove any trace of ethanol. Ti samples were placed in a 24-well plate and incubated with 1 mL of *S. epidermidis* $(1 \times 10^5$ CFU/mL) for 2 h at 37 °C. The medium containing planktonic bacteria was then aspirated and the samples were rinsed three times with sterile PBS. Afterwards, disks were transferred in sterile tubes containing 1 mL of 50% Mueller-Hinton in sterile PBS (MH-PBS), and adherent bacteria were detached by 10 min vortexing. To make sure that dislodging of bacteria from the surfaces was effective, after the first vortexing step the disks were transferred in new sterile tubes containing 1 mL of MH-PBS and vortexed again for 5 min. Bacterial suspensions from each vortexing step were then serially diluted in MH-PBS and seeded on BHI agar plates. The plates were incubated at 37 °C for 24 h and the resulting colonies counted. All experiments were performed in triplicate for each type of surface.

2.7.3. Scanning Electron Microscopy (SEM)

The morphology of *S. epidermidis* adhered to Ti samples was studied by SEM (Quanta250 SEM, FEI, Oregon, USA) operated in secondary electron detection mode. The working distance was adjusted in order to obtain the suitable magnification; the accelerating voltage was set to 30 kV. SEM was performed in duplicate for each sample. Briefly, upon 2 h incubation as described above, all samples were rinsed three times with filtered sterile PBS, fixed with 2.5% (v/v) glutaraldehyde for 30 min at 4 °C, rinsed three times with filtered sterile PBS and MilliQ ultrapure water, and dehydrated in graded series of ethanol solutions (20 min each). Immediately prior to SEM analysis, samples were sputter-coated with gold (Sputter Coater K550X, Emitech, Quorum Technologies Ltd, UK).

2.7.4. Bacterial growth kinetics on titanium surfaces

Ti samples, placed in triplicate into 48-well plates, were immersed in 1 mL of *S. epidermidis* $(6 \times 10^4$ CFU/mL) suspension in MH for 2 h. The medium containing planktonic bacteria was removed, Ti disks were rinsed with sterile PBS, and adherent bacteria were allowed to grow at 37 °C for 22 h in fresh MH medium supplemented with 10% (v/v) PrestoBlue® metabolic dye. Bacterial growth kinetics were monitored fluorometrically according to PrestoBlue® manufacturer's instructions by using a Multimode Plate Reader (EnSpire™ 2300, PerkinElmer, Waltham, MA, USA).

2.8. Cell culture

The human osteoblast-like MG-63 cell line was obtained from ATCC (Manassas, VA, USA) and maintained in Dulbecco's Modified Eagle Medium (DMEM), in a humidified incubator at 37 °C and 5% CO_2 atmosphere. DMEM medium was supplemented with 10% (v/v) heat inactivated FBS, 2 mM L-glutamine, 100 units/mL penicillin and 100 μg/mL streptomycin.

2.8.1. Cell adhesion and viability assay

The biocompatibility of Ti samples was evaluated by measuring viability of the MG-63 cell line by using the metabolic dye PrestoBlue®. Cells were seeded onto Ti samples in a 48-well plate at a density of 4×10^4 cells/well in complete medium and allowed to adhere for 4 h at 37 °C. Thereafter the medium was aspirated, cells were rinsed with sterile PBS and incubated at 37 °C for 90 min in fresh complete medium containing 10% (v/v) PrestoBlue®. Cell metabolic activity was measured fluorometrically according to PrestoBlue® manufacturer's instructions by using a Multimode Plate Reader (EnSpire™ 2300, PerkinElmer, Waltham, MA, USA). All experiments were performed in triplicate for each type of surface.

2.8.2. Cell-bacteria co-culture

This assay was performed according to previously reported studies [12,54]. Ti samples were incubated with 1 mL of *S. epidermidis* $(6 \times 10^4$ CFU/mL) in a 48-well plate for 2 h at 37 °C as described above. The medium was then removed and the samples were washed three times in sterile PBS. Next, MG-63 cells, freshly resuspended in DMEM medium without penicillin and streptomycin, supplemented with 2% MH broth, were seeded on bacteria-covered surfaces at a density of 4×10^4 cells/well. Bacteria and MG-63 cells were incubated at 37 °C in humidified 5% CO_2 for 6 and 24 h. At these time points, samples were fixed in 3% Paraformaldehyde, stained with Alexa Fluor 488-phalloidin and Hoechst 33,342 and examined by Confocal Laser Scanning Microscopy (CLSM) with a Leica TCS SP8 X microscope (Leica Microsystems GmbH, Wetzlar, Germany). Images were analysed using ImageJ 1.51 w software (NIH, Bethesda, MD, USA) to determine cell area and surface coverage. All experiments were performed in duplicate for each type of surface.

2.9. Statistical analysis

Data, presented as mean values ± standard deviations, were analysed by a non-parametric Mann-Whitney U test (IBM SPSS Statistics 20 software, Armonk, NY, USA). Statistical significance was set at P value <0.05.

3. Results and discussion

3.1. Coupling strategy and physicochemical characterization of titanium samples

The cathelicidin derived peptide BMAP27(1–18), previously shown to possess potent bactericidal activity also upon immobilization on solid support [46], was covalently linked to Ti disks by using the maleimide-thiol chemistry. To this aim, the selected peptide sequence was modified at the N-terminus by adding a spacer and an anchoring moiety bearing a free thiol. The peptide derivative is hereafter referred to as B27(1–18)^{SH}. This modification did not significantly affect the antimicrobial properties of the original peptide, as assessed by determining minimum inhibitory concentration (MIC) against representative Gram-positive and Gram-negative bacterial species (Table 1).

The selected coupling strategy has been previously applied for functionalization of titanium and tantalum with, respectively, the antimicrobial peptide hLF1-11, and the cell adhesive RGD peptide, both for osseointegrative applications [32,33,55]. In the present study this simple and linear functionalization procedure, schematically illustrated in Fig. S1 (see Supplementary material), was used for covalent anchoring of B27(1–18)^{SH} to titanium *via* its N-terminus. Ti disks (Ti) were first treated with oxygen plasma (Ti_Pl) to generate hydroxyl groups required for the subsequent silanization of the metal surface with the aminosilane APTES. The amino group of the organosilane was then exploited to introduce the bifunctional crosslinker SMP, bearing the maleimide function (Ti_A) which was subsequently used to react with the thiol on the peptide N-terminus (Ti_A_B27(1–18)^{SH}) (see Fig. S1 in Supplementary material).

To verify whether the functionalization procedure was successful, Ti samples first underwent physicochemical characterization by static contact angle (CA) measurements and XPS. As expected, CA analysis (Table 2) showed a substantial change in wettability upon plasma treatment (Ti_Pl *vs.* Ti samples) as well as upon silanization (Ti_A *vs.* Ti_Pl), and subsequent peptide coupling (Ti_A_B27(1–18)^{SH} *vs.* Ti_Pl, and Ti_A_B27(1–18)^{SH} *vs.* Ti_A).

High resolution XPS spectra were then recorded to obtain the chemical composition of the modified Ti surfaces, reported in Fig. 1. Silanization of samples was supported by the presence of silicon (Si 2p) and by the increase in carbon (C 1s) and nitrogen (N 1s) content in Ti_A *vs.* Ti disks. An additional increase of both carbon and nitrogen, and decrease in percent oxygen (O 1s) and titanium (Ti 2p) in Ti_A_B27(1–18)^{SH} samples, with respect to Ti_A disks, indicated stable and strong attachment of peptide molecules to the silanized metal surfaces, thus confirming that the applied procedure for peptide tethering to titanium was both sound and reliable.

The peptide layer formed on the Ti surface was quantified using Quartz Crystal Microbalance with Dissipation monitoring (QCM-D), which is a very sensitive tool to measure masses in the ng/cm^2 range [56]. The technique is based on monitoring the resonance frequency of an appropriate piezoelectric sensor crystal, which decreases proportionally to the adsorbed mass (defined as "adlayer") on the surface of the crystal itself. The additional monitoring of the dissipation factor enables a more accurate mass estimate by taking into account the contribution of the adsorbed water to the adlayer mass [57].

In the present study, in order to record the formation of a peptide layer covalently linked to titanium, Ti crystal sensors were used and, prior to peptide addition, the surface of the Ti sensor was treated with O$_2$ plasma, APTES and crosslinker, as described above for Ti disks, and extensively rinsed with PBS. Upon addition of peptide solution, changes in resonance frequency (ΔF, Fig. 2A) and dissipation (ΔD, Fig. 2B) indicated deposition of a stable layer with a rapid drop in ΔF, corresponding to a rapid increase in ΔD, during the first 5–6 min. This

was followed by stabilization of both parameters during the next 15–20 min. Replacement of the peptide solution by PBS after 80 min monitoring did not result in appreciable modifications of the registered traces, consistent with the formation of a stable peptide monolayer over the silanized surface. By fitting data to the Voigt model [53], an average surface mass density of 456.32 ± 7.61 ng/cm^2 and a layer thickness of 3.08 ± 0.06 nm were determined. Although it is difficult to make direct comparisons, these values are in the same order of magnitude as the QCM-D data obtained by Castellanos et al. using cell-adhesive peptides [52] and by Corrales Urena et al. using antimicrobial peptides [58] adsorbed onto CoCr and Ti sensors, respectively. The peptide layer thickness was comparable to that achieved by a basically similar coupling scheme for the antimicrobial peptide Dhvar5 grafted on chitosan [29], and for the covalently bound lactoferrin peptide [33], both determined by ellipsometry. Regarding the surface peptide density on titanium, it is interesting to note that our data are comparable to those obtained by others with colorimetric methods [29,30]. Collectively the physicochemical data support successful functionalization of Ti disks with the cathelicidin peptide derivative B27(1–18)^{SH}.

3.2. Analysis of antimicrobial properties of titanium samples

The antimicrobial efficacy of Ti-anchored peptide was first tested in terms of bacterial adhesion inhibition. Adhesion of microorganisms to surfaces of implanted biomedical devices is the first and crucial step in bacterial colonization of implants so its prevention should likely prevent the development of infection. Ti samples were exposed to a suspension of *Staphylococcus epidermidis* ATCC 35,984, a reference strain with a well-documented biofilm-forming ability [8]. Notably, this feature is considered to be related to the pathogenicity of this otherwise harmless microorganism [2,8]. Bacteria were allowed to adhere to Ti samples for 2 h at 37 °C, then planktonic cells were washed away and surface attached bacteria recovered by a two-step vortexing procedure. As shown in Fig. 3, the colony forming units (CFU) of *S. epidermidis*, recovered from Ti_A_B27(1–18)^{SH} disks, were significantly less than those recovered from both controls, *i.e.* Ti and Ti_A samples. This would suggest that bacteria were killed upon contact with the peptide-functionalized Ti, and/or that their adhesion to Ti_A_B27(1–18)^{SH} disks was in some way hindered.

To clarify events occurring at the metal surface during staphylococcal adhesion, the morphology of the attached bacteria was determined by SEM in parallel to CFU counting. As shown in Fig. 4, this analysis revealed a remarkable difference in *S. epidermidis* cells adhered to the different substrata. Bacterial cells on control Ti samples were opaque, round in shape, with smooth surface and with division septa clearly evident (Fig. 4B, F). Individual bacteria were on average of the expected size with diameter values ranging from 0.55 μm to 0.85 μm. Dividing microorganisms were very frequent, indicating that bacteria on bare titanium were viable and growing (Fig. 4B, F–G). Often several dozens of bacterial cells were clustered together (Fig. 4A, C). Such bacterial agglomerates were covered by a dense and grey layer resembling a blanket (Fig. 4A, C and G). Individual cells were tightly associated with each other and connected by junctions (Fig. 4C, E). In addition, in most instances there was a halo surrounding the bacteria at the contact interface between bacterial cell and Ti surface (Fig. 4C, G). In some clusters, fimbriae-like surface appendages, connecting bacteria to Ti, were also visible (Fig. 4D,E). All these elements likely represent extracellular matrix components and/or adhesion structures, indicating biofilm initiation [59–61], in line with the well-known biofilm forming properties of *S. epidermidis* ATCC 35,984, which is known to be a heavy matrix producer [8,9]. Notably, we did not observe significant morphological differences between bacteria adhered to bare Ti (Ti; Fig. 4A–E) and those adhered to silanized Ti disks (Ti_A; Fig. 4F - G). In contrast to controls, bacteria adhered to Ti_A_B27(1–18)^{SH} samples were not only

fewer in number, but also showed dramatically different morphologies (Fig. 4I). They showed increased size and elongated shapes, and division septa were conspicuously missing (Fig. 4J). In addition, bacteria had a knobbly appearance, many were collapsed and deflated and appeared embedded in a layer of amorphous material deposited on the Ti surface (Fig. 4H - J). In many cases, these ghost-like bacterial cells were surrounded by an empty circle (Fig. 4K), and for some bacteria what appeared to be the extrusion of cytoplasmic material out of the cell was observed (Fig. 4L). Such dramatic changes in morphology pointed to the impairment of microbial cell growth as well as of cell division, which is normally accomplished through formation of the division septum. The observed structures could reasonably derive from dead bacteria. However, the "deflated bag" appearance, in the absence of evident surface lesions such as blebs or holes [62], would suggest that digestion of bacterial content has occurred, possibly upon activation of autolytic enzymes [63].

In Ti_A_B27(1–18)^{SH} samples, the observed changes in morphology matched the reduction in CFUs, thus highlighting killing ability of Ti-immobilized B27(1–18)^{SH}. This finding was not unexpected, considering that BMAP27(1–18) proved able to kill staphylococci when N-terminally anchored to a model support [46]. However, a question arises about its mode of action in the immobilized state. The bactericidal activity of this peptide in solution is based on its ability to perturb microbial membranes, and is intimately related to its ability to adopt an amphipathic conformation [47,64]. In our case however, it appears quite obvious that, presuming their limited mobility, the anchored peptide molecules may interact only with superficial components of the bacterial cell, and thus, the killing action likely differs from that displayed by this type of peptides in solution [47,62,64]. In this respect, it is worth noting that the staphylococci adhered to peptide-functionalized Ti (this study, Fig. 4) were remarkably different from those observed in a previous study after treatment with the sheep cathelicidin SMAP-29 in solution [62]. In this latter case, surface roughening and blebbing of SMAP29-treated microorganisms was interpreted as morphological evidence of the potent permeabilizing activity of this alpha-helical peptide in solution [62], while the bactericidal mode of action of immobilized SMAP-29 [41], or indeed BMAP-27 [65], has not as yet been elucidated.

It is very likely that the negatively charged bacteria were initially attracted by the highly cationic B27(1–18)^{SH} (net charge +10 [46]), but were killed upon their contact/adhesion to the metal, in keeping with what suggested also by other authors [31,44]. The observed changes in morphology could be the result of events triggered by a peptide-induced perturbation at the bacterial surface, as reported for free peptides in solution [63,66,67], and also suggested for immobilized AMPs [44,68].

It is interesting to note however, that in Ti_A_B27(1–18)^{SH} samples, besides dead or heavily damaged bacteria, microcolonies with normal appearance were also occasionally observed (Fig. 4H). This prompted us to investigate whether the surviving bacteria could be able to regrow. To this end, Ti samples were exposed to a suspension of *S. epidermidis* for 2 h as above and, after removal of planktonic microorganisms and washings, the incubation was extended for additional 22 h in fresh MH broth. Since the presence of metal disks in the wells would not allow optical density measurements, growth was kinetically monitored by the PrestoBlue® dye, which emits fluorescence upon conversion by metabolically active microorganisms. As shown in Fig. 5, bacterial growth on control Ti disks (Ti and Ti_A) became detectable at 7–8 h post-adhesion, with an exponential phase between 10–15 h, and a final plateau at 18–20 h. The surviving bacteria on Ti_A_B27(1–18)^{SH} samples showed an about 1.5-h delay both for the beginning of growth and onset of the exponential growth phase, presumably related to their decreased initial number, in keeping with the results of bacterial adhe-

sion assays. Hence, inhibition of the initial bacterial adhesion remains crucial for long lasting antimicrobial efficacy [14].

It is worth stressing in this respect that the experimental conditions used in our *in vitro* assays, such as a relatively high initial inoculum, are likely different from those occurring in clinical settings where a possible bacterial contamination would take origin from a very low bacterial number, as also confirmed by animal model studies [69,70]. In agreement with what has been suggested by other authors [30], one could reasonably expect a more effective protection under medically relevant conditions, with only few bacteria present at the implant surface thanks to strictly antiseptic surgical procedures.

3.3. Evaluation of compatibility of titanium samples to osteoblast cells

In the general context of the prosthetic settings, one should take into consideration the complex dynamics of events occurring during and upon implantation, such as osteoblast attachment, growth and differentiation, that collectively should lead to complete implant integration. With this perspective, it was mandatory to assess the biocompatibility of our Ti samples to osteoblast cells. To address this issue, Ti samples were seeded with the osteosarcoma-derived MG-63 cells, used as a model, in a 48-well plate. Adherent cells after 4 h incubation were quantified by a PrestoBlue® metabolic assay. As shown in Fig. 6, metabolic activity of cells on Ti_A and Ti_A_B27(1–18)^{SH} samples was comparable to that of MG-63 cells on bare Ti, which is known for its biocompatibility. This means that cells were vital and able to adhere to various substrata without appreciable toxic effects neither by the peptide nor by other organic molecules present on Ti (*e.g.* Ti_A). This result adds to previous reports concerning the virtual absence of cytotoxic effects of BMAP27(1–18) against different host cell types, both in solution [47,48,64], and upon immobilization [46].

Given the cytocompatibility of the functionalized Ti samples we next investigated their antimicrobial efficacy in a more complex context by addressing the issue of "race for the surface". This concept stems from the observation that, in order to achieve successful and long lasting tissue integration of the implanted prosthesis, the surface of an ideal implant should be resistant to bacterial colonization but at the same time prone to colonization by host tissue cells [10,12,71].

To investigate to what extent the colonizing capacity of osteoblast cells might be hampered by bacteria present on Ti itself, a co-culture experiment of MG-63 cells and bacteria was set up. *S. epidermidis* was allowed to adhere to Ti samples as in the antimicrobial assays described above. After withdrawal of planktonic bacteria and washings, Ti disks contaminated by adherent bacteria were seeded with freshly resuspended MG-63 cells in antibiotic-free DMEM medium supplemented with 2% MH, and incubated for additional 6 h and 24 h. At these time points, Ti disks were processed and analysed by fluorescence microscopy in order to evaluate MG-63 cell number and morphology.

Data and representative CSLM images are shown in Fig. 7. Data were calculated as percent cell surface coverage respect to bacteria-free Ti controls (Fig. 7A, B), and mean cell area (Fig. 7C, D). It is evident that the presence of bacteria affected cell adhesion and spreading on distinct Ti samples to different extents. For example, at a 6 h time point, osteoblast adhesion to Ti and Ti_A samples was inhibited by about 40% for bacterial adhered samples, whereas cell adhesion to Ti_A_B27(1–18)^{SH} samples was not impaired but rather enhanced (Fig. 7A). Since at this time point cell size (Fig. 7C) and morphology (Fig. 7, images in the upper row) were on average highly comparable, the increased surface coverage on Ti_A_B27(1–18)^{SH} samples could be reasonably ascribed to a higher number of adhered MG-63 cells. This finding would suggest that the bactericidal action exerted by peptide-functionalized Ti, as observed by SEM (Fig. 5H-L) and confirmed by CFU counts (Fig. 3), was effective enough to allow displacement of bacteria

by MG-63 cells, which could thus predominate and spread onto the surface. This hypothesis seems further supported by the increment in both surface coverage (Fig. 7B) and mean cell area (Fig. 7D) observed after 24 h co-incubation on peptide-functionalized samples. However, although BMAP27(1–18) proved neutral with respect to MG-63 cell growth and differentiation in a previous study [46], we cannot exclude specific effects on cells by the Ti-anchored peptide. It is interesting to note that at 24-h time point a slight improvement of cell adhesion and spreading compared to bacteria-free control was observed in Ti and Ti_A samples, which were devoid of antimicrobial properties (Figs. 3–5). This would suggest that besides bacterial killing, one should take into consideration other phenomena in the complex network of multiple interactions between implant surfaces, bacteria, and relevant tissue cells [10,54,72]. In the light of what has been reported for the oral environment [73,74], at present we cannot rule out possible stimulating effects of bacteria on tissue cell expression of adhesion molecules that would in turn improve cell adhesion and spreading.

4. Conclusions

In order to obtain titanium with anti-infective surface, in this study Ti disks were successfully functionalized with the cathelicidin derived α-helical peptide B27(1–18)^{SH}, as assessed by contact angle, XPS, and QCM-D analyses. Adhesion of *S. epidermidis* to peptide-functionalized samples was markedly reduced and alterations in bacterial morphology revealed by SEM indicate a contact-killing effect of the anchored peptide, suggesting a possibly different mode of action respect to that displayed by this peptide in solution. In this respect, a more profound knowledge of the bactericidal mechanism of surface-immobilized peptide should help design improved peptide derivatives, spacers, and coupling strategies, in order to increase the antimicrobial performance of the functionalized Ti. Importantly, the immobilized peptide did not produce any cytotoxic effect on osteoblast-like cells, which adhered and spread better on functionalized Ti when co-cultured with bacteria compared to non-coated surfaces. For further improvement in view of orthopaedic applications, it would be worth investigating the stability/efficacy of Ti-anchored peptide in the presence of human serum and/or other relevant biological components such as hyaluronic acid, or in the presence of proteases. Although these aspects have not yet been addressed, results obtained in the present study are promising, highlighting the potential of BMAP27(1–18) for the development of biomaterials refractory to microbial contamination.

Declaration of Competing Interest

The authors declare no competing financial interest.

Acknowledgements

Appendix A. Supplementary data

Supplementary material related to this article can be found, in the online version, at doi:https://doi.org/10.1016/j.colsurfb.2019.110586.

References

[1] A.J. Tande, R. Patel, Prosthetic joint infection, Clin. Microbiol. Rev. 27 (2014) 302–345, https://doi.org/10.1128/CMR.00111-13.
[2] C.R. Arciola, D. Campoccia, P. Speziale, L. Montanaro, J.W. Costerton, Biofilm formation in Staphylococcus implant infections. A review of molecular mechanisms and implications for biofilm-resistant materials, Biomaterials. 33 (2012) 5967–5982, https://doi.org/10.1016/j.biomaterials.2012.05.031.
[3] H.O. Gbejuade, A.M. Lovering, J.C. Webb, The role of microbial biofilms in prosthetic joint infections, Acta Orthop. 86 (2015) 147–158, https://doi.org/10.3109/17453674.2014.966290.
[4] G. Batoni, G. Maisetta, S. Esin, Antimicrobial peptides and their interaction with biofilms of medically relevant bacteria, Biochim. Biophys. Acta Biomembr. 1858 (2016) 1044–1060, https://doi.org/10.1016/j.bbamem.2015.10.013.
[5] T.F. Moriarty, R. Kuehl, T. Coenye, W.-J. Metsemakers, M. Morgenstern, E.M. Schwarz, M. Riool, S.A.J. Zaat, N. Khana, S.L. Kates, R.G. Richards, Orthopaedic device-related infection: current and future interventions for improved prevention and treatment, EFORT Open Rev. 1 (2016) 89–99, https://doi.org/10.1302/2058-5241.1.000037.
[6] M. Taha, H. Abdelbary, F.P. Ross, A.V. Carli, New innovations in the treatment of PJI and biofilms—clinical and preclinical topics, Curr. Rev. Musculoskelet. Med. (2018) https://doi.org/10.1007/s12178-018-9500-5.
[7] P.C. Matthews, A.R. Berendt, M.A. McNally, I. Byren, Diagnosis and management of prosthetic joint infection, BMJ. 338 (2009) https://doi.org/10.1136/bmj.b1773, b1773–b1773.
[8] M. Sabaté Brescó, L.G. Harris, K. Thompson, B. Stanic, M. Morgenstern, L. O'Mahony, R.G. Richards, T.F. Moriarty, Pathogenic mechanisms and host interactions in Staphylococcus epidermidis device-related infection, Front. Microbiol. 8 (2017) https://doi.org/10.3389/fmicb.2017.01401.
[9] P.D. Fey, M.E. Olson, Current concepts in biofilm formation of Staphylococcus epidermidis, Future Microbiol. 5 (2010) 917–933, https://doi.org/10.2217/fmb.10.56.
[10] A. Gristina, Biomaterial-centered infection: microbial adhesion versus tissue integration, Science (80-.) 237 (1987) 1588–1595, https://doi.org/10.1126/science.3629258.
[11] G. Subbiahdoss, R. Kuijer, D.W. Grijpma, H.C. van der Mei, H.J. Busscher, Microbial biofilm growth vs. tissue integration: "The race for the surface" experimentally studied, Acta Biomater. 5 (2009) 1399–1404, https://doi.org/10.1016/j.actbio.2008.12.011.
[12] M. Godoy-Gallardo, J. Guillem-Marti, P. Sevilla, J.M. Manero, F.J. Gil, D. Rodriguez, Anhydride-functional silane immobilized onto titanium surfaces induces osteoblast cell differentiation and reduces bacterial adhesion and biofilm formation, Mater. Sci. Eng. C. 59 (2016) 524–532, https://doi.org/10.1016/j.msec.2015.10.051.
[13] D. Campoccia, L. Montanaro, C.R. Arciola, A review of the biomaterials technologies for infection-resistant surfaces, Biomaterials. 34 (2013) 8533–8554, https://doi.org/10.1016/j.biomaterials.2013.07.089.
[14] J. Gallo, M. Holinka, C. Moucha, Antibacterial surface treatment for orthopaedic implants, Int. J. Mol. Sci. 15 (2014) 13849–13880, https://doi.org/10.3390/ijms150813849.
[15] A.E. Eltorai, J. Haglin, S. Perera, B.A. Brea, R. Ruttiman, D.R. Garcia, C.T. Born, A.H. Daniels, Antimicrobial technology in orthopedic and spinal implants, World J. Orthop. 7 (2016) 361, https://doi.org/10.5312/wjo.v7.i6.361.
[16] F. Costa, I.F. Carvalho, R.C. Montelaro, P. Gomes, M.C.L. Martins, Covalent immobilization of antimicrobial peptides (AMPs) onto biomaterial surfaces, Acta Biomater. 7 (2011) 1431–1440, https://doi.org/10.1016/j.actbio.2011.005.
[17] S.A. Onaizi, S.S.J. Leong, Tethering antimicrobial peptides: current status and potential challenges, Biotechnol. Adv. 29 (2011) 67–74, https://doi.org/10.1016/j.biotechadv.2010.08.012.
[18] M. Riool, A. de Breij, J.W. Drijfhout, P.H. Nibbering, S.A.J. Zaat, Antimicrobial peptides in biomedical device manufacturing, Front. Chem. 5 (2017) 1–13, https://doi.org/10.3389/fchem.2017.00063.
[19] A.T.Y. Yeung, S.L. Gellatly, R.E.W. Hancock, Multifunctional cationic host defence peptides and their clinical applications, Cell. Mol. Life Sci. 68 (2011) 2161–2176, https://doi.org/10.1007/s00018-011-0710-x.
[20] G. Wang, B. Mishra, K. Lau, T. Lushnikova, R. Golla, X. Wang, Antimicrobial peptides in 2014, Pharmaceuticals. 8 (2015) 123–150, https://doi.org/10.3390/ph8010123.
[21] L.T. Nguyen, E.F. Haney, H.J. Vogel, The expanding scope of antimicrobial peptide structures and their modes of action, Trends Biotechnol. 29 (2011) 464–472, https://doi.org/10.1016/j.tibtech.2011.05.001.
[22] A. Tossi, B. Skerlavaj, F. D'Este, R. Gennaro, Structural and functional diversity of cathelicidins, in: G. Wang (Ed.), Antimicrob. Pept. Discov. Des. Nov. Ther. Strateg, 2nd ed., CABI, 2017, pp. 20–48 https://lccn.loc.gov/2017016223.

[23] N. Strempel, J. Strehmel, J. Overhage, Potential application of antimicrobial peptides in the treatment of bacterial biofilm infections, Curr. Pharm. Des. 21 (2015) 67–84 http://www.ncbi.nlm.nih.gov/pubmed/25189860.

[24] T. Koprivnjak, A. Peschel, Bacterial resistance mechanisms against host defense peptides, Cell. Mol. Life Sci. 68 (2011) 2243–2254, https://doi.org/10.1007/s00018-011-0716-4.

[25] ECDC, European Centre for disease prevention and control, Surveillance of Surgical Site Infections in Europe 2010–2011, 2013 https://doi.org/10.2900/90271.

[26] D. Kraus, J. Deschner, A. Jäger, M. Wenghoefer, S. Bayer, S. Jepsen, J.P. Allam, N. Novak, R. Meyer, J. Winter, Human β-defensins differently affect proliferation, differentiation, and mineralization of osteoblast-like MG63 cells, J. Cell. Physiol. 227 (2012) 994–1003, https://doi.org/10.1002/jcp.22808.

[27] M. Kittaka, H. Shiba, M. Kajiya, T. Fujita, T. Iwata, K. Rathvisal, K. Ouhara, K. Takeda, T. Fujita, H. Komatsuzawa, H. Kurihara, The antimicrobial peptide LL37 promotes bone regeneration in a rat calvarial bone defect, Peptides. 46 (2013) 136–142, https://doi.org/10.1016/j.peptides.2013.06.001.

[28] Z. Zhang, J.E. Shively, Acceleration of bone repair in NOD/SCID mice by human monoosteophils, novel LL-37-Activated monocytes, PLoS One 8 (2013)e67649 https://doi.org/10.1371/journal.pone.0067649.

[29] F.M.T.A. Costa, S.R. Maia, P.A.C. Gomes, M.C.L. Martins, Dhvar5 antimicrobial peptide (AMP) chemoselective covalent immobilization results on higher antiadherence effect than simple physical adsorption, Biomaterials. 52 (2015) 531–538, https://doi.org/10.1016/j.biomaterials.2015.02.049.

[30] B. Mishra, G. Wang, Titanium surfaces immobilized with the major antimicrobial fragment FK-16 of human cathelicidin LL-37 are potent against multiple antibiotic-resistant bacteria, Biofouling. 33 (2017) 544–555, https://doi.org/10.1080/08927014.2017.1332186.

[31] B. Nie, H. Ao, C. Chen, K. Xie, J. Zhou, T. Long, T. Tang, B. Yue, Covalent immobilization of KR-12 peptide onto a titanium surface for decreasing infection and promoting osteogenic differentiation, RSC Adv. 6 (2016) 46733–46743, https://doi.org/10.1039/C6RA06778F.

[32] M. Godoy-Gallardo, C. Mas-Moruno, M.C. Fernández-Calderón, C. Pérez-Giraldo, J.M. Manero, F. Albericio, F.J. Gil, D. Rodríguez, Covalent immobilization of hLf1-11 peptide on a titanium surface reduces bacterial adhesion and biofilm formation, Acta Biomater. 10 (2014) 3522–3534, https://doi.org/10.1016/j.actbio.2014.03.026.

[33] M. Godoy-Gallardo, C. Mas-Moruno, K. Yu, J.M. Manero, F.J. Gil, J.N. Kizhakkedathu, D. Rodriguez, Antibacterial properties of hLf1-11 peptide onto titanium surfaces: a comparison study between silanization and surface initiated polymerization, Biomacromolecules. 16 (2015) 483–496, https://doi.org/10.1021/bm501528x.

[34] W. Lin, C. Junjian, C. Chengzhi, S. Lin, L. Sa, R. Li, W. Yingjun, Multi-biofunctionalization of a titanium surface with a mixture of peptides to achieve excellent antimicrobial activity and biocompatibility, J. Mater. Chem. B Mater. Biol. Med. 3 (2015) 30–33, https://doi.org/10.1039/C4TB01318B.

[35] S. Makihira, T. Shuto, H. Nikawa, K. Okamoto, Y. Mine, Y. Takamoto, M. Ohara, K. Tsuji, Titanium immobilized with an antimicrobial peptide derived from histatin accelerates the differentiation of osteoblastic cell line, MC3T3-E1, Int. J. Mol. Sci. 11 (2010) 1458–1470, https://doi.org/10.3390/ijms11041458.

[36] L. Zhou, Y. Lai, W. Huang, S. Huang, Z. Xu, J. Chen, D. Wu, Biofunctionalization of microgroove titanium surfaces with an antimicrobial peptide to enhance their bactericidal activity and cytocompatibility, Colloids Surf. B Biointerfaces 128 (2015) 552–560, https://doi.org/10.1016/j.colsurfb.2015.03.008.

[37] C.-P. Chen, R.-Y. Jing, E. Wickstrom, Covalent attachment of daptomycin to Ti6Al4V alloy surfaces by a thioether linkage to inhibit colonization by Staphylococcus aureus, ACS Omega2 (2017) 1645–1652, https://doi.org/10.1021/acsomega.6b00567.

[38] N. Masurier, J.-B. Tissot, D. Boukhriss, S. Jebors, C. Pinese, P. Verdié, M. Amblard, A. Mehdi, J. Martinez, V. Humblot, G. Subra, Site-specific grafting on titanium surfaces with hybrid temporin antibacterial peptides, J. Mater. Chem. B Mater. Biol. Med. 6 (2018) 1782–1790, https://doi.org/10.1039/C8TB00051D.

[39] P. Wadhwani, N. Heidenreich, B. Podeyn, J. Bürck, A.S. Ulrich, Antibiotic gold: tethering of antimicrobial peptides to metal nanoparticles maintains conformational flexibility of peptides and improves trypsin susceptibility, Biomater. Sci. 5 (2017) 817–827, https://doi.org/10.1039/c7bm00069c.

[40] G. Gao, J.T.J. Cheng, J. Kindrachuk, R.E.W. Hancock, S.K. Straus, J.N. Kizhakkedathu, Biomembrane interactions reveal the mechanism of action of surface-immobilized host defense IDR-1010 peptide, Chem. Biol. 19 (2012) 199–209, https://doi.org/10.1016/j.chembiol.2011.12.015.

[41] J.W. Soares, R. Kirby, L.A. Doherty, A. Meehan, S. Arcidiacono, Immobilization and orientation-dependent activity of a naturally occurring antimicrobial peptide, J. Pept, Sci. 21 (2015) 669–679, https://doi.org/10.1002/psc.2787.

[42] A. Rai, S. Pinto, M.B. Evangelista, H. Gil, S. Kallip, M.G.S. Ferreira, L. Ferreira, High-density antimicrobial peptide coating with broad activity and low cytotoxicity against human cells, Acta Biomater. 33 (2016) 64–77, https://doi.org/10.1016/j.actbio.2016.01.035.

[43] M. Bagheri, M. Beyermann, M. Dathe, Mode of action of cationic antimicrobial peptides defines the tethering position and the efficacy of biocidal surfaces, Bioconjug. Chem. 23 (2012) 66–74, https://doi.org/10.1021/bc200367f.

[44] K. Hilpert, M. Elliott, H. Jenssen, J. Kindrachuk, C.D. Fjell, J. Körner, D.F.H. Winkler, L.L. Weaver, P. Henklein, A.S. Ulrich, S.H.Y. Chiang, S.W. Farmer, N. Pante, R. Volkmer, R.E.W. Hancock, Screening and Characterization of Surface-Tethered Cationic Peptides for Antimicrobial Activity, Chem. Biol. 16 (2009) 58–69, https://doi.org/10.1016/j.chembiol.2008.11.006.

[45] M. Bagheri, M. Beyermann, M. Dathe, Immobilization reduces the activity of surface-bound cationic antimicrobial peptides with No influence upon the activity Spectrum, Antimicrob. Agents Chemother. 53 (2009) 1132–1141, https://doi.org/10.1128/AAC.01254-08.

[46] F. D'Este, D. Oro, G. Boix-Lemonche, A. Tossi, B. Skerlavaj, Evaluation of free or anchored antimicrobial peptides as candidates for the prevention of orthopaedic device-related infections, J. Pept. Sci. 23 (2017) 777–789, https://doi.org/10.1002/psc.3026.

[47] B. Skerlavaj, R. Gennaro, L. Bagella, L. Merluzzi, A. Risso, M. Zanetti, Biological characterization of two novel cathelicidin-derived peptides and identification of structural requirements for their antimicrobial and cell lytic activities, J. Biol. Chem. 271 (1996) 28375–28381, https://doi.org/10.1074/jbc.271.45.28375.

[48] M. Benincasa, B. Skerlavaj, R. Gennaro, A. Pellegrini, M. Zanetti, In vitro and in vivo antimicrobial activity of two α-helical cathelicidin peptides and of their synthetic analogs, Peptides. 24 (2003) 1723–1731, https://doi.org/10.1016/j.peptides.2003.07.025.

[49] S. Bauer, P. Schmuki, K. von der Mark, J. Park, Engineering biocompatible implant surfaces, Prog. Mater. Sci. 58 (2013) 261–326, https://doi.org/10.1016/j.pmatsci.2012.09.001.

[50] A.M. Khorasani, M. Goldberg, E.H. Doeven, G. Littlefair, Titanium in biomedical applications—properties and fabrication: a review, J. Biomater. Tissue Eng. 5 (2015) 593–619, https://doi.org/10.1166/jbt.2015.1361.

[51] M. Godoy-Gallardo, Z. Wang, Y. Shen, J.M. Manero, F.J. Gil, D. Rodriguez, M. Haapasalo, Antibacterial coatings on titanium surfaces: a comparison study between in vitro single-species and multispecies biofilm, ACS Appl. Mater. Interfaces7 (2015) 5992–6001, https://doi.org/10.1021/acsami.5b00402.

[52] M.I. Castellanos, C. Mas-Moruno, A. Grau, X. Serra-Picamal, X. Trepat, F. Albericio, M. Joner, F.J. Gil, M.P. Ginebra, J.M. Manero, M. Pegueroles, Functionalization of CoCr surfaces with cell adhesive peptides to promote HUVECs adhesion and proliferation, Appl. Surf. Sci. 393 (2017) 82–92, https://doi.org/10.1016/j.apsusc.2016.09.107.

[53] F. Höök, B. Kasemo, T. Nylander, C. Fant, K. Sott, H. Elwing, Variations in coupled water, viscoelastic properties, and film thickness of a Mefp-1 protein film during adsorption and cross-linking: A quartz crystal microbalance with dissipation monitoring, ellipsometry, and surface plasmon resonance study, Anal. Chem. 73 (2001) 5796–5804, https://doi.org/10.1021/ac0106501.

[54] B. Zhao, H.C. Van Der Mei, G. Subbiahdoss, J. De Vries, M. Rustema-Abbing, R. Kuijer, H.J. Busscher, Y. Ren, Soft tissue integration versus early biofilm formation on different dental implant materials, Dent. Mater. 30 (2014) 716–727, https://doi.org/10.1016/j.dental.2014.04.001.

[55] C. Mas-Moruno, B. Garrido, D. Rodriguez, E. Ruperez, F.J. Gil, Biofunctionalization strategies on tantalum-based materials for osseointegrative applications, J. Mater. Sci. Mater. Med. 26 (2015) 1–12, https://doi.org/10.1007/s10856-015-5445-z.

[56] K.A. Marx, Quartz crystal microbalance: a useful tool for studying thin polymer films and complex biomolecular systems at the solution - Surface interface, Biomacromolecules. 4 (2003) 1099–1120, https://doi.org/10.1021/bm020116i.

[57] M. Rodahl, B. Kasemo, A simple setup to simultaneously measure the resonant frequency and the absolute dissipation factor of a quartz crystal microbalance, Rev. Sci. Instrum. 67 (1996) 3238–3241, https://doi.org/10.1063/1.1147494.

[58] Y.R. Corrales Ureña, L. Wittig, M. Vieira Nascimento, J.L. Faccioni, P.N. Lisboa Filho, K. Rischka, Influences of the pH on the adsorption properties of an antimicrobial peptide on titanium surfaces, Appl. Adhes. Sci. 3 (2015) 7, https://doi.org/10.1186/s40563-015-0032-6.

[59] D.L. Williams, R.D. Bloebaum, Observing the biofilm matrix of Staphylococcus epidermidis ATCC 35984 grown using the CDC biofilm reactor, Microsc. Microanal. 16 (2010) 143–152, https://doi.org/10.1017/S143192760999136X.

[60] B. Valdez-Salas, E. Beltrán-Partida, S. Castillo-Uribe, M. Curiel-Álvarez, R. Zlatev, M. Stoytcheva, G. Montero-Alpírez, L. Vargas-Osuna, In vitro assessment of early bacterial activity on Micro/Nanostructured Ti6Al4V surfaces, Molecules. 22 (2017) 832, https://doi.org/10.3390/molecules22050832.

[61] P. Cao, Y. Yang, F. Uche, S. Hart, W.-W. Li, C. Yuan, Coupling plant-derived cyclotides to metal surfaces: an antibacterial and antibiofilm study, Int. J. Mol. Sci. 19 (2018) 793, https://doi.org/10.3390/ijms19030793.

[62] B. Skerlavaj, M. Benincasa, A. Risso, M. Zanetti, R. Gennaro, SMAP-29: a potent antibacterial and antifungal peptide from sheep leukocytes, FEBS Lett. 463 (1999) 58–62, https://doi.org/10.1016/S0014-5793(99)01600-2.

[63] M. Wilmes, M. Stockem, G. Bierbaum, M. Schlag, F. Götz, D. Tran, J. Schaal, A. Ouellette, M. Selsted, H.-G. Sahl, Killing of staphylococci by θ-Defensins involves membrane impairment and activation of autolytic enzymes, Antibiotics. 3 (2014) 617–631, https://doi.org/10.3390/antibiotics3040617.

[64] E.K. Lee, Y.-C. Kim, Y.H. Nan, S.Y. Shin, Cell selectivity, mechanism of action and LPS-neutralizing activity of bovine myeloid antimicrobial peptide-18 (BMAP-18) and its analogs, Peptides. 32 (2011) 1123–1130, https://doi.org/10.1016/j.peptides.2011.03.024.

[65] K. Rapsch, F.F. Bier, M. Tadros, M. von Nickisch-Rosenegk, Identification of antimicrobial peptides and immobilization strategy suitable for a covalent surface coating with biocompatible properties, Bioconjug. Chem. 25 (2014) 308–319, https://doi.org/10.1021/bc4004469.

[66] A. Müller, A. Wenzel, H. Strahl, F. Grein, T.N.V. Saaki, B. Kohl, T. Siersma, J.E. Bandow, H.-G. Sahl, T. Schneider, L.W. Hamoen, Daptomycin inhibits cell envelope synthesis by interfering with fluid membrane microdomains, Proc. Natl. Acad. Sci. 113 (2016) E7077–E7086, https://doi.org/10.1073/pnas.1611173113.

[67] K. Scheinpflug, M. Wenzel, O. Krylova, J.E. Bandow, M. Dathe, H. Strahl, Antimicrobial peptide cWFW kills by combining lipid phase separation with autolysis, Sci. Rep. 7 (2017) 44332, https://doi.org/10.1038/srep44332.

[68] X. Chen, H. Hirt, Y. Li, S. Gorr, C. Aparicio, Antimicrobial GL13K peptide coatings killed and ruptured the wall of Streptococcus gordonii and prevented formation and growth of biofilms, PLoS One 9 (2014)e111579https://doi.org/10.1371/journal.pone.0111579.

[69] R. Southwood, J. Rice, P. McDonald, P. Hakendorf, M. Rozenbilds, Infection in experimental hip arthroplasties, J. Bone Joint Surg. Br. 67-B (1985) 229–231, https://doi.org/10.1302/0301-620X.67B2.3980532.

[70] D. Vidlak, T. Kielian, Infectious dose dictates the host response during Staphylococcus aureus orthopedic-implant biofilm infection, Infect. Immun. 84 (2016) 1957–1965, https://doi.org/10.1128/IAI.00117-16.

[71] V.T.H. Pham, V.K. Truong, A. Orlowska, S. Ghanaati, M. Barbeck, P. Booms, A.J. Fulcher, C.M. Bhadra, R. Buividas, V. Baulin, C.J. Kirkpatrick, P. Doran, D.E. Mainwaring, S. Juodkazis, R.J. Crawford, E.P. Ivanova, "Race for the Surface": Eukaryotic Cells Can Win, ACS Appl. Mater. Interfaces8 (2016) 22025–22031, https://doi.org/10.1021/acsami.6b06415.

[72] K.G. Neoh, X. Hu, D. Zheng, E.T. Kang, Balancing osteoblast functions and bacterial adhesion on functionalized titanium surfaces, Biomaterials. 33 (2012) 2813–2822, https://doi.org/10.1016/j.biomaterials.2012.01.018.

[73] M. Engels-Deutsch, S. Rizk, Y. Haïkel, Streptococcus mutans antigen I/II binds to α5β1 integrins via its A-domain and increases β1 integrins expression on periodontal ligament fibroblast cells, Arch. Oral Biol. 56 (2011) 22–28, https://doi.org/10.1016/j.archoralbio.2010.08.010.

[74] P.R. Kramer, A. JanikKeith, Z. Cai, S. Ma, I. Watanabe, Integrin mediated attachment of periodontal ligament to titanium surfaces, Dent. Mater. 25 (2009) 877–883, https://doi.org/10.1016/j.dental.2009.01.095.